

**GEOLOGICAL SETTING, NATURE AND EVOLUTION OF REDUCED INTRUSIONS AND GOLD
BEARING QUARTZ VEINS OF THE 4021 PROSPECT, GOODPASTER DISTRICT, EAST-
CENTRAL ALASKA.**

by

KATHERINE M. DILWORTH

B.Sc. Honours, Queen's University – Kingston, Ontario, 2000

A THESIS SUBMITTED IN PARTIAL FULFILMENT OF
THE REQUIREMENTS FOR THE DEGREE OF

MASTER OF SCIENCE

in

THE FACULTY OF GRADUATE STUDIES

(Department of Earth and Ocean Sciences)

We accept this thesis as conforming
to the required standard

THE UNIVERSITY OF BRITISH COLUMBIA

July 2003

© Katherine M. Dilworth, 2003

In presenting this thesis in partial fulfilment of the requirements for an advanced degree at the University of British Columbia, I agree that the Library shall make it freely available for reference and study. I further agree that permission for extensive copying of this thesis for scholarly purposes may be granted by the head of my department or by his or her representatives. It is understood that copying or publication of this thesis for financial gain shall not be allowed without my written permission.

Department of Earth and Ocean Sciences

The University of British Columbia
Vancouver, Canada

Date July 21 2003

ABSTRACT

Gold deposits associated with Cretaceous reduced granitic rocks are common in Yukon and Alaska. The Liese zone and spatially related prospects in the Goodpaster district, east-central Alaska, are associated with an arcuate, easterly trending belt of Cretaceous reduced granite to tonalite that compose the older of two Early Cretaceous intrusive suites. A younger suite of calc-alkaline diorite rocks (~94 Ma) are slightly more oxidized and are unrelated to the gold mineralization. Both calc-alkalic suites have low magnetic susceptibilities and oxidation states. The older suite, which includes a phase of the Goodpaster Batholith, is weakly peraluminous and contains monazite and zircon. Biotite is common and hornblende is subordinate to absent. Older granitoids of the suite are deformed and syn- to- late kinematic to regional metamorphism at about 109-107 Ma (U-Pb; zircon and monazite). Post-kinematic intrusions of the suite are as young as 104 Ma (U-Pb SHRIMP-RG). Sulphide deposition at ~104.3 Ma in the Liese Zone, inferred by a Re-Os date on molybdenite, indicates a temporal overlap.

Gold veins in the region have a reduced sulphide assemblage (löllingite and pyrrhotite stable) and are characterized by an Au-Bi-Te geochemical signature. Fluid inclusions from gold veins and pegmatite are similar and contain ubiquitous aqueous-carbonic fluid inclusions \pm CH₄. Locally, complex saline fluids coexist with CO₂-rich fluids. Sulphide minerals from the Liese zone and gold prospects have Pb isotopic values ($^{206}\text{Pb}/^{204}\text{Pb}$ = 19.4-19.5) that generally overlap with those of the reduced granite to tonalite ($^{206}\text{Pb}/^{204}\text{Pb}$ = 19.4-19.6). The sulphide Pb isotopic values extend to slightly higher $^{206}\text{Pb}/^{204}\text{Pb}$ values, likely due to fluid rock interaction with the isotopically heterogeneous host gneiss of the Yukon-Tanana terrane. The diorite suite has lower values ($^{206}\text{Pb}/^{204}\text{Pb}$ = 19.1-19.2) than most of the sulphides, and thus is precluded from contributing Pb to the bulk of the sulphides.

Gold in the Pogo area is related to a suite of reduced granite to tonalite intrusions that were emplaced late- to post-kinematic to regional deformation in the late Early Cretaceous. Gold-bearing quartz veins formed from magmatic-hydrothermal fluids exsolved from the reduced granites and were focused along shallowly dipping regional foliation.

TABLE OF CONTENTS

Abstract.....	ii
Table of Contents.....	iii
List of Figures.....	vii
List of Tables.....	x
Foreword.....	xii
Acknowledgements.....	xiii

CHAPTER ONE

GENERAL INTRODUCTION

Gold-Bearing Quartz Veins Related to Reduced Intrusions.....	1
Objectives.....	3
Exploration History.....	4
Previous Work.....	5
Methodology.....	5
Presentation.....	6
Chapter 2.....	7
Chapter 3.....	7
Chapter 4.....	7
Appendices.....	8
References.....	9

CHAPTER TWO

PETROGRAPHIC, GEOCHEMICAL AND LEAD ISOTOPIC CHARACTERISTICS OF REDUCED GRANITOIDS IN THE GOODPASTER DISTRICT, EAST-CENTRAL ALASKA

Abstract.....	11
Introduction.....	13
Regional Geology.....	15

Geological Setting of the Goodpaster District.....	17
Petrographic and Geochronological Data.....	22
Granite Suite.....	25
Tonalite Suite.....	29
Diorite Suite.....	31
Controls on Intrusive Emplacement.....	32
Geochemistry of the Intrusive Suites in the Goodpaster District.....	36
Analytical Methods.....	36
Major Element Geochemistry.....	36
Trace and Rare Earth Element Geochemistry.....	43
Tectonic Discrimination.....	47
Bulk Magnetic Susceptibility.....	50
Oxidation State.....	51
Lead Isotope Study.....	52
Discussion.....	57
Evolution of the Granitoid Suites in the Goodpaster District.....	57
Magmatic Source.....	59
Relationship to Other Reduced Intrusions Related to Gold Deposits.....	60
Depth of Emplacement.....	61
Correlation with Cretaceous Plutonic Suites in Yukon.....	62
Conclusions.....	64
References.....	66

CHAPTER THREE

GOLD-BEARING QUARTZ VEINS RELATED TO REDUCED INTRUSIONS AT THE 4021 PROSPECT, GOODPASTER DISTRICT, EAST-CENTRAL ALASKA

Abstract.....	73
Introduction.....	74
Regional Geological Setting.....	79

District Scale Geology.....	80
Gold-Bearing Quartz Veins of the Goodpaster District.....	82
4021 Prospect.....	85
Alteration.....	87
<i>Quartz-sericite ± K-feldspar ± albite</i>	87
<i>Chlorite</i>	89
<i>Ankerite-sericite-carbonate</i>	90
<i>Calcite-quartz</i>	90
<i>Surface weathering</i>	91
Quartz Vein Morphology.....	91
<i>Early shear zones</i>	94
<i>Main stage veins / veinlets</i>	94
<i>Post-mineral faulting</i>	96
Quartz Vein Textures.....	97
Ore Mineralogy.....	100
Metal Association and Distribution.....	102
Fluid Inclusions.....	105
Microthermometry.....	109
Pegmatite.....	112
Quartz Veins.....	113
<i>99-2076 (flat quartz vein)</i>	114
<i>276-192 (steeply dipping quartz veinlet)</i>	115
Bladed Calcite.....	116
Interpretation of Fluid Inclusions.....	116
Pressure Estimates.....	120
Lead Isotopic Compositions as a Source Indicator.....	123
Discussion.....	128
Comparison of the 4021 Prospect to the Liese Zone.....	129
Timing of Mineralization in Relation to Metamorphism, Deformation and Cretaceous	
Magmatism.....	129
Magmatic Linkages and Depths of Formation.....	132

Orogenic Versus Reduced Intrusion-Related Gold Deposits.....	133
Conclusions.....	134
References.....	136

CHAPTER FOUR

CONCLUSIONS, EXPLORATION POTENTIAL AND CONSIDERATIONS FOR FUTURE RESEARCH

General Conclusions and Exploration Considerations.....	143
Cretaceous Intrusive Rocks.....	143
4021 Prospect Gold-Bearing Quartz Veins.....	145
Classification.....	147
References.....	148

APPENDICES

Appendix A – U-Pb Geochronology.....	149
Conventional U-Pb Geochronology Data.....	152
SHRIMP-RG U-Pb Geochronology Data.....	162
Appendix B – Geochemistry Detection Limits and Standards.....	166
Appendix C – Fluid Inclusion Microthermometric Measurements.....	171

LIST OF FIGURES

CHAPTER ONE

Figure 1-1. Location of the Goodpaster district in east-central Alaska.....	2
---	---

CHAPTER TWO

Figure 2-1. Location of the Tintina Gold Belt in Yukon and Alaska, and the major gold deposits and gold occurrence associated with reduced intrusions.....	14
Figure 2-2. Map of late Early and early Late Cretaceous plutonic and volcanic rocks in Yukon and east-central Alaska.....	18
Figure 2-3. Simplified regional geology map of east-central Alaska.....	19
Figure 2-4. Geological map of the Goodpaster district.....	21
Figure 2-5. Geochronology summary	27
Figure 2-6. Photographs of granite suite samples.....	26
Figure 2-7. Photographs of tonalite and diorite suite samples.....	30
Figure 2-8. Rose diagrams of foliation and pegmatite/granite orientations in drill core.....	33
Figure 2-9. Schematic relationships of intrusive phases relative to foliation.....	34
Figure 2-10. Photograph of granite exploiting shallowly dipping foliation.....	35
Figure 2-11. Total alkalis versus silica plot for plutonic rocks	36
Figure 2-12. Shands peraluminosity index.....	42
Figure 2-13. Harker variation diagrams.....	44
Figure 2-14. Chondrite and primitive mantle normalized rare earth element diagrams.....	45
Figure 2-15. Tectonodiscrimination diagrams.....	48
Figure 2-16. Intrusive rocks samples normalized to North American shale	49
Figure 2-17. Magnetic susceptibility diagram.....	50

Figure 2-18. $\text{Fe}_2\text{O}_3/\text{Fe}_2\text{O}_3 + \text{FeO}$ ratios of the intrusive rocks.....	52
Figure 2-19. $^{208}\text{Pb}/^{204}\text{Pb}$ versus $^{206}\text{Pb}/^{204}\text{Pb}$ diagram and $^{207}\text{Pb}/^{204}\text{Pb}$ versus $^{206}\text{Pb}/^{204}\text{Pb}$ covariation diagrams	55

CHAPTER THREE

Figure 3-1. Location of the Goodpaster district in east-central Alaska.....	75
Figure 3-2. Geological map of the Goodpaster district.....	78
Figure 3-3. Photograph of flat-lying structures evident in topography at the 4021 prospect...83	
Figure 3-4. Geological Map of the 4021 prospect.....	86
Figure 3-5. Photographs of alteration assemblages at the 4021 prospect.....	88
Figure 3-6. Geological long section of 4021 prospect.....	92
Figure 3-7. Cross section A-A' of the 4021 prospect.....	93
Figure 3-8. Photographs of quartz veins.....	95
Figure 3-9. Photomicrographs of quartz grain textures.....	99
Figure 3-10. Photomicrographs of ore mineral assemblages and relationships.....	101
Figure 3-11. Interpreted mineralization and alteration paragenetic sequence.....	103
Figure 3-12. Fluid inclusion photomicrographs.....	108
Figure 3-13. Fluid inclusion homogenization temperature histograms	111
Figure 3-14. Depressed CO_2 melting temperatures in aqueous-carbonic fluids.....	117
Figure 3-15. Proposed fluid evolution at the 4021 prospect.....	119
Figure 3-16. Pressure estimates based on isochores.....	121
Figure 3-17. Depth estimates.....	123
Figure 2-18. $^{208}\text{Pb}/^{204}\text{Pb}$ versus $^{206}\text{Pb}/^{204}\text{Pb}$ diagram and $^{207}\text{Pb}/^{204}\text{Pb}$ versus $^{206}\text{Pb}/^{204}\text{Pb}$ covariation diagrams	126

APPENDIX A

Figure A-1. Location of samples used for geochronology.....	150
Figure A-2. U-Pb concordia plots for intrusive samples from the Goodpaster district using conventional U-Pb methods.....	159
Figure A-3. U-Pb Concordia plot for sample Mapt-7 using SHRIMP-RG.....	165

LIST OF TABLES

CHAPTER TWO

Table 2-1. Summary of the Cretaceous intrusive rocks in the Goodpaster district.....	23
Table 2-2a. Location and descriptions of Cretaceous intrusive rocks samples used for geochemistry.....	37
Table 2-2b: Major element compositions of Cretaceous intrusive rocks.....	38
Table 2-2c: Trace and rare earth element compositions of Cretaceous intrusive rocks.....	39
Table 2-3. Lead isotopic values from the granite, tonalite and diorite suite intrusive rocks in the Goodpaster district.....	54
Table 2-4. Summary of the mid-Cretaceous intrusive suites in Yukon and Alaska.....	63

CHAPTER THREE

Table 3-1. General characteristics of intrusion-related gold deposits and mesothermal orogenic lode-gold deposits.....	76
Table 3-2. Summary of the three intrusive suites in the Goodpaster district.....	81
Table 3-3. Correlation coefficients between gold and various elements	105
Table 3-4. Fluid inclusion types and general characteristics.....	107
Table 3-5. Summary of fluid inclusions microthermometric data.....	110
Table 3-6. Summary of fluid inclusion composition data.....	110
Table 3-7. Lead isotopic analyses from sulphide mineral separates from gold-bearing quartz veins	125

APPENDIX A

Table A-1. Geochronology sample descriptions.....	151
Table A-2. Conventional U-Pb analytical data for intrusive rocks in the Goodpaster District, Alaska	156

Table A-3. U-Pb analytical data (SHRIMP-RG) for sample MAPT-7.....	164
--	-----

APPENDIX B

Table B-1. Geochemistry data from volcanic rocks samples.....	168
Table B-2. Detection limits.....	169
Table B-3. Duplicate and standard analyses.....	170

APPENDIX C

Type 1A microthermometric data.....	172
Type 1B microthermometric data.....	173
Type 2 and Type 4 microthermometric data.....	175
Type 3 microthermometric data.....	177
Bladed calcite microthermometric data.....	178

FOREWORD

This thesis is comprised of two papers that were produced at the University of British Columbia. The purpose of this foreword is to properly acknowledge the contributions of several collaborators.

The paper that comprises Chapter 2 was prepared for submission to the Canadian Journal of Earth Sciences and will be coauthored by Shane Ebert, Richard Tosdal and Jim Mortensen. Shane Ebert contributed to the field-work on which this thesis is based. Jim Mortensen provided all conventional U-Pb ages on the intrusive rocks and provided the report found in Appendix A. Richard Tosdal undertook SHRIMP-RG and provided an age for one sample. All co-authors were involved in the development of ideas and contributed editorially.

The paper that comprises Chapter 3 is co-authored by Shane Ebert and Richard Tosdal. These authors played an editorial role and provided guidance and supervision in all aspects of the papers. Shane Ebert supervised the fluid inclusion portion of the paper. Moira Smith (TeckCominco Ltd.) provided all common Pb-Pb analyses from the Liese zone and North zone.

Acknowledgments

This thesis has benefited from the help of many people. I would like to extend my gratitude to my supervisors Richard Tosdal and Shane Ebert for their guidance during this thesis and for their continuous patience and encouragement. Thank you for providing me with numerous opportunities beyond my thesis, such as field trips and conferences which were invaluable to learning. Shane Ebert is gratefully acknowledged for his prompt reviews of many, many revisions of these chapters and for numerous discussions. Thanks to Jim Mortensen for his wealth of knowledge on the Canadian Cordillera, geochemistry, geochronology and for serving on my committee.

Many thanks to fellow graduate students who provided me with a source of fun and distraction, and made UBC an enjoyable place to spend the last two and half years. I would especially like to thank Nathalie Lefebvre for listening when I needed to vent. Thanks to Geoff Bradshaw for the Tuesday lattes, Dave Smithson for his discussions on everything porphyry copper related, Simon Haynes, Lawrence Winter and Angie Carter for making my first year at UBC enjoyable and for having some great parties. Scott Heffernan is thanked for all his advice, for his constant optimism, and for providing me with all the papers I ever needed....is there any paper that you don't have? Thanks to Brigitte Petrie for the fun travels in Peru.

Mati Raudsepp is thanked for his invaluable assistance with the SEM and microprobe. Alex Allen is thanked for her help with UBC red tape and for knowing everything! Janet Gabites is thanked for her help and discussions about common Pb isotopes.

During the last two years, I have had the privilege of working with several geologists. I would like to thank them for sharing their ideas, insights and support. Finally, thank you to Moira Smith, Paul Robers and Jack DiMarchi of Teckcominco for their discussions while at Pogo camp. Thanks to Cameron Rombach for his discussions on the Liese zone and making camp such a fun place to be - green acres is the place to be!

Thank you to my family for their support during the course of my thesis. Your early morning wake up calls over the last two and half years has not gone unnoticed. Finally, I would like to thank my fiancé Martin Telford for his understanding and constant emotional support during the last two and a half years. It has been a long two years apart.

CHAPTER ONE

GENERAL INTRODUCTION

GOLD-BEARING QUARTZ VEINS RELATED TO REDUCED INTRUSIONS

The Goodpaster district in east-central Alaska is located within the Tintina Gold Belt (TGB), which is characterized by various styles of precious- and base-metal mineralization thought to be genetically associated with reduced Cretaceous intrusions (Thompson and Newberry, 2000; Lang et al., 2001) (Figure 1-1). Gold-rich deposits within the TGB are principally associated with the early Late Cretaceous Tombstone Plutonic Suite (TPS), although younger and older deposits are known (Thompson and Newberry, 2000; Hart et al., 2000). The deposits are part of the reduced intrusion-related gold deposit (IRGD) class as described by Thompson et al. (1999), Lang et al. (2000), and Thompson and Newberry (2000). Deposit styles in the IRGD class are highly variable and include sheeted gold-bearing quartz (\pm feldspar) veins, auriferous polymetallic replacement bodies, auriferous breccias, disseminated ores, gold-rich skarns (Hart et al., 2002) and Au-rich shear-zone hosted quartz veins (Thompson and Newberry, 2000). Despite the numerous reviews of the intrusion-related gold deposit class, there have been few detailed studies on specific gold deposits related to reduced intrusions, or of the proposed causative intrusive complex.

The Goodpaster district contains an easterly trending belt of gold-bearing quartz veins, the largest of which is the Liese zone. The 4021 prospect, the second best exposed of all the prospects, is located 5 km east of the Liese zone and likely formed during the same mineralizing event as the Liese zone. The prospects are spatially and temporally associated with an arcuate, easterly trending belt of reduced late Early Cretaceous granitic to tonalitic intrusions. The gold-bearing quartz veins in the Liese zone and the 4021 prospect are hosted in shear zones, bordered by sericite-carbonate altered rocks, and contain low-salinity, aqueous-carbonic fluids (Rombach

et al., 2002; this study). These are common characteristics similar to both intrusion-related gold deposits (Thompson and Newberry, 2000) and orogenic gold deposits related to metamorphic processes (Goldfarb et al., 1997).

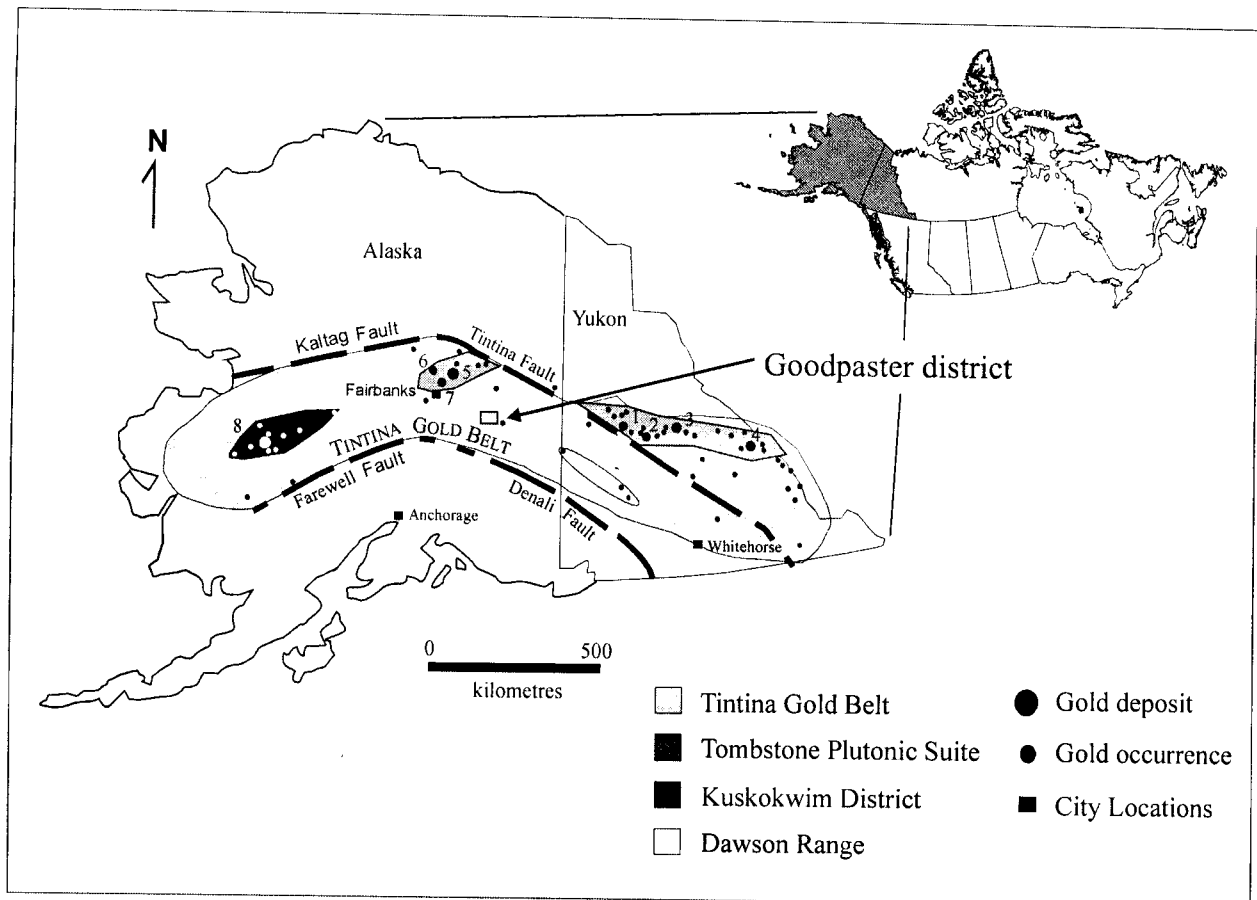


Figure 1-1: Location and extent of the Tintina Gold Belt in Yukon and Alaska. The small square denotes the location of the Goodpaster district in east-central Alaska. Major gold deposits (large circles), gold occurrences (small circles) and the extent of the Tombstone Plutonic Suite, Kuskokwim District plutonic rocks, and Dawson Range Plutonic Suite are shown. The gold deposits are associated with plutonic rocks. Numbers denote gold deposits: 1-Brewery Creek; 2- Clear Creek; 3-Dublin Gulch; 4-Emerald Lake; 5-Fort Knox; 6- True North; 7-Ryan Lode; 8-Donlin Creek. Figure modified after Mortensen et al.(2000).

OBJECTIVES

This thesis is part of a larger study focusing on the regional geologic framework and deposit specific exploration models for intrusion-related gold mineralization in Yukon and Alaska. This project was designed to advance the understanding of the diverse styles and ages of intrusion-related gold deposits in Yukon and Alaska and to develop exploration models based on detailed studies of individual deposits. The project was supported by the Mineral Deposit Research Unit at the University of British Columbia, eight mining companies (AngloGold North America Inc., Barramundi Gold Ltd., Barrick Gold Corporation, Homestake Canada Inc., Newmont Exploration, Placer Dome Exploration, Teck Exploration Inc. [presently TeckCominco Ltd.], and WMC Exploration Inc.) and the Natural Sciences and Engineering Research Council of Canada (NSERC Cooperative Research and Development Program). TeckCominco Inc. provided additional logistical and financial support for this study during two field seasons. An NSERC Post Graduate Scholarship (PGS-A) and a Thomas and Marguerite MacKay scholarship from the University of British Columbia provided additional funding.

The three main objectives of this thesis were to 1) establish the regional intrusive framework in the Goodpaster district, 2) to better understand the timing, nature, and origin of alteration and mineralization at the 4021 prospect and 3) to assess the relationship between the intrusive rocks and the gold-bearing quartz veins in the district. A major focus of the research was to develop a genetic model for the 4021 prospect and prove, or disprove, the magmatic-hydrothermal component in ore formation.

Research on the largest gold veins in the Goodpaster district, the Liese zone, is the subject of a current PhD thesis by Cameron Rombach at the University of Alaska in Fairbanks. The gold-bearing quartz veins at the 4021 prospect shares several characteristics with the quartz

veins of the Liese zone and this study and the study of Rombach et al., (2002) have reached similar conclusions.

EXPLORATION HISTORY

The discovery of the high-grade Liese zone in the Goodpaster district resulted from several years of systematic exploration in an area of promising geology but very little prior mining history. In 1981, the Alaskan subsidiary of Watts Grifffis McOuat (WGM) followed up on the regional-scale stream sediment-sampling program in the Goodpaster River area by the USGS and found that Pogo and Liese Creeks returned weak gold and multi-element anomalies. Further geochemical sampling identified a multi-element anomaly and mineralized quartz float on the ridge adjacent to Pogo creek. The area lay dormant until 1991, when WGM formed the Stone Boy Venture (JC) with partners Sumitomo Metal Mining Arizona Inc., Conroy Petroleum, and Noranda-Hemlo Inc. Following withdraw of the latter two companies in 1993, WGM operated the project on behalf of Sumitomo until 1997, when Teck Inc. earned a 40% interest and became operator. In 1994, three holes were drilled to test the anomaly and intersected gold in quartz veins that are now known as the Liese Zone. Drilling continued with 13 holes in 1995, 23 holes in 1996, and 41 holes in 1997. Originally, the Liese zone was inferred to comprise a series of parallel, steeply dipping veins. However, following drilling in 1997, it became evident the veins were relatively flat-lying. The early recognition of the shallowly dipping geometry was important to the evaluation of the Liese zone and critical for exploration in the Goodpaster district.

PREVIOUS WORK

The Liese zone and surrounding area has been the subject of several studies. The studies have focused mainly on the Liese zone and include work by exploration and mine geologists, the United States Geological Survey, graduate students, and a structural study by the Mineral Deposit Research Unit at the University of British Columbia. Relevant references include Smith et al. (1999), Smith et al. (2000), Moore (2000), Rombach et al. (2002), Dilworth et al. (2002a), Dilworth et al., (2002b), Day et al., (2002), Day et al. (2003), Rhys et al. (2003) and Dilworth et al., (2003).

Thirteen intrusive rock samples were collected for U-Pb dating by various workers, prior to the author arriving to begin the project. Jim Mortensen at the University of British Columbia, Vancouver, analyzed these samples and his report is included in Appendix A. Shane Ebert spent six weeks mapping in the region prior to the author starting the project and provided a regional geological base map for the intrusive rock study.

METHODOLOGY

A combination of detailed geological mapping, petrography, geochronology, geochemistry, fluid inclusion microthermometry and a lead isotope study were integrated to understand the distribution of the intrusive rocks in the Goodpaster district and to constrain the origin of gold-bearing quartz veins at the 4021 prospect.

Fieldwork during 2001 and 2002 largely focused on detailed geological mapping and defining the distribution of the intrusive rocks in the district as well as the field relationships of the intrusions in the vicinity of the 4021 prospect. Samples were collected specifically for petrographic, geochemical, lead isotopes, and fluid inclusion studies.

Most of the observations from the 4021 prospect are based on examination and logging of alteration, ore mineralogy and structure in drill core. Samples collected from drill core were cut and prepared as polished thin sections and doubly polished thin sections for petrography and fluid inclusion microthermometry respectively. Semi-quantitative analysis using the scanning electron microscope (SEM) was used to identify unknown minerals. The electron microprobe was used for thermobarometry on two hornblende samples for preliminary emplacement depths of the Goodpaster Batholith. Fluid inclusion microthermometry was undertaken to provide constraints on the physico-chemical conditions (pressure-temperature-composition) of the gold-bearing ore fluid.

Lead isotope compositions of sulphide minerals and intrusive rock samples were analysed to identify metal sources and assess the degree of fluid rock interaction. All lead isotopic compositions from the Liese zone are from Smith et al., (1999). Janet Gabites analysed all Pb isotope samples at the Pacific Centre for Isotope and Geochemical Research at the University of British Columbia, Vancouver.

PRESENTATION

This thesis is presented in manuscript format, in accordance with the University of British Columbia guidelines. Results are presented as two individual research papers in Chapter 2 and Chapter 3. These papers will be submitted for publication in the Canadian Journal of Earth Sciences and Mineralium Deposita respectively. Supplementary information is provided in the appendices. As these chapters are stand-alone papers, repetition is unavoidable in order to provide clarity and context for each chapter.

CHAPTER 2

Petrographic, geochemical and isotopic characteristics of reduced granitoids in the Goodpaster district, east-central Alaska

Katherine Dilworth, Shane Ebert, Jim Mortensen and Richard Tosdal

This chapter focuses on the Cretaceous intrusive rocks in the Goodpaster district and describes the regional distribution of the intrusive rocks, their ages, and their spatial and temporal relation to gold mineralization at the 4021 prospect. Field mapping, geochemistry, petrography, and lead isotopes subdivide the Cretaceous rocks into three suites. New U-Pb ages are reported for the Goodpaster Batholith, the Shawnee Peak intrusion and a tonalite rock three kilometers east of the Liese zone. This chapter also provides a detailed geological history of the district.

CHAPTER 3

Gold bearing quartz veins related to reduced intrusions at the 4021 prospect, Goodpaster district, east-central Alaska

Katherine Dilworth, Shane Ebert and Richard Tosdal

This chapter provides a detailed overview of the geology of the 4021 prospect. Descriptions of the alteration, ore mineralogy, quartz vein textures and elemental associations are discussed. The above, combined with geochronology, lead isotopes and fluid inclusion microthermometry were used to confirm a magmatic-hydrothermal origin for the gold-bearing quartz veins of the 4021 prospect.

CHAPTER 4

General Conclusions

This chapter outlines the overall conclusions of the research presented in chapter two and chapter three. Exploration and future research considerations are also discussed.

APPENDICES A

Appendix A provides sample locations and sample descriptions of rocks used for U-Pb dating. A report prepared by Jim Mortensen at the Pacific Center for Isotopic and Geochemical Research at the University of British Columbia, Vancouver, discusses the detailed methodology and interpretation of 13 intrusive rocks in the Goodpaster district dated by conventional U-Pb methods. A report for sample MAPT-7 whose age was determined by SHRIMP-RG by Richard Tosdal at Stanford University, California is also included.

Appendix B discusses the methodology, detection limits, and duplicate analyses (to test for precision) used for geochemical data. Samples were analysed at ALS-Chemex, North Vancouver. Geochemical data for two volcanic rocks that were not used in this study are provided.

Appendix C provides fluid inclusion observations and microthermometric measurements from the fluid inclusion study.

REFERENCES

- Day, W.D., Aleinikoff, J.N., Dusel-Bacon, C., Goldfarb, R., Gough, L.P. and O'Neill, J.M., 2002, Complex Mesozoic deformation in the central part of the Yukon Tanana Uplands, Alaska -Implications for gold deposition in the Tintina Gold Province, Geological Society of America Programs with Abstracts.
- Day, W.C., Aleinikoff, J.N., Roberts, P., Smith, M., Gamble, B.M., Henning, M.W., Gough, L.P., and Morath, L.C. 2003, Geological Map of the Big Delta B-2 Quadrangle, east-central Alaska. U.S. Department of the Interior and U.S. Geological Survey; Geological Investigations series I-2788. Scale 1: 63 360.
- Dilworth, K.M., Ebert, S.E., Mortensen, J.K., Rombach, C., Tosdal, R.M., 2002. Reduced granites and gold veins in the Pogo Area, east-central Alaska. Geological Society of America, v. 34, no. 6, p. 114.
- Dilworth, K.M., Ebert, S.E., Mortensen, J.K., Tosdal, R.M., 2002. Petrography of reduced intrusions on the Pogo Property, east-central Alaska, *In* Geological Association of Canada, Program with Abstracts.
- Dilworth, K.M., Ebert, S.E., Mortensen, J.K., Tosdal, R.M., 2003, Reduced granites and gold veins in the Pogo region, east-central Alaska, Geological Association of Canada Annual Meeting, Program with Abstracts.
- Goldfarb, R.J., Miller, L.D., Leach, D.L., and Snee, L.W., 1997. Gold deposits in metamorphic rocks of Alaska: Economic Geology Monograph 9, p. 151-190.
- Hart, C.J.R., Baker, T., and Burke, M., 2000. New exploration concepts for country-rock hosted, intrusion-related gold systems. *In* The Tintina Gold Belt: Concepts, exploration, and discoveries, British Columbia and Yukon Chamber of Mines Cordilleran Roundup Special Volume 2, Vancouver, British Columbia, p. 132-145.
- Hart, C.J.R., McCoy, D.T., Goldfarb, R.J., Smith, M., Roberts, P., Hulstein, R., Bakke, A.A., and Bundtzen, R.K., 2002, Geology, Exploration, and Discovery in the Tintina Gold Province, Alaska and Yukon, *in* Society of Economic Geologists Special Publication 9, p. 241-274.
- Lang, J.R., Baker, C.J.R. Hart, and J.K. Mortensen. 2000, An exploration model for intrusion-related gold systems: Society of Economic Geologists Newsletter. v. 40,1, 6-15.
- Lang, J. R, Thompson, J.F., Mortensen, J.K., Baker, C.J.R., Cousin, I.M., Duncan, R., and Aloof, T., 2001. Tombstone-Tungsten Belt. *In* Lang, J., *eds* Regional and system-scale controls on the formation of copper and/or gold magmatic-hydrothermal mineralization. Mineral Deposit Research Unit, Special Publication Number 2, January 2001.

- Mortensen, J.K., Hart, C.J.R., Murphy, D.C., and Heffernan, S., 2000. Temporal evolution of Early and Mid-Cretaceous magmatism in the Tintina Gold Belt. *In* The Tintina Gold Belt: Concepts, exploration, and discoveries, British Columbia and Yukon Chamber of Mines Cordilleran Roundup Special Volume 2, Vancouver, British Columbia, pp. 49-57.
- Moore, K., 2000. Geology of the gold-bearing L1 and L2 Liese quartz zones, Pogo Deposit, east-central Alaska: Masters Thesis, Colorado School of Mines, June 2000.
- Rhys, D., DiMarchi, J., Rombach, C., Smith, M., Friesen, R. (2003). Structural setting, style and timing of vein-hosted gold mineralization at the Pogo deposit, east-central Alaska: 38 p. Mineralium Deposita.
- Rombach, C., Newberry, R.J., Gordfarb, R.J., Smith, M., 2002. Geochronology and mineralization of the Liese zones, Pogo Deposit, Alaska. Geological Society of America, v 34, no. 6, p. 114.
- Smith M, Thompson J, Bressler J, Layer P, Mortensen J, Abe I, Takaoka H, (1999), Geology of the Liese zone, Pogo property, East-central Alaska. SEG Newsletter 38: 1, 12-21.
- Smith M, Thompson J, Moore KH, Bressler J, Layer P, Mortensen J, Abe I, Takaoka H (2000) The Liese zone, Pogo property: A new high-grade gold deposit in Alaska. In: Tucker T, and Smith M.T., (eds) The Tintina Gold Belt: Concepts, Exploration and Discoveries. B.C. and Yukon Chamber of Mines, Special Volume 2, pp 131-144.
- Thompson, J.F.H., and R.J. Newberry. 2000, Gold deposits related to reduced granitic intrusions, *in* Hagemann, S.G., and Brown, P.E., eds., Gold in 2000: Reviews in Economic Geology. v.13 ,377-400.
- Thompson J.F.H., Sillitoe RH, Baker T, Lang J.R., Mortensen J.K. (1999). Intrusion-related gold deposits associated with tungsten-tin provinces. Mineralium Deposita 34: 323-334.

CHAPTER TWO

Petrographic, geochemical and Pb-isotopic characteristics of reduced granitoids in the Goodpaster district, east-central Alaska

ABSTRACT

The >5 M oz gold veins of the Liese Zone and nearby prospects in the Goodpaster district of east-central Alaska are spatially and temporally associated with an arcuate, easterly trending belt of reduced felsic plutons that compose two late Early Cretaceous suites: a granite suite and a tonalite suite. A younger, early Late Cretaceous diorite suite is intermediate in composition.

The granite suite consists of several pulses of syn- to post-kinematic biotite \pm hornblende granite, granodiorite, pegmatite, and two-mica granite. Accessory garnet is common. Older granitoids of this suite are deformed and syn- to late-kinematic to regional deformation and metamorphism at about 114-107 Ma. Younger granitoids (~107 Ma) are not foliated and emplacement of some phases exploits a shallowly dipping regional fabric. The tonalite suite forms small to large bodies of post-kinematic hornblende-biotite granodiorite to tonalite, with rare granite, and includes an older phase of the Goodpaster Batholith and the Shawnee Peak intrusion. Newly reported ages for the tonalite suite suggest it was emplaced between 105.7 ± 0.3 Ma (Goodpaster Batholith; U-Pb, monazite) and 103.2 ± 2.2 Ma (U-Pb, zircon). A U-Pb monazite age indicates the Shawnee Peak pluton crystallized at 106.9 ± 1.3 Ma. The youngest, Late Cretaceous diorite suite consists of small, steeply dipping stocks of hornblende-biotite \pm pyroxene-bearing diorite, quartz diorite, monzodiorite and tonalite. A younger phase of the Goodpaster Batholith (93.7 Ma) is included in this suite.

Both the granite and tonalite suites are weakly peraluminous and contain variable amounts of monazite and zircon. The diorite suite has a metaluminous mineralogy and contains

< 5 % primary magnetite. Monazite is notably absent. All plutonic suites are subalkalic, calc-alkaline and have low magnetic susceptibilities and oxidation states ($\text{Fe}_2\text{O}_3 / \text{FeO} + \text{Fe}_2\text{O}_3 = 0.02$ to 0.45). High LILE/HFSE ratios and depleted Nb and Ti combined with ubiquitous inherited zircon suggest the rocks are likely subduction related and were highly contaminated by continental crust. Preliminary depth estimates from the Al-in-hornblende barometer indicates the Goodpaster Batholith was emplaced at depths of 5-9 km.

Locally, dykes of aplite and pegmatite grade into mineralized quartz veins and cross cut the granite, and parts of the tonalite, suites. The timing of sulphide deposition in the Liese Zone (~ 104.2 Ma; $^{187}\text{Re}/^{187}\text{Os}$, molybdenite) overlaps the timing of the tonalite, and possibly the granite, suite. The diorite suite is inferred to postdate all gold-bearing quartz veins.

Lead isotopic compositions for the granite and diorite suites form isotopically distinct fields. Granite has higher $^{206}\text{Pb}/^{204}\text{Pb}$ values (19.4 to 19.6) and diorite has much lower $^{206}\text{Pb}/^{204}\text{Pb}$ values (19.1). The tonalite suite $^{206}\text{Pb}/^{204}\text{Pb}$ values overlap both the diorite and granite suite fields (19.2 to 19.5). The granite suite overlaps the least radiogenic values of the Devonian-Mississippian gneiss of the Yukon Tanana Terrane. Gold-bearing quartz veins at the Liese zone and 4021 prospect have $^{206}\text{Pb}/^{204}\text{Pb}$ values (19.4 to 19.6) that overlap the granite suite and suggest they shared a similar source.

Gold-bearing quartz veins in the Goodpaster district are related to a suite of reduced granitic-tonalitic intrusions that were emplaced late- to post-kinematic to regional metamorphism and deformation in the late Early Cretaceous. These veins and intrusive rocks are 12-15 m.y. older than the reduced granites of the Tombstone Plutonic Suite (92 ± 1 Ma) and form the western equivalent of the Anvil Suite in Yukon.

INTRODUCTION

Gold related to reduced intrusions is a relatively newly recognized type of mineral deposit (McCoy et al., 1997; Thompson et al., 1999; Lang et al., 2000; Rowins, 2000; Thompson and Newberry 2000; Hart et al., 2002). The genetic models for this deposit type are based largely on deposits and occurrences in Yukon Territory and Alaska. The most widely known of these deposits are associated with the 92 ± 1 Ma Tombstone Plutonic Suite (TPS) (Thompson et al., 1999) and include the Fort Knox (169 Mt @ 0.93 g/t Au; Bakke et al. 1995) and Brewery Creek mines (43.8 Mt @ 1.03 g/t Au; Park 1999) and the Dublin Gulch prospect (99 Mt @ 1.1 g/t Au; Hart et al., 2000) (Figure 2-1). The Liese Zone, located on the Pogo property in the Goodpaster district of east-central Alaska, is one of the highest-grade gold deposits included within this new deposit type with a current resource of 13.5 Mt with an average grade of 0.52 opt Au (Teck Cominco Limited website, December 31, 2002). Other deposits of this type worldwide include Timbarra and Kidston in Australia (Mustard, 2001), Korri Kolli in the Bolivian polymetallic belt and Mokrsko in the Czech Republic (Thompson et al., 1999). Despite numerous reviews of the ore deposit type, there have been surprisingly few detailed studies on specific gold deposits related to reduced intrusions, or of the proposed causative intrusive complex. Furthermore, the origins of some deposits placed within the gold deposits related to reduced granites class are controversial, as some have characteristics that overlap orogenic gold deposits (Goldfarb et al., 2000).

Granitic rocks are inferred or demonstrated to be genetically associated with reduced intrusion-related gold deposits. Despite their importance in the genetic model, only limited detailed work has been carried out on the plutonic rocks related to the deposits. In Alaska and Yukon, only the Emerald Lake Pluton within the Tombstone Plutonic Suite in Yukon has thus far been studied in any detail (Coulsen et al., 2000; Duncan, 1999). The remainders of the reduced

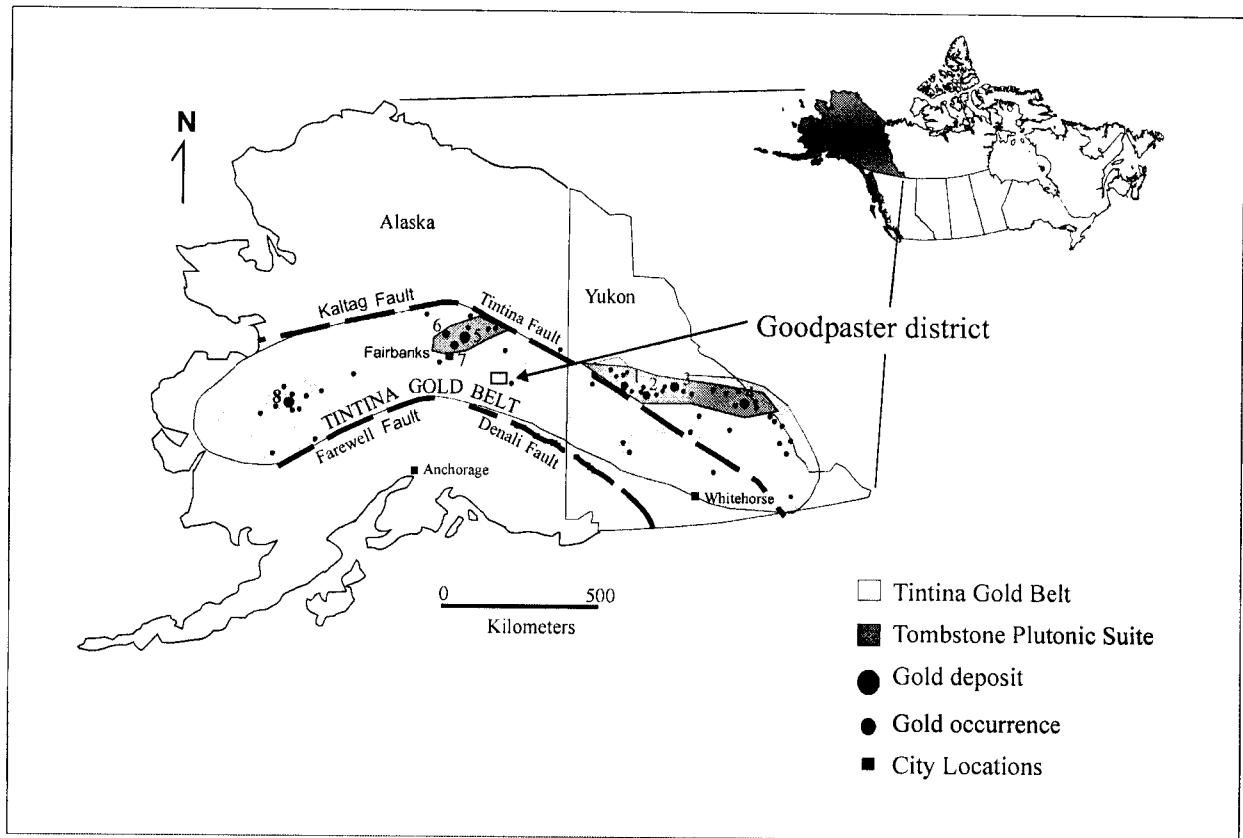


Figure 2-1: Location and extent of the Tintina Gold Belt in the northwestern Canadian Cordillera and Alaska. The small square denotes the location of the Goodpaster district in east-central Alaska. The major gold deposits (large circles) and gold occurrences (small circles) are shown: 1- Brewery Creek; 2- Clear Creek; 3-Dublin Gulch; 4-Emerald Lake; 5-Fort Knox; 6-True North; 7-Ryan Lode; 8-Donlin Creek. The extent of the Tombstone Plutonic Suite is shaded. Figure modified after Mortensen et al., (2000).

plutonic complexes associated with gold occurrences are only known in a reconnaissance manner (Lang et al., 2001). Most are reduced, metaluminous, ilmenite series, multiphase felsic intrusive rocks with low fO_2 (McCoy et al., 1997; Thompson et al., 1999).

This chapter focuses on the igneous rocks associated with Cretaceous plutonic phases in the Goodpaster district. The Liese zone and associated prospects are spatially and temporally associated with late Early Cretaceous intrusive rocks (Smith et al., 2000; Dilworth et al., 2002) that are syn- to late kinematic with respect to regional deformation and metamorphism (Smith et al., 1999; Moore, 2000; Dilworth et al., 2002). These are about 12-15 m.y. older than the better-

studied Tombstone Plutonic Suite rocks. The recognition of these late Early Cretaceous intrusive rocks associated with the gold-bearing quartz veins in the Goodpaster district extends both the geographic and temporal range of plutonic complexes in Yukon and eastern Alaska that are prospective for gold mineralization.

REGIONAL GEOLOGY

The Goodpaster District lies within the Tintina Gold Belt, a belt of gold occurrences associated with granitic complexes that extends from southwest Northwest Territories, through Yukon and into southwestern Alaska (Figure 2-1). Most gold deposits and prospects in the Tintina Gold Belt are associated with the Tombstone Plutonic Suite (TPS). This suite forms a belt of ~92 Ma, lithologically diverse syenite to gabbro intrusions in Yukon that is offset 450 km dextrally along the Tintina Fault with the western continuation present near Fairbanks (Figure 2-1; Mortensen et al., 2000). The Goodpaster district lies south of the TPS belt of intrusions, 145 kilometers east of Fairbanks in east-central Alaska but is associated with older granitic complexes. Still younger Late Cretaceous deposits (~70 Ma), form in the western extension of the Tintina Gold Belt in the Kuskokwim Belt (e.g., Donlin Creek; Ebert et al., 2000; Burdtsen and Miller, 2000).

East-central Alaska is composed of a number of accreted terranes with continental, oceanic and island arc affinities (Foster et al., 1994). The largest is the Yukon-Tanana Terrane, a pericratonic terrane with continental affinities that consists primarily of metamorphosed pre-Devonian quartzitic, pelitic and calcic sedimentary rocks (Foster et al., 1994; Aleinikoff et al., 2000). Devonian and Mississippian plutonic rocks intrude the sedimentary sequence and collectively the rocks are interpreted to represent components of a Devonian to Mississippian igneous arc built on a submerged continental margin (Aleinikoff and Nokleberg, 1985; Dusel-

Bacon and Aleinikoff, 1985; and Dusel-Bacon and Hanson, 1992; Aleinikoff et al, 2000). The terrane was metamorphosed to amphibolite facies at intermediate pressures (Foster et al., 1994); however, the timing of metamorphism and deformation remains poorly understood. Mid-Paleozoic, Jurassic and Early Cretaceous metamorphic events have been suggested by Foster et al. (1994), Dusel-Bacon and Aleinikoff (1985) and Aleinikoff et al. (2000) and a number of workers suggest that metamorphism began during a Jurassic collisional event and culminated in widespread metamorphism and tectonism during the Early Cretaceous (Pavlis et al., 1993; Aleinikoff and Nokleberg, 1985; Wilson et al., 1985; Dusel-Bacon and Aleinikoff, 1996; Day et al., 2002). Uranium-lead ages presented in this study indicate that metamorphism and deformation in the Goodpaster district locally continued as late as 107 Ma, and that Early Cretaceous metamorphism and deformation may be the dominant event in the Goodpaster district (Day et al., 2002).

Felsic and intermediate plutonic rocks intruded the Yukon-Tanana Terrane during the Late Triassic to Early Jurassic (215 to 188 Ma), the late Early Cretaceous to Late Cretaceous (115 to 85 Ma) and the Late Cretaceous to early Tertiary (50-74 Ma) (Foster et al. 1994; Wilson et al., 1985; Mortensen et al., 2000). Each Phanerozoic intrusive event may reflect a period of subduction and arc magmatism superimposed on the Paleozoic Yukon-Tanana Terrane protolith (Foster et al., 1994; Newberry, 2000). Of particular importance for the Goodpaster district is the widespread late Early Cretaceous to early Late Cretaceous plutonic event that is known throughout most of Yukon Territory and east-central Alaska. These intrusive rocks apparently intruded at a time coinciding with a period of plate reorganization accompanying accretion of the Wrangellia Composite Terrane with the Yukon Tanana Terrane (Plafker and Berg, 1994, Aleinikoff et al., 2000). The plutonic rocks are divided into several plutonic suites based on spatial distribution, age, lithology and geochemistry (Figure 2-2) (Mortensen et al., 2000). In

general, the Cretaceous rocks have more variable chemical compositions and generally contain more normative quartz than the Jurassic event (Foster et al., 1994).

During the Eocene, oblique subduction (Plafker and Berg, 1994) may have initiated dextral strike slip movement along the northwest striking Tintina and Denali Faults, to the north and south of the Goodpaster region, respectively. Large, northeast striking, steeply dipping oblique sinistral faults developed contemporaneously with the main dextral strike-slip faults (Page et al., 1995) and cut the region into narrow panels that now expose different crustal levels of the Yukon-Tanana Terrane. These northeast trending faults are widespread in Alaska (Newberry, 2000) and are present at various scales.

The Yukon-Tanana Terrane in the Goodpaster district is referred to as the "Y1" subterrane (Churkin et al., 1982), or the "Lake George subterrane" (Nokleberg et al., 1993). The subterrane lies southeast of the northeast-trending Shaw Creek Fault, where batholith-sized bodies of augen gneiss are diagnostic (Dusel-Bacon and Hansen, 1991) and Cretaceous plutons intrude the regionally metamorphosed Yukon Tanana Terrane (Figure 2-3). The dominant rock types in the Goodpaster district are paragneiss consisting of quartz-feldspar-plagioclase-biotite gneiss, quartz-muscovite schist, and quartzite; orthogneiss occurs as quartz-feldspar-biotite gneiss and augen gneiss. Lesser amounts of amphibolite, calc-silicate gneiss, and ultramafic gneiss are also present.

GEOLOGICAL SETTING OF THE GOODPASTER DISTRICT

The Goodpaster district covers an area of approximately 20 km by 16 km. Outcrops in the district are widely scattered and scarce, as Pleistocene glaciation did not affect the region. Thus, the distribution and geometry of the intrusive rocks and their contact relationships with the country rocks are largely inferred from available outcrop, diamond drill holes, mapping talus,

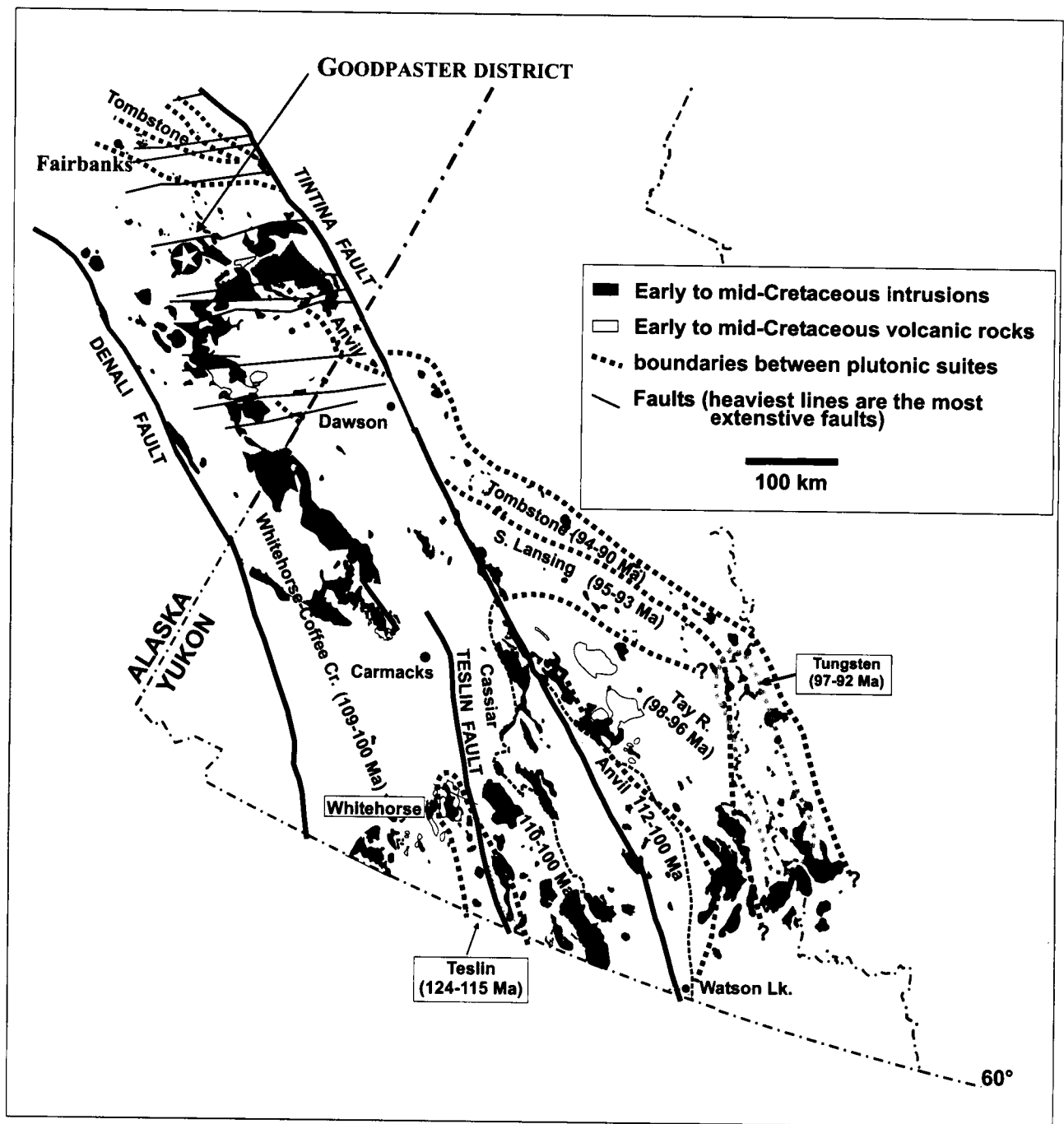
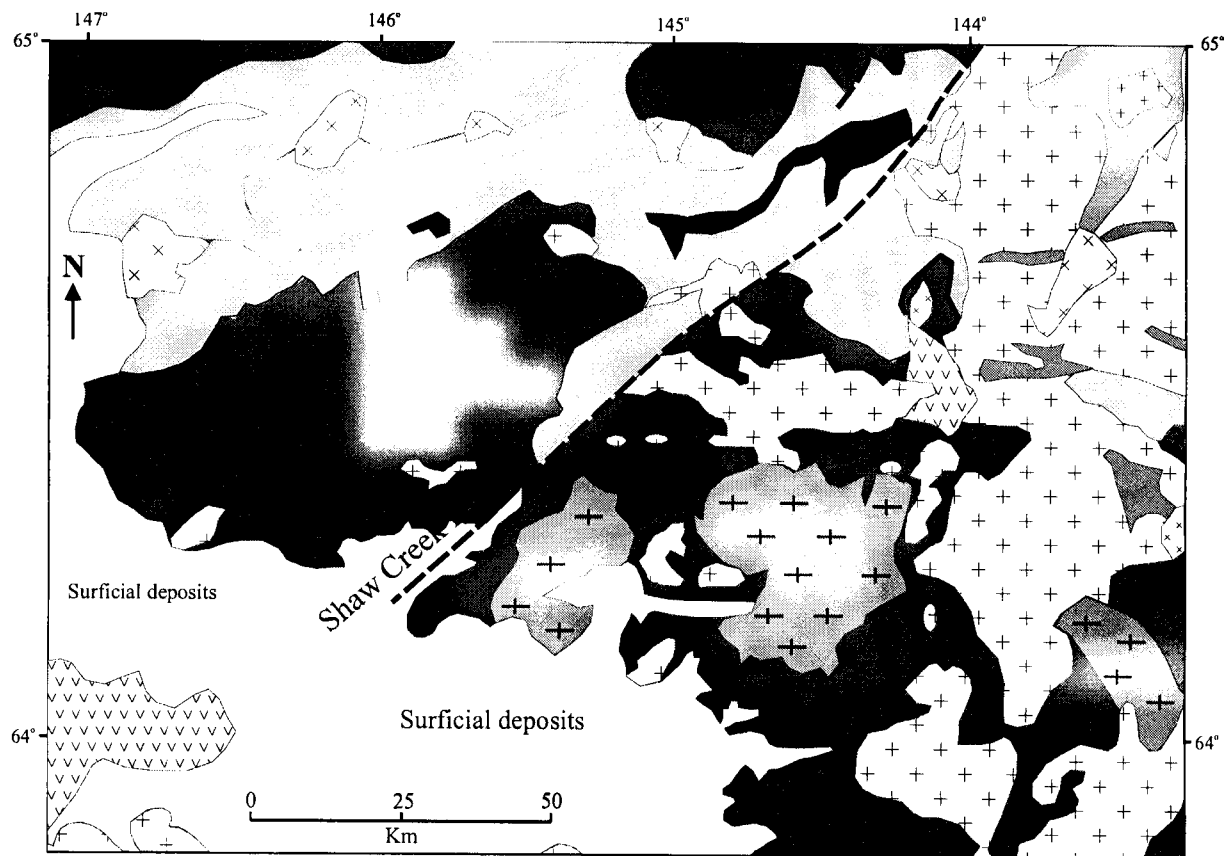







Figure 2-2: Early and Late Cretaceous plutonic and volcanic rocks in southern Yukon Territory and east-central Alaska. Plutonic suites shown are those of Mortensen et al. (2000). The star denotes the Goodpaster district.



Paleozoic to late Early Cretaceous Metamorphic Rocks

-  Pumpellyite-greenschist facies: schist, semischist, quartzite, marble, greenstone and phyllite.
-  Amphibolite facies: high to intermediate pressure pelitic schist, pelitic gneiss, quartzite, orthogneiss, calc-silicate and amphibolite.
-  Amphibolite facies: schist, gneiss, amphibolite, quartzite, and minor marble.
-  Amphibolite facies: augen orthogneiss
-  Ultramafic rocks.

Post Metamorphic Igneous Rocks

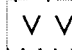
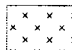
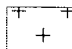
-  Unmetamorphosed volcanic and/or sedimentary rocks
-  Tertiary granite
-  Cretaceous granite

Figure 2-3. Simplified Geology of east-central Alaska. The star denotes the Goodpaster district. Modified after Dusel-Bacon and Foster (1993).

and from airborne geophysical surveys. Faults are interpreted from airphotos, topography, aeromagnetic maps, and from mapped offsets of rock lithologies.

Gold-bearing quartz vein systems within the district, of which the Liese zone is the largest, are associated with an arcuate, easterly trending belt of reduced granitoids emplaced into the paragneiss, and lesser orthogneiss, of the Yukon Tanana Terrane. The plutonic rocks form an elongate composite body approximately 10 km long by 2 km wide that lies approximately two kilometers south of the Goodpaster Batholith, the largest intrusive body in the region (Figure 2-4). Small granitic bodies occur sporadically outside the elongate composite pluton. South of this arcuate belt, minor dykes and small plugs of mafic dykes and Eocene hypabyssal rhyolite crop out.

Paragneiss is the dominant metamorphic rock and consists dominantly of fine- to medium-grained quartz-biotite-potassium feldspar-plagioclase, with 1-5 mm subidioblastic almandine garnet porphyroblasts (Moore, 2000) comprising up to 5% of the rock. Gneissic compositional layering of the paragneiss dips moderately to steeply towards the northeast near the Liese zone (Smith et al. 2000; Rhys et al., 2003) and towards the southeast in surface outcrops south of the arcuate belt of granitoids. In detail, however, the gneissic foliation is mesoscopically and microscopically folded and possesses variable dips. It is deformed by a northwest-striking D2 event, that produced a strong, shallow northeast-dipping domainal gneissosity (S2) that is axial planar to the folds. Locally, domains of intense S2 separate, or truncate folded S1, resulting in abrupt changes in foliation orientation (Rhys et al., 2003). The S1 fabric in these areas is transposed into the S2 or is completely obliterated. A third deformation event, D3, was observed north of Central Creek (Figure 2-4) and cuts the S2 fabric at a shallow angle. Generally, S3 foliation dips shallowly towards the north and is associated with E-W trending, low angle faults.

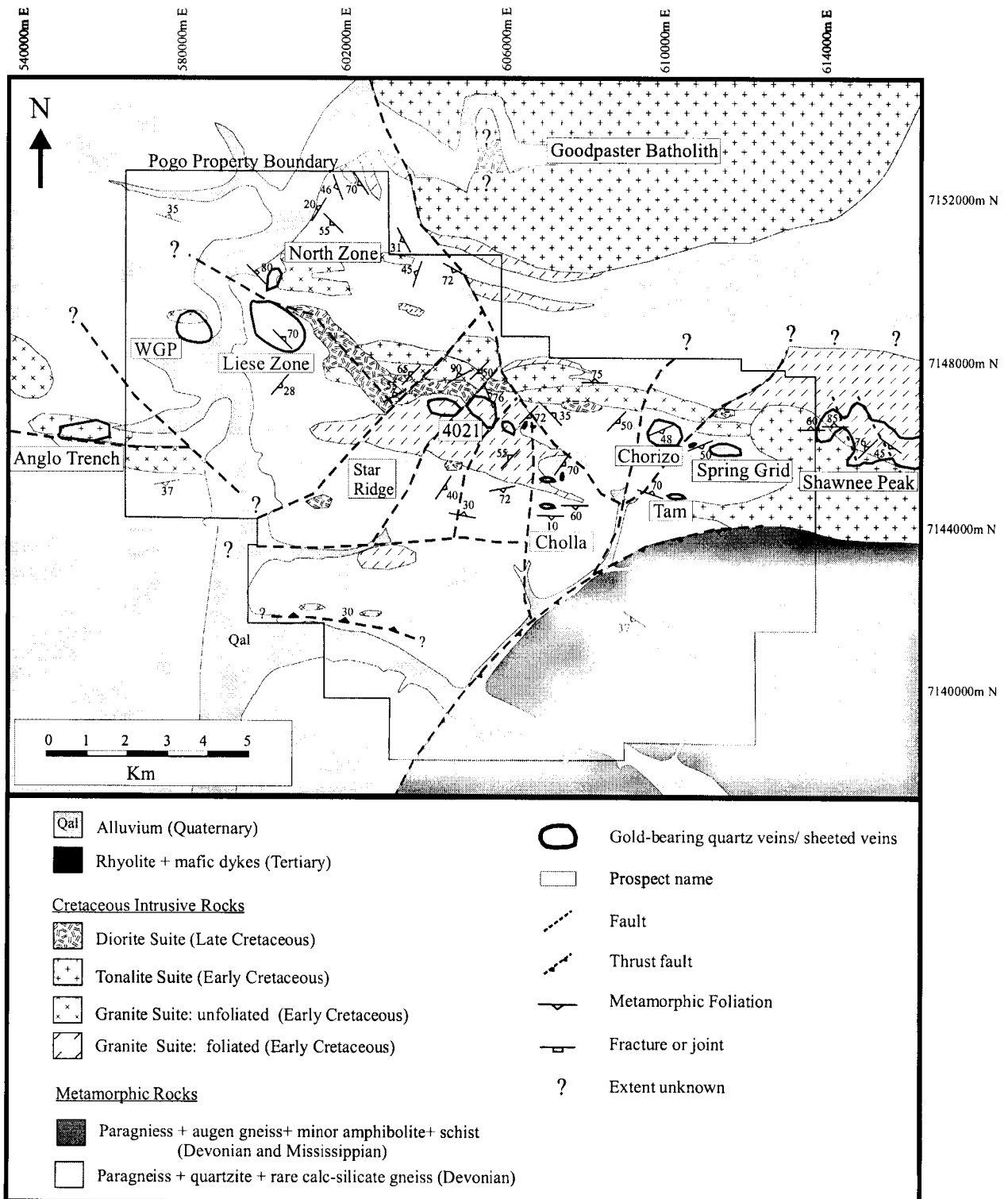


Figure 2-4. Geology map of the Goodpaster district showing the distribution of the Cretaceous intrusive rocks and associated gold-bearing quartz veins.

Numerous, mainly northeast-trending faults occur at all scales in the region (Smith et al., 1999). Rhys et al. (2003) mapped several fault generations in the Liese zone: early north- to northwest moderately dipping normal faults, south-southeast dipping normal faults, northeast-trending sinistral faults and rare northwest trending faults. Several low-angle faults have also been identified in the region (Weber et al., 1978).

PETROGRAPHIC AND GEOCHRONOLOGICAL DATA

Field data, petrography, geochemistry, and geochronology subdivide the Cretaceous plutonic rocks into three intrusive suites: a granitic suite (~107 Ma), a tonalitic suite (~105 Ma) and a dioritic suite (~94 Ma). All intrusive rock classifications are based on visual modal estimates using the International Union of Geological Sciences (IUGS) classification of Streckeisen (1976). Table 2-1 summarizes the major textural, mineralogical, geochemical and geochronological features of the three intrusive suites in the Goodpaster district. Sparse, narrow quartz-feldspar phyric rhyolite dikes, dated at 54.5 +/- 0.5 Ma to 51.8 +/- 0.3 Ma (U-Pb: zircon, this study) and feldspar-phyric mafic dykes dated at 92.7 Ma (^{40}Ar - ^{39}Ar ; Rhys et al., 2003) represent the youngest intrusive events in the region. These rock units are not discussed further.

Most Cretaceous intrusive rocks in the Goodpaster district are fine- to medium-grained with grain sizes less than 2 mm, although locally feldspar phenocrysts up to 1.5 cm are present. In this study, relative grain sizes are reported: grain sizes less than 0.5 mm are termed aplitic, between 0.5 mm and 1 mm are fine-grained, between 1 mm to 2 mm are medium-grained, between 2 and 5 mm are coarse-grained and greater than 5 mm are pegmatitic.

Petrography and geochronology indicate that metamorphism and early pluton emplacement occurred essentially simultaneously and plutonism was syn- to post-kinematic with respect to development of the main deformation fabrics in the area. It is unclear how many

Table 2-1: Summary of petrology, geochemistry, geochronology, oxidation state and magnetic susceptibility of the Cretaceous intrusive suites in the Goodpaster district

Intrusive Suite	Rock Types	Petrology	Kinematics	Geochemistry	Sample	Rock type	Age (Ma) ^a	Mineral	System	Fe ₂ O ₃ / FeO + Fe ₂ O ₃	Magnetic Susceptibility
Granite	granitic orthogneiss, granite, leucogranite, granodiorite, pegmatite and aplite	strongly foliated to unfoliated, medium grained, 5 % fine-grained, euhedral biotite. Accessory fine-grained garnet is common. Biotite is predominant, hornblende is rare to absent. Trace mineralogy includes ilmenite and monazite. Forms small bodies and small, tabular sheets	syn- to post-kinematic	subalkaline, calc-alkaline SiO ₂ wt. % 70 to 87 weakly metaluminous to peraluminous	OGNU 98-93	hbl-bt orthogneiss	109.2 ± 0.4	monazite	U-Pb	0.07 - 0.32	0.00 - 0.21
					OGNU 98-93	orthogneiss	107.0 ± 0.6	zircon	U-Pb		
					98-176	granite gneiss	107.3 ± 0.8	monazite	U-Pb		
					97-71	bi-rich granodiorite	107.3 ± 0.8	monazite	U-Pb		
					97-75	bi-poor granodiorite	107.1 ± 0.6	monazite	U-Pb		
					MAPT-21	pegmatite	108.0 ± 1.0	monazite	U-Pb		
Tonalite	tonalite and granodiorite minor granite and quartz diorite	equigranular to weakly seriate, medium-grained, biotite and hornblende are the predominant mafic minerals. Trace mineralogy includes ilmenite and monazite. Forms stocks and batholiths	post-kinematic	subalkaline, calc-alkaline SiO ₂ wt.% 62 to 72.2 peraluminous	PEGM-98-93	pegmatite	107.5 ± 2.0	monazite	U-Pb		
					Pogo-00-16	bi-mu leucogranite	107.9 ± 1.2	monazite	U-Pb		
					SP-00-14	bi-granodiorite	106.9 ± 1.3	monazite	U-Pb	0.10 - 0.24	0.02 - 0.15
					MAPT-14	hbl-bt tonalite	105.7 ± 0.3	monazite	U-Pb		
					MAPT-7	bi-granodiorite	103.4 ± 2.2	zircon	SHRIMP		
Diorite	diorite, quartz diorite, monzodiorite, tonalite	equigranular, medium- to coarse-grained, hornblende, biotite ± pyroxene are the predominant mafic minerals. Trace mineralogy includes magnetite and ilmenite. Forms steeply dipping dykes and small bodies. Chlorite alteration is ubiquitous	post-kinematic	subalkaline, calc-alkaline SiO ₂ wt % 49.6 to 56.7 weakly metaluminous to weakly peraluminous	105-745	pxn-bi-hbl diorite	94.5 ± 0.2	zircon	U-Pb	0.13 - 0.33	0.21 - 0.135
					Kgg-14	hbl-bt tonalite	93.7 ± 0.2	zircon	U-Pb		

^a All errors are reported as 2σ

Abbreviations: bt = biotite; hbl = hornblende; mu = muscovite; pxn = pyroxene

System: All ages determined by conventional U-Pb methods at the Pacific Center for Isotopic and Geochemical Research (PCIGR), University of British Columbia, Vancouver with the exception of sample MAPT-7 which was analysed by SHRIMP-RG at Stanford University, California, by Richard Tosdal.

generations of magmatism are represented in the area. U-Pb ages from thirteen representative plutonic suite samples were analyzed by conventional methods at the Pacific Centre for Isotopic and Geochemical Research (PCIGR) at the University of British Columbia, Vancouver, using the sample preparation procedures described by Mortensen (1995). One sample was dated using the SHRIMP-RG at Stanford University, California. A summary of the geochronological data is shown schematically in Figure 2-5. Analytical results, with uncertainties presented at the 2σ level, are provided in Appendix A.

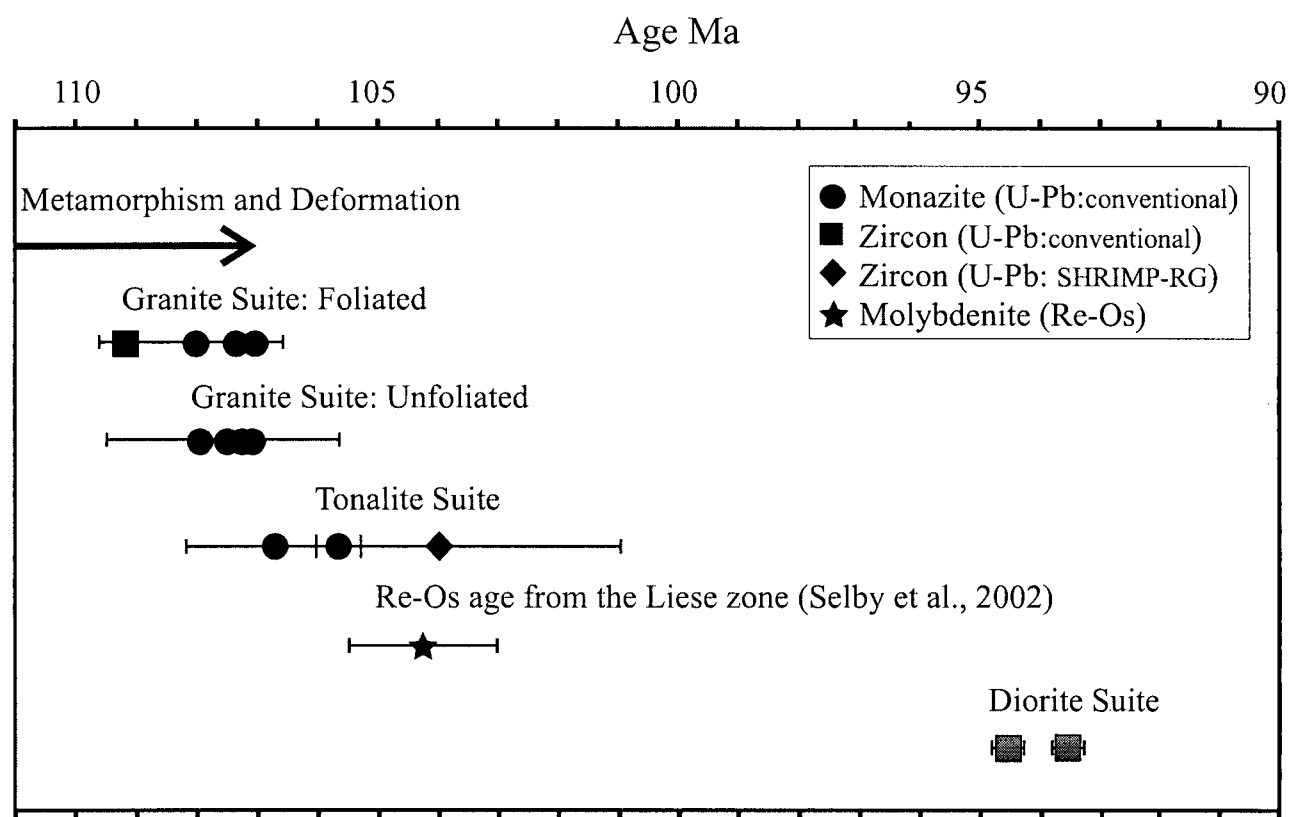


Figure 2-5. Geochronology summary of the intrusive rocks and metamorphism and deformation in the Goodpaster District, east-central Alaska during the early Late to late Early Cretaceous. The $^{187}\text{Re}/^{187}\text{Os}$ isochron age from the Liese zone quartz veins (Selby et al., 2002) is included for reference.

GRANITE SUITE

The granite suite is comprised of syn-to post-kinematic granite to granodiorite with lesser amounts of leucogranite, aplite and pegmatite. The suite is subdivided into orthogneiss, represented by plutonic rocks with a strong to weak foliation, and granitoids that contain no foliation. The suite was emplaced during the oldest of the late Early Cretaceous events between 107 and 109 Ma. Several of the youngest phases (~107 Ma) crop out as small subhorizontal dykes and tabular sheets that have a similar morphology to the flat lying quartz veins at the 4021 prospect (Chapter 3) and the Liese zone (Smith et al., 1999, 2000).

Euhedral to subhedral plagioclase, biotite, potassium feldspar, and interstitial quartz form the main constituent minerals. The trace mineralogy in order of abundance includes apatite, zircon, ilmenite, monazite, pyrite, allanite, xenotime, thorite, and rare scheelite. Accessory fine-grained garnet is almandine-spessartine \pm grossular in composition based on semi-quantitative scanning electron microscope (SEM) analysis. Garnet is considered a primary igneous phase because it occurs as inclusions within quartz, microcline, feldspar, and granophyre. Garnet grains are typically 1-2 mm in diameter and occur as subhedral crystals or anhedral granules that outline the shape of a single crystal. In the foliated phases, garnet is associated with biotite and is locally altered to chlorite \pm sericite \pm potassium feldspar. In general, biotite is the predominant ferromagnesian mineral, though locally foliated intrusions contain abundant biotite and up to 8% hornblende.

White mica is a rare primary phase and forms euhedral to separate subhedral coarse-grains that are not associated with any particular mineral. Based on semi-quantitative SEM analysis, this white mica is Li-rich (lepidolite). The white mica coexists with biotite in the two-mica leucogranite that forms small plugs north of the Liese zone and near the 4021 prospect.

The two-mica leucogranite is medium- to coarse-grained and locally weakly foliated (Figure 2-6d).

Granitic to granodioritic orthogneiss is the predominant host-rock to the gold-bearing quartz veins of the 4021 prospect. The orthogneiss is fine- to medium-grained and ranges from strongly foliated, with mineral segregation occurring at 1-3 mm (Figure 2-6a, top), to diffusely foliated defined by discontinuous alignment of coarse biotite flakes. In places, subhedral megacrystic potassium feldspar grains up to 1.5 cm in length are weakly aligned with biotite in a coarse-grained phase of granitic orthogneiss (Figure 2-6a, bottom). Locally, the orthogneiss grades into lenses of unfoliated granite with diffuse boundaries that are typically less than 1.5 meters wide. U-Pb ages from biotite-rich orthogneiss (sample OGNU 98-93) returned zircon and monazite ages of 109.2 ± 0.4 Ma and 107.0 ± 0.6 Ma respectively, and monazite from biotite-poor granitic orthogneiss (sample 98-176) returned an age of 107.3 ± 0.8 Ma (Appendix A).

Granite to granodiorite is interpreted to be late- to post-kinematic based on the following observations. In drill core, unfoliated granite occurs as small dykes and lenses 5-30 cm to many meters wide. Granite is typically fine- to coarse-grained and is dominantly equigranular (Figure 2-6b). Locally, it is slightly foliated as defined by biotite and feldspar alignment (Figure 2-6c).

Most granitic rocks show weak to moderate alteration of biotite to chlorite +/- clinozoisite and minor sericite. Biotite is red-brown and titaniferous, as SEM analysis detects titanium and secondary chlorite commonly contains randomly oriented needles of rutile. Fine-grained sericite \pm calcite selectively replaces plagioclase and replaces potassium feldspar crystals. Sericite alteration is most abundant in the late- to post-kinematic phases of the suite and is inferred to be dueteric because the enclosing orthogneisses often show little evidence of alteration. Where sericite alteration is pervasive, protolith lithologies are unrecognizable and the rocks become grey, green or tan. The small igneous 1-2 mm pink almandine-spessartine garnets

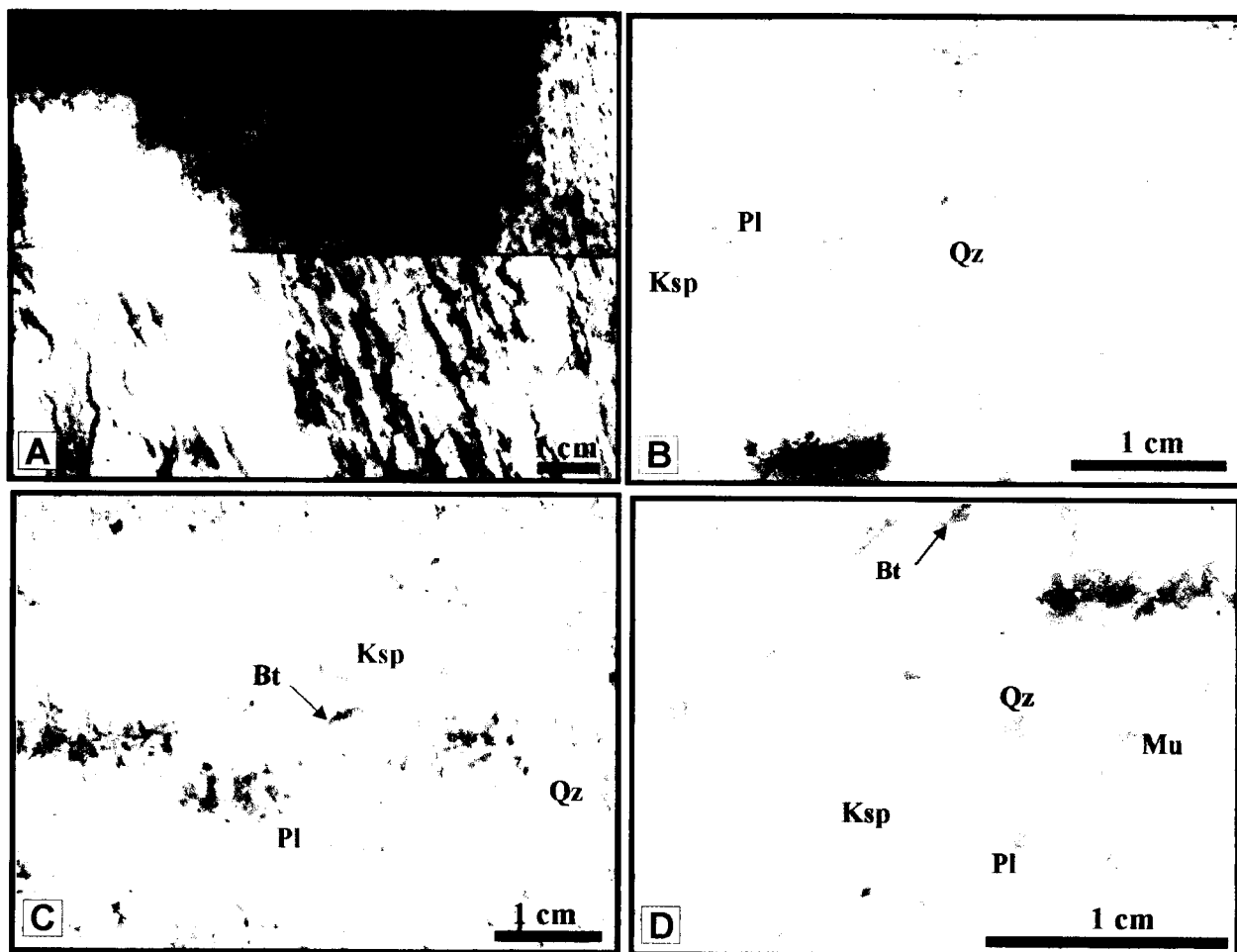


Figure 2-6: Photographs of granite suite samples from the Goodpaster district. All samples are stained with sodiumcobaltnitrate. Potassium feldspar (Ksp) is yellow, plagioclase (Pl) is white, quartz (Qz) is grey and mafic minerals [biotite (Bt) and hornblende (Hb)] are black. Muscovite is white (Mu). **A)** Syn-kinematic biotite-rich orthogneiss (top) and granite orthogneiss (bottom) from the Liese zone and 4021 prospect respectively. Samples 98-75 and 249-799. **B)** Late-kinematic, weakly foliated, medium-grained granite. Sample Pogo-00-R6. **C)** Post-kinematic, fine-grained granodiorite. Sample 00-R12. **D)** Late- to post-kinematic, medium-grained biotite-muscovite leucogranite. Sample 00-R14.

are very distinct where the rocks are pervasively sericitically altered.

Ubiquitous granitic aplite and pegmatite dykes and sills have a close spatial relationship to granite and quartz veins. Locally, coarse-grained patches of pegmatite are intergrown with granite aplite and can comprise up to 25-35% of the rock. Biotite-rich and biotite-poor pegmatites are present in the region. Biotite-rich pegmatite consists of euhedral feldspar and interstitial quartz with up to 25% coarse-grained biotite. Biotite-poor pegmatite of granite composition is the most common and consists of graphic, milky white potassium feldspar crystals up to 10 cm in length and interstitial quartz, albite, biotite, muscovite and accessory subhedral almandine-spessartine garnet. Quartz-rich pegmatite contains trace amounts of apatite, pyrite, pyrrhotite, arsenopyrite, chalcopyrite, galena, zircon, rutile, molybdenite, ilmenite, and scheelite. Locally, these quartz-rich pegmatites grade into gold-bearing quartz veins (Chapter 3; Moore, 2000), although the pegmatites themselves lack any gold values.

Granular quartz veins have a sugary texture in hand sample. Quartz grains are anhedral, and rarely euhedral, and occur with interstitial potassium feldspar and sericite or are poikilitically enclosed within potassium feldspar grains (Chapter 3; Moore, 2000). Locally these granular quartz veins contain no interstitial feldspars. The relict intrusive texture, combined with similar mineralogy to the pegmatite, suggests the granular quartz veins are the transitional link between pegmatite and gold-bearing quartz veins.

U-Pb monazite ages of 107.3 ± 0.8 Ma to 107.1 ± 0.6 Ma have been determined from undeformed biotite-rich granodiorite (sample GDIB 97-71) and biotite-poor granite (sample 97-75), respectively from the Liese zone (Appendix A). These ages essentially overlap with the younger phases of orthogneiss (~ 107 Ma, Figure 2-5), indicating the granite intrusive suite was contemporaneous with and slightly postdates regional metamorphism and deformation. A folded pegmatite dyke within the Liese zone returned an U-Pb monazite age of 108.0 ± 1.0 Ma (sample

MAPT-21) and a large, undeformed pegmatite body from the Liese zone returned an U-Pb monazite age of 107.5 ± 2.0 Ma (sample PEGM 98-93) (Appendix A). These ages demonstrate a temporal association between the pegmatite and the granite suite.

TONALITE SUITE

The tonalite suite is post-kinematic and is comprised of dominantly hornblende-biotite bearing tonalite to granodiorite. This suite is represented by batholiths, stocks and minor sheets and includes the Goodpaster Batholith and Shawnee Peak stock (Figure 2-4) are included in this suite. The suite typically consists of medium- to coarse-grained, euhedral to subhedral plagioclase, biotite, hornblende and interstitial quartz and minor potassium feldspar. Outcrop-scale variations in quartz, hornblende and potassium feldspar content are common (Figure 7 a, b, c). Accessory and trace minerals in order of abundance include apatite, ilmenite, zircon, monazite, epidote, allanite, pyrite, chalcopyrite, galena, and scheelite. No garnet was observed in any of the tonalite suite samples.

The Shawnee Peak stock forms a non-foliated, massive body which underlies the western flank of Shawnee Peak and the eastern portion of the Goodpaster district (Figure 2-4). It forms an ~ 50 km² composite pluton that varies in composition from biotite-hornblende granite to quartz diorite. The stock texturally varies from crowded megacrystic to equigranular.

The various phases of the Goodpaster Batholith are characteristically coarse-grained, equigranular and homogeneous with fresh, euhedral biotite containing abundant zircon, apatite and ilmenite inclusions. The Goodpaster Batholith is predominantly a biotite \pm hornblende-bearing tonalite but varies from granite to tonalite. Finer grained, biotite-bearing tonalite phases of the Goodpaster Batholith that crop out about 2 kilometers south occur as small bodies and sheets.

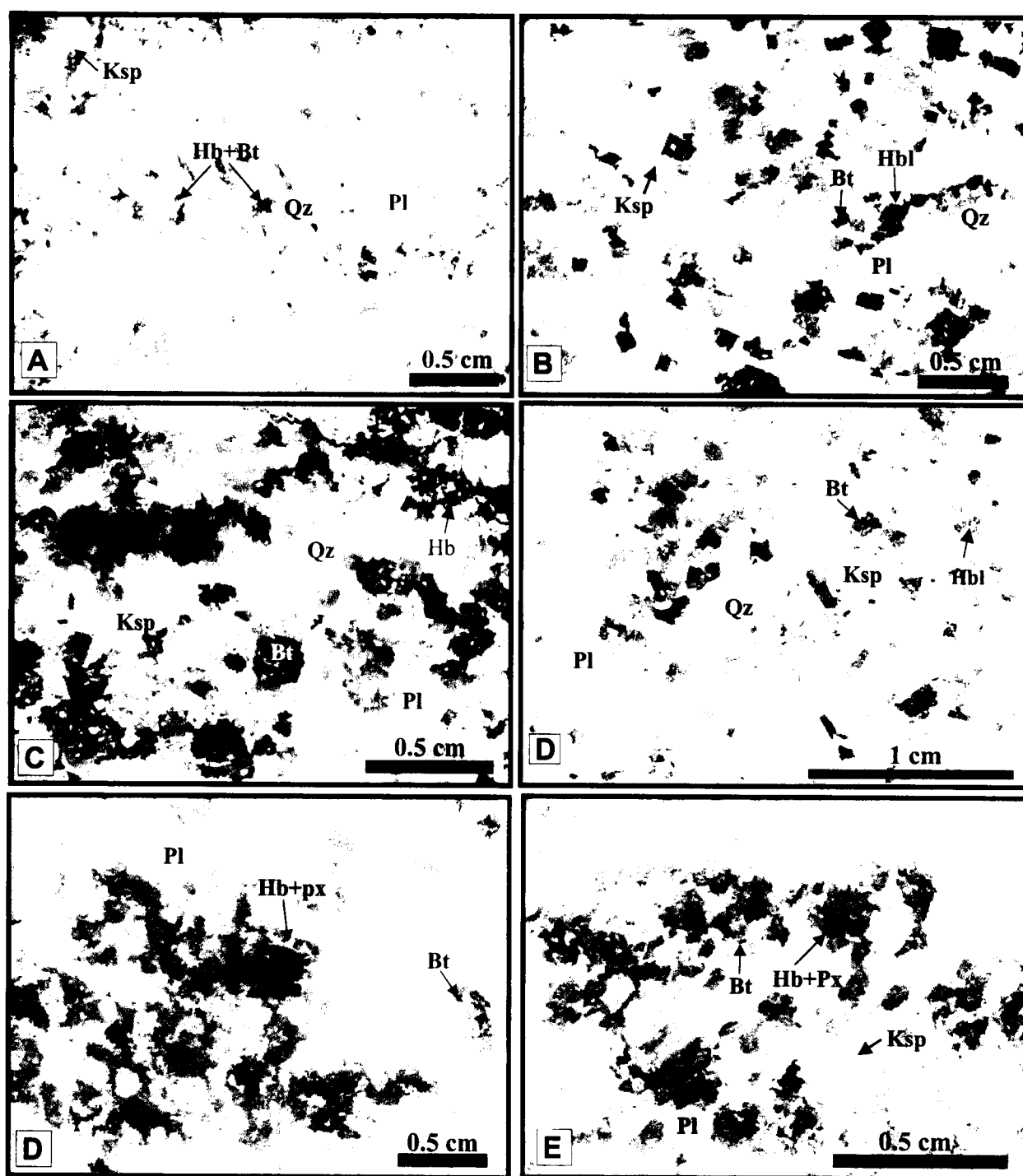


Figure 2-7: Photographs of tonalite suite and diorite suite samples from the Goodpaster district. All samples are stained with sodiumcobaltinitrate. Potassium feldspar (Ksp) is yellow, plagioclase (Pl) is white, quartz (Qz) is grey and mafic minerals [biotite (bt), hornblende (Hb) and pyroxene (pxn)] are black. **A)** Fine-grained biotite tonalite from the Football Field, west of the 4021 Prospect. Sample Mapt-7 (~103 Ma) **B)** Coarse-grained hornblende-biotite tonalite of the Goodpaster Batholith. Sample MAPT-14 (~105.7 Ma) **C)** Coarse-grained hornblende-biotite tonalite of the Goodpaster Batholith. Sample KGG-14 (~93.7 Ma). **D)** Coarse-grained hornblende-biotite granite from Shawnee Peak. Sample Pogo-00-02 (~107 Ma). **E)** Coarse-grained pyroxene-hornblende-biotite diorite from Liese Creek. Sample Pogo-00-R134. (~94.5 Ma) **F)** Coarse-grained hornblende-pyroxene-biotite diorite from north of the 4021 prospect. Sample Pogo-00-R32.

Rocks of the tonalite suite are typically very weakly altered. In places, biotite is interleaved along cleavage planes with secondary chlorite \pm rutile and rare clinozoisite. Twinned hornblende is characteristic and poikilitically encloses euhedral plagioclase, biotite, zircon, and apatite. Hornblende is variably altered to chlorite \pm titanite \pm calcite along cleavage planes. Feldspars are weakly sericitized and plagioclase is weakly sausserized. Limited late magmatic or sub-solidus deformation is evidenced by undulose extinction and minor subgrain development in quartz.

Conventional U-Pb dating on monazite from biotite-hornblende bearing tonalite of the Goodpaster Batholith returned an age of 105.7 ± 0.3 Ma (sample MAPT-14) (Appendix A). Zircon grains from biotite-bearing tonalite (sample MAPT-7), located 2 km east of the Liese zone in the composite plutonic belt, returned a weighted mean U-Pb SHRIMP-RG age of 103.4 ± 2.2 Ma (Appendix A). Biotite-hornblende bearing granodiorite from Shawnee Peak (sample SP-00-14) returned a U-Pb zircon of age of 106.9 ± 1.3 Ma (Appendix A).

DIORITE SUITE

The post-kinematic diorite suite, comprised of diorite and quartz diorite, with lesser amounts of monzodiorite and tonalite, represents a younger, early Late Cretaceous event in the Goodpaster district. The rocks are typically medium- to coarse-grained and equigranular (Figure 2-7 d, e, f) and occur as steeply dipping dykes, sills and plugs. The Liese diorite is the largest body and crops out in the valley north of the Liese zone. Constituent minerals are plagioclase, hornblende, pyroxene, chlorite, potassium feldspar, and quartz. Accessory and trace minerals in order of abundance include apatite, ilmenite, pyrite, epidote, zircon, and magnetite. In one location, the rocks are locally seriate with very coarse-grained, elongate hornblende.

The diorite suite is characterized by the presence of minor primary magnetite, absence of monazite and abundant modal hornblende \pm pyroxene as the primary ferromagnesian minerals. Lesser biotite is also present. Magnetite is interpreted to be primary based on the equilibrium textural relationship to other framework silicate minerals, the presence of ilmenite exsolution textures, and the lack of any evidence that the magnetite is an alteration product of other iron-bearing minerals.

Chlorite interleaved with, or completely replacing, biotite is ubiquitous. Pyroxene contains inclusion-rich cores and is typically mantled by actinolite which in turn is altered to chlorite and calcite. Plagioclase has well formed albite twinning and oscillatory-zoned grains with moderate sausserization of the cores. Chalcopyrite, pyrrhotite, galena, and sphalerite are common. Locally, weak brittle deformation is evident by broken albite twins.

Near the 4021 prospect, diorite contains numerous gneissic xenoliths and locally shows chilled margins and hornfelsing of the gneiss. Diorite is inferred to cross cut the gold-bearing quartz veins in the Liese zone (Smith et al., 2000) and at the 4021 prospect (Chapter 3). Small, thin pegmatite veins less than 2 cm wide and rare quartz veins also cut the diorite. Gold-bearing quartz veins however, are not known to cross cut the diorite suite.

A conventional U-Pb zircon age of 95.4 ± 0.2 Ma was obtained from diorite north of the Liese zone (sample 107-945) (Appendix A). A young phase of the Goodpaster Batholith (sample Kgg-#14) returned a conventional U-Pb zircon age of 93.7 ± 0.2 Ma (Appendix A).

CONTROLS ON INTRUSIVE EMPLACEMENT

Structural controls on the emplacement of igneous rocks in the region are difficult to ascertain because of the lack of outcrop. Vertically drilled diamond drill core from the 4021 prospect, and to a lesser extent observations from outcrop along Central Creek, approximately

five kilometers south of the Liese zone, provides some structural constraints. The S1 foliation in the drill core is intensely folded and is cut by a generally shallowly dipping S2 foliation. Rhys et al. (2003) noted a similar relationship in the underground exposures in the Liese zone. The S2 fabric there always dips gently to the northeast although the dip azimuth is variable (Rhys et al., 2003). The relative constant dip direction of the S2 fabric thus offers a means to orient the drill core and examine semi-quantitatively the structural control on magma emplacement. The angle made by S1 and S2 foliation and granitic intrusion contact orientations, including pegmatite, with the vertical drill core was measured and is summarized in Figure 2-8.

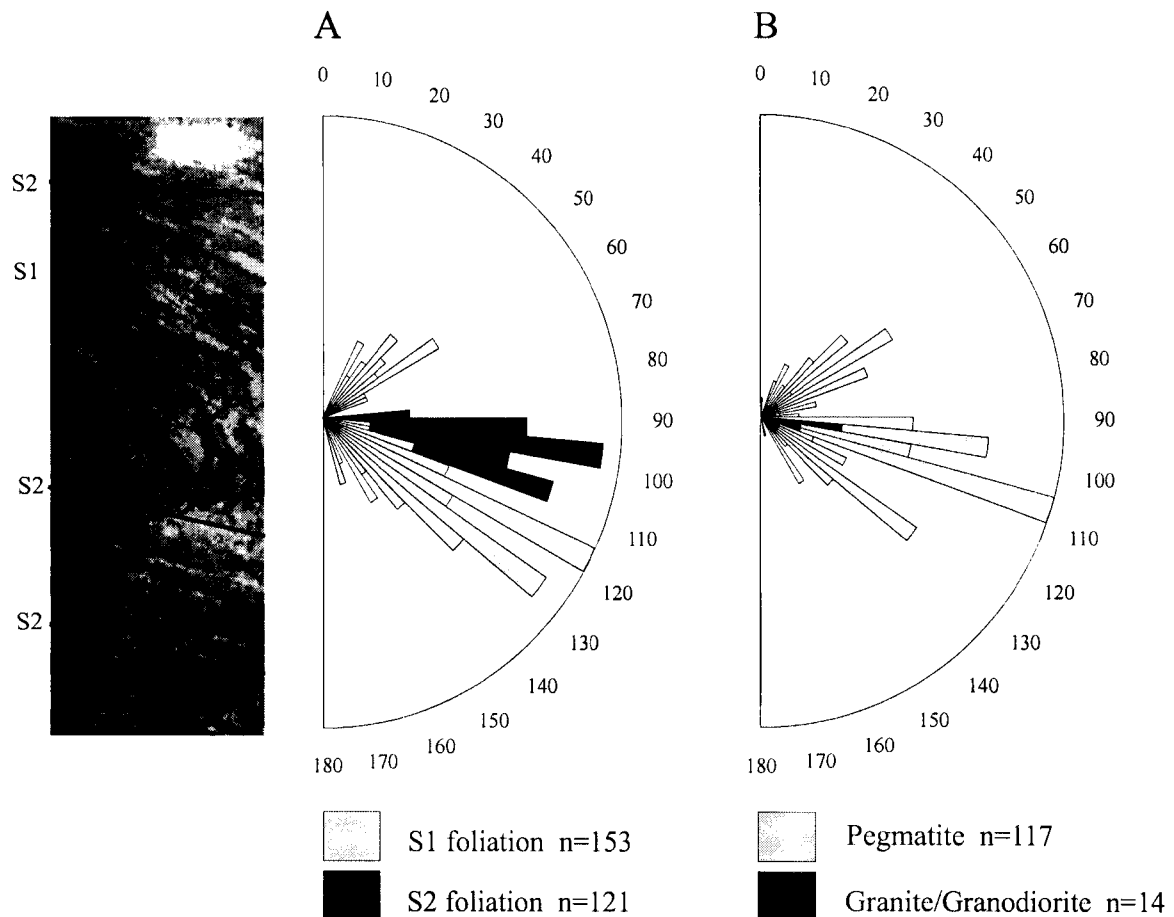


Figure 2-8: Half rose diagrams of foliation (A) and intrusive contact orientations (B) measured from drill core. All measurements are from vertical drill holes from the 4021 prospect. Plunges were recorded by measuring the angles of the foliation clockwise from vertical, relative to the drill core axis, assuming a shallow dip for the S2 foliation. The shallow dip for S2 is inferred from regional measurements and from Rhys et al. (2003).

All measurements were recorded clockwise from vertical after orienting S2 to be shallowly dipping to the northeast. The S2 fabric always lies at high angles to the vertical drill core while S1 occurs at variable but generally shallow angles to drill core (Figure 2-8a).

Contacts of the felsic intrusive phases with foliated orthogneiss suggest three geometries of intrusion emplacement. 1) Syn- to late-kinematic intrusive phases are foliated and are locally folded by S2. 2) Late- to post-kinematic intrusive phases exploit the S2 fabric and 3) post-kinematic intrusive phases cross cut all deformational fabrics. A schematic diagram depicting the relationships of the intrusive phases to the S1 and S2 foliation is shown in Figure 2-9.

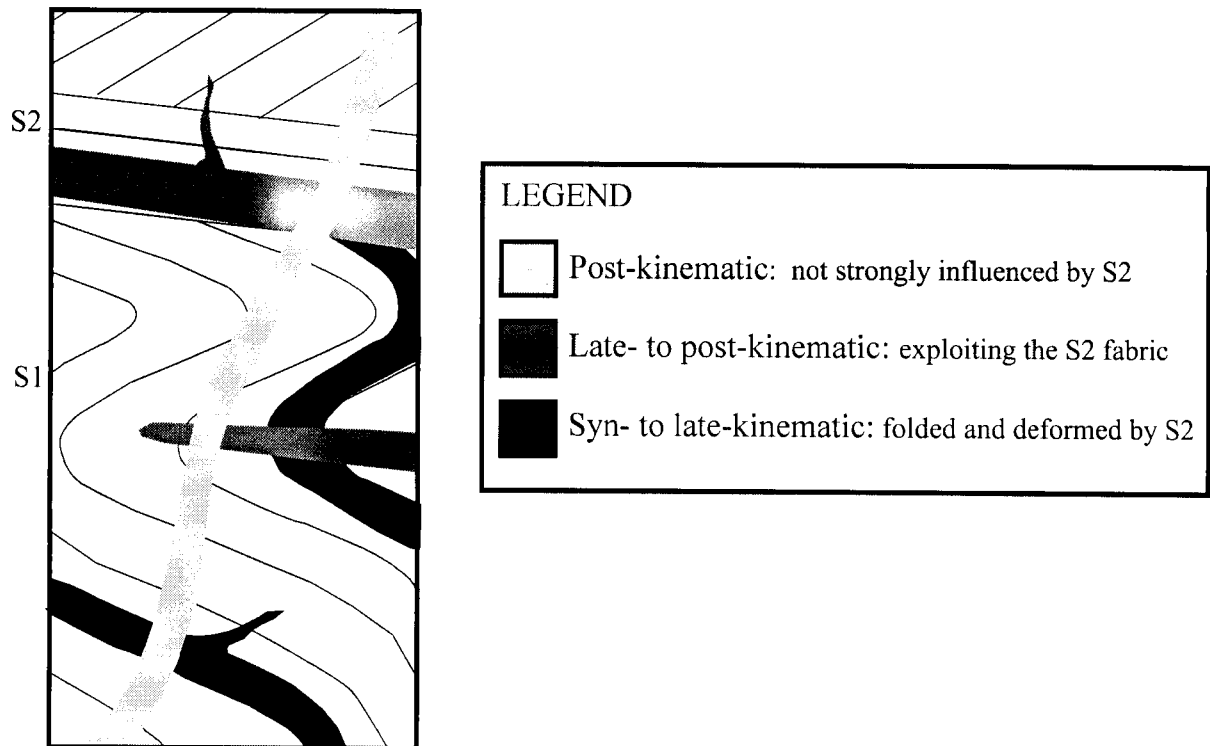


Figure 2-9: Schematic relationships of the intrusive phases relative to foliation.

North of Central Creek, mapping has shown that granite intrusions exploited the S2 fabric (Figure 2-10). Here, granite sheets also intrude what was mapped as a northerly, shallowly

dipping S3 fabric and other low-angle faults. Several intrusive bodies south of the arcuate belt also outcrop as elongate east-west trending bodies and may reflect sub-horizontal dykes. Moreover, several E-W trending thrust faults in the region west of Shaw Creek have a number of intrusive bodies intruding along them (Figure 2-3).

These mesoscopic drill core and map-scale relationships provide the basis for the hypothesis that the granite and tonalite suites locally intrude as flat lying tabular intrusive sheets exploiting a shallowly dipping structure, either the S2 foliation or low angle faults late- to post-kinematic. If the hypothesis is valid, the east-west distribution of the composite felsic intrusions in the Goodpaster district logically may be inferred to be controlled by shallowly dipping syn-metamorphic faults. The post-mineralization diorite on the other hand appears to dip steeply, based on diamond drill core correlations at the 4021 deposit and aeromagnetic data.



Figure 2-10. Polydeformed foliation in outcrop north of Central Creek. Granite is exploiting the shallowly dipping foliation.

GEOCHEMISTRY OF THE INTRUSIVE SUITES IN THE GOODPASTER DISTRICT

ANALYTICAL METHODS

Whole rock analyses of major, minor, and rare earth element compositions were obtained from 56 least altered intrusive rock samples in the Goodpaster district (Table 2-2). Major elements and selected trace element concentrations were determined by X-ray fluorescence spectrometry (XRF). Rare earth elements (REE) and remaining trace elements were determined by inductively coupled plasma mass spectrometry (ICP-MS). All analyses were completed at Chemex Laboratories, North Vancouver, Canada.

MAJOR ELEMENT GEOCHEMISTRY

The major element data classifies all the intrusive rocks in the district as calc-alkalic (after the classification of Irvine and Baragar, 1971) and subalkaline. In Figure 2-11, the intrusive rock samples on the total alkali versus silica diagram of LeBas et al. (1986), modified for plutonic rocks (Wilson, 1989), show a range of compositions from diorite to alkali granite.

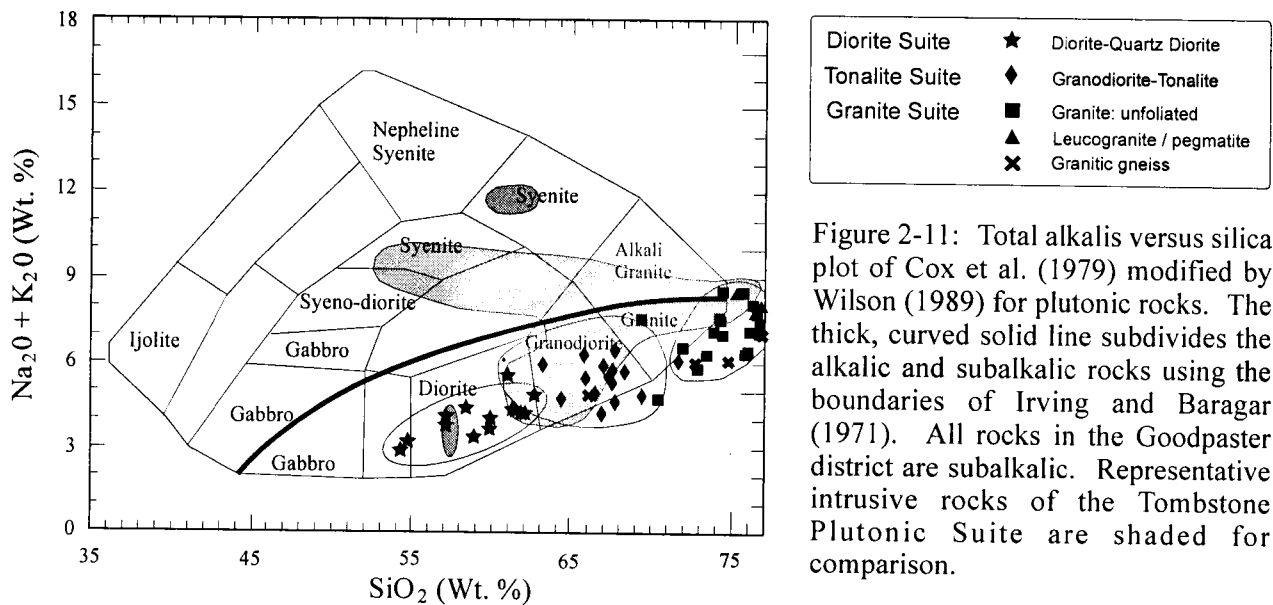


Figure 2-11: Total alkalis versus silica plot of Cox et al. (1979) modified by Wilson (1989) for plutonic rocks. The thick, curved solid line subdivides the alkalic and subalkalic rocks using the boundaries of Irving and Baragar (1971). All rocks in the Goodpaster district are subalkalic. Representative intrusive rocks of the Tombstone Plutonic Suite are shaded for comparison.

Table 2-2a: Location and descriptions of samples used for geochemistry.

SAMPLE	Location	Northing	Easting	Diamond Drill Hole	Description
POGO-00-R6	4021 prospect	605083	7146776	-	granite orthogneiss
POGO-00-R12	North Zone	600991	7149610	-	granite
POGO-00-R14	North Zone	600320	7149928	-	leucogranite
POGO-00-R16	North Zone	600456	7149719	-	leucogranite
POGO-00-R17	North Zone	600502	7149800	-	orthogneiss
POGO-00-R29	4021 prospect	605603	7147520	-	quartz monzonite
POGO-00-R32	4021 prospect	604971	7147494	-	px-hbl-bt diorite
POGO-00-R34	4021 prospect	603782	7147178	-	bt-granodiorite / tonalite
POGO-00-R38	Tam Prospect	610518	7144668	-	hbl-bt quartz diorite
POGO-00-R39	Star Ridge	602124	7145266	-	altered granite
POGO-00-R51	North of 4021 prospect	604896	7148188	-	bt-tonalite
POGO-00-R52	North of 4021 prospect	604896	7148188	-	bt-tonalite
POGO-00-R90	Football Field	603085	7146606	-	granite orthogneiss
POGO-00-R94	Football Field	603140	7147236	-	hbl-bt-pxn diorite
POGO-00-R95	Football Field	603488	7147720	-	hbl-bt-diorite
POGO-00-R96	Football Field	603397	7147847	-	bt-granite
POGO-00-R97	Football Field	603236	7147903	-	tonalite
POGO-00-R99	Football Field	603335	7148071	-	bt-hbl quartz diorite
POGO-00-R100	Football Field	603370	7148389	-	tonalite
POGO-00-R105	East of 4021 prospect	606721	7146823	-	mafic dyke
POGO-00-R114	Ogopogo	605147	7153607	-	bt-hbl tonalite
POGO-00-R117	Spring Grid	608375	7147096	-	hbl-bt quartz diorite
POGO-00-R119	Spring Grid	610217	7145596	-	mafic dyke
POGO-00-R134	Liese Creek	601200	7148967	-	hbl-px-bt diorite
SP-00-09	Shawnee Peak	615487	7145436	-	bt-hbl granite
SP-00-12	Shawnee Peak	615641	7146237	-	granite orthogneiss
SP-00-14	Shawnee Peak	615622	7146190	-	bt-granodiorite
MAPT-14	North Goodpaster	604981	7147822	-	hbl-bt tonalite
MAPT-7	Football Field	603314	7147600	-	bt-granodiorite
KGG -14	North Goodpaster	605308	7152204	-	bt-hbl tonalite
POGO-01-100B	Central Creek	604597	7142801	-	transitional intrusive
POGO-01-101B	Central Creek	605075	7143137	-	transitional intrusive
POGO-01-104	Central Creek	603886	7141272	-	pegmatite
POGO-01-106	Chorizo	610025	7146821	-	granodiorite
POGO-01-109	Chorizo	611042	7146942	-	bt-hbl diorite
POGO-01-122	4021 prospect	604647	7147095	-	bt-granite
POGO-01-123	4021 prospect	604647	7147095	-	bt-mu leucogranite
POGO-01-126	4021 prospect	604791	7147375	-	diorite
POGO-01-129	4021 prospect	604812	7147660	-	diorite
POGO-01-131	North of 4021 prospect	604866	7147974	-	biotite tonalite
POGO-01-137	West Goodpaster	594310	7148555	-	granite
POGO-01-144	Goodpaster Batholith	604492	7152752	-	bt-hbl granodiorite
POGO-01-152	Anglo Property	595474	7146710	-	hbl-bt monzonite
POGO-01-162	Spring Grid	601033	7144450	-	highly altered intrusive
POGO-01-165	Spring Grid	611010	7145688	-	bt-granite (w. fol'd)
POGO-01-167	Spring Grid	608314	7145918	-	bt-granodiorite
POGO-01-169	West of Football Field	601674	7147820	-	granite (w. fol'd)
POGO-01-170	West Goodpaster	601611	7147983	-	diorite
POGO-01-171	West Goodpaster	598207	7149051	-	altered granite
DDH- 00-248	4021 prospect	-	-	00-248	granodiorite
DDH- 00-254	4021 prospect	-	-	00-254 150 ft	hbl-bt diorite
DDH-00-254 600'	4021 prospect	-	-	00-254 600 ft	hbl-bt quartz diorite
POGO-02 98-93	4021 prospect	-	-	98-93 885 ft	bt-hbl rich orthogneiss
POGO-02 98-176	4021 prospect	-	-	98-176 588 ft	granitic orthogneiss
POGO-02 97-75	4021 prospect	-	-	97-75 1260 ft	bt-poor gnt granodiorite
POGO-02 247-318	4021 prospect	-	-	00-247 318 ft	bt granodiorite
POGO-02 98-105-745	4021 prospect	-	-	98-105 745 ft	hbl-pxn-bt diorite
POGO-02 263-286	4021 prospect	-	-	00-263 286 ft	granite
POGO-02 00-249-386	4021 prospect	-	-	00-249 386 ft	bt-gnt granitic orthogneiss
POGO-02 249-799	4021 prospect	-	-	00-249 799 ft	c.g. orthogneiss
POGO-02 249-1010	4021 prospect	-	-	00-249 1010 ft	bt-gnt granite
POGO-02 249-512	4021 prospect	-	-	00-249 512 ft	bt-gnt granite
POGO-02 247-661	4021 prospect	-	-	00-247 661 ft	c.g. bt granitic orthogneiss
POGO-02 263-744.5	4021 prospect	-	-	00-263 744.5 ft	granite

Abbreviations: gnt=garnet; mu=muscovite, bt=biotite; hbl=hornblende; pxn=pyroxene, w. fol'd= weakly foliated

Table 2-2b: Major element geochemistry for representative rocks in the Goodpaster district

SAMPLE	Majors											TOTAL	FeO
	Al ₂ O ₃	CaO	FeO (T)	K ₂ O	MgO	MnO	Na ₂ O	P ₂ O ₅	SiO ₂	TiO ₂	LOI		
POGO-00-R6	13.50	2.27	2.43	2.31	0.57	0.05	3.63	0.12	72.78	0.35	0.68	98.69	1.99
POGO-00-R12	14.48	2.90	2.95	2.91	0.78	0.05	2.79	0.12	71.31	0.43	0.61	99.33	2.35
POGO-00-R14	14.21	0.43	0.71	4.52	<0.01	0.03	3.29	0.20	74.79	0.07	1.03	99.28	0.11
POGO-00-R16	14.46	0.61	0.95	4.78	0.09	0.04	3.50	0.21	73.74	0.08	0.58	99.04	0.68
POGO-00-R17	14.93	3.07	4.13	1.94	1.59	0.04	2.22	0.18	68.88	0.50	1.35	98.83	2.97
POGO-00-R29	17.45	7.05	9.77	1.96	3.69	0.16	3.24	0.68	51.82	2.20	1.56	99.58	6.77
POGO-00-R32	16.84	8.45	9.90	1.35	5.66	0.18	1.67	0.15	51.17	0.94	3.29	99.60	7.38
POGO-00-R34	15.81	4.27	4.93	2.89	1.69	0.08	2.45	0.15	65.12	0.71	1.14	99.24	3.87
POGO-00-R38	17.04	5.46	6.75	2.41	3.10	0.12	2.90	0.23	58.09	0.93	2.48	99.51	5.26
POGO-00-R39	15.91	4.18	7.30	2.54	3.35	0.11	3.09	0.32	55.88	0.98	5.78	99.44	5.93
POGO-00-R51	16.11	3.99	4.77	2.30	1.51	0.08	2.82	0.15	64.80	0.66	1.95	99.14	3.84
POGO-00-R52	14.94	3.39	7.12	2.22	1.35	0.10	2.30	0.14	64.32	0.68	2.93	99.49	3.51
POGO-00-R90	13.55	3.07	3.89	3.55	0.74	0.08	2.29	0.08	70.44	0.38	0.64	98.71	2.93
POGO-00-R94	17.17	8.39	8.81	1.57	4.77	0.15	2.07	0.12	54.60	0.85	0.80	99.30	6.19
POGO-00-R95	16.72	7.48	8.86	1.88	5.28	0.16	2.08	0.12	54.61	0.81	1.59	99.59	6.73
POGO-00-R96	15.18	2.90	2.38	3.42	0.67	0.03	2.97	0.12	69.95	0.35	0.68	98.65	1.88
POGO-00-R97	17.13	5.45	5.76	2.62	1.91	0.11	3.10	0.30	60.53	0.84	1.42	99.17	4.13
POGO-00-R99	16.18	4.78	5.46	2.03	1.68	0.12	2.75	0.14	64.04	0.69	0.83	98.70	4.25
POGO-00-R100	16.15	5.70	6.33	2.24	2.26	0.12	2.35	0.16	62.05	0.81	1.29	99.46	4.90
POGO-00-R105	18.59	7.32	8.36	2.33	3.57	0.11	2.76	0.38	52.73	1.10	2.03	99.28	6.67
POGO-00-R114	16.04	4.49	4.54	2.79	1.68	0.09	2.59	0.13	65.26	0.64	0.79	99.04	3.57
POGO-00-R117	15.24	6.62	7.51	2.17	4.50	0.14	1.99	0.12	59.01	0.73	1.19	99.22	5.79
POGO-00-R119	16.41	8.46	9.13	1.17	4.20	0.16	2.07	0.11	56.21	0.88	0.28	99.08	6.07
POGO-00-R134	15.59	7.68	8.44	1.81	4.73	0.15	2.08	0.09	57.40	0.73	0.43	99.13	5.84
SP-00-09	15.29	2.95	3.35	4.12	1.27	0.08	3.30	0.15	67.78	0.41	0.61	99.51	2.67
SP-00-12	12.72	1.38	1.58	3.82	0.20	0.04	3.02	0.05	74.70	0.19	0.79	98.49	1.31
SP-00-14	14.04	2.47	2.83	3.46	0.51	0.06	2.70	0.10	71.57	0.38	0.58	98.70	2.42
MAPT-14	16.23	4.52	4.43	2.99	1.70	0.09	2.76	0.12	64.88	0.61	0.60	98.93	3.28
MAPT-7	15.15	3.27	2.40	3.06	0.77	0.03	2.94	0.13	69.85	0.38	0.78	98.76	2.01
KGG -14*	15.92	4.29	3.82	2.49	1.58	0.09	3.07	0.13	66.31	0.54	1.35	99.69	2.96
POGO-01-100B	5.59	0.72	1.60	0.92	0.39	0.02	1.22	0.04	87.61	0.28	0.58	98.98	0.98
POGO-01-101B	14.03	2.54	0.98	1.48	0.38	0.03	4.28	0.10	74.03	0.15	0.72	98.79	0.70
POGO-01-104	12.16	0.28	0.55	4.54	0.21	0.02	3.29	0.06	76.56	0.08	0.75	98.51	0.24
POGO-01-106	15.77	4.06	4.79	3.02	1.59	0.09	2.54	0.16	65.00	0.64	1.19	99.06	3.66
POGO-01-109	15.99	5.97	7.67	2.12	3.15	0.14	1.90	0.13	58.82	0.78	2.47	99.34	6.04
POGO-01-122	13.24	1.58	1.50	4.04	0.06	0.07	2.81	0.04	74.19	0.08	0.71	98.39	0.85
POGO-01-123	14.01	0.87	0.80	4.47	0.06	0.04	3.09	0.08	74.56	0.04	0.82	98.84	0.57
POGO-01-126	14.53	7.12	7.47	2.16	4.88	0.13	1.98	0.12	57.95	0.71	1.13	98.35	5.29
POGO-01-129	16.54	9.08	9.65	1.00	5.38	0.17	1.66	0.15	49.62	0.91	4.43	98.66	7.18
POGO-01-131	15.90	4.63	4.79	1.77	1.48	0.08	2.69	0.14	64.87	0.69	1.30	98.56	3.86
POGO-01-137	14.49	1.69	1.86	3.96	0.54	0.03	2.95	0.12	71.49	0.30	1.24	98.76	1.46
POGO-01-144	16.36	4.87	5.02	2.66	1.97	0.09	2.60	0.15	63.08	0.72	1.08	98.69	3.58
POGO-01-152	15.42	3.42	4.62	3.55	1.77	0.08	2.63	0.18	64.44	0.69	1.57	98.56	3.32
POGO-01-162	13.90	0.54	2.82	3.53	0.78	0.05	2.53	0.10	72.34	0.32	2.13	99.13	1.56
POGO-01-165	14.08	1.17	1.27	5.85	0.23	0.04	2.42	0.10	72.05	0.21	0.75	98.27	0.89
POGO-01-167	16.20	3.90	5.10	3.25	2.09	0.09	2.86	0.18	63.50	0.74	1.09	99.22	4.07
POGO-01-169	13.89	1.99	1.91	3.79	0.42	0.05	3.03	0.11	72.14	0.26	0.63	98.35	1.49
POGO-01-170	16.21	6.21	7.40	1.95	3.68	0.13	2.09	0.15	58.70	0.80	1.57	99.03	5.32
POGO-01-171	7.46	0.48	1.51	2.72	0.28	0.01	1.07	0.03	83.87	0.26	0.78	98.50	0.79
DDH- 00-248	16.48	4.03	5.24	2.09	2.12	0.06	1.89	0.12	62.66	0.64	3.61	99.02	3.90
DDH- 00-254	14.67	6.21	6.78	2.63	4.21	0.12	2.03	0.13	59.72	0.69	1.49	98.84	5.20
DDH-00-254 600'	14.97	7.10	7.91	1.65	5.44	0.13	1.83	0.12	56.70	0.73	2.27	99.00	6.35
POGO-02 98-93	14.16	4.21	6.84	2.20	3.33	0.13	2.54	0.12	64.02	0.81	0.87	99.23	5.72
POGO-02 98-176	12.07	0.51	1.16	5.66	0.12	0.05	2.39	0.03	76.98	0.11	0.59	99.67	0.96
POGO-02 97-75	13.87	0.75	0.87	5.36	0.10	0.05	3.02	0.19	74.39	0.06	0.90	99.56	0.71
POGO-02 247-318	14.05	3.92	5.00	1.89	1.42	0.09	2.68	0.08	67.77	0.59	2.14	99.63	3.99
POGO-02 98-105-745	15.63	7.94	8.27	1.72	5.06	0.16	2.55	0.10	56.38	0.70	0.83	99.34	6.63
POGO-02 263-286	12.27	1.51	1.64	4.86	0.16	0.06	2.36	0.03	74.35	0.12	0.65	98.12	1.42
POGO-02 00-249-386	12.67	1.70	1.95	3.45	0.45	0.06	3.56	0.08	74.70	0.25	0.28	99.35	1.48
POGO-02 249-799	12.64	2.19	2.50	4.00	0.38	0.06	2.36	0.05	74.87	0.22	0.47	99.84	1.99
POGO-02 249-1010	13.68	1.59	2.27	4.23	0.37	0.07	3.15	0.22	72.76	0.23	0.86	99.51	1.87
POGO-02 249-512	13.68	1.05	0.77	4.20	0.11	0.06	3.42	0.05	75.11	0.04	0.59	99.09	0.64
POGO-02 247-661	13.60	1.80	2.01	3.70	0.46	0.06	3.75	0.09	72.35	0.27	0.44	98.75	1.67
POGO-02 263-744.5	13.71	0.90	0.79	4.96	0.07	0.06	2.93	0.07	74.46	0.04	0.97	99.00	0.64
POGO-02 249-1020	18.89	8.16	9.34	1.92	4.45	0.17	1.77	0.19	51.81	1.04	0.97	98.79	7.85

1. All analyses were completed at ALS Chemex Labs Ltd., North Vancouver, British Columbia

2. Major element abundances are reported as weight percents

* - note that only a very small sample was analysed (30g)

Table 2-2c: Trace and rare earth element (REE) geochemistry on intrusive rocks from the Goodpaster district

SAMPLE	Trace/REE (ppm)											
	Ba	Ce	Cs	Co	Cu	Dy	Er	Eu	Gd	Ga	Hf	Ho
POGO-00-R6	1580	150.5	1.3	21.0	25.0	2.6	1.3	1.5	4.1	13.0	4.0	0.6
POGO-00-R12	1205	123.5	2.4	16.0	15.0	3.3	1.6	1.4	5.8	17.0	6.0	0.7
POGO-00-R14	108	14.5	8.0	21.5	15.0	1.6	0.9	0.1	1.1	18.0	1.0	0.3
POGO-00-R16	165.5	11.5	9.7	12.5	<dl	2.5	1.3	0.3	1.4	18.0	<1	0.5
POGO-00-R17	276	62.5	2.5	18.5	15.0	4.4	3.3	1.6	4.0	18.0	2.0	1.1
POGO-00-R29	915	93.5	1.5	26.0	25.0	7.9	4.7	2.5	8.9	21.0	8.0	1.9
POGO-00-R32	504	37.0	5.2	32.5	15.0	3.6	2.1	1.1	3.6	18.0	3.0	0.8
POGO-00-R34	1680	43.0	4.4	16.0	20.0	3.3	1.9	1.2	3.8	19.0	4.0	0.7
POGO-00-R38	1155	78.5	3.9	20.5	25.0	3.0	1.8	1.5	4.0	21.0	5.0	0.7
POGO-00-R39	837	62.5	1.9	18.0	15.0	3.3	1.7	1.1	4.4	20.0	5.0	0.7
POGO-00-R51	1490	38.5	2.7	16.5	10.0	2.9	1.5	1.3	3.4	20.0	4.0	0.6
POGO-00-R52	1955	45.0	3.6	24.5	20.0	2.7	1.4	1.1	3.3	18.0	3.0	0.6
POGO-00-R90	565	72.0	3.9	16.0	10.0	4.4	2.8	1.2	4.2	17.0	5.0	1.0
POGO-00-R94	917	36.0	2.6	38.0	25.0	3.6	2.1	1.1	3.5	18.0	3.0	0.9
POGO-00-R95	1660	33.0	3.4	33.5	25.0	3.2	2.1	1.0	3.3	18.0	3.0	0.8
POGO-00-R96	1925	52.0	2.7	17.0	10.0	1.7	0.8	1.2	3.0	20.0	4.0	0.3
POGO-00-R97	1635	92.0	2.1	20.5	15.0	3.2	1.8	1.6	4.3	21.0	5.0	0.7
POGO-00-R99	1175	49.5	4.3	19.0	10.0	2.9	1.6	1.2	3.4	20.0	4.0	0.6
POGO-00-R100	1410	47.0	3.3	20.5	10.0	3.5	2.1	1.2	4.0	20.0	4.0	0.8
POGO-00-R105	1275	47.0	5.5	23.5	20.0	5.0	2.9	1.4	5.3	23.0	3.0	1.1
POGO-00-R114	601	70.0	3.5	18.5	10.0	4.6	2.7	1.2	4.8	20.0	6.0	1.0
POGO-00-R117	944	45.0	3.9	30.5	25.0	3.7	2.2	1.0	3.9	17.0	4.0	0.9
POGO-00-R119	707	34.5	1.4	68.5	10.0	3.7	2.4	1.1	3.6	18.0	3.0	0.9
POGO-00-R134	899	38.5	3.0	36.0	25.0	3.4	2.3	0.9	3.5	17.0	4.0	0.8
SP-00-09	1380	64.0	6.0	28.5	5.0	2.8	1.5	1.0	4.3	20.0	4.0	0.5
SP-00-12	318	93.0	2.1	31.0	5.0	7.2	4.5	0.6	6.5	18.0	8.0	1.7
SP-00-14	1140	103.5	2.1	16.5	<dl	5.0	2.9	1.3	6.2	17.0	5.0	1.0
MAPT-14	777	73.0	3.4	14.0	<dl	6.1	3.5	1.3	6.2	20.0	6.0	1.2
MAPT-7	2160	57.5	2.7	19.5	<dl	2.6	1.1	1.4	4.5	20.0	4.0	0.4
KGG -14	553	18.0	2.9	34.5	5.0	3.0	2.0	0.9	2.8	19.0	4.0	0.6
POGO-01-100B	259	30.5	0.9	21.5	15.0	1.3	0.8	0.4	1.6	5.0	6.0	0.3
POGO-01-101B	378	25.5	1.0	19.0	<dl	2.9	1.7	1.0	2.5	11.0	1.0	0.6
POGO-01-104	265	8.0	1.4	18.0	<dl	1.7	1.2	0.3	1.3	10.0	<1	0.4
POGO-01-106	1420	58.5	3.6	29.0	140.0	3.0	1.5	1.1	3.9	17.0	3.0	0.5
POGO-01-109	1260	41.0	3.5	19.0	30.0	3.8	2.2	0.9	4.2	15.0	3.0	0.8
POGO-01-122	584	54.5	1.0	19.5	<dl	6.0	3.9	0.9	5.8	13.0	4.0	1.3
POGO-01-123	32.5	19.0	4.3	19.5	<dl	4.0	2.4	0.1	2.8	14.0	1.0	0.8
POGO-01-126	1200	40.5	2.8	29.5	35.0	3.2	1.8	0.9	3.5	14.0	3.0	0.6
POGO-01-129	443	34.5	4.2	30.5	10.0	3.2	1.8	1.0	3.4	16.0	2.0	0.7
POGO-01-131	1290	46.0	5.4	11.5	<dl	1.2	0.5	1.0	2.0	16.0	3.0	0.1
POGO-01-137	659	45.5	2.4	11.0	<dl	3.1	1.8	0.7	3.3	14.0	3.0	0.6
POGO-01-144	615	122.0	2.7	13.5	<dl	4.1	2.2	1.0	5.4	17.0	4.0	0.8
POGO-01-152	1295	68.0	11.4	13.0	20.0	3.1	1.5	1.0	4.0	17.0	5.0	0.5
POGO-01-162	771	78.0	5.1	11.5	<dl	4.6	2.4	0.8	5.2	15.0	4.0	0.8
POGO-01-165	749	52.5	3.0	12.5	<dl	2.8	1.4	0.6	3.4	14.0	2.0	0.5
POGO-01-167	1425	64.5	4.2	15.0	<dl	3.0	1.6	1.1	4.1	18.0	4.0	0.6
POGO-01-169	919	73.5	2.0	12.5	<dl	3.3	1.5	0.7	4.2	14.0	4.0	0.5
POGO-01-170	974	43.5	2.4	19.5	5.0	3.3	2.0	1.0	3.9	16.0	3.0	0.7
POGO-01-171	409	42.0	3.1	16.0	20.0	2.4	1.2	0.5	2.6	8.0	5.0	0.4
DDH- 00-248	550	47.5	4.9	11.5	15.0	4.0	2.5	1.0	4.2	18.0	3.0	0.8
DDH- 00-254	1240	50.0	3.8	24.0	35.0	3.7	2.0	0.8	3.9	14.0	4.0	0.7
DDH-00-254 600'	1015	40.0	3.3	29.0	40.0	3.0	1.8	0.8	3.4	14.0	3.0	0.6
POGO-02 98-93	651	84.5	2.8	47.5	45.0	5.2	3.1	1.5	6.5	20.0	6.0	1.1
POGO-02 98-176	216	82.0	1.0	52.5	15.0	5.5	3.8	0.3	6.2	18.0	5.0	1.2
POGO-02 97-75	185	13.5	3.7	36.0	15.0	2.5	1.4	0.3	1.7	17.0	<1	0.5
POGO-02 247-318	484	64.0	4.8	26.0	15.0	4.4	2.5	1.0	5.2	19.0	5.0	0.9
POGO-02 98-105-745	1230	37.5	2.5	40.5	35.0	3.7	2.2	0.9	4.0	18.0	3.0	0.8
POGO-02 263-286	776	73.0	2.3	37.0	15.0	6.5	4.0	0.8	6.5	15.0	4.0	1.3
POGO-02 00-249-386	1740	146.0	0.8	27.0	<dl	3.2	1.7	1.2	5.1	13.0	4.0	0.6
POGO-02 249-799	730	77.5	1.1	37.5	20.0	4.0	2.5	1.1	5.1	14.0	5.0	0.8
POGO-02 249-1010	538	45.0	4.2	30.5	5.0	4.7	2.4	0.8	4.8	17.0	2.0	0.9
POGO-02 249-512	115.5	16.0	5.9	47.5	5.0	3.3	2.1	0.3	2.2	14.0	<1	0.7
POGO-02 247-661	1705	153.5	2.1	36.0	10.0	3.7	2.1	1.3	5.9	15.0	4.0	0.7
POGO-02 263-744.5	300	18.5	4.3	41.5	<dl	2.8	1.7	0.3	2.3	15.0	<1	0.6
POGO-02 249-1020	484	42.5	2.2	37.5	25.0	5.7	3.5	1.6	5.6	20.0	2.0	1.2

1. All analyses were completed at Chemex Labs Ltd., North Vancouver, British Columbia
2. Trace and REE abundance are reported as parts per million (ppm)
3. <dl = below detection limits

Table 2-2c. Continued

SAMPLE	Trace/REE (ppm)											
	La	Pb	Lu	Nd	Ni	Nb	Pr	Rb	Sm	Sr	Ta	Tb
POGO-00-R6	91.5	20.0	0.1	42.5	<5	91.0	14.5	81.0	6.1	451.0	12.5	0.6
POGO-00-R12	64.0	15.0	0.1	49.0	<5	14.0	14.4	105.5	8.0	360.0	6.5	0.8
POGO-00-R14	8.5	25.0	0.1	5.0	<5	15.0	1.6	237.0	1.0	36.6	14.0	0.3
POGO-00-R16	6.0	15.0	0.2	4.5	<5	14.0	1.4	276.0	1.5	51.1	8.5	0.4
POGO-00-R17	31.5	35.0	0.5	26.0	15.0	13.0	7.4	123.0	4.6	246.0	5.0	0.8
POGO-00-R29	44.5	55.0	0.6	49.0	30.0	27.0	12.2	56.2	10.4	449.0	3.0	1.6
POGO-00-R32	19.0	20.0	0.3	18.5	25.0	7.0	4.7	55.2	3.9	284.0	1.5	0.7
POGO-00-R34	22.0	25.0	0.2	20.0	5.0	9.0	5.4	116.5	4.3	269.0	3.5	0.7
POGO-00-R38	42.5	30.0	0.2	30.5	15.0	11.0	8.9	93.6	5.2	433.0	2.5	0.7
POGO-00-R39	31.5	20.0	0.2	28.5	20.0	9.0	7.8	111.0	5.4	305.0	1.5	0.7
POGO-00-R51	19.5	35.0	0.1	18.5	5.0	12.0	4.9	88.8	4.2	353.0	5.0	0.6
POGO-00-R52	22.0	800.0	0.1	19.5	10.0	10.0	5.3	79.2	3.8	286.0	7.0	0.5
POGO-00-R90	35.0	25.0	0.4	28.5	5.0	15.0	8.1	142.5	5.2	183.0	5.5	0.8
POGO-00-R94	18.0	25.0	0.3	17.5	15.0	6.0	4.5	59.2	3.8	304.0	5.0	0.6
POGO-00-R95	16.5	20.0	0.3	16.0	20.0	6.0	4.1	73.4	3.4	382.0	2.5	0.6
POGO-00-R96	26.5	30.0	<0.1	22.0	<5	9.0	6.3	115.0	4.1	312.0	6.5	0.4
POGO-00-R97	50.5	30.0	0.2	34.5	15.0	44.0	10.1	97.0	5.6	580.0	7.0	0.7
POGO-00-R99	26.0	20.0	0.2	21.5	5.0	9.0	5.9	85.4	4.0	328.0	5.0	0.6
POGO-00-R100	23.0	25.0	0.3	21.5	5.0	10.0	5.8	85.6	4.5	342.0	4.0	0.7
POGO-00-R105	21.5	20.0	0.3	25.5	5.0	9.0	6.3	101.0	6.1	470.0	3.5	1.0
POGO-00-R114	33.5	30.0	0.4	28.5	5.0	13.0	8.1	131.0	5.5	258.0	5.5	0.8
POGO-00-R117	22.5	30.0	0.3	21.0	30.0	8.0	5.6	88.6	4.4	261.0	4.5	0.7
POGO-00-R119	16.5	15.0	0.3	17.5	5.0	11.0	4.5	40.2	3.9	297.0	17.5	0.7
POGO-00-R134	18.5	20.0	0.3	17.5	15.0	6.0	4.7	68.8	3.7	247.0	4.5	0.6
SP-00-09	34.5	45.0	0.3	25.0	5.0	13.0	6.8	162.0	4.6	418.0	8.5	0.6
SP-00-12	45.5	20.0	0.6	37.5	5.0	15.0	10.9	156.0	7.5	71.6	13.0	1.3
SP-00-14	54.5	5.0	0.4	41.0	<5	19.0	11.7	113.0	7.2	190.5	8.0	1.0
MAPT-14	38.0	20.0	0.6	30.0	<5	15.0	8.2	116.5	6.1	290.0	5.5	1.1
MAPT-7	32.5	20.0	0.1	24.5	<5	12.0	6.9	105.0	5.5	321.0	10.0	0.6
KGG -14	9.0	25.0	0.3	8.5	10.0	13.0	1.9	104.0	2.6	227.0	5.0	0.5
POGO-01-100B	15.0	15.0	0.1	11.0	5.0	7.0	3.2	33.2	1.7	72.8	6.5	0.2
POGO-01-101B	13.0	20.0	0.2	10.0	<5	7.0	2.8	31.8	2.2	297.0	6.0	0.4
POGO-01-104	6.0	30.0	0.2	4.0	<5	18.0	1.2	164.5	1.0	78.9	6.0	0.2
POGO-01-106	29.5	125.0	0.2	23.0	<5	13.0	6.3	105.0	4.5	325.0	7.5	0.6
POGO-01-109	20.0	25.0	0.3	17.5	5.0	8.0	4.7	66.4	3.8	269.0	1.5	0.6
POGO-01-122	25.0	20.0	0.7	23.5	<5	13.0	6.2	107.0	5.6	162.0	6.0	0.9
POGO-01-123	9.0	20.0	0.4	8.0	<5	17.0	2.2	162.5	2.1	41.6	9.0	0.6
POGO-01-126	19.5	15.0	0.3	17.5	35.0	8.0	4.6	73.4	3.6	222.0	2.0	0.5
POGO-01-129	17.0	50.0	0.3	15.0	20.0	7.0	3.9	38.2	3.4	272.0	<0.5	0.5
POGO-01-131	25.0	5.0	<0.1	15.5	5.0	9.0	4.6	63.8	2.3	260.0	1.0	0.2
POGO-01-137	22.5	15.0	0.3	17.5	<5	14.0	4.9	141.5	3.5	178.5	4.0	0.5
POGO-01-144	60.5	15.0	0.3	37.5	5.0	11.0	11.7	98.6	5.8	255.0	1.5	0.8
POGO-01-152	34.5	25.0	0.2	25.0	5.0	12.0	7.2	149.0	4.7	323.0	1.5	0.5
POGO-01-162	38.0	15.0	0.3	30.5	5.0	17.0	8.3	136.5	5.9	134.5	2.5	0.8
POGO-01-165	26.0	20.0	0.2	20.0	5.0	10.0	5.6	157.5	4.0	161.5	4.0	0.5
POGO-01-167	33.0	35.0	0.2	25.0	5.0	12.0	7.0	127.0	4.8	360.0	1.5	0.6
POGO-01-169	36.0	25.0	0.2	27.5	<5	12.0	7.8	133.5	4.8	234.0	3.5	0.6
POGO-01-170	21.0	20.0	0.3	18.5	10.0	8.0	4.9	69.6	4.0	279.0	1.0	0.6
POGO-01-171	20.0	25.0	0.1	15.0	5.0	9.0	4.3	100.5	2.8	96.7	5.0	0.4
DDH- 00-248	23.5	30.0	0.4	20.5	5.0	11.0	5.5	127.5	4.2	215.0	1.5	0.6
DDH- 00-254	24.0	15.0	0.3	20.0	25.0	8.0	5.4	96.4	4.1	228.0	1.5	0.6
DDH-00-254 600'	19.0	5.0	0.3	17.0	35.0	7.0	4.4	67.8	3.2	255.0	1.0	0.5
POGO-02 98-93	40.5	5.0	0.5	32.5	55.0	17.0	9.3	100.0	6.2	243.0	10.0	0.9
POGO-02 98-176	38.5	20.0	0.6	30.0	5.0	15.0	9.0	202.0	6.2	50.1'	19.0	0.9
POGO-02 97-75	6.0	30.0	0.2	5.0	5.0	15.0	1.6	244.0	1.5	69.7	15.5	0.4
POGO-02 247-318	30.0	10.0	0.4	25.0	5.0	10.0	7.0	115.0	5.0	235.0	6.0	0.7
POGO-02 98-105-745	18.0	20.0	0.4	16.0	20.0	7.0	4.4	60.0	3.5	306.0	5.0	0.6
POGO-02 263-286	34.0	25.0	0.7	28.0	<5	9.0	8.0	158.5	6.1	187.5	13.0	1.0
POGO-02 00-249-386	87.5	10.0	0.3	37.0	<5	113.0	12.9	113.5	5.2	334.0	14.5	0.6
POGO-02 249-799	37.5	20.0	0.5	28.5	<5	13.0	8.2	112.0	5.2	196.5	12.5	0.7
POGO-02 249-1010	20.5	30.0	0.4	18.0	<5	23.0	5.0	182.0	4.6	160.0	12.5	0.8
POGO-02 249-512	7.0	35.0	0.3	6.0	<5	15.0	1.8	173.5	1.7	74.0	18.0	0.5
POGO-02 247-661	91.0	10.0	0.3	41.5	5.0	118.0	13.9	125.0	6.1	348.0	20.5	0.7
POGO-02 263-744.5	9.0	35.0	0.3	6.5	5.0	14.0	2.1	173.5	1.9	82.0	15.5	0.4
POGO-02 249-1020	19.0	10.0	0.6	20.0	5.0	8.0	5.2	65.6	4.8	333.0	5.5	0.9

Table 2-2c. Continued

SAMPLE	trace/REE (ppm)										
	Ti	Th	Tm	Sn	W	U	V	Yb	Y	Zn	Zr
POGO-00-R6	-	53.0	0.1	2.0	203.0	4.0	35.0	1.1	14.5	25.0	179.0
POGO-00-R12	-	29.0	0.2	1.0	152.0	2.0	45.0	1.4	16.0	40.0	214.0
POGO-00-R14	-	2.0	0.1	19.0	230.0	5.0	<5	1.0	10.0	30.0	66.0
POGO-00-R16	-	3.0	0.2	15.0	144.0	3.0	<5	1.6	13.5	30.0	23.5
POGO-00-R17	-	12.0	0.6	1.0	115.0	2.0	95.0	3.3	30.0	70.0	84.5
POGO-00-R29	-	9.0	0.7	2.0	33.0	2.5	140.0	4.2	45.0	120.0	312.0
POGO-00-R32	-	4.0	0.3	1.0	31.0	1.5	265.0	2.0	20.0	90.0	106.5
POGO-00-R34	-	10.0	0.3	1.0	79.0	2.0	60.0	1.8	19.5	65.0	135.5
POGO-00-R38	-	13.0	0.3	1.0	49.0	3.5	125.0	1.7	16.5	85.0	187.0
POGO-00-R39	-	12.0	0.3	3.0	35.0	2.0	140.0	1.6	17.5	70.0	176.0
POGO-00-R51	-	6.0	0.2	1.0	101.0	2.5	45.0	1.4	15.5	80.0	131.0
POGO-00-R52	-	6.0	0.2	1.0	173.0	2.0	70.0	1.2	14.5	2530.0	106.0
POGO-00-R90	-	16.0	0.5	4.0	112.0	2.0	70.0	2.8	26.0	45.0	157.5
POGO-00-R94	-	5.0	0.3	1.0	112.0	2.0	255.0	2.1	20.5	85.0	115.5
POGO-00-R95	-	5.0	0.3	1.0	54.0	2.0	250.0	1.9	19.0	90.0	99.5
POGO-00-R96	-	9.0	<0.1	<1	145.0	2.5	15.0	0.7	8.5	25.0	117.5
POGO-00-R97	-	10.0	0.2	<1	112.0	3.0	65.0	1.5	17.0	80.0	204.0
POGO-00-R99	-	9.0	0.3	<1	110.0	2.5	65.0	1.6	15.5	85.0	125.0
POGO-00-R100	-	10.0	0.3	<1	99.0	2.0	90.0	2.1	20.0	95.0	119.0
POGO-00-R105	-	7.0	0.4	1.0	88.0	1.5	200.0	2.4	26.5	65.0	101.5
POGO-00-R114	-	16.0	0.4	3.0	118.0	2.0	90.0	2.6	25.0	60.0	169.5
POGO-00-R117	-	9.0	0.4	1.0	107.0	2.0	175.0	2.1	21.0	80.0	124.5
POGO-00-R119	-	4.0	0.4	<1	453.0	0.5	275.0	2.3	21.0	85.0	103.0
POGO-00-R134	-	8.0	0.4	1.0	112.0	2.5	250.0	2.1	20.5	75.0	109.0
SP-00-09	-	18.0	0.2	5.0	224.0	4.5	50.0	1.3	15.0	60.0	123.5
SP-00-12	-	30.0	0.7	1.0	297.0	6.5	15.0	4.0	42.0	20.0	227.0
SP-00-14	-	18.0	0.4	2.0	159.0	2.5	45.0	2.4	25.5	40.0	156.0
MAPT-14	-	17.0	0.5	3.0	99.0	3.0	70.0	3.5	26.5	55.0	162.0
MAPT-7	-	13.0	0.1	1.0	214.0	3.5	15.0	0.8	9.5	25.0	112.5
KGG -14	-	4.0	0.3	2.0	112.0	1.5	65.0	2.1	19.0	55.0	136.5
POGO-01-100B	-	7.0	0.1	1.0	177.0	1.5	15.0	0.9	8.0	10.0	213.0
POGO-01-101B	-	5.0	0.2	1.0	145.0	2.0	5.0	1.6	18.0	<5	38.5
POGO-01-104	-	1.0	0.1	4.0	146.0	0.5	<5	1.4	12.5	<5	14.5
POGO-01-106	-	8.0	0.1	5.0	185.0	3.0	55.0	1.3	16.5	210.0	120.5
POGO-01-109	-	7.0	0.3	<1	52.0	1.5	130.0	2.2	22.0	80.0	119.5
POGO-01-122	-	13.0	0.6	<1	160.0	2.0	<5	4.7	37.0	5.0	124.0
POGO-01-123	-	5.0	0.4	4.0	168.0	4.0	<5	2.5	27.0	10.0	33.0
POGO-01-126	-	6.0	0.3	1.0	65.0	1.5	155.0	1.9	19.0	95.0	130.0
POGO-01-129	-	5.0	0.3	1.0	27.0	2.0	225.0	1.9	18.5	105.0	98.0
POGO-01-131	-	4.0	<0.1	<1	48.0	0.5	35.0	0.5	5.5	95.0	122.0
POGO-01-137	-	8.0	0.3	2.0	79.0	1.5	25.0	1.8	18.0	15.0	98.0
POGO-01-144	-	15.0	0.3	1.0	51.0	0.5	85.0	2.0	22.0	60.0	154.5
POGO-01-152	-	15.0	0.1	2.0	55.0	3.5	65.0	1.3	16.0	90.0	188.0
POGO-01-162	-	12.0	0.3	1.0	67.0	3.0	20.0	2.4	24.5	30.0	152.5
POGO-01-165	-	9.0	0.2	1.0	97.0	2.0	5.0	1.4	15.5	15.0	85.0
POGO-01-167	-	14.0	0.2	<1	43.0	4.0	70.0	1.3	16.0	75.0	155.0
POGO-01-169	-	13.0	0.2	1.0	92.0	2.0	15.0	1.3	16.0	25.0	126.5
POGO-01-170	-	5.0	0.3	<1	44.0	1.5	115.0	2.1	19.5	95.0	121.5
POGO-01-171	-	8.0	0.1	1.0	130.0	2.0	15.0	1.3	14.0	30.0	190.0
DDH- 00-248	-	6.0	0.4	<1	142.0	1.5	90.0	2.4	22.0	30.0	110.5
DDH- 00-254	-	9.0	0.3	1.0	48.0	3.0	130.0	2.0	19.5	75.0	144.0
DDH-00-254 600'	-	7.0	0.2	<1	42.0	2.0	145.0	1.8	17.0	75.0	94.5
POGO-02 98-93	-	17.0	0.5	3.0	232.0	3.0	130.0	2.8	27.0	60.0	199.5
POGO-02 98-176	-	48.0	0.6	2.0	444.0	8.5	5.0	3.6	28.5	15.0	101.0
POGO-02 97-75	-	4.0	0.2	11.0	322.0	10.0	<dl	1.5	13.5	15.0	25.0
POGO-02 247-318	-	15.0	0.4	7.0	160.0	3.5	100.0	2.2	22.0	50.0	144.0
POGO-02 98-105-745	-	8.0	0.3	2.0	122.0	2.0	235.0	2.1	20.0	80.0	95.0
POGO-02 263-286	0.5	26.0	0.6	2.0	325.0	6.5	10.0	4.0	35.0	15.0	98.5
POGO-02 00-249-386	<0.5	72.0	0.3	2.0	227.0	29.0	35.0	1.7	17.0	15.0	151.5
POGO-02 249-799	<0.5	25.0	0.4	4.0	316.0	6.5	35.0	2.6	23.0	35.0	126.0
POGO-02 249-1010	0.5	12.0	0.4	5.0	257.0	5.0	20.0	2.4	24.0	40.0	70.0
POGO-02 249-512	0.5	6.0	0.3	6.0	415.0	13.5	<5	2.1	21.5	25.0	20.0
POGO-02 247-661	<0.5	72.0	0.3	1.0	298.0	18.5	30.0	2.0	19.5	15.0	160.0
POGO-02 263-744.5	0.5	8.0	0.3	6.0	364.0	20.5	5.0	1.6	17.5	20.0	23.5
POGO-02 249-1020	<0.5	6.0	0.5	3.0	133.0	1.5	225.0	3.3	31.0	80.0	77.0

These rock names are reasonably consistent with names based on visually estimated modal mineral percentages.

The intrusive rocks are all dominantly weakly peraluminous to weakly metaluminous ($Al/CNK < 1.2$) with a few moderately peraluminous samples (Figure 2-12). Based on mineralogy, the granite and tonalite suites are more peraluminous whereas the younger diorite suite is notably metaluminous. General compositional fields for rocks of the Tombstone Plutonic Suite of Yukon Territory and east-central Alaska are included in the diagrams as shaded areas for comparison. Figure 2-11 demonstrates that the rocks of the Goodpaster district are generally of the same geochemical character as the TPS rocks, however no alkalic rocks, which are a minor but important component of the TPS (Lang et al., 2001), are known.

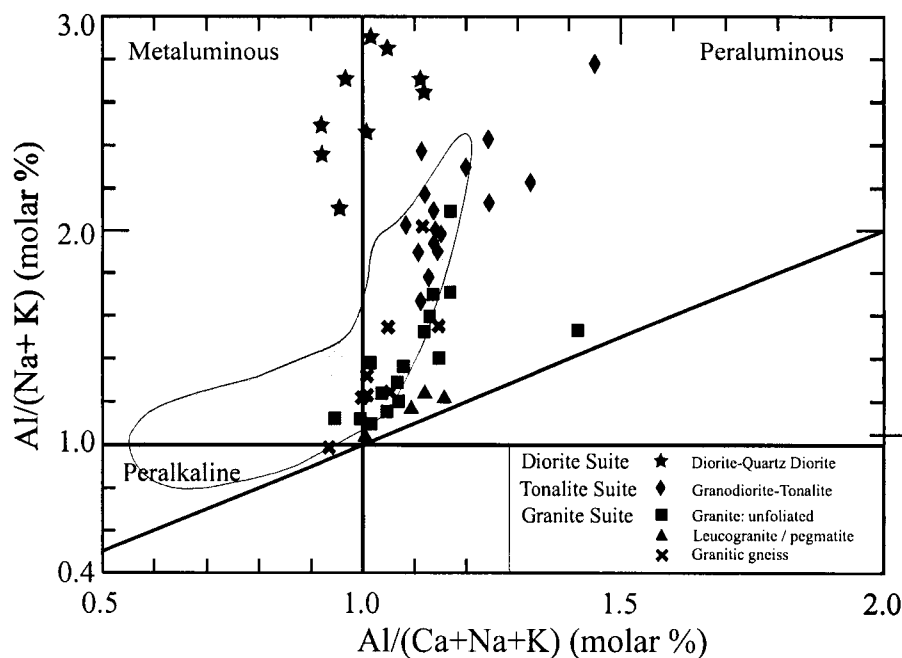


Figure 2-12. Shand's peraluminosity index (Maniar and Piccoli, 1989). The intrusive rocks in the Goodpaster district are weakly metaluminous to weakly peraluminous. The shaded field represents rocks of the Tombstone Plutonic Suite (Lang et al., 2001).

Silica content for the granite suite ranges from 70 to 87 wt.%, the tonalite suite ranges from 62 to 72 wt. % and the diorite suite ranges from 50 to 63 wt. %. Fine-grained quartz-rich intrusive rocks (SiO_2 between 74 and 87 wt. %) of the granite suite may be transitional into the quartz veins. These samples were obtained from granitic phases exploiting shallowly dipping fabrics as shown in Figure 2-10.

Harker variation diagrams (Figure 2-13) show common trends within each of the three suites. Harker variation diagrams are not shown to demonstrate a differentiation trend between the three suites because the three suites are temporally distinct and are probably not comagmatic. Silica in each of the three suites demonstrate strongly negative correlations with TiO_2 , FeO , Fe_2O_3 , MnO , MgO , and CaO whereas K_2O and Na_2O show a weakly positive correlation, Al_2O_3 is poorly correlated and P_2O_5 shows a constant correlation. Alkaline elements show some scatter possibly reflecting post emplacement alteration and alkali exchange. Distinct compositional gaps occur between 1 to 1.5 wt. % MgO and 2.0 to 2.5 wt. % MgO (Figure 2-13, center). Although this may be due to sampling bias, these gaps seem to represent a fundamental change in whole rock geochemistry between the three suites.

TRACE AND RARE EARTH ELEMENT GEOCHEMISTRY

Rare earth element (REE) data of the representative intrusive suite rocks are listed in Table 2-2 and are graphically presented as chondrite normalized (REE_{CN}) and primitive mantle normalized (REE_{PM}) diagrams on Figure 2-14. The data is normalized to chondrite and primitive mantle REE values of Sun and McDonough (1989). Intrusive rocks of the Tombstone Plutonic Suite rocks are represented by the shaded pattern and are shown in the background for comparison.

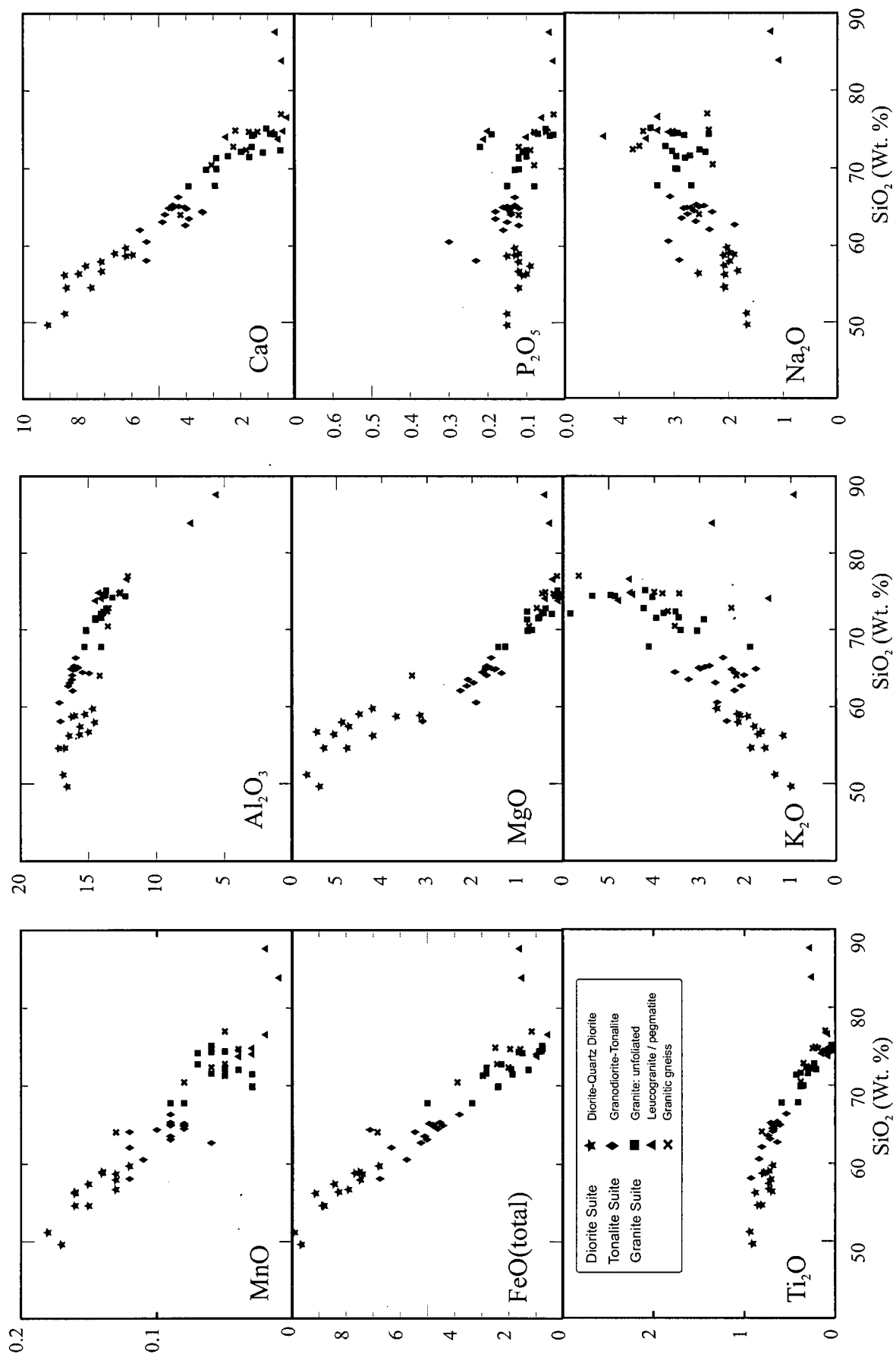


Figure 2-13: Harker variation diagrams showing the trends within each of the three plutonic suites. The two triangles that are silica-rich (> 80 wt. % SiO_2) are from quartz-rich intrusive rocks that exploit shallowly dipping structures such as shown in Figure 2-10.

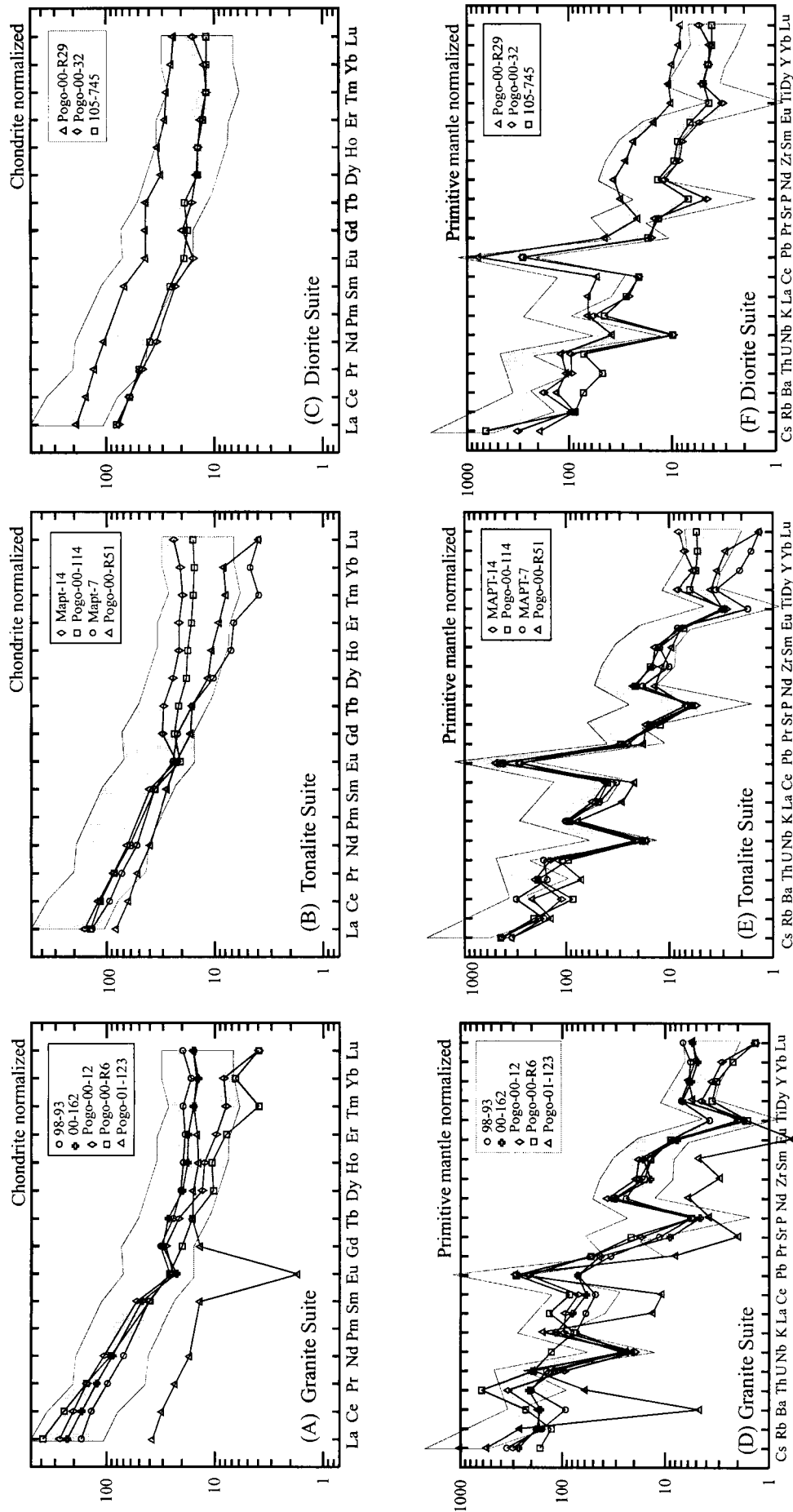


Figure 2-14: Chondrite-normalized rare earth element (REE_{CN}) plots for (A) granite suite samples and (C) diorite suite samples. Primitive mantle normalized extended plots (REE_{PM}) for representative intrusive rocks of the (D) granite suite and (F) diorite suite. Normalizing values for chondrite and primitive mantle values are from Sun and McDonough (1989). Granite Suite sample descriptions: 98-93: fine-grained biotite-hornblende granitic orthogneiss, 00-262: medium- to coarse-grained biotite granite, Pogo-00-R12: coarse-grained, weakly foliated biotite-hornblende biotite tonalite, Pogo-00-114: coarse-grained mica granite (and representative of pegmatite). Tonalite Suite sample descriptions: Mapt-14: coarse-grained hornblende-biotite tonalite, Pogo-00-114: coarse-grained hornblende-biotite tonalite, Pogo-00-R51: fine-grained biotite tonalite. Diorite Suite sample descriptions: Pogo-00-R29: coarse-grained hornblende-rich quartz monzodiorite, Mapt-7: fine-grained biotite-hornblende diorite, 106-745: medium-grained biotite-pyroxene-hornblende diorite.

Medium- to coarse-grained rocks of the granite suite, including orthogneiss and granite (samples 98-93 and 01-165 respectively), show enriched (105-130X), moderately sloping light rare earth element (LREE) patterns and weakly enriched (20X), dish shaped patterns of heavy rare earth elements (HREE) on REE_{CN} diagrams (Figure 14-a). This dish shaped pattern is suggestive of hornblende being present as a residual phase (Rollinson, 1993). Negative europium anomalies are moderate to small. Finer-grained granite suite samples (Pogo-00-12 and Pogo 00-R6) have a similar LREE enrichment and slope, however HREE patterns slope steeply with an absent to weak negative Eu anomaly. The presence of residual garnet in the source may be indicated by this large HREE depletion (Rollinson, 1993). An explanation for the differences in HREE is not obvious, but could reflect mineralogical differences due to sample sizes of coarser grained material. REE_{PM} diagrams for both fine- and coarse-grained samples generally exhibit large negative Nb and Ti anomalies (Figure 2-14d).

Differentiated phases of pegmatite and leucogranite, represented by sample Pogo-01-123 (Figure 2-14a), display a less enriched (20-30X), shallowly sloping LREE pattern and a weakly enriched (4-10X), relatively flat pattern for HREEs. Although distribution coefficients for the LREE in most minerals predict that these minerals should behave incompatibly during crystallization and increase with fractionation (Miller and Mittlefehldt, 1982), the more fractionated pegmatite and aplite show a progressive decrease in the LREE contents. This behaviour is attributed to the fractionation of accessory monazite or allanite (Miller and Mittlefehldt, 1982) and is consistent with the greater degree of fractionation of a volatile-rich melt (Pearce et al. 1984; Christiansen and Keith, 1996). The overall flattening of the REE patterns is consistent with increased differentiation of a peraluminous pluton (Miller and Mittlefehldt, 1982). The differentiated phases also exhibit variable Eu anomalies and negative Ti and Nb anomalies on primitive mantle normalized diagrams (Figure 2-14d).

Tonalite suite samples show similar REE_{CN} patterns to the granite suite but have more shallowly sloping and less enriched LREE patterns (80-105X)(Figure 2-14b). Negative europium anomalies are small to absent. Two HREE patterns are present that are similar to those found in the granite suite: coarse-grained, hornblende-biotite tonalite from the Goodpaster Batholith (MAPT-14 and Pogo-00-114) has a dish-shaped HREE pattern while fine-grained biotite granodiorite to tonalite (MAPT-7 and Pogo-00-R51) has a steeper HREE pattern. These fine-grained samples intruded ~ 2 km south of the Goodpaster Batholith. The change in the HREE pattern may be attributed to the presence of hornblende in the coarse-grained samples, which concentrates more HREE-bearing minerals (i.e. zircon; Rollinson, 1993). All tonalite samples have large to moderate negative Nb and Ti anomalies on REE_{PM} diagrams (Figure 2-14e)

Intrusive rocks of the diorite suite show distinct REE_{PM} patterns when compared to the granite and tonalite suites. Rocks of the diorite suite have an overall shallow sloping REE_{CM} pattern, with moderately enriched (100X) LREEs and weakly enriched (10X) HREEs (Figure 2-14c). Negative europium anomalies are very small to absent. Europium anomalies, large negative Nb anomalies, and small negative Ti anomalies are shown on the REE_{PM} diagram. (Figure 2-14f).

TECTONIC DISCRIMINATION

Nb/Y and Rb/Y+Nb tectonomagmatic discrimination diagrams of Pearce et al. (1984) are presented in Figure 2-15. A majority of the rocks have compositions consistent with volcanic arc magmatism, with the exception of three granitic orthogneiss samples which have elevated Nb values and plot in the within plate field. This effect may be attributable to fractionation (Pearce et al., 1984) rather than a change in magmatic setting.

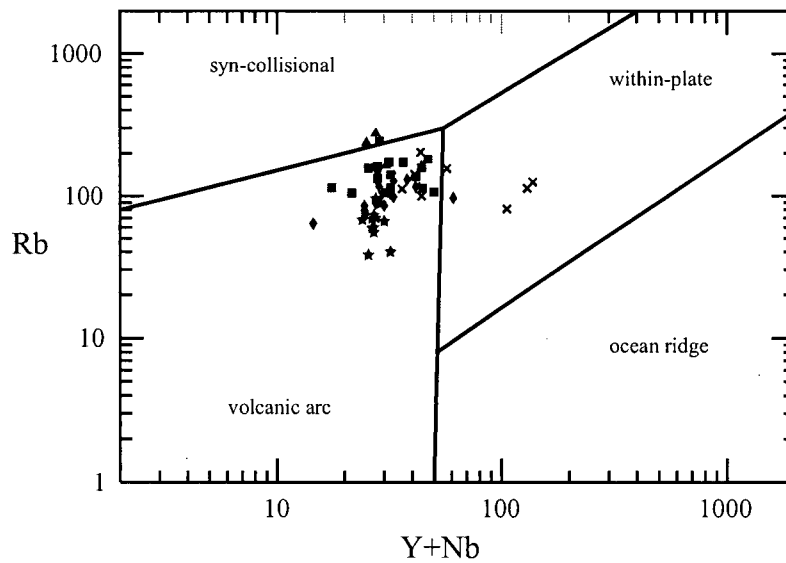
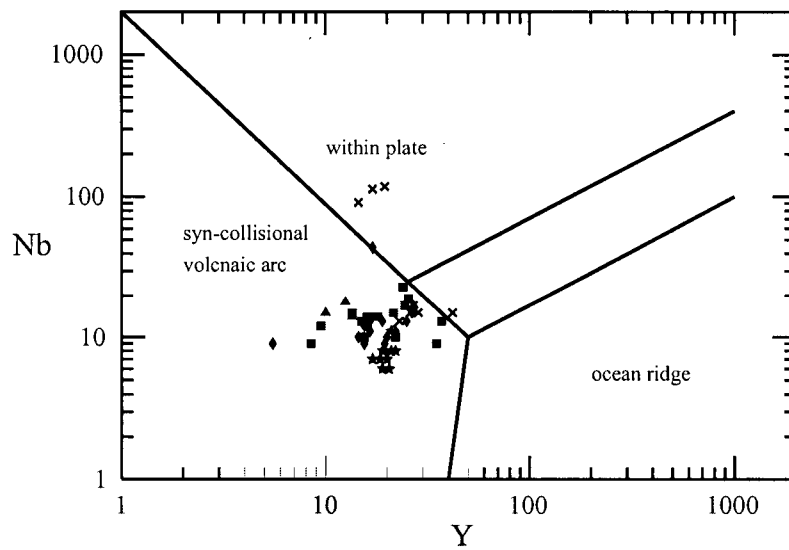


Figure 2-15: Tectonodiscrimination diagrams after Pearce et al. (1984). The intrusive suites show an affinity for a volcanic arc setting, with the exception of three orthogneiss samples which have elevated Nb values and fall in the within plate field. This effect may be attributable to fractionation (Pearce, 1994) rather than a change in magmatic setting. Symbols are the same as those used in Harker variation diagrams (Figure 2-13)

Incompatible trace element distributions (Figure 3-14), except for the highly differentiated samples, are typical of calc-alkaline arc magmas (Perfit et al., 1980). They are characterized by large ion lithophile element (LILE) enrichment and high field strength (HFSE) depletion resulting in high LILE/HFSE ratios. This, coupled with low normalized abundances of Nb, Ti and P with respect to primitive mantle values, is also characteristic of typical I-type subduction related granitoids formed in a magmatic arc setting (Wilson, 1989; Chappell and White, 1992; Christiansen and Keith, 1996).

The intrusive rocks normalized to the North American shale curve (Gromet et al., 1984) produce a relatively flat pattern near unity (Figure 2-16). This suggests there was a significant chemical contribution to intrusions from continentally derived sediments, as the curve represents average sedimentary rocks in continental platforms. This observation is consistent with the presence of abundant inherited zircon in most of the samples dated in this study.

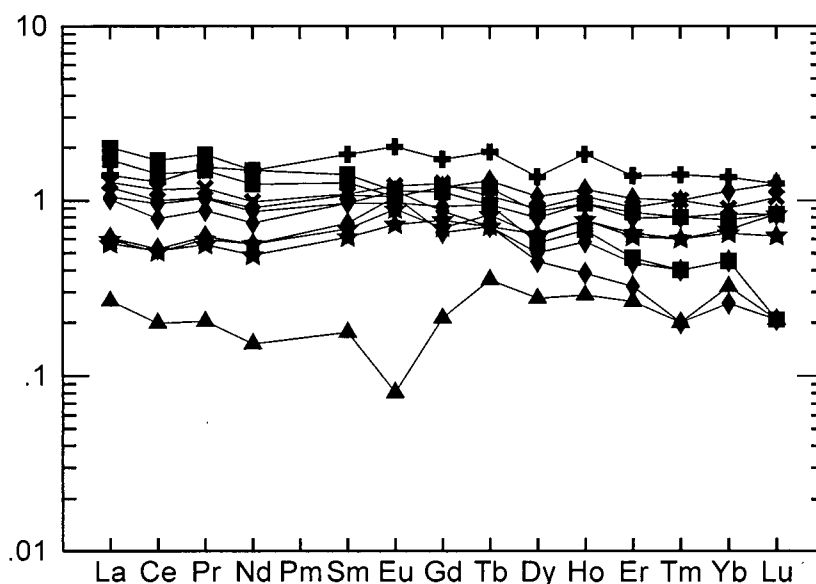


Figure 2-16: Selected intrusive rock samples normalized to the North American Shale Curve (Gromet 1984). All values are near unity. Data and symbols are the same as those used in REECN and REEPM plots in Figure 2-12.

BULK MAGNETIC SUSCEPTIBILITY

Bulk magnetic susceptibility was measured with a hand held Exploranium KT-9 Kappa meter on 45 hand samples of representative intrusive rocks. Magnetic susceptibility is a measure of the abundance of ferromagnetic minerals (i.e. magnetite), and to a lesser extent paramagnetic minerals (i.e. hornblende and pyroxene) in a rock sample.(Reynolds, 1997).

The granite and tonalite suites are defined by very low magnetic susceptibility values (0-0.2) and the diorite suite is defined by slightly higher values (0.2-1.29) (Figure 2-17). The higher values for the diorite suite are consistent with the presence of trace primary magnetite, abundant paramagnetic minerals, and correlation with magnetic highs on the aeromagnetic map of the region. Although the diorite suite values are higher relative to the granite and tonalite suite rocks, overall values are still very low, less than 1.29×10^{-3} SI units.

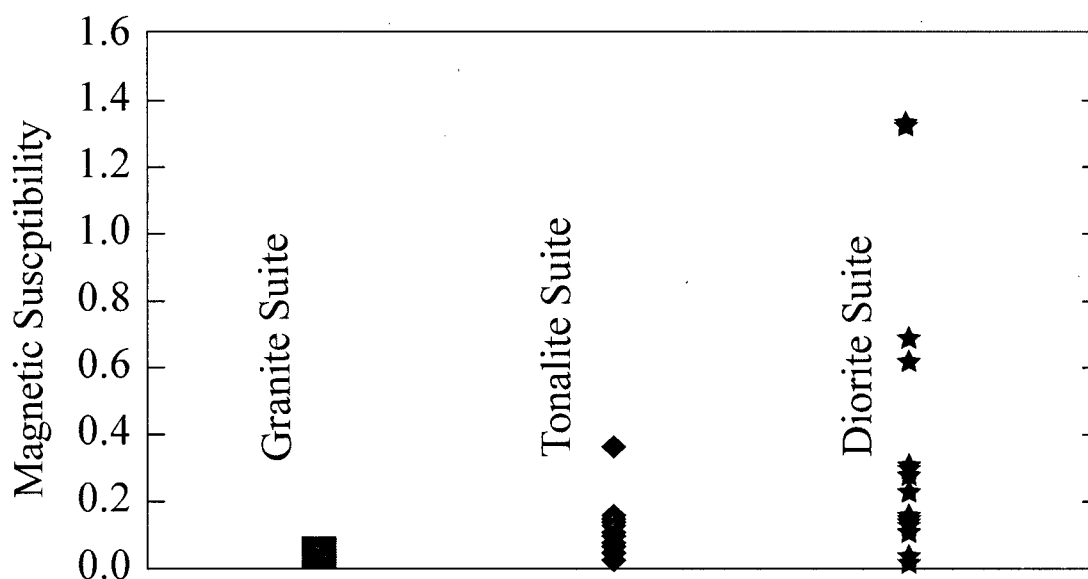


Figure 2-17. Magnetic susceptibility ($\times 10$ S.I. units) of 45 intrusive rocks samples. Uncertainty increases systematically with reading magnitude (Duncan, 1999). Number of samples measured: granite suite ($n = 19$), tonalite suite ($n = 11$), diorite suite ($n = 15$)

OXIDATION STATE

The oxidation state for the intrusive rocks was calculated using the Fe_2O_3 (T) and FeO analysis obtained from whole rock geochemistry. The reported Fe_2O_3 (T) is the value of total iron in a sample analysed by X-ray fluorescence (XRF) assuming all iron is ferric. The reported FeO is the actual ferrous value of the sample determined by HCl-HF acid digestion and titrimetric finish. The oxidation state ($\text{Fe}_2\text{O}_3 / \text{FeO} + \text{Fe}_2\text{O}_3$) was constructed by converting Fe_2O_3 (T) to Fe_2O_3 (actual ferric value) using the equation $\text{Fe}_2\text{O}_3 = \text{Fe}_2\text{O}_3 \text{ (T)} - (1.1113)(\text{FeO})$.

$\text{Fe}_2\text{O}_3 / \text{FeO} + \text{Fe}_2\text{O}_3$ ratios of intrusive rocks in the Goodpaster district range between 0.06-0.45, averaging 0.18 (Figure 2-18). These values are consistent with the oxidation state of reduced granite in Alaska associated with productive gold occurrences (Leveille et al., 1988; Burns et al., 1991) which have $\text{Fe}_2\text{O}_3 / \text{FeO} + \text{Fe}_2\text{O}_3$ values less than 0.6. The very low oxidation state is also supported by the presence of abundant accessory ilmenite and rare primary magnetite. Two samples (tonalite and leucogranite) have anomalously high ferric values. This may be attributed to moderate hydrothermal alteration and/or surface weathering (Duncan, 1999); they have been omitted from the diagram.

McCoy et al. (1997) attribute the reduced oxidation state of the intrusive rocks in the Fairbanks district to interaction and assimilation with the reduced sedimentary rocks of the Yukon-Tanana Terrane or due to assimilation of reduced gases derived from the sedimentary strata. These same reducing processes are likely to have occurred in Goodpaster district as well and are consistent with the petrological and geochemical evidence for significant crustal contamination of the magmas. Carbonaceous material is common throughout the Yukon-Tanana Terrane and rare graphite schist observed in drill core from the Liese zone indicates highly reduced metasedimentary rocks locally underlie the region. Minor primary magnetite occurs only in the diorite suite rocks and may reflect slightly more oxidizing conditions for this younger

intrusive suite. The low oxidation state generally correlates with the observed low magnetic susceptibilities.

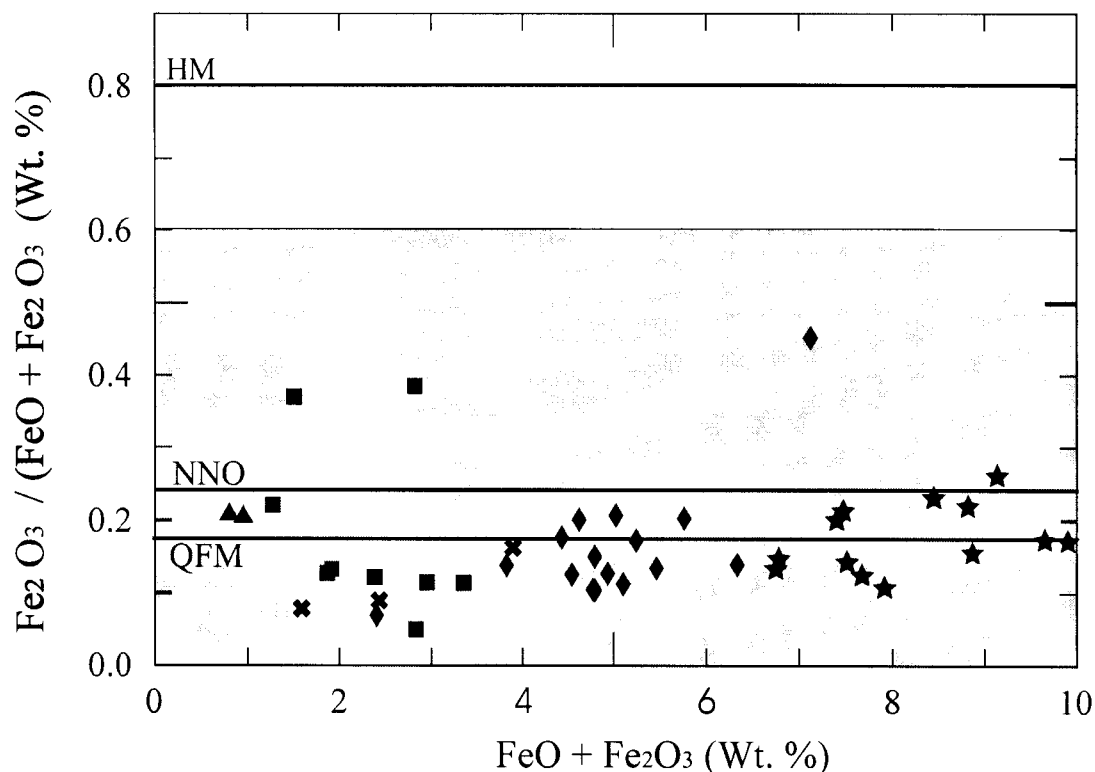


Figure 2-18: $\text{Fe}_2\text{O}_3 / (\text{FeO} + \text{Fe}_2\text{O}_3)$ (wt. %) versus $\text{FeO} + \text{Fe}_2\text{O}_3$ (wt. %) values for intrusive rocks in the Goodpaster district. The quartz-magnetite-fayalite (QFM), nickel nickel-oxide (NNO) and hematite-magnetite (HM) buffers (after Duncan, 1999) are shown for reference. The shaded area represents the oxidation state for productive granitic rocks in Alaska (Leveille et al., 1998). Symbols are the same as those used in geochemical diagrams. Squares, triangles and X's = granite suite, diamonds = tonalite suite and stars = diorite suite.

PB ISOTOPE STUDY

A lead isotope study was undertaken to help characterize the various igneous rock suites, to obtain information on the source of magmas, and to help provide a framework to evaluate metal sources for the gold-bearing quartz veins. Eleven feldspar separates from the various intrusive suites in the district were analysed for their lead isotopic compositions, in addition to fourteen sulphide mineral separates from gold-bearing quartz veins and one base metal vein.

The feldspar and sulphide lead isotopic compositions are commonly interpreted as initial values because little uranium is incorporated into these minerals. This limits the change in isotopic composition through time-integrated growth

Lead isotopic compositions were determined using a modified VG54R thermal ionization mass spectrometer at the PCIGR Laboratory at the University of British Columbia, Vancouver. Measured isotopic compositions were corrected for instrumental mass fractionation of 0.15 % per mass unit based on replicate analyses of NBS SRM981 and the recommended values of Todt et al. (1996).

Results from the intrusive rocks are reported in Table 2-3 and plotted on $^{208}\text{Pb}/^{204}\text{Pb}$ versus $^{206}\text{Pb}/^{204}\text{Pb}$ and $^{207}\text{Pb}/^{204}\text{Pb}$ versus $^{206}\text{Pb}/^{204}\text{Pb}$ covariation diagrams (Figure 2-19). The shale curve of Godwin and Sinclair (1982) has been plotted in the figures for isotopic reference. This curve was developed for the northern Cordillera in western Canada and represents the time-integrated Pb isotopic history of the Canadian miogeocline and also approximates the evolution of upper crustal lead in the Yukon Tanana Terrane (Lang et al., 1993). Lead isotopic compositions are also plotted for Cretaceous to Tertiary granite (McCoy et al., 1997; Aleinikoff et al., 2000) and Devonian to Mississippian gneiss from east-central Alaska (Aleinikoff et al., 2000) for comparison. They are represented as light grey and dark grey shades respectively. No isotopic values are available for the metasedimentary rocks in east-central Alaska.

The granite and diorite suites, the oldest and youngest suites in the Goodpaster district respectively, define two distinct Pb isotopic populations (Figure 2-19a). The granite suite, which includes orthogneiss, granite, two-mica granite, and pegmatite has higher $^{206}\text{Pb}/^{204}\text{Pb}$ values and a fairly homogenous Pb isotope population ($^{206}\text{Pb}/^{204}\text{Pb}$ = 19.39 to 19.50, $^{207}\text{Pb}/^{206}\text{Pb}$ = 0.80 to 0.81; $^{208}\text{Pb}/^{204}\text{Pb}$ = 39.45 to 39.67, $^{208}\text{Pb}/^{206}\text{Pb}$ = 2.02 to 2.04). The diorite suite has lower Pb isotopic values ($^{206}\text{Pb}/^{204}\text{Pb}$ = 19.15, $^{207}\text{Pb}/^{204}\text{Pb}$ = 15.70, $^{208}\text{Pb}/^{204}\text{Pb}$ = 39.13, $^{208}\text{Pb}/^{206}\text{Pb}$ = 40.0),

Table 2-3: Lead isotope analytical data from feldspar mineral separates of the granite suite, tonalite suite, diorite suite and a rhyolite dyke in the Goodpaster district.

Sample ¹	Location	Rock type ²	Mineral ³	²⁰⁶ Pb/ ²⁰⁴ Pb	Error %	²⁰⁷ Pb/ ²⁰⁴ Pb	Error %	²⁰⁸ Pb/ ²⁰⁴ Pb	Error %	²⁰⁷ Pb/ ²⁰⁶ Pb	Error %	²⁰⁸ Pb/ ²⁰⁶ Pb	Error %
Granite Suite													
POGO 16-b	North Zone	bt-mu leucogranite	pl	19.403	0.018	15.764	0.016	39.501	0.047	0.812	0.000	2.036	0.001
MAPT 21 -c	Liese Zone	pegmatite	pl	19.481	0.008	15.755	0.010	39.555	0.034	0.809	0.000	2.030	0.001
GDI97-71	Liese Zone	bt-granodiorite	fs	19.481	0.009	15.766	0.010	39.614	0.035	0.809	0.000	2.033	0.001
98-176	Liese Zone	orthogneiss	pl	19.786	0.012	15.798	0.011	39.997	0.040	0.798	0.000	2.022	0.001
OGNU 98-93 -a	Liese Zone	orthogneiss	pl	19.434	0.009	15.749	0.010	39.602	0.035	0.810	0.000	2.038	0.001
PEGM 98-93 -b	Liese Zone	pegmatite	pl	19.448	0.008	15.759	0.010	39.556	0.034	0.810	0.000	2.034	0.001
Tonalite Suite													
SP00-14	Shawnee peak	bt-hbl granite	kf	19.499	0.009	15.744	0.011	39.624	0.035	0.807	0.000	2.032	0.001
MAPT 14 -c	Goodpaster Batholith	bt-hbl tonalite	pl	19.478	0.010	15.781	0.011	39.566	0.037	0.810	0.000	2.031	0.001
MAPT 7 -b	Football Field	bt granodiorite	pl	19.186	0.010	15.739	0.011	39.211	0.036	0.820	0.000	2.044	0.001
Diorite Suite													
105-745 -b	Liese Creek	bt-px-hbl diorite	pl	19.150	0.008	15.702	0.010	39.126	0.034	0.820	0.000	2.043	0.001
Rhyolite Dyke													
Mapt-5	Star	rhyolite dyke	pl	19.567	0.020	15.726	0.023	39.351	0.076	0.804	0.000	2.011	0.002

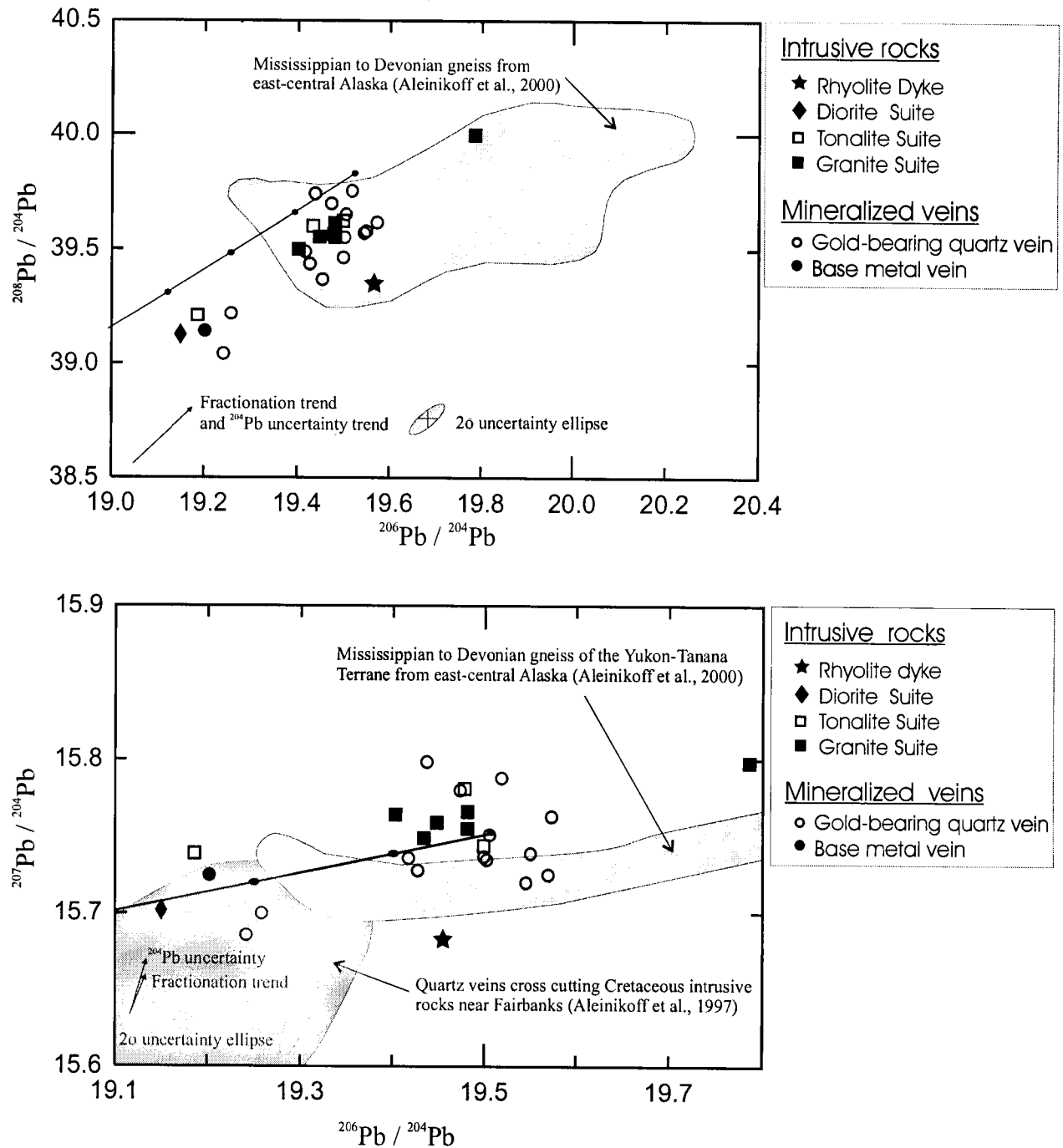
1. All analyses analysed by Janet Gabites at the PCIGR Laboratory at the University of British Columbia, Vancouver.

All ratios corrected for isotopic fractionation (0.15‰ per atomic mass unit), based on repeated analyses of NBS SRM981 lead standard.

2. Bt = biotite, hbl = hornblende, px = pyroxene

3. Minerals analysed: fs = feldspar undifferentiated, pl = plagioclase, kf = potassium feldspar

Uncertainties are obtained by numerically propagating all mass fractionation and analytical uncertainties through the calculations and are presented at the 2σ level.



though only one sample was analysed. The diorite sample analysed is from Pogo creek and is inferred to cut the Liese zone quartz veins (Smith et al., 1999). One granitic orthogneiss sample (98-176) has an anomalously high Pb isotope value ($^{206}\text{Pb}/^{204}\text{Pb} = 19.8$). This sample is highly sericitically altered and the anomalous value may reflect hydrothermal alteration of the feldspars.

The tonalite suite, which includes the Goodpaster Batholith and Shawnee Peak stock, has Pb isotopic compositions that overlap the fields defined for both the granite and the diorite suites. An explanation for this is not obvious. It could reflect the slightly more mafic composition of the tonalite suite in comparison to the granite suite, and thus potentially represent a varying mix between magmas of similar Pb isotopic character as the older granite suite and younger diorite suite. It is also equally important to recognize that Pb isotopic data is available for only three samples within the tonalite suite. Thus, it is uncertain whether the tonalite suite actually has two distinct Pb isotopic populations, or whether a more complete data set would show a continuum between the two fields of isotopic composition. Note that Pb isotopic compositions were not obtained from the youngest tonalite sample of the Goodpaster Batholith (sample Kgg-14; 93.7 Ma). Eocene quartz-feldspar phyric rhyolite dykes have Pb isotopic values that are distinct from the Cretaceous intrusive rocks. They likely derived their Pb isotopic signature from the Yukon Tanana Terrane.

The granite suite has higher $^{206}\text{Pb}/^{204}\text{Pb}$ values than those reported for Cretaceous to Tertiary granite rocks from east-central Alaska (Aleinikoff et al., 2000; McCoy et al., 1997) and overlaps the lower $^{206}\text{Pb}/^{204}\text{Pb}$ values of Devonian to Mississippian gneiss in east-central Alaska (Aleinikoff et al., 2000) as shown in Figure 2-19. The diorite suite overlaps with the lower $^{206}\text{Pb}/^{204}\text{Pb}$ values of Cretaceous to Tertiary granite rocks from east-central Alaska (Aleinikoff et al., 2000; McCoy et al., 1997).

Sulphides from gold-bearing quartz veins from various prospects in the Goodpaster district also show two isotopically distinct fields. Sulfide minerals from gold-bearing quartz veins of the Liese zone and nearby prospects form a relatively tight Pb isotopic population, with $^{206}\text{Pb}/^{204}\text{Pb}$ values of about 19.5 to 19.6. These values overlap the granite suite, and some of the tonalite suite, and suggest they shared a common Pb source. The sulphide minerals range to slightly higher $^{206}\text{Pb}/^{204}\text{Pb}$ values, which could be explained by some fluid-rock interaction with the highly radiogenic host gneiss.

A base metal vein containing stibnite, galena, and pyrite from Shawnee Peak and two distal gold-bearing quartz veins have low Pb isotopic values ($^{206}\text{Pb}/^{204}\text{Pb}= 19.1$ to 19.3). These samples have Pb isotopic compositions similar to the younger, early Late Cretaceous diorite suite and one of the tonalite suite samples. These veins may not be related to the main gold-mineralizing event. For a comprehensive discussion of Pb isotopic values for the gold-bearing quartz veins, see Chapter 3.

DISCUSSION

EVOLUTION OF THE GRANITIC SUITES IN THE GOODPASTER DISTRICT

Three plutonic suites were emplaced into paragneiss of the Yukon Tanana Terrane in the Goodpaster district during the late Early Cretaceous and early Late Cretaceous. The three suites are subdivided on the basis of field relationships, geochronology, geochemistry, and lithology: a granite suite (~109-107 Ma), a tonalite suite (~107-103 Ma) and a diorite suite (~94 Ma). The plutonic suites were emplaced syn-to post-kinematic into a complex, polydeforming terrane. Early intrusive phases emplaced ~109 Ma are deformed (Dilworth et al., 2002) and were emplaced during final stages of regional metamorphism and ductile deformation, whereas the younger ones are only weakly deformed to undeformed. Undeformed varieties have U-Pb ages

similar to those of the weakly deformed granites. An U-Pb zircon age of 107.3 ± 0.2 Ma for foliated gneiss provides the minimum age of regional metamorphism in the area (Appendix A). Deformation and metamorphism were complete by $107.3 + 0.8$ Ma, when the oldest unfoliated granite was emplaced.

Similar relationships that constrain the timing of regional metamorphism to the late Early Cretaceous are demonstrated in the Mount Haynes Quadrangle, approximately 55 km south of the Goodpaster district. Granitic plutonic rocks there intruded during the waning stage of major regional amphibolite facies metamorphic conditions during the Early Cretaceous (Nokleberg and others, 1996; Aleinikoff et al., 2000) and thus are broadly synchronous with that documented in the Goodpaster district.

The granite suite, and possibly some of the tonalite suite, is inferred to locally intrude as flat lying sheets that exploit shallowly dipping structures. These tabular granitic sheets may be apophyses off a larger, unrecognized pluton at depth or injected as tongues, veins or dykes extending from the Goodpaster Batholith into the Goodpaster district. The relationship between shallowly dipping fabrics and granite sheets suggests that shallowly dipping regional structures are important and may have provided a structural pathway for magma migration. Whether pluton emplacement occurred by instigation of its own sub-horizontal fracture pattern during emplacement at depth or exploited the mechanical anisotropy created by the S2 foliation or low angle syn-metamorphic faults cannot be established with available data.

The Goodpaster Batholith, the largest intrusion in the Goodpaster district, has a narrow range of whole rock and mineral compositions based on the southern portion which was part of this study. Although it is interpreted that much of the Batholith crystallized during the late Early Cretaceous at about 106 Ma, a petrologically identical younger phase crystallized during the early Late Cretaceous at 93.7 Ma. The petrologic similarity coupled with lack of outcrop makes

it impossible to map individual intrusive phases within the Goodpaster Batholith. Although no lead isotopic analyses were acquired from the younger sample, the variable lead isotopic data from the tonalite suite combined with the two U-Pb ages suggests the Goodpaster Batholith has a complex history, and is composed of multiple intrusive phases that were not previously recognized.

MAGMATIC SOURCE

The REE profiles, primitive mantle normalized trace element patterns, and negative Nb and Ti anomalies all suggest that the intrusive rocks in the Goodpaster district were derived from a mantle source (Peccerillo et al., 1988) in a magmatic arc setting. However, the intrusive rocks in the Goodpaster district lack the large negative Eu anomalies that are expected due to differentiation of a mantle-derived magma from subduction processes (Selby et al., 1999). Therefore, although there is an affinity for subduction related processes, the trace element subduction signature may also be produced by partial melting of material previously related to subduction processes (Johnston and Wyllie, 1988; Morris and Hooper, 1997) and thus does not rule out the possibility that the rocks are entirely crustally derived and have inherited the arc signature (Whalen et al., 1998; Taylor and McLennan, 1985).

Mantle-derived rocks have low initial lead concentrations and therefore the Pb isotopic composition of a granite commonly reflects the crust with which it is associated (Farmer and DePaolo, 1983; Davidson, 1996). The Pb isotope compositions of the granite, and parts of the tonalite suite, have elevated $^{206}\text{Pb}/^{204}\text{Pb}$ values which is consistent for rocks of old, upper crustal origin (Tosdal et al., 1999). Conversely, the lower $^{206}\text{Pb}/^{204}\text{Pb}$ values seen in the younger diorite suite, and parts of the tonalite suite, indicate a lesser influence by old radiogenic crust (Tosdal et al., 1999). This trend is consistent with the Pb isotopic variation documented in the Cretaceous

to Tertiary intrusive rocks of east-central Alaska: the intrusive rocks become less radiogenic with decreasing age (Aleinikoff et al., 2000; Goldfarb et al., 2000).

No Sr or Nd isotopic data are available for intrusive rocks in the Goodpaster district. However, samples of Cretaceous granitic rocks from east-central Alaska are characterized by a decrease in $^{87}\text{Sr}/^{86}\text{Sr}$ values (0.7413 to 0.7064) and an increase in ϵNd values (–21.4 to –5.8) with decreasing age (Aleinikoff et al., 2000). It is probable that intrusive rocks in the Goodpaster district would show similar Sr and ϵNd isotopic characteristics.

Snyder et al. (2002) suggest the Yukon Tanana Terrane in southern Yukon is less than 10 km thick. If this is also the case in east-central Alaska then the magma in the Goodpaster district would probably have interacted mainly with thicker underlying North American continental crust. The Pb isotopic data indicates either significant crustal contamination of a mantle-derived magma, or complete partial melting of continental crust to produce the granitoids in the Goodpaster district. The mildly peraluminous nature of the intrusive rocks, ubiquitous inherited zircon component, rare earth element geochemistry and local presence of garnet and two-mica granite all suggest that the continental crust played an important role in the magma genesis. The degree of crustal involvement, however, is difficult to assess as little is known about the thickness and composition of the crust underlying the Yukon Tanana Terrane in east-central Alaska (Snyder et al., 2002).

RELATIONSHIP TO OTHER REDUCED INTRUSIONS RELATED TO GOLD DEPOSITS

The intrusive rocks in the Goodpaster district are typical of reduced intrusions associated with gold mineralizing events in Alaska and Yukon (McCoy et al., 1997; Leveille et al., 1988; Lang et al., 1999). The reduced granitoids have oxidation states less than 0.45, and have a spatial and temporal association with reduced gold-bearing quartz veins (Chapter 3). Although

the rocks locally have S-type affinities, overall they are classified as reduced I-type intrusions (Chappell and White, 1992; Lang et al., 1999). The reduced nature of the intrusions is supported by the presence of abundant ilmenite, rare magnetite and the low magnetic susceptibilities. The low oxidation state may be attributed to interaction and reduction of the magma with reduced metasedimentary rocks of the Yukon Tanana Terrane (McCoy et al., 1997, Aleinikoff et al., 2000).

DEPTH OF EMPLACEMENT

The lack of coeval Cretaceous volcanic rocks and mariolitic cavities, and the occurrence of intrusions of batholith proportions are consistent with relatively deep emplacement levels for the felsic granitoids in the Goodpaster district (Flannigan et al., 2000). Preliminary Al-in-hornblende barometry on two samples from the Goodpaster Batholith indicate the granitoids in the Pogo region were emplaced at a depth of 5-9 km, based on pressure estimates averaging $\sim 2 \pm 1$ kbar (range: 1.32 – 2.55 kbar).

Note that the iron-rich, low fO_2 granites that characterize the intrusive phases in the Goodpaster district may not be amenable to application of the hornblende barometer. All the intrusive rocks in the Goodpaster district straddle the QFM buffer and none of the empirical calibrations have been conducted at low fO_2 at or below the QFM buffer. The role of fO_2 is fundamentally important, as low fO_2 can cause calculated pressures to be higher by a factor or two or more (Anderson and Smith, 1995). The hornblende Fe/Fe + Mg ratio from the two samples (0.62-0.69) also lies slightly above the acceptable range of 0.40 to 0.65 (Anderson and Smith, 1995). The ~ 2 kbar pressure estimate is also at the lower end of the calibrated limit of 2 kbar for which the barometer is experimentally based.

Nevertheless, the ~2 kbar pressure estimate is consistent with the 1.4 to 2.4 kbar pressure estimates obtained from fluid inclusion from gold-bearing quartz veins of the 4021 prospect and the felsic intrusions were emplaced at 7 ± 2 km depths. For a detailed study on the fluid inclusion pressure estimates see Chapter 3.

CORRELATION WITH CRETACEOUS PLUTONIC SUITES IN YUKON

Numerous mid-Cretaceous plutonic suites have been recognized and described in Yukon (Figure 2-3) based on lithology, age and geochemistry (Mortensen et al. 2000; Lang et al., 2001). Table 2-4 summarizes the main features of each of the plutonic suites, based mostly from intrusions in Yukon. The continuation of these suites into east-central Alaska, with the exception of the Tombstone plutonic suite, is poorly understood. A number of the plutonic suites (e.g. Anvil, Tay River and South Lansing suite) appear to overlap in east-central Alaska and no longer form spatially distinct suites (Mortensen, personal communication 2003).

The intrusive rocks in the Goodpaster district are not related to the Tombstone Plutonic Suite (TPS) on the basis of spatial distribution, age, and lithology. The TPS lies north of the Goodpaster district (Figure 2-1) and forms younger (93-86 Ma; McCoy et al., 1997), smaller bodies. Intrusive rocks of batholithic proportions that are prevalent in eastern Alaska, such as the Goodpaster Batholith are notably absent in the TPS (Mortensen, personal communication 2003). Furthermore, the intrusive rocks of the Goodpaster district are more peraluminous, lack the alkalic and porphyritic phases that are typical of the TPS and contain monazite, which are not present in TPS intrusions (Lang et al., 2001).

Although the granite and tonalite suites in the Goodpaster district are age equivalent to the Whitehorse-Coffee Creek Suite (111-99 Ma; Mortensen, 2000) they most closely resemble intrusive rocks of the more northerly Anvil Suite of Yukon Territory (112-100 Ma) and may be

Table 2-4. Summary of the Cretaceous Intrusive suites in Yukon and Alaska (Mortensen et al., 2000; Lang and others, 2001)

	Tombstone Plutonic Suite	Anvil Suite	Cassiar Suite	Tay River Suite ^C	South Lansing Suite	Whitehorse-Coffee Creek Suite
Age	89 to 94.5 Ma	100 to 107 Ma, 112 Ma ^a	110-99 Ma	98-95 Ma	93 to 95 Ma	99 to 111 Ma
Geochemistry	subalkaline to alkaline metaluminous	subalkaline peraluminous	subalkaline peraluminous minor metaluminous	subalkaline weakly peraluminous	subalkaline strongly peraluminous	subalkaline metaluminous
Texture	Porphyritic to K-feldspar megacrystic, with lesser seriate to equigranular phases. Lacks monazite.	weakly foliated, equigranular		equigranular to seriate		equigranular to porphyritic
Main Lithologies	Bt ± hbl granodiorite to quartz monzonite	Bt-Mu quartz monzonite, granite, and granite	biotite granite and granodiorite	hbl-bt granodiorite and quartz monzonite aplite and pegmatite common	granodiorite to quartz monzonite biotite only mafic mineral, contains monazite	bt-hbl granodiorite and quartz monzonite, monzodiorite
Subordinate Lithologies	syenite, gabbro, diorite and lamprophyre	hornblende + plagioclase phyric diorite dykes	Mu or Hbl-bearing of granodiorite to granite	quartz diorite, monzonite		Bt-Mu quartz monzonite, quartz diorite and granite.
Examples	Emerald Lake Batholith Tombstone Range	Anvil Batholith (Mt. Mye phase ^a) Mt. Carmacks Batholith Fanning Batholith Mt. Billings	Logtung porphyry	Anvil Batholith (Marjore and Orchard Phase) Coal River Batholith	Moose Creek pluton MacArthur Range Pluton South Lansing Pluton	Whitehorse batholith Dawson Range Batholith Casino Plutonic Suite

Abbreviations: Bt=biotite; Mu=muscovite; Hbl=hornblende

A = U-Pb age for the Mt. Carmacks pluton and intrusions in the Finlayson Lake region

B = Anvil Suite from Pigage and Anderson (1985)

C = Tay River suite is the former Transitional Suite of Gordey and Anderson (1993)

the western continuation of the Anvil suite into east-central Alaska (Mortensen et al., 2000). The plutonic rocks of the Anvil suite are subalkaline and consist of peraluminous muscovite-biotite granite and metaluminous to peraluminous hornblende-biotite granodiorite to granite. The Mt. Billings Batholith (106.4 ± 0.4 Ma; Heffernan and Mortensen, 1999) is age equivalent to the Goodpaster Batholith and Shawnee Peak intrusions and forms equigranular, biotite-hornblende bearing monzonite to granodiorite. The Anvil suite is also syn- to post-kinematic with respect to deformation and metamorphism (Pigage and Anderson, 1985).

The early Late Cretaceous diorite suite resembles the Tay River Suite of Mortensen et al., (2000) (formerly the "transitional plutons" of Gordey and Anderson, 1993), although it is less widespread in Alaska than in Yukon. The Tay River Suite is age equivalent (98 to 95 Ma) to the diorite suite rocks. Most intrusions of the Tay River suite are hornblende-biotite granodiorite with rare quartz diorite. Additionally, no mineralization is known to be associated with this suite (Mortensen et al., 2000).

CONCLUSIONS

Whole rock geochemistry, petrography and geochronology permit the division of the intrusive granitoids in the Goodpaster district into three Cretaceous suites: a granite, tonalite, and diorite suite. New U-Pb ages presented in this study, in addition to mapping, demonstrate the late Early Cretaceous granite and tonalite suites are more widespread than previously recognized and are more dominant than the younger, early Late Cretaceous diorite suite. The granite and tonalite suites differ from the younger diorite suite based on the presence of the trace minerals monazite and allanite, and the generally more peraluminous mineralogy. In contrast, the diorite suite lacks monazite, has a metaluminous mineralogy, and contains primary magnetite.

The granite and tonalite suites form an arcuate, easterly belt of intrusions ~ 2 km south of the Goodpaster Batholith with which the Liese zone and related prospects are spatially related. Geochronology indicates that the tonalite suite (~105 Ma) is roughly coeval with gold deposition (~104 Ma) and Pb-isotopic data show Pb in the granite suite, and some of the tonalite suite, samples have a similar source of Pb to the gold-bearing quartz veins.

The Goodpaster Batholith contains phases that are older than previously suggested (Smith et al., 1999; Smith et al., 2000) and forms a composite granodiorite to tonalite intrusion. Based on pressure estimates from the Al-in-hornblende geothermobarometer, the Goodpaster Batholith was emplaced at depths of 5-9 km.

All intrusive rocks in Goodpaster district are reduced, ilmenite series granitoids. Shallowly dipping regional fabrics or faults appear to play an important role during early pluton emplacement by providing structural pathways and producing the elongate east-west trending belt of granite to tonalite intrusions. Geochemical data suggest that the plutons were probably mantle-derived but were extensively contaminated by continental crust. Lead isotope compositions are consistent with the granite suite having been derived from, or contaminated by, either the North American or Yukon Tanana Terrane crustal rocks. The diorite suite has distinctly less radiogenic lead isotopic compositions. Plutonic rocks in the Goodpaster district are not related to the Tombstone Plutonic Suite. Instead, the granite and tonalite suites may be the western continuation of the Anvil Suite into east-central Alaska. The Late Cretaceous diorite suite is most likely the western equivalent of the Tay River Suite.

REFERENCES:

- Aleinikoff, J.N., and Nokleberg, W.J., 1985a, Age of intrusions and metamorphism of a granodiorite in the Lake George subterrane, northeastern Mount Hayes Quadrangle, *In* Bartsch-Winkler, S., and Reed, K.M., eds., The United States Geological Survey in Alaska; Accomplishments during 1983: U.S. Geological Survey Circular 945, p. 62-65.
- Aleinikoff, J.N., Farmer, G.L. Rye, R.O., and Nokleberg, W.J. 2000. Isotopic evidence for the sources of Cretaceous and Tertiary granitic rocks, east-central Alaska; implications for the tectonic evolution of the Yukon-Tanana terrane. *Canadian Journal of Earth Sciences*, **37**: 945-956.
- Anderson, J.L., and Smith, D.R., 1995. The effects of temperature and fO_2 on the Al-in-hornblende barometer. *In*: *American Mineralogist*, v. 80, p. 549-559.
- Bakke, A.A., 1995, The Fort Knox 'porphyry' gold deposit-Structurally controlled stockwork and shear quartz vein, sulfide-poor mineralization hosted by a Late Cretaceous pluton, east-central Alaska, *in* Schroeter, T.G., ed., Porphyry deposits of the North-western Cordillera of North America: Canadian Institute of Mining, Metallurgy and Petroleum Special, v. 46, p. 795-802.
- Bundtzen, T.K. and Miller, M.L., 1997, Precious metals associated with Late Cretaceous - Early Tertiary igneous rocks of southwestern Alaska, *in* Goldfarb, R.J., and Miller, L.D., eds., Mineral deposits of Alaska: Economic Geology Monograph 9
- Burns, L.E., Newberry, R.J., and Solie, D.N., 1991, Quartz normalative plutonic rocks of interior Alaska and their favourability for association with gold: Alaska Division of Geological and Geophysical Survey Reports of Investigations, 91-3, 58 p.
- Chappell, B.W., and White, A. J. R. 1992. I- and S-type granites in the Lachlan fold belt. *Transactions of the Royal Society of Edinburgh*, **83**: 1-26.
- Christiansen, E.H., and Keith, J.D. 1996. Trace element systematics in silicic magmas. A metallogenic perspective. *In* Trace element geochemistry of volcanic rocks: Applications for massive sulphide exploration: Geological Association of Canada, Short Course notes. Edited by D.A. Wymann, **12**: 115-151
- Churkin, M., Jr., Foster, H.L., Chapmand, R.M. and Weber, F.R., 1982. Terranes and suture zones in east-central Alaska: *Journal of Geophysical Research*, v. 87, no. B5, p. 3718-3730.
- Coulsen, I.M., Villeneuve, M.E., Dipple, G.M., Duncan, R.A., Russell, J.K. and Mortensen, J.K., 2002. Time-scales of assembly and thermal history of a composite felsic pluton: constraints from the Emerald Lake area, northern Canadian Cordillera, Yukon. *Journal of Volcanology and Geothermal Research*, **114**: 331-356.

- Cox, K.G., Bell, J.D. and Pankhurst, R.J., 1979, The interpretation of igneous rocks. George, Allen and Unwin, London.
- Davidson, J.P., 1996, Deciphering mantle and crustal signatures in subduction zone magmatism: American Geophysical Union Monograph 96, p. 251-262.
- Day, W.D., Aleinikoff, J.N., Dusel-Bacon, C., Goldfarb, R., Gough, L.P. and O'Neill, J.M., 2002, Complex Mesozoic deformation in the central part of the Yukon Tanana Uplands, Alaska -Implications for gold deposition in the Tintina Gold Province, Geological Society of America Programs with Abstracts.
- Dilworth, K.M., Ebert, S.E., Mortensen, J.K., Rombach, C., Tosdal, R.M., 2002. Reduced granites and gold veins in the Pogo Area, east-central Alaska. Geological Society of America Programs with Abstracts.
- Duncan, R. A., 1999. Physical and Chemical Zonation in the Emerald Lake Pluton, Yukon Territory: Masters Thesis, University of British Columbia, 179 p.
- Dusel-Bacon, Cynthia, and Foster, H.L., 1983, A sillimanite gneiss dome in the Yukon crystalline terrane, east-central Alaska: Petrography and garnet-biotite geothermometry: U.S. Geological Survey Professional Paper 1170-E, 25 p.
- Dusel-Bacon, C., and Aleinikoff, J.N., 1985. Petrology and tectonic significance of augen gneiss from a belt of Mississippian granitoids in the Yukon-Tanana terrane, east-central Alaska. Geological Society of American Bulletin, 96: 411-425.
- Dusel-Bacon, C., and Aleinikoff, J.N., 1996, U-Pb zircon and titanite ages for augen gneiss from the divide mountain area, eastern Yukon-Tanana Upland, Alaska, and Evidence for the composite nature of the Fiftymile Batholith, *in* Moore, T.E and Dumoulin, J.A., eds, Geologic Studies in Alaska by the U.S. Geological Survey Bulletin 2552, p. 131-141.
- Dusel-Bacon, C., and Hanson, V.L., 1991, High-pressure, medium-temperature early Mesozoic metamorphism and deformation within the Yukon-Tanana composite terrane, eastern Alaska [abs]: Geological Society of America Abstracts with Programs, v. 23, p. 20.
- Dusel-Bacon, C., and Hanson, V.L., 1992, High-pressure amphibolite-facies metamorphism and deformation within the Yukon Tanana Terrane and Taylor Mountain terranes east-central Alaska, *in* Bradley, D.W., and Dusel-Bacon, C., eds., Geological Survey Bulletin 2041, p. 140-158.
- Ebert, S., Miller, L., Petsel, S., Dodd, S., and Kowalczyk, P., 2000, Geology, Mineralization, and Exploration at the Donlin Creek Project, Southwest Alaska: *in* The Tintina Gold Belt: Concepts, Exploration, and Discoveries, Special Volume 2, British Columbia and Yukon Chamber of Mines, pp. 99-114.

- Farmer, G.L., and DePaolo, D.J., 1983, Origin of Mesozoic and Tertiary granite in the western United States and implications for pre-Mesozoic crustal signature: 1, Nd and Sr isotopic studies in the geocline of the northern Great Basin: *Journal of Geophysical Research*, v. 88, p. 3379-3401.
- Flannigan, B., Freeman, C., McCoy, D., and Hart, C., 2000. Paleo-Reconstruction of the Tintina Gold Belt-Implications for mineral exploration. In *The Tintina Gold Belt: Concepts, exploration, and discoveries*, British Columbia and Yukon Chamber of Mines Cordilleran Roundup Special Volume 2, Vancouver, British Columbia, p. 34-48.
- Foster, H.L., Keith, T.E., and Menzie, W.D. 1994. Geology of the Yukon-Tanana terrane of east-central Alaska. In *the geology of Alaska: Boulder, Colorado, Geological Society of America, The geology of North America*, v. G-1. *Edited by G. Plafker and H.C. Berg*, pp. 205-240.
- Godwin, C.I., and Sinclair, A.J. 1982. Average lead isotope growth curves for shale-hosted zinc-lead deposits, Canadian Cordillera. *Economic Geology*, 77: 208-211.
- Goldfarb, Hart, C., Miller, M., Miller, L., Farmer, G.L., Groves, D., 2000, The Tintina Gold Belt-A Global Perspective, *In The Tintina Gold Belt: Concepts, exploration, and discoveries*, British Columbia and Yukon Chamber of Mines Cordilleran Roundup Special Volume 2, Vancouver, British Columbia, pp. 5-34.
- Gordey, S.P., and Anderson, R.J., 1993, Evolution of the northern Cordilleran miogeocline, Nahanni map area (1051), Yukon and Northwest Territories: *Geological Survey of Canada Memoir* 428, 214 p.
- Gromet, L.P., Dymek, R.F., Haskin, L.A., Korotev, R.L. 1984. The "North American shale composite": its compilation, major and trace element characteristics. *Geochemica et Cosmochimica Acta*, 48: 2469-2482.
- Hart, C.J.R., Baker, T., and Burke, M., 2000. New exploration concepts for country-rock hosted, intrusion-related gold systems. *In The Tintina Gold Belt: Concepts, exploration, and discoveries*, British Columbia and Yukon Chamber of Mines Cordilleran Roundup Special Volume 2, Vancouver, British Columbia, p. 132-145.
- Hart, C.J.R., McCoy, D.T., Goldfarb, R.J., Smith, M., Roberts, P., Hulstein, R., Bakke, A.A., and Bundtzen, R.K., 2002, *Geology, Exploration, and Discovery in the Tintina Gold Province, Alaska and Yukon*, in *Society of Economic Geologists Special Publication* 9, p. 241-274.
- Heffernan, R.S., and Mortensen, J.K., 1999, Age, geochemical, and metallogenic investigations of Cretaceous intrusions in southwestern Yukon and southwestern NWT: A preliminary report, In *Yukon Exploration and Geology*, Esmond, D.S and L.H. Weston (eds), p. 145-149.

- Irvine, T.N., and Baragar, W.R.A., 1971. A guide to the chemical classification of the common volcanic rocks. *Canadian Journal of Earth Sciences*, **8**: 523-548.
- Lang, I. M., Nokleberg, W.J., Newkirk, S.R., Aleinikoff, J.M. Church, S.E., and Krouse, H.R., 1993. Devonian volcanogenic massive sulphide deposits and occurrences, southern Yukon-Tanana terrane, eastern Alaska Range, Alaska: Economic
- Lang, J.R., Baker, C.J.R. Hart, and J.K. Mortensen. 2000, An exploration model for intrusion-related gold systems: *Society of Economic Geologists Newsletter*, v 40,1, 6-15.
- Lang, J. R, Thompson, J.F., Mortensen, J.K., Baker, C.J.R., Coulsen, I.M., Duncan, R., and Maloof, T., 2001. Tombstone-Tungsten Belt. *In* Lang, J., *eds* Regional and system-scale controls on the formation of copper and/or gold magmatic-hydrothermal mineralization. Mineral Deposit Research Unit, Special Publication Number 2, January 2001.
- LeBas, M.J., Le Maitre, R.W., Streckeisen, A., and Zanettin, B., 1986. A chemical classification of volcanic rocks based on the total alkali-silica diagram. *Journal of Petrology*, **27**: 745-750.
- Leveille, R.A., Newberry, R.J. & Bull, K.F. (1988). An oxidation state-alkalinity diagram for discriminating some gold-favourable plutons: an empirical and phenomenological approach. *Geological Society of America, Abstracts with program* 20, A142.
- Johnston, A.D., and Wyllie, P.J., 1988. Constraints on the origin of Archean trochjemetes based on phase relations of the Nuk gneiss with H₂O at 15 kbar. *Contributions to Mineralogy and Petrology*, v 100: 35-46.
- Maniar, P.D. and Piccoli, P.M. 1989. Tectonic discrimination of granitoids. *Geological Society of America Bulletin*, **101**: 635-643.
- McCoy, D., Newberry, R.J., Layer, P., Dimarchi, J.J., Bakke, A., Masterman, J.S. & Minehane, D.L. 1997. Plutonic-related gold deposits of interior Alaska. *In* Mineral deposits of Alaska, Economic Geology Monograph 9, *Edited by* R.J. Goldfarb and L.D. Miller, pp. 191-241.
- Miller, C. F., and Mittlefehdt, D.W. 1982. Depletion of light rare-earth elements in felsic magmas. *Geology*, **10**: 129-133.
- Moore, K., 2000. Geology of the gold-bearing L1 and L2 Lise quartz zones, Pogo Deposit, east-central Alaska: Masters Thesis, Colorado School of Mines, June 2000.
- Morris, G.A., and Hooper, P.R. 1997. Petrogenesis of the Colville igneous complex, northeast Washington: implications for Eocene tectonics in the northern U.S. Cordillera. *Geology*, v. 25: 831-834.

- Mortensen, J.K., Ghosh, D., and Ferri, F., 1995, U-Pb age constraints of intrusive rocks associated with Copper-Gold porphyry deposits in the Canadian Cordillera, *in* Schroeter, T.G., ed., *Porphyry deposits of the northwestern Cordillera of North America*: Canadian Institute of Mining and Metallurgy, Special Volume 46, pp. 142-158.
- Mortensen, J.K., Hart, C.J.R., Murphy, D.C., and Heffernan, S., 2000. Temporal evolution of Early and Mid-Cretaceous magmatism in the Tintina Gold Belt. *In* *The Tintina Gold Belt: Concepts, exploration, and discoveries*, British Columbia and Yukon Chamber of Mines Cordilleran Roundup Special Volume 2, Vancouver, British Columbia, pp. 49-57.
- Nokleburg, W.J., Aleinikoff, J.N., and Lange, I.M., 1993, Origin and accretion of Andean-type and island arc terranes of Paleozoic age juxtaposed along the Hines Creek fault, Mount Hayes Quadrangle, eastern Alaska Range, Alaska: *Geological Society of America Abstracts with Programs*, v. 15, p. 427.
- Newberry, R.J. 2000. Mineral deposits and associated Mesozoic and Tertiary igneous rocks within the interior Alaska and adjacent Yukon portions of the "Tintina Gold Belt": A progress report. *In* *The Tintina Gold Belt: Concepts, exploration, and discoveries*, British Columbia and Yukon Chamber of Mines Cordilleran Roundup Special Volume 2, Vancouver, British Columbia, pp. 59-88.
- Page, R.A., Plafker, G., and Pulpan, H., 1995, Block rotation in east-central Alaska: A framework for evaluation earthquake potential?: *Geology*, v. 23, p. 629-632.
- Park, V., 1999. Brewery Creek project 1998 exploration progress report, January 20th, 1999. Viceroy exploration (Canada) Inc. company report.
- Pavlis, T.L., Sisson, V.B., Foster, H.L., Nokleberg, W.J., and Plafker, George, 1993, Mid-Cretaceous extensional tectonics of the Yukon-Tanana terrane: Trans-Alaska Crustal Transect (TACT), east-central Alaska, *Tectonics*, v. 12, p. 1031-1042.
- Pearce, J.A., Harris, N.B.W., and Tindle, A.G. 1984. Trace element discrimination diagrams for the tectonic interpretation of granitic rocks. *Journal of Petrology*, 25: 956-983.
- Peccerillo, A., Poli, G., and Serri, G. 1988. Petrogenesis of andesitic and kamafugitic rocks from central Italy. *Canadian Mineralogist*, v. 26: 45-65.
- Pigage, L.C., and Anderson, R.G., 1985, The Anvil plutonic suite, Faro, Yukon Territory. *Canadian Journal of Earth Sciences*, 22, 1204-1216.
- Perfit, M.R., Gust, D.A., and Bence, A.E., Arculus, R.J., and Taylor, S.R. 1980. Chemical characteristics of island-arc basalts: implications for mantle sources. *Chemical Geology*, v. 30: 227-256.

- Plafker, G., and Berg, H.C. 1994. Overview of the geology and tectonic evolution of Alaska. *In* The geology of Alaska: Boulder, Colorado, Geological Society of America, The geology of North America, v. G-1. *Edited by* G. Plafker and H.C. Berg, pp. 989-1021.
- Reynolds, J.M. 1997, An introduction to Applied and Environmental Geophysics. Chichester: John Wiley & Sons.
- Rhys, D., DiMarchi, J., Rombach, C., Smith, M., Friesen, R. (in press). Structural setting, style and timing of vein-hosted gold mineralization at the Pogo deposit, east-central Alaska: 38 p.
- Rollinson, H.R. 1993. Using geochemical data: evaluation, presentation, and interpretation. Longman Group Limited, Essex, England, 352 p.
- Rowins, S. M., 2000. Reduced porphyry copper-gold deposits: A new variation on an old theme. *Geology*, v. 28; no. 6; p. 491-494.
- Selby D, Creaser RA, Hart C.J., Rombach C.S., Thompson J.F.H., Smith M. T., Bakke A, Goldfarb R., (in press). Timing of sulphide and gold mineralization at the Fort Knox and Pogo gold deposits, Tintina Gold Belt, Alaska: Evidence from Re-Os molybdenite dates for distinct gold mineralization episodes. *Geology*: v. 30, No. 9, pp. 791-794.
- Selby, D., Creaser, R.A., and Nesbitt, B.E. 1999. Major and trace element compositions and Sr-Nd-Pb systematics of crystalline rocks from the Dawson Range, Yukon, Canada. *Canadian Journal of Earth Sciences*, **36**: 1463-1481.
- Smith, M., Thompson, J., Bressler, J., Layer, P., Mortensen, J., Takaoka, I., 1999. Geology of the Liese Zone, Pogo Property, East-Central Alaska: Society of Economic Geologists Newsletter, No. 38, p. 11-21.
- Smith, M.T., J.F.H. Thompson, K.H. Moore, J.R. Bressler, P. Layer, J.K. Mortensen, I. Abe, and H. Takaoka. 2000, The Liese zone, Pogo Property: A new high-grade gold deposit in Alaska, *in* Tucker, T.L., and Smith, M.T., eds., The Tintina Gold Belt: Concepts, exploration and discoveries: British Columbia- Yukon Chamber of Mines, Cordilleran Round-Up Special Volume 2, p. 131-144.
- Snyder, D.B., Clowes, R.M., Cook, F.A., Erdmer, P, Evenchick, C.A., Van der Velden, A.J. and Hall, K.W., 2002. Proterozoic Prism Arrests Suspect Terranes: Insights into the Ancient Cordilleran Margin from Seismic Reflection Data. *GSA Today*, v. 12, no. 10, pp. 4-10.
- Streckeisen, A. (1976). To each plutonic rock its proper name. *Earth Science Reviews*, 12, 1-33.
- Sun, S.S., and McDonough, W.F. 1989. Chemical and isotopic systematics of oceanic basalts: implications for mantle composition and processes. *In* Magmatism in the ocean basins, Geological Society Special Publication 42. *Edited by* A.D. Saunders and M.J. Norry, pp. 313-345.

- Taylor, S.R., and McLennan, S.M. 1985. The continental crust: its composition and evolution. Blackwell Scientific Publications, Oxford, U.K., 311 pp.
- Thompson, J.F.H., and R.J. Newberry. 2000, Gold deposits related to reduced granitic intrusions, *in* Hagemann, S.G., and Brown, P.E., eds., Gold in 2000: Reviews in Economic Geology, v.13 ,377–400.
- Thompson J.F.H., Sillitoe RH, Baker T, Lang J.R., Mortensen J.K. (1999). Intrusion-related gold deposits associated with tungsten-tin provinces. *Mineral Deposita* 34: 323-334.
- Todt, W., Cliff, R.A., Hanser, A., and Hofman, A.W., 1996. Evaluation of a $^{202}\text{Pb}/^{205}\text{Pb}$ double spike for high-precision lead isotope analysis: *Geophysical Monograph*, v. 95, p. 429-437.
- Tosdal, R.M., Wooden, J.L., and Bouse, R.M. 1999. Pb isotopes, ore deposits and metallogenic terranes: *Economic Geology Reviews*, **12**: 1-28.
- Weber, F., R., Foster, H.L., Keith, T.E.C., and Dusel-Bacon, C., 1978, Preliminary geological map of the Big Delta Quadrangle: U.S. Geological Survey Open-File Report 78-529-A, scale 1:150,000.
- Whalen, J.B., Jenner, G.A., Currie, K.L., Barr, S.M., Longstaffe, F.J., and Hegner, E., 1994. Geochemical and isotopic characteristics of granitoids of the Avalon Zone, southern New Brunswick: Possible evidence for repeated delamination events. *Journal of Geology*, **102**:269-282.
- Wilson F.H., Smith, J.G., and Shew, Nora, 1985, Review of radiometric data from the Yukon crystalline terrane, Alaska and Yukon Territory: *Canadian Journal of Earth Sciences*, v. 22, p. 525-537.
- Wilson, M., 1989, *Igneous petrogenesis*: London, Unwun Hayman.

CHAPTER THREE

Gold-bearing quartz veins related to reduced intrusions at the 4021

Prospect, Goodpaster district, east-central Alaska

ABSTRACT

The 4021 prospect is one of many auriferous quartz veins within the Goodpaster district, east-central Alaska. The most well known of the prospects are the > 5 Moz gold-bearing quartz veins of the Liese zone. The 4021 prospect is hosted within syn- to late-kinematic late Early Cretaceous granitic orthogneiss and lies south of an arcuate, easterly-trending belt of composite late Early Cretaceous reduced granite to tonalite intrusions that intrude paragneiss of the Yukon-Tanana Terrane. The veins are spatially and temporally associated with ~109-103 Ma biotite \pm hornblende granitic to tonalitic intrusions. The quartz veins are inferred to be cut by ~94.5 Ma dioritic rocks.

The 4021 prospect consists of at least two shallowly dipping, easterly striking shear hosted quartz veins. Steeply dipping sheeted quartz veinlets are abundant. Quartz veins contain approximately 3-5 vol. % arsenopyrite, pyrite, pyrrhotite, chalcopyrite, löllingite, native bismuth, gold, bismuth telluride minerals and undifferentiated Au-Bi-Te \pm S minerals. Gold occurs as free grains, and commonly as complex intergrowths with Bi - Te \pm S minerals in quartz, arsenopyrite, and pyrite. The veins may contain narrow sericite \pm carbonate alteration envelopes, and lesser K-feldspar \pm albite alteration locally occurs within veins and along quartz vein margins. Pegmatite and granite dykes and sills are spatially and temporally associated with the quartz veins. Gold-bearing quartz veins and pegmatite have a similar mineralogy, texture and flat lying morphology: both are inferred to exploit shallowly dipping regional structures.

Fluid inclusion compositions from gold-bearing quartz veins and pegmatite are complex and both contain primary, low salinity, aqueous-carbonic ($\pm \text{CH}_4$) fluid inclusions that coexist with rare saline and hypersaline fluids. The onset of gold and sulphide deposition began during aqueous-carbonic fluid immiscibility between 225 and 390°C. Pressure estimates from isochores and decrepitation range between 2.1 and 2.4 kbar, suggesting emplacement depths of 5–9 km.

Sulphide minerals from the quartz veins of the 4021 prospect and Liese zone have Pb isotopic values ($^{206}\text{Pb}/^{204}\text{Pb} = 19.5\text{--}19.6$) that generally overlap those of the reduced granite to tonalite suites in the Goodpaster district ($^{206}\text{Pb}/^{204}\text{Pb} = 19.4\text{--}19.5$), thereby suggesting they share a common lead source. The sulphide Pb isotopic values extend to slightly higher $^{206}\text{Pb}/^{204}\text{Pb}$ values than the igneous rocks due to fluid rock interaction with the more isotopically heterogeneous host gneiss of the Yukon Tanana Terrane. Diorite has lower Pb values ($^{206}\text{Pb}/^{204}\text{Pb} = 19.2$) than most of the sulphides, and thus is precluded from contributing lead to the bulk of the sulphides.

The 4021 prospect is a smaller-scale, lower-grade analogy to the quartz veins in the Liese zone. Gold-bearing quartz veins at the 4021 prospect formed from magmatic-hydrothermal fluids that exsolved from reduced granite to tonalite intrusions at depths of 7 ± 2 km.

INTRODUCTION

The Goodpaster district, located 145 kilometers east of Fairbanks in east-central Alaska, is hosted within the Tintina Gold Belt, a belt widely known for gold deposits related to reduced intrusions (Figure 3-1)(Hart et al., 2002). The Goodpaster district contains an easterly trending belt of gold-bearing quartz vein prospects. Of all the prospects, the Liese zone is the best known and highest-grade with a current resource estimate of 10.7 Mt at an average grade 0.52 oz/ton Au, or a resource of 5.6 Moz Au (Smith et al., 2000). The Liese zone, as well as the 4021

prospect, contains characteristics similar to intrusion-related gold systems (McCoy et al., 1997; Thompson and Newberry, 2000; Baker and Lang, 2000; Hart et al., 2002) and mesothermal, orogenic lode-gold systems (Goldfarb et al., 2000). For example, the gold-bearing quartz veins are associated with sericite-carbonate alteration, have ubiquitous low salinity aqueous-carbonic fluid inclusions, and are hosted in shear zones (Smith et al., 2000). Thus, the origin and classification of the Liese zone and satellite quartz veins are controversial. A summary of general characteristics for intrusion-related gold systems and orogenic gold systems is presented in Table 3-1.

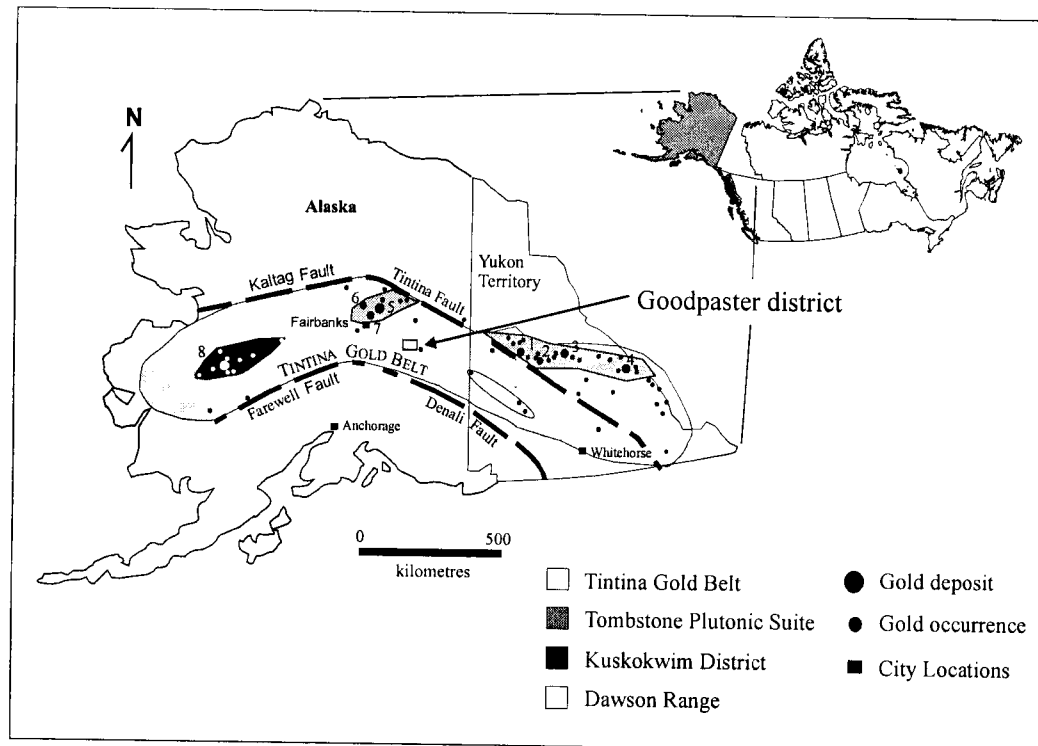


Figure 3-1: Location and extent of the Tintina Gold Belt in the northwestern Canadian Cordillera and Alaska. The small square denotes the location of the Goodpaster district in east-central Alaska. Major gold deposits (large circles), gold occurrences (small circles) and the extent of the Tombstone Plutonic Suite, Kuskokwim District and Dawson Range Suite are shown. The deposits are all associated with plutonic rocks. Numbers denote gold deposits: 1-Brewery Creek; 2- Clear Creek; 3-Dublin Gulch; 4-Emerald Lake; 5-Fort Knox; 6- True North; 7-Ryan Lode; 8-Donlin Creek. Figure modified after Mortensen et al., (2000).

Table 3-1. General characteristics of intrusion related gold deposits (IRGD) and mesothermal orogenic lode-gold deposits.

	Intrusion-Related Gold Systems ^{A,B}	Mesothermal Orogenic Lode-Gold systems ^C
Geochemical Signature	Au-Bi-Te-W- Mo-Sb with low Pb-Zn-Cu	Au-Ag ± As-Sb-Te-W-Mo-Bi with low Cu-Pb-Zn
Kinematics	Mineralization is post-metamorphism and deformation	Mineralization is syn- to post-peak metamorphism occurring during compressive deformation
Alteration	Alteration dominated by sericite-carbonate with lesser potassium feldspar ± albite. Narrow selvages around veins	Alteration dominated by silicification, carbonitization, sericitization, tourmalinization and albitization+ pyrrhotite-pyrite-scheelite. Halos are a few centimeters to meters
Redox State	Reduced ore mineral assemblage with pyrite-pyrrhotite to pyrite-arsenopyrite stable. Pyrite, arsenopyrite, pyrrhotite ± löllingite, maldonite, native Bi and Bi-Te minerals are common.	Redox state is generally reducing, controlled by the hematite-magnetite buffer. Pyrite, arsenopyrite, chalcopyrite, galena and stibnite are common.
Ore Assemblage		
Temperature and depth of Ore mineralization	>500°C to <300°C Various depths < 1 to >2 kbar	250°C to 400°C 1-3 kbar (at the brittle-ductile transition)
Granitoids	Temporally and spatially related to gold veins. Plutons are reduced and ilmenite-series in composition. Pegmatite and aplite are abundant and may be auriferous	Granitoids are spatially related to the gold deposits Tonalite-trochilite-granite in composition
Geological setting	Back-arc setting Belts dominated by continental sedimentary sequences	Accreted terranes and collisional settings Greenstone metavolcano-sedimentary terranes (Archean) and marine sedimentary rocks (Phanerozoic)
Ore veins	Sheeted or stockwork veins hosted intrusions. Veins, replacements and shear zones peripheral to intrusions	Veins are structurally controlled and associated with major faults, typically on second- or higher-order splays. Shear zones are hosted in dominantly reverse or strike slip regimes
Carbonate minerals	calcite or dolomite	Ankerite or siderite
Fluid Inclusions	Abundant low salinity aqueous-carbonic fluids (CO ₂ -rich) ± high-salinity fluids.	Uniformly low fluid salinities (<5% NaCl wt.% equivalent) with < 50% CO ₂
Metal zoning	Within intrusion: Au-Bi-Sn - W ± Mo Peripheral: Au-As-Sb Distal: Zn-Pb-Ag Depth: Increase in Bi and decrease in As	Mineralization is uniform with no zoning with respect to intrusions. No zoning parallel to fluid conduits within deposits

^A: For simplicity, skarn deposits which are included under the intrusion-related gold deposit class are not included

^B: Intrusion-related gold deposit characteristics based on McCoy et al. (1997) and Thompson and Newberry, (2000)

^C: Characteristics common to Archean, Paleozoic and Mesozoic orogenic gold systems from McCuaig and Kerrich, (1994), Bierlein and Crowe, (2000) and references therein.

Intrusion related gold deposit (IRGD) characteristics are primarily documented from gold deposits and occurrences associated with the mid-Cretaceous Tombstone Plutonic Suite in the northern Cordillera of Canada and east-central Alaska (McCoy et al., 1997; Thompson et al., 1999; Thompson and Newberry, 2000). These deposits are typically low-grade and high tonnage, and examples include the Fort Knox and Brewery Creek mines [169 Mt @ 0.93 g/t Au (Bakke et al., 1995) and 43.8 Mt @ 1.03 g/t Au (Park, 1999) respectively] and the Dublin Gulch prospect (99 Mt @ 1.1 g/t Au; Hart et al., 2000). Deposits in western Alaska associated with Late Cretaceous intrusions (i.e. Donlin Creek) are also included within the IRGD classification (Baker and Lang, 2000; Hart et al., 2000; Ebert and others, 2000). Global analogies include Timbarra and Kidston, Australia (Mustard, 2000), Salave, Spain, and Kori Kollo, Bolivia (Thompson et al., 1999).

Several auriferous quartz veins with similar morphology and alteration to the Liese zone are identified in the district. One of the largest prospects is the 4021 prospect, located five kilometers east of the Liese zone (Figure 3-2). The prospect shares the same shear hosted, shallowly dipping vein geometry, vein composition, and vein-controlled alteration as the Liese zone. The prospect is hosted within reduced granitic orthogneiss and is intimately associated with pegmatite, which has the same shallowly dipping morphology as the quartz veins.

This chapter assesses the magmatic component in the formation of the 4021 prospect. Field relationships, petrography, fluid inclusion microthermometry and lead isotopes provide compelling evidence to suggest a temporal, spatial and genetic link between the differentiated phases of the granite, or possibly tonalite, suite and gold-bearing quartz veins.

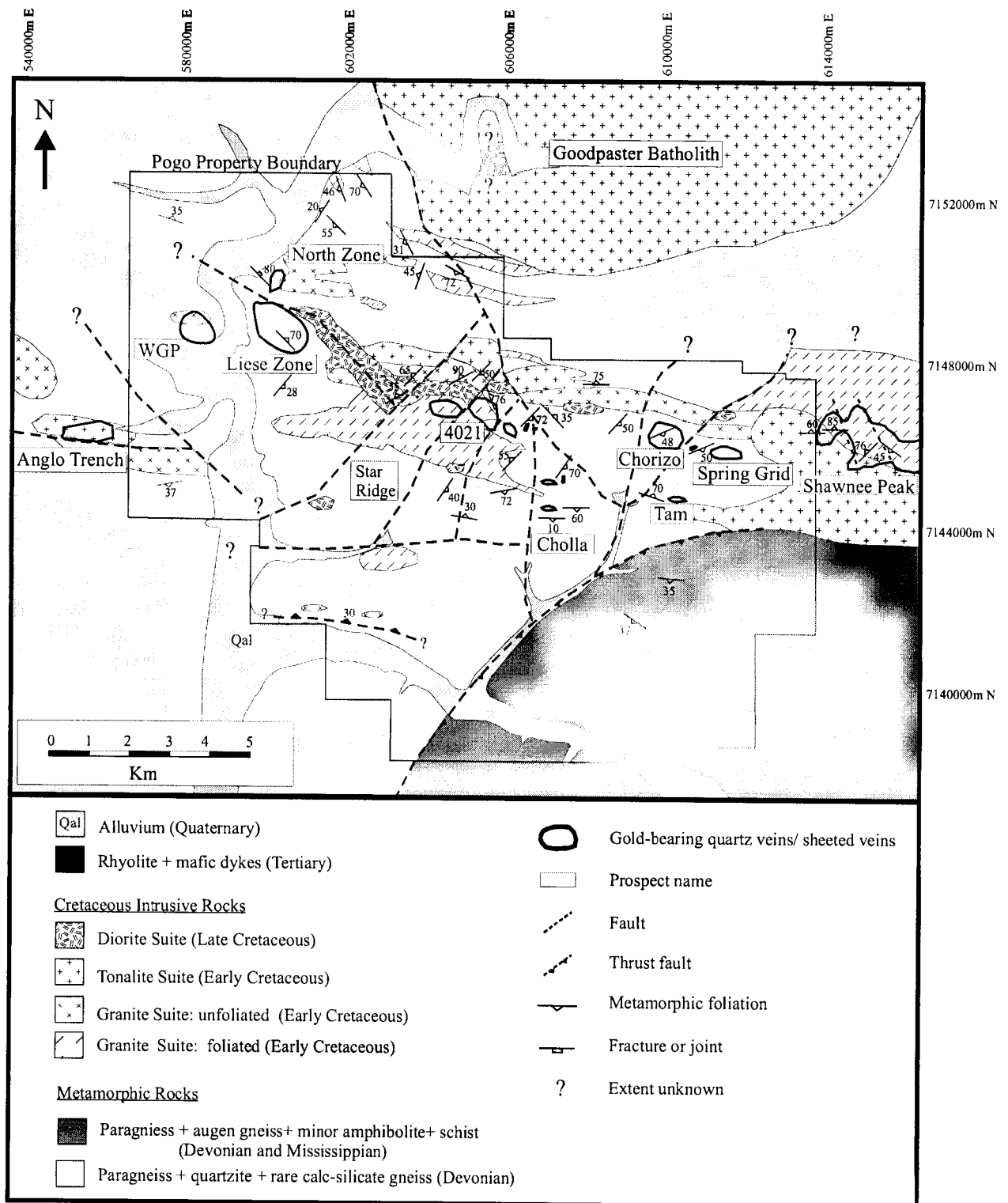


Figure 3-2. Geological map of the Goodpaster district and the distribution of the Cretaceous intrusive rocks and associated gold-bearing quartz vein prospects.

REGIONAL GEOLOGICAL SETTING

The Goodpaster district is located in the pericratonic Yukon Tanana Terrane, a terrane that underlies much of western Yukon and east-central Alaska (Aleinikoff and Nokleberg, 1985a; Mortensen, 1992; Dusel-Bacon and Aleinikoff, 1997). Metamorphosed pre-Devonian sedimentary rocks, intruded by Devonian to Mississippian plutonic rocks, comprise this composite terrane and represent a continental margin setting that culminated into a submarine magmatic arc (Aleinikoff et al., 2000; Dusel-Bacon and Aleinikoff, 1985). The terrane was subsequently intensely deformed and metamorphosed up to amphibolite facies conditions at intermediate pressures (Foster et al., 1994). The timing of metamorphism remains unresolved but has been proposed to involve mid-Paleozoic, Early Jurassic and Early Cretaceous events (Hansen and Dusel-Bacon, 1998; Aleinikoff et al., 2000). In the Goodpaster district, granitoids intruded syn- to post-regional metamorphism and deformation during the Cretaceous. Deformation and metamorphism ended by the late Early Cretaceous at about 107 Ma (Smith et al., 2000; Day et al., 2003; this study), the age of the oldest undeformed granite.

Three periods of igneous activity intruded the Yukon Tanana Terrane during the Mesozoic and Cenozoic (Foster et al., 1994; Mortensen et al., 2000). Of particular importance is the widespread Cretaceous plutonism that affected most of Yukon Territory and east-central Alaska, as a number of gold occurrences are spatially and temporally associated with them. Sparse volcanic rocks intruded during the Mesozoic and Tertiary (Dusel-Bacon and Aleinikoff, 1985).

The Goodpaster district lies east of the northeast-striking Shaw Creek Fault, where Paleozoic augen gneiss and Cretaceous plutons of batholithic proportions are widespread. The largest pluton is the Goodpaster Batholith, which intrudes the northern portion of the district. The dominant host rocks to the intrusive rocks are paragneiss and orthogneiss, with lesser

amphibolite, calc-silicate and ultramafic gneiss. These rocks, especially the augen gneiss, compose the Lake George subterrane of the Yukon Tanana Terrane (Nokleberg et al., 1993; Dusel-Bacon and Aleinikoff, 1996). The rocks are well foliated and polydeformed (Foster et al., 1994). Southeast-directed extension and exhumation occurred in the Yukon Tanana Terrane during the Early Cretaceous (Hansen and Dusel-Bacon, 1998; and Dusel-Bacon et al., 2002). A period of low magnitude northwest-southeast to north-south directed extension identified in the Liese zone may have occurred at this time (Rhys et al., 2003). Northeast-striking, steeply dipping oblique sinistral faults, contemporaneous with movements along the Denali and Tintina faults in the Cenozoic (Wilson et al., 1985; Newberry et al., 2000), are widespread in the region and cut the region into structural domains. In addition, several low-angle faults have also been identified (Weber et al., 1978).

DISTRICT SCALE GEOLOGY

The orthogneiss and paragneiss of the Yukon Tanana Terrane in the Goodpaster district are intruded by three Cretaceous plutonic suites. The oldest suite consists of a 109-107 Ma syn- to late-kinematic granite suite characterized by biotite-bearing granite and granodiorite, two-mica granite, pegmatite and aplite. An intermediate suite consists of a 107-103 Ma post-kinematic tonalite suite characterized by hornblende-biotite bearing tonalite and granodiorite with lesser granite and monzonite. The youngest suite consists of a 95 Ma diorite suite characterized by post-kinematic biotite-hornblende \pm pyroxene bearing diorite, quartz diorite and lesser monzonite and tonalite. Minor dykes and small plugs of Eocene hypabyssal quartz-feldspar phyric rhyolite dykes intrude the area and are the youngest intrusions known in the district. For a comprehensive description of the intrusive rocks in the Goodpaster district, see Chapter 2. A brief summary is presented in Table 3-2.

Table 3-1: Summary of the petrology, geochemistry and geochronology of the Cretaceous intrusive rocks in the Goodpaster district.

Intrusive Suite	Intrusive Rock Types	Petrology	Geochemistry	Age (Ma)
Granite	granitic to granodioritic orthogneiss, granite, granodiorite, leucogranite, pegmatite and aplite	strongly foliated to unfoliated, fine- to medium-grained, 5-10 % euhedral biotite. Garnet is a common accessory mineral. Trace minerals include ilmenite, monazite, and zircon. Forms small bodies and tabular dykes and sills	subalkaline, calc-alkaline SiO ₂ wt. %: 72 to 87 weakly metaluminous to peraluminous	Foliated: 109.2 ± 0.4 to 107.0 ± 0.6 Non foliated: 108.0 ± 1.0 to 107.3 ± 0.8
Tonalite	tonalite and granodiorite with minor granite and quartz diorite	equigranular to weakly seriate, medium- to coarse-grained with fresh, euhedral biotite. Biotite and hornblende are the predominant mafic minerals. Trace minerals include ilmenite, monazite, and zircon. Forms voluminous bodies including the Goodpaster Batholith and Shawnee Peak stock	subalkaline, calc-alkaline SiO ₂ wt.% 69.85 to 72.15 weakly peraluminous	105.7 ± 0.3 to (103.4 ± 2.2)
Diorite	diorite, quartz diorite, monzodiorite, monzonite and tonalite	equigranular, medium- to coarse-grained, abundant hornblende, biotite +/- pyroxene. Chlorite alteration is ubiquitous. Trace mineralogy includes magnetite, zircon and ilmenite. Monazite is absent. Forms small, steeply-dipping bodies	subalkaline, calc-alkaline SiO ₂ wt.% 49.62 to 56.7 weakly metaluminous to weakly peraluminous	94.5 ± 0.2 to 93.7 ± 0.2

All ages determined by conventional U-Pb methods on zircon or monazite at the PCIGR Laboratory at the University of British Columbia, Vancouver. An exception is the parenthesis, sample within parenthesis whose zircon age was determined by SHRIMP-RG at Stanford University, California

Outcrop in the district is sparse, and thus the interpretation of intrusive relationships and structural geometry is hindered. Nonetheless, some constraints on the intrusive geometry can be inferred from surface outcrop, exploration drill core and underground workings. A pervasive gneissic compositional layering (S1) in the para- and orthogneiss trends northwest with a moderate to steep northeast dip (Weber et al., 1978; Rhys et al., 2003; this study) on the north side of the property near the Liese zone and has a southern dip on the southern side. A northwest-striking D2 event macroscopically and microscopically folds S1, producing a strong, northeast-dipping domainal gneissosity that is shallowly dipping and axial planar to the folds. A third fabric (S3) locally cuts the S2 fabric at a shallow angle. Generally, S3 foliation dips shallowly towards the north and may be associated with E-W trending faults (Rhys et al., 2003).

Northeast-striking, sinistral faults inferred from topography, airphoto lineaments, lithological changes, and aeromagnetic data are widespread in the region. Shallowly dipping structures (i.e. S2 and S3), though not readily apparent, are evident in flat lying topography observed in the field (Figure 3-3). It is interpreted that some of the syn- to post-kinematic felsic intrusive phases exploited these shallow fabrics forming flat lying, tabular sheets (see Chapter 2). The gold-bearing quartz veins at the 4021 prospect have a similar flat-lying morphology as these felsic intrusive phases. This suggests the quartz veins and the felsic intrusive phases may have a similar emplacement style, exploiting regional sub-horizontal features.

GOLD-BEARING QUARTZ VEIN PROSPECTS

Numerous prospects hosting gold-bearing quartz veins are identified in the district along an easterly trending belt. They are from west to east the Anglo Trench, WGP, North zone, Liese zone, 4021, Chorizo, Cholla, Tam, and Shawnee Peak prospects (Figure 3-2). The quartz veins are mainly hosted within pre-Devonian paragneiss and late Early Cretaceous granitic

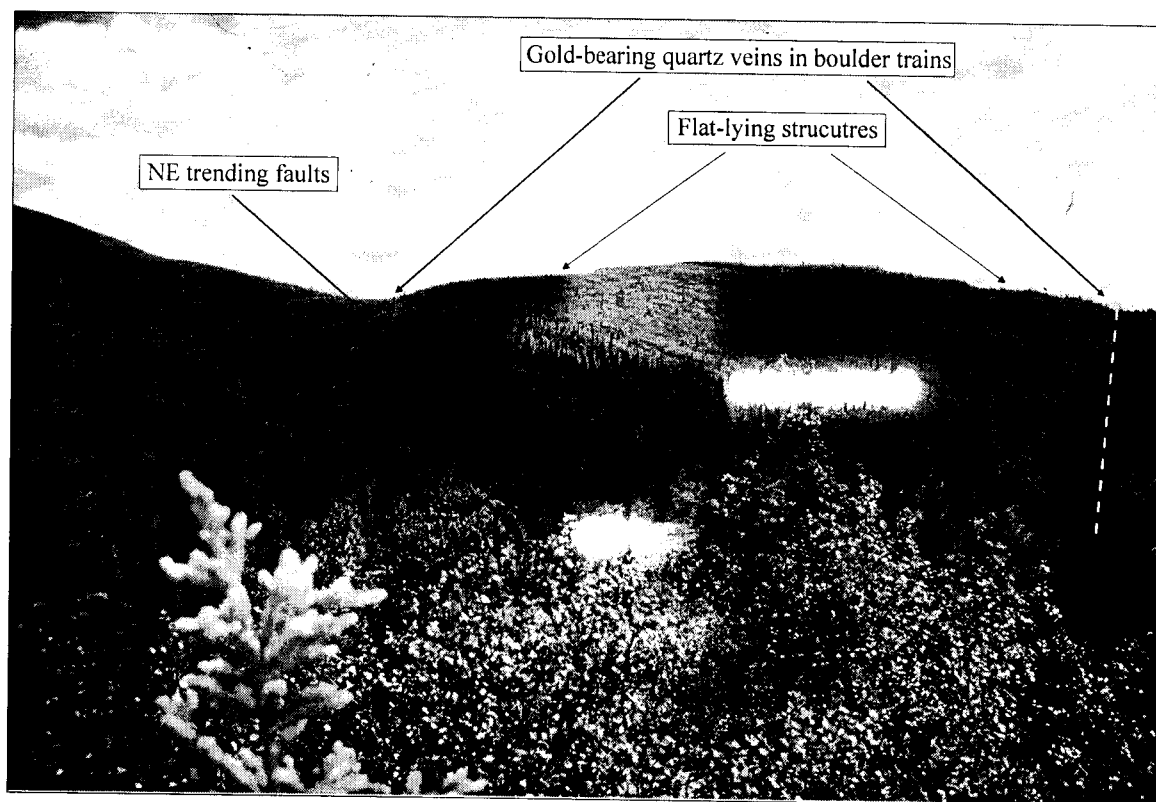


Figure 3-3. View looking south towards the 4021 prospect showing flat-lying topography and scarcity of outcrop. Hill 4021 is to the left of the diagram. Quartz bolder trains subcrop on both sides of the knoll. The prospect is cut by several northeast-trending faults causing a general displacement of lithologies towards the northeast.

orthogneiss, with minor mineralization in unfoliated late Early Cretaceous granitic rocks. The mineralized trend follows the arcuate, easterly-trending belt of early Late Cretaceous plutonic rocks that intrude approximately 2 km south of the Goodpaster Batholith.

The prospects are identified in the field by gold-bearing quartz boulders at surface and anomalous gold, bismuth, tellurium, and arsenic in soil geochemistry. Most prospects are inferred to contain shallowly dipping quartz veins surrounded by steeply dipping sheeted veinlets. The Tam and Cholla veins, the most southern prospects, are an exception as they are inferred to be steeply dipping based on limited diamond drilling. The Anglo Trench prospect in the western part of the district consists of thin, steeply dipping quartz veins within unfoliated

biotite \pm hornblende-bearing granodiorite and surrounding paragneiss. At the Shawnee Peak prospect, a 0.3 to 2.3 m wide quartz vein dips moderately along a biotite-orthogneiss and leucocratic granitic orthogneiss contact that probably marks a fault contact (Ebert, 2001).

Minor base metal-bearing veins crop out at Shawnee Peak and Star Ridge, 15 km east and 4 km south-southeast of the Liese zone respectively. At Shawnee Peak, a 20 cm wide quartz vein hosted in biotite orthogneiss contains 5% stibnite, sphalerite, arsenopyrite, galena, pyrite, chalcostibnite and cassiterite (Ebert, 2001). At Star Ridge, numerous quartz boulders with coarse-grained stibnite and minor sphalerite occur as float and rubble crop. In the Liese zone, 2-4 mm wide quartz veins with minor ankerite and coarse-grained sphalerite, galena and pyrite cross cut the gold-bearing quartz veins (Moore, 2000; Smith et al., 2000).

The Liese zone, the largest and highest-grade gold zone known in the Goodpaster district, has been the focus of numerous studies. As such, many aspects of the deposit have been previously described by Smith et al. (1999), Moore (2000), Smith et al. (2000), Thompson and Newberry (2000), Rhys et al. (2003), and Rombach et al. (2002). A PhD thesis on the Liese zone is in progress by Cameron Rombach at the University of Alaska, Fairbanks.

The Liese zone consists of a series of three or more stacked, subparallel, shallowly dipping quartz veins. The main L1 and L2 quartz veins are up to 20 m thick and extend laterally for over 1300 and 600 meters respectively. These main veins dip 25-30° towards the north and exploit earlier biotite-rich shear zones (Smith et al., 2000; Rhys et al., 2003). The veins are hosted primarily in quartz-feldspar-biotite paragneiss and locally within unfoliated felsic intrusive rocks. Extensional veinlets form steep offshoots off the main veins and are present in the hanging-wall and footwall, particularly where the host rock is intrusive. The quartz veins contain ~3 vol. % arsenopyrite, pyrite, pyrrhotite, chalcopyrite, löllingite, native bismuth, Bi-Te \pm S minerals and native gold (Smith et al., 2000). Gold occurs as free grains, or as

complex intergrowths with native bismuth and $\text{Bi-Te} \pm \text{S} \pm \text{Au}$ minerals. The sulphide minerals form in linear bands or webby aggregates parallel to the quartz vein contacts (Moore, 2000; Rhys et al., 2002).

4021 PROSPECT

The gold-bearing quartz veins of the 4021 prospect underlie a small knoll just west of hill 4021, the highest point in the Goodpaster district. The 4021 prospect consists of two or more shallowly dipping shear-hosted quartz veins that trend approximately east-west, parallel to the arcuate felsic composite plutonic body exposed in talus to the north (Figure 3-4). These veins are enveloped by abundant steeply dipping sheeted quartz veinlets that are inferred to strike northeast and dip steeply. The quartz veins and veinlets are hosted within two texturally distinct varieties of orthogneiss and rarely within paragneiss. The younger granitic to granodioritic orthogneiss (~107 Ma) hosts the upper quartz veins and is coarse-grained with potassium feldspar megacrysts up to 1.5 cm in length. The slightly older hornblende-biotite orthogneiss (~109 to 107 Ma, Appendix A) is fine- to medium-grained, contains more abundant biotite and lacks the feldspar megacrysts. Steeply dipping, medium- to coarse-grained diorite intrudes the northern part of the prospect. Diorite is inferred to cross cut the gold-bearing quartz veins because quartz veins and veinlets appear to terminate in the diorite in drill core correlations. No gold-bearing quartz veins are known to cross cut the diorite. Fine-grained mafic dykes, locally feldspar phyric, are observed in drill core. Similar dykes in the Liese zone exploit post-mineral faults (Rhys et al., 2003) and may be related to dioritic rocks.

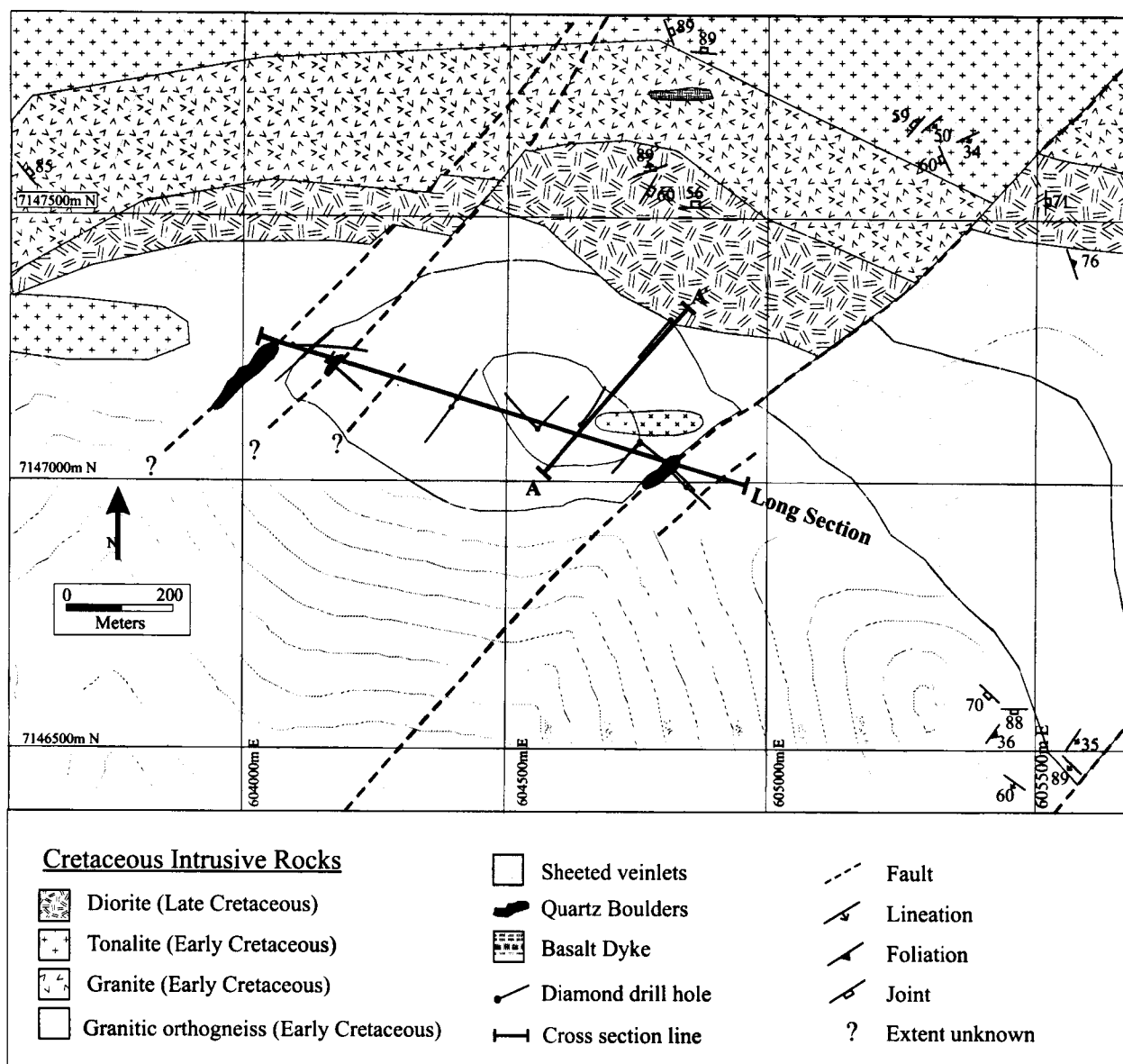


Figure 3-4. Geological map of the 4021 prospect showing the distribution of sheeted quartz veins and gold-bearing quartz boulders. Intrusive rocks outcrop in talus to the north of the prospect in approximately the same east-southeasterly trend as the quartz veins. The upper gold-bearing quartz vein is offset by faults in the saddles flanking the knoll. Northeast striking faults have sinistral separation and have a predominantly strike slip displacement.

ALTERATION

Four simple hydrothermal alteration assemblages are observed at the 4021 prospect. Alteration episodes are subdivided based on their relative timing and relationship to the gold-bearing quartz veins, which are discussed below. The four alteration assemblages consist of silica-sericite \pm K-feldspar \pm albite \pm carbonate \pm chlorite, chlorite, ankerite-sericite, and calcite-quartz. Surface weathering overprints all alteration types.

Quartz-sericite \pm K feldspar \pm albite \pm carbonate \pm chlorite

Quartz veining and localized silicification of wall rocks is the earliest alteration event in the district. Gold-bearing quartz veins and sheeted veinlets typically contain sericite-dominant alteration (+ pyrite \pm carbonate) envelopes less than 5 cm in width (Figure 3-5a). Rock outside the sericite envelopes exhibits little to no macroscopic alteration. Where sheeted veinlet densities are high, sericite alteration forms pervasive zones as alteration envelopes overlap. Although there is no relationship between sericite alteration intensity and gold grade, this alteration type is generally most intense where sulphides, in particular arsenopyrite, are abundant. In some gold-bearing quartz veins, sericite altered margins are absent. Sericite-dominant alteration also affects pegmatite and granite dykes that intrude the orthogneiss, however, the enclosing orthogneiss remains essentially unaltered (Figure 3-5b). Where sericite-dominant alteration is pervasive, only equigranular or foliated protolith textures are preserved, reminiscent of an intrusive rock or a gneissic rock respectively.

Sericitization is typified by the development of light green to colourless fine-grained sericite causing the host rocks to become pale green-yellow. Potassium feldspar is altered to sericite, and plagioclase is altered to sericite + calcite in the core and sericite in the rim,

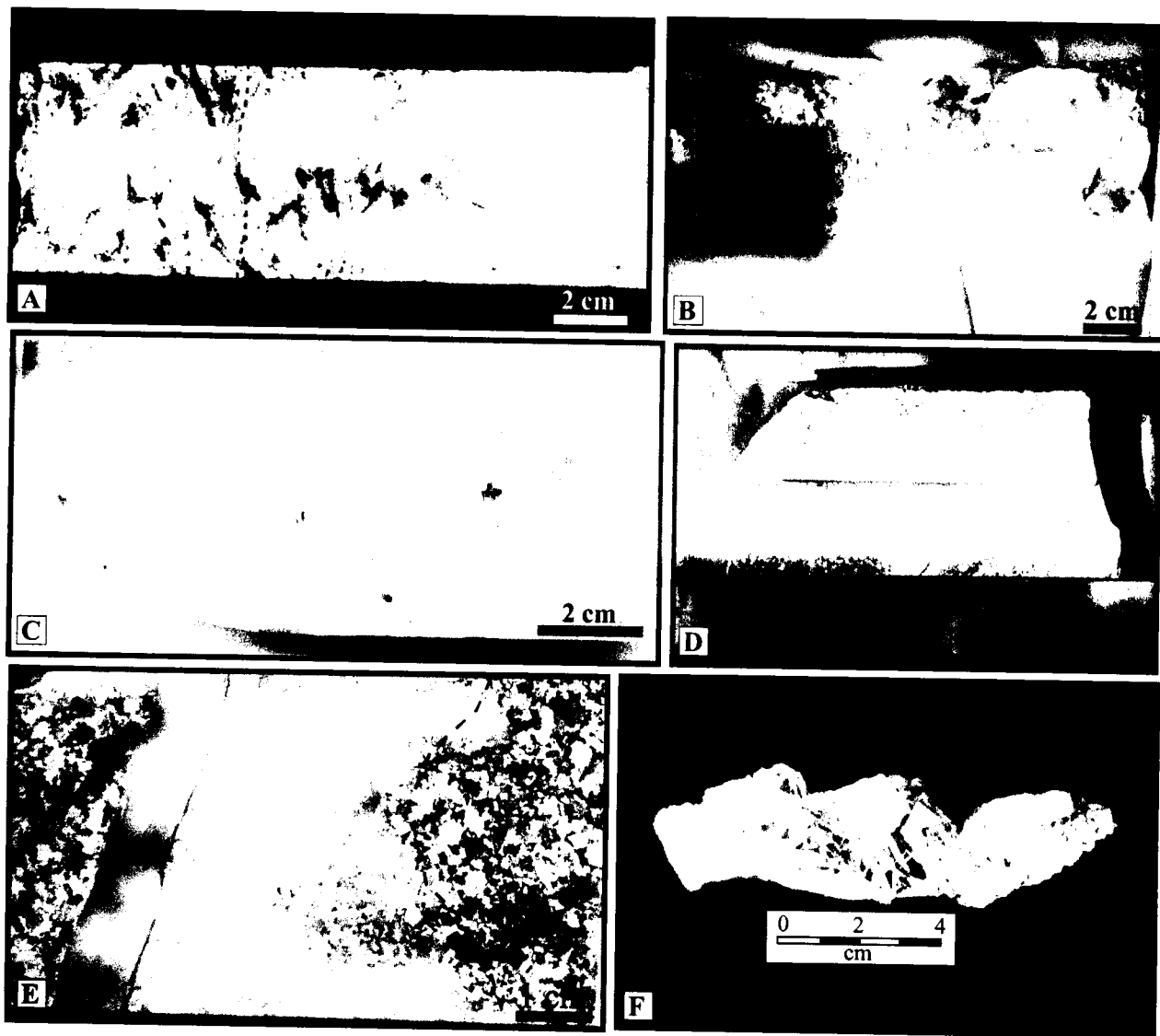


Figure 3-5. Alteration photographs. A) Quartz (+ feldspar) vein with a 5 cm sericite \pm carbonate alteration envelope. B) Sericite-dominant alteration imparting a pale green colour to pegmatite. The enclosing orthogneiss is unaltered. C) Late ankerite veinlets cross cutting a quartz vein. Where the ankerite veinlets cross cut the quartz vein, pyrite \pm pyrrhotite is deposited in the fractures. D) Ankerite veinlet with typical 1 cm sericite+carbonate alteration envelopes (bottom). Pervasive ankerite alteration occurs where alteration envelopes overlap (top). E) Late calcite (\pm quartz) vein cross cutting diorite and bleaching the wall rock margins. F) Coarse-grained bladed calcite vein which cross cuts orthogneiss.

presumably reflecting primary variations in the calcium content. Biotite is replaced by fine-grained sericite-rutile \pm pyrite \pm chlorite.

Potassium feldspar \pm albite occurs within quartz veins and locally as 1-2 mm, discontinuous white selvages on the quartz vein margins. Rarely selvages may extend up to 1 cm away from the vein. Secondary potassium feldspar is perthitic, weakly sericite-altered and locally rims cores of sericite-carbonate altered plagioclase. Albite selectively replaces potassium feldspar as unaltered, euhedral, albite twinned grains that form a coarse checkerboard texture. In places, veins with potassium feldspar altered margins grade outward into sericite-pyrite \pm carbonate alteration. This suggests these alteration types were likely coeval.

Chlorite

Chlorite alteration is intimately associated with diorite and mafic dykes and is therefore unrelated to the gold mineralizing event. Chlorite alteration ranges in intensity. It is ubiquitous in the dioritic rocks and locally overprints quartz-sericite altered rocks. Chlorite completely replaces biotite or is interleaved along cleavage planes and occurs with ilmenite \pm titanite \pm rutile. Hornblende and pyroxene are altered to chlorite-carbonate \pm sericite \pm titanite along cleavage planes. Plagioclase is weakly altered to sericite-carbonate \pm chlorite. Narrow, 1-3 mm wide chlorite-carbonate \pm pyrite \pm pyrrhotite veinlets cross cut the host gneiss and all intrusive phases, but are most abundant in the dioritic rocks.

In addition, chlorite alteration is pervasive within the early, flat-lying shear zones and may alter the country rock up to 0.3 m away from the shear zone margins. Chlorite locally occurs as ragged, randomly oriented felted masses up to 1 cm from quartz vein margins and also occurs within quartz veins. The presence of randomly oriented needles of rutile + ilmenite in the chlorite suggests it may have completely replaced hydrothermal titaniferous biotite.

Ankerite-sericite-carbonate

Ankerite veinlets are fracture controlled, 1-3 mm wide, and cross cut gold-bearing quartz veins. Ankerite veinlets have narrow sericite-carbonate alteration envelopes up to 2 cm thick, with coarse-grained sericite on the veinlet margins. Small, euhedral pyrite and pyrrhotite grains occupy 1-2 vol. % of the veinlets and also occur within the alteration envelope. Where ankerite veinlets coalesce, alteration becomes pervasive (Figure 3-5d). Ankerite veinlets are commonly spatially associated with quartz veins, but cut across quartz grains and sulphide minerals in random and discontinuous orientations (Figure 3-5c). Ankerite is magnesium-rich based on semi-quantitative scanning electron microscope (SEM) analysis. Moore (2000) refers to this alteration as DOS in the Liese zone, as the carbonate mineral is iron-rich dolomite. Ankerite alteration is pervasive along some faults, resulting in complete destruction of original protoliths and leaving only remnant gneissic, intrusive and phenocryst textures.

Calcite-quartz

Calcite \pm quartz veins form white coatings on fractures in numerous orientations in all rocks types but are most intensely developed in diorite and mafic dykes. Calcite veinlets locally cross cut the quartz veins. Calcite filled fractures are 1-10 mm wide and contain 1 vol. % fine-grained pyrrhotite, pyrite, ilmenite \pm chalcopyrite and 1-2 vol. % fine-grained quartz crystals. Coarse-grained sericite grows inwards at the vein margins. Calcite \pm quartz veins have white, strongly bleached margins because biotite, hornblende, pyroxene and plagioclase are altered to variable mixtures of carbonate + sericite + chlorite \pm epidote \pm titanite \pm rutile (Figure 3-5e).

Rarely, 3-6 cm wide coarse-grained bladed calcite veins occur (Figure 3-5f) in drill core and bleach the wall up to a few centimeters with similar alteration to calcite fractures. Fine-

grained quartz and pyrite occur within the calcite blades and euhedral magnesium-rich ankerite grows into the open space between the bladed calcite laths.

Grey quartz \pm calcite \pm pyrite \pm pyrrhotite veins are commonly spatially associated with the calcite veins although lack the intense bleaching of the wallrock. Typically, they have no macroscopic alteration envelopes. These veins cross cut the diorite, suggesting they are part of a later, but minor, quartz-veining event.

Surface Weathering Effects

Surface weathering and oxidation occurs to a depth of 50-75 meters and extends to greater depths along high-angle faults and fractured zones. Oxidation of iron sulphides to iron oxides and alteration of mafic minerals to clay imparts a pervasive, pale yellow-orange colour to the rocks. Jarosite and covellite occur as alteration minerals of pyrite and chalcopyrite respectively. Pyrrhotite is commonly altered to a fine-grained mixture of iron oxides. Arsenopyrite is rarely weathered.

QUARTZ VEIN MORPHOLOGY

The 4021 prospect consists of two, possibly three, shallowly dipping quartz veins hosted in flat-lying, chloritized ductile shear zones. The veins are enveloped by abundant, steeply dipping sheeted quartz veinlets. The upper quartz vein obtains a maximum true thickness of 3.4 m and has been traced over an area of 810 m by 420 m (Figure 3-6 and 3-7). This vein averages about 0.3 meters in thickness. The upper quartz vein subcrops in the two saddles flanking the knoll and quartz boulder trails can be followed for a few meters. A second gold-bearing quartz vein occurs 30-50 m deeper and lies subparallel to the upper quartz vein. The extent of the

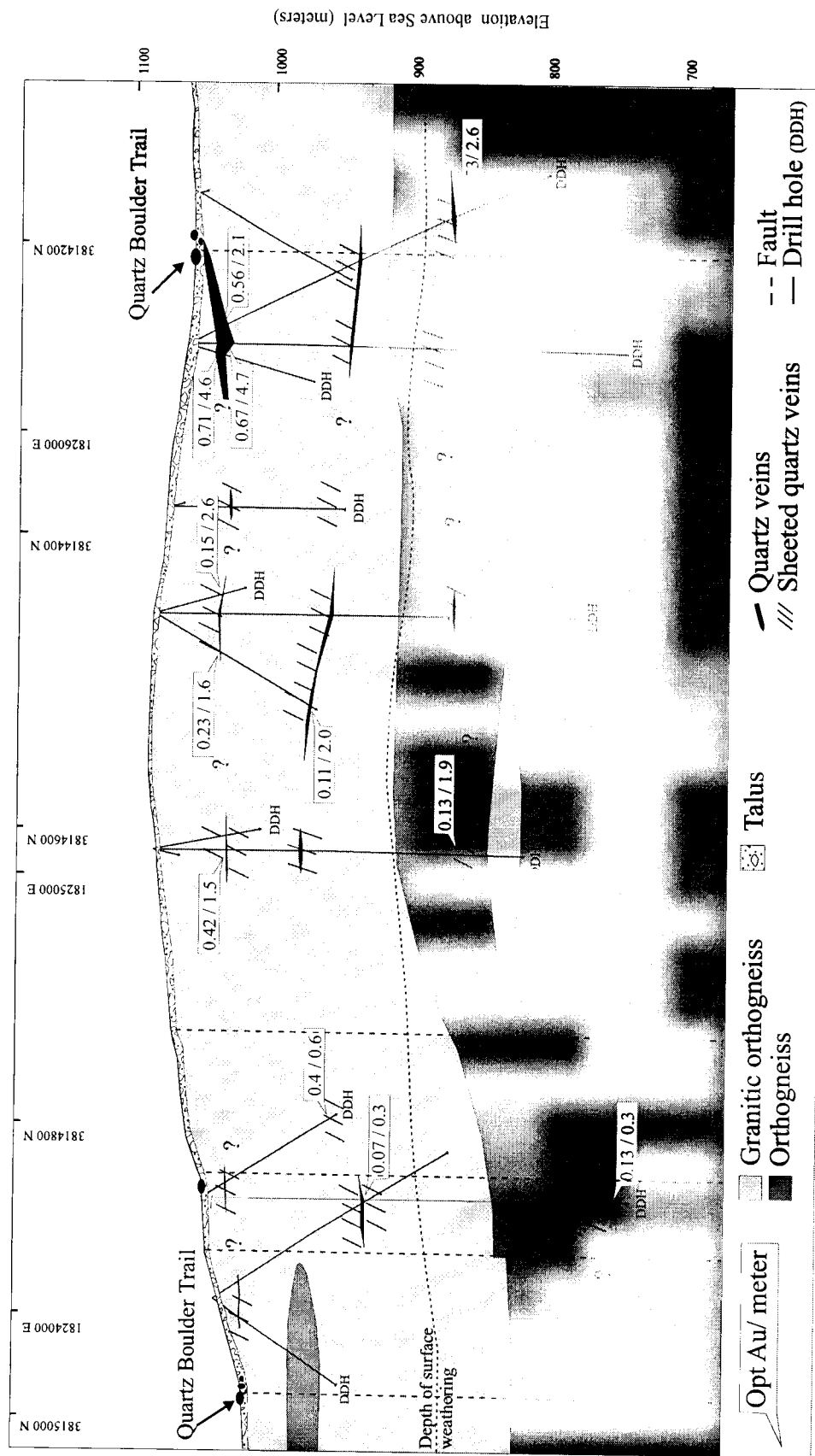


Figure 3-6. Long section of the 4021 prospect looking towards the north northeast. The angle between the sheeted quartz veinlets and shallowly dipping quartz veins is typically 60-90 degrees, however there are no constraints on their dip direction. Based on the narrow veinlets which cross cut the composite plutonic body to the north, the sheeted veinlets strike northeast. The orientation and thickness of the sheeted quartz veinlets is schematic and only high density areas of sheeted quartz veinlets are shown. The northeast trending faults are inferred to dip steeply and have a dominantly sinistral strike slip separation with little vertical displacement.

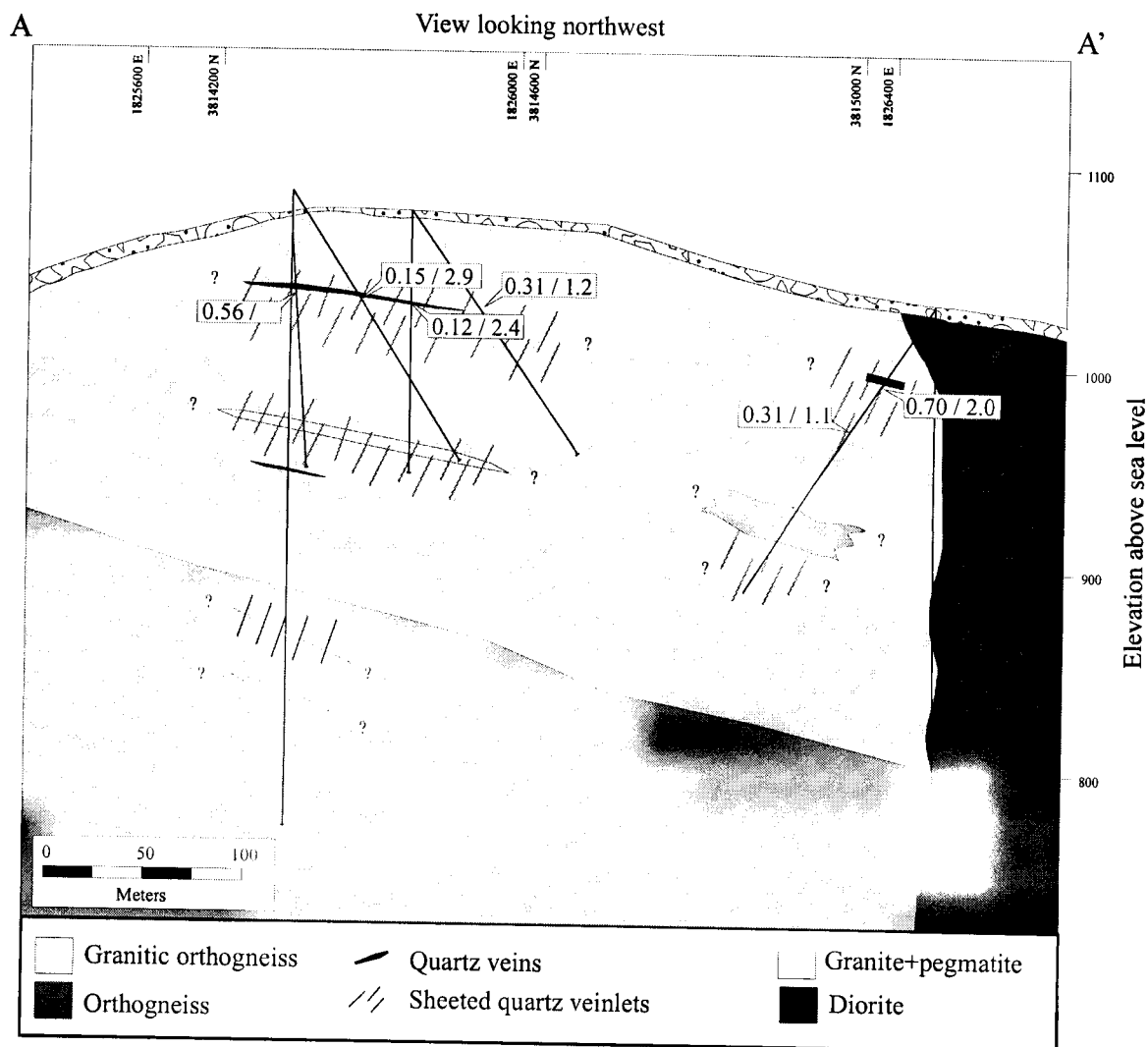


Figure 3-7. Cross section A-A'. View is to the north northwest. Diorite is steeply dipping and is inferred to cross cut the gold-bearing quartz veins and veinlets. The angle between sheeted veinlets and shallowly dipping quartz veins is typically 60 to 90 degrees, however there are no geological constraints on their dip direction. Based on narrow veins which cross cut the composite plutonic body to the north, the sheeted veinlets strike northeast.

deeper vein is not as well constrained and it does not outcrop. A third vein is encountered at depth in some, but not all, drill holes and the continuity of this vein is unknown.

Early shear zones

Chloritized shear zones at the 4021 prospect are commonly thin and diffuse but may range up to 0.3 m thick. Ductile shear zones are evident on both the hanging-wall and footwall of some main-stage quartz veins and are inferred to be shallowly dipping based on their high angles of intersection with vertical drill core and inferred continuity between drill holes. Discontinuous quartz laminations with milky white and dark grey quartz define a planar fabric and are rarely separated and disrupted by highly fissile, phyllosilicate chloritic shear horizons and dark grey shears. In places, country rock fragments within the shear zone are altered to chlorite and locally are silicified (Figure 3-8a).

Main stage veins / veinlets

The main generation of quartz veins is flat lying and exploits chloritized shear zones. These quartz veins can be massive and voluminous. They thicken and thin over short lateral distances, and are up to 3.4 meters in the thickest vein intercept. Although shear zones do not always have quartz veins within them, the presence of shear structures may aid in identifying lateral quartz veins. Quartz is commonly massive, but locally has a granular texture.

Main-stage quartz veins may contain multiple, 1-2 cm wide bands of webby textured arsenopyrite, pyrrhotite, pyrite \pm löllingite \pm chalcopyrite \pm calcite. Less abundant fine-grained native bismuth, bismuth-telluride minerals and native gold occur as inclusions within the webby textured sulphides or proximal to the webby sulphides as disseminated inclusions within quartz. In some zones, the massive quartz is porcelain white with <1 vol. % fine-grained disseminated

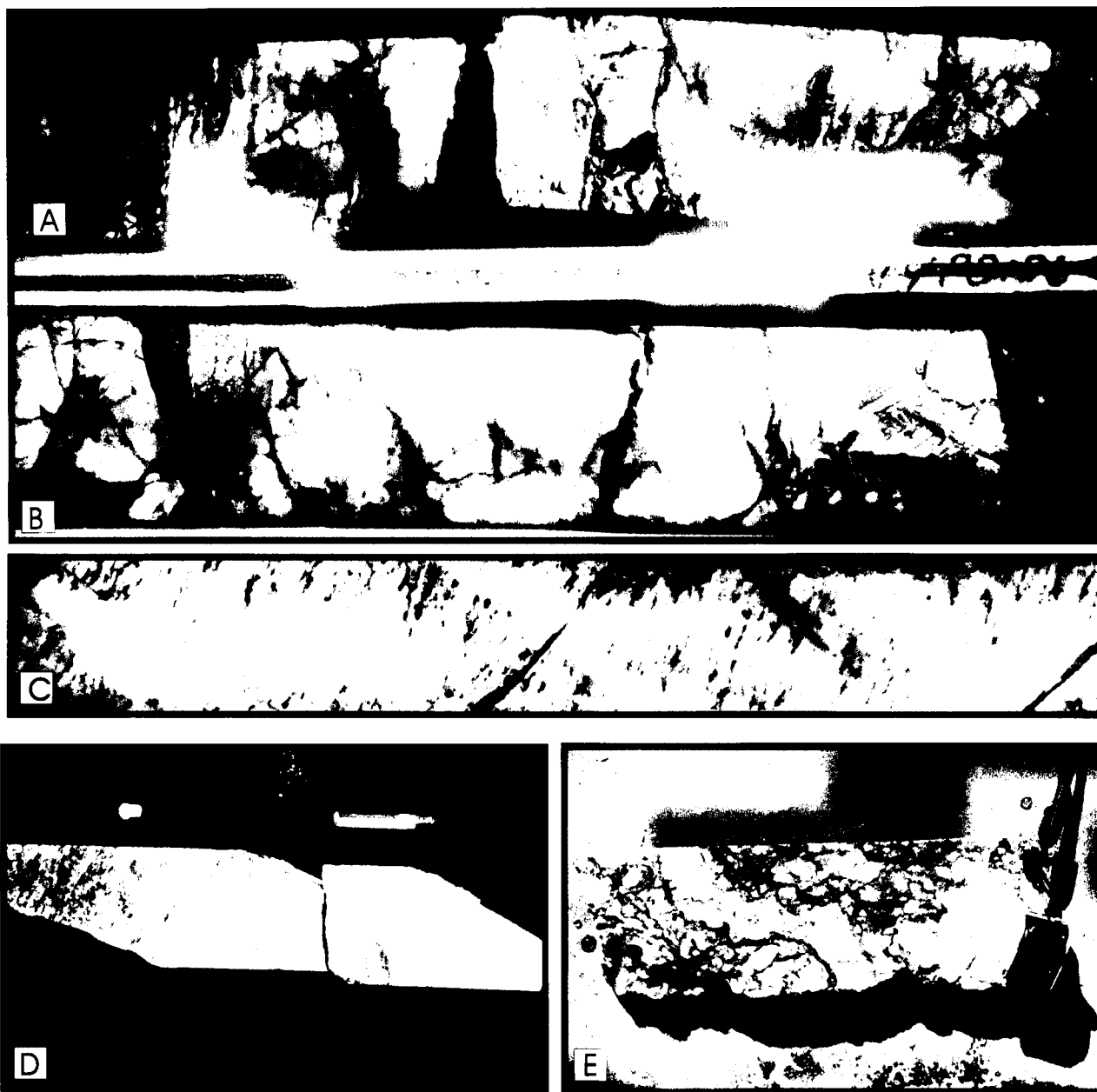


Figure 3-8. Photographs of various quartz veins and veinlets. A) Ductile shear zones (left and right sides of the photo) with discontinuous laminations of quartz and dark grey shear horizons. Silicification of the wall rocks and porcelain white massive quartz are evident in the center of the photo between the shear zones. B) Massive, porcelain white quartz veins with arsenopyrite + pyrite fractures in numerous orientations. Stylolites with pyrite and arsenopyrite accumulation are evident on the right side of the photo. C) Steeply dipping, subparallel sheeted quartz veinlets cross cut granitic orthogneiss. D) Fragments of chloritized wall rock within a quartz vein. Several calcite veinlets cross cut the quartz vein at shallow angles to the drill core margin. The quartz vein has a narrow K-feldspar \pm albite alteration envelope. E). Brecciated quartz vein with subangular quartz fragments within an arsenopyrite and pyrite matrix. Locally, quartz heals the breccia fragments.

sulphides and ore minerals (Figure 3-8b). Typically these zones contain low to negligible gold grades although locally some contain visible gold. Fragments of chloritized wall rock locally occur within the main-stage veins (Figure 3-8c) and may be parallel to the quartz vein margins. Quartz vein boundaries are commonly sharp, but are diffuse where steeply dipping sheeted veinlets splay off the main vein. Main stage quartz veins have gold grades that vary between <0.01 and 9.7 ounces per tonne (opt) Au, averaging approximately 0.3 opt Au. The higher gold grades are typically associated with the webby sulphide bands and proximal to ductile shear fabrics.

Steeply dipping sheeted quartz veinlets are abundant at the 4021 prospect and are generally orthogonal to the shallowly dipping main-stage veins. Sheeted quartz veinlets are <1 to >20 cm thick but average 1-2 cm. They are planar and subparallel (Figure 3-8c). Quartz veinlet densities average 4-6 veinlets per meter in areas of high density and less dense zones with fewer than two veinlets per meter are widespread. Sheeted quartz veinlets have similar mineralogy and textures to the main stage quartz veins, suggesting they are coeval. Low gold grades up to a few grams per tonne (g/t) generally typify the steep veinlets although they locally contain visible gold and have high grades up to 11 opt Au. Minor, 1-3 mm quartz veinlets locally coalesce into masses of narrow, anastomosing veins. They do not contain significant gold concentrations. Paragenetic relationships between the veinlet types were not apparent in drill core.

Post-mineral brittle faulting

Two generations of faulting in the vicinity of the 4021 prospect are identified based on drill core and field relationships: brittle faults with brecciated quartz and steeply dipping, northeast trending faults.

Brecciated quartz is commonly associated within, or flanking, the massive shear hosted quartz veins. The breccia consists of angular, mottled white to moderate grey, 0.5 to 3 cm quartz fragments within a fine-grained arsenopyrite and pyrite matrix (Figure 3-8e). Locally, the breccia is healed by light grey quartz. Arsenopyrite and pyrite may account for 5-30 vol. % of the rock and quartz fragments locally contain fine disseminations of arsenopyrite. Brecciated quartz is identified in a few quartz vein intercepts and can be traced between closely spaced drill holes. These breccia zones may be subhorizontal and could represent a syn-late brittle manifestation, or reactivation, of the early ductile shear structure controlling mineralization. The temporal and geometric relationship of the faulting to the quartz veins however cannot be confirmed by drill core data. Some of these zones may represent late, high angle brittle faults transecting the quartz veins.

Numerous steeply dipping, northeast-trending faults are inferred to cut the 4021 prospect based on lithology offsets and changes in topography. In drill core, faults typically contain 1-5 cm angular fragments of gneissic or intrusive rock in a clay or gouge matrix. Fault zones may be up to 3 meters wide, though are typically less than 0.5 meters. Zones of intense brittle faulting and cataclasis have a weak, steeply dipping fabric and contain 1-6 mm subangular to subrounded rotated clasts of quartz in a fine-grained, dark grey, rock powder matrix. In places, slivers of sheared, gouged wall rocks with small quartz fragments occur within the fault zones, however only remnant intrusive, gneissic textures or phenocryst textures (reminiscent of rhyolite or feldspar phyric mafic dykes) remain as they are pervasively altered to ankerite-sericite and/or chlorite. Thin, calcite and quartz veinlets locally occur within the faults in random orientations. These faults are inferred to be steeply dipping based on their oxidation well below depths of surface oxidation. Based on the interpreted continuity of the quartz veins (Figure 2-6), these steeply dipping faults do not appear to have significant vertical displacements.

QUARTZ TEXTURES

Granular and massive textural varieties of quartz are distinguished in the quartz veins. Quartz in granular veins has a sugary texture in hand sample and is composed of anhedral to rounded quartz grains 0.5 to 4 mm in diameter. Microcline, albite and muscovite (Figure 3-9b) are interstitial to the rounded quartz grains although locally the granular veins contain no potassium feldspar (Figure 3-9c). Similar vein textures were documented in the Liese zone by Moore (2000). Moore (2000) identified rare, 6-sided euhedral to subhedral quartz grains that indicate the granular quartz is a primary feature. The granular quartz is texturally similar to granular textured pegmatite and aplite (Figure 3-9a).

Some pegmatitic sills are quartz-rich and contain interstitial sulphides, with pegmatite locally enveloping quartz rich centers. In one locality, biotite-quartz-feldspar pegmatite grades from coarse granular quartz with 5-10% feldspar into coarse granular quartz (\pm feldspar \pm sulfide \pm biotite). A continuum from feldspar-bearing granular quartz veins into massive, anhedral quartz (\pm feldspar) veins is seen in some drill core and pegmatite and quartz veins share a similar, flat lying morphology (Figure 3-10, see Chapter 2). Taken together, the spatial, mineralogical and geometric relationships imply a direct transitional link of the granular quartz veins to pegmatite/aplite and gold-bearing quartz veins.

Massive quartz veins are milky white and contain 0.2 to 6 mm interlocking anhedral quartz grains (Figure 3-9d). White quartz is generally unstrained where not recrystallized and quartz grain boundaries are slightly sutured. Minor interstitial microcline and sericite are common accessories along quartz grain boundaries. Where the quartz veins are sheared and strained, the quartz is mottled light gray to dark grey with extreme undulatory extinction and subgrain boundary development. Locally, polygonal crystals characteristic of recrystallization during deformation occur.

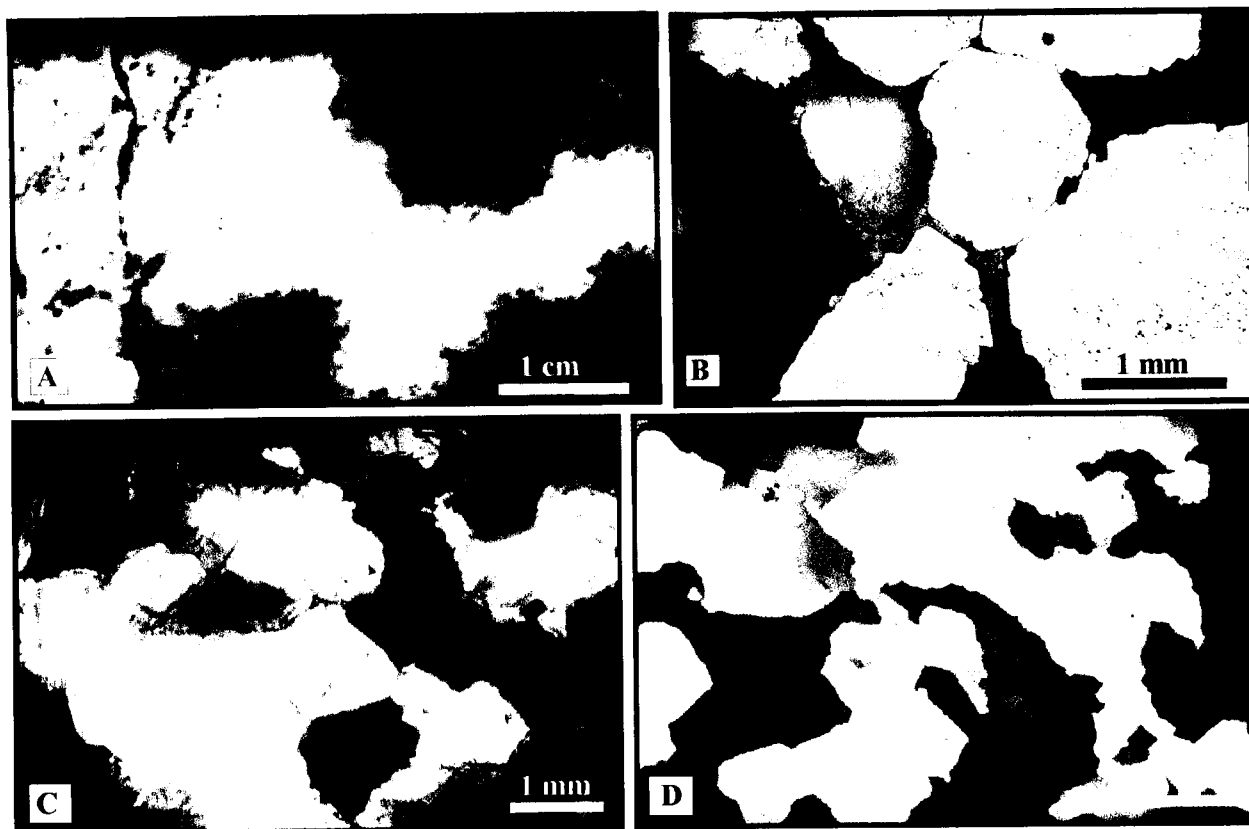


Figure 3-9 Quartz vein textures from the Goodpaster district.. **A)** Photograph showing the transition from pegmatite (lower left) grading into a granular quartz vein (upper right). 4021 prospect. **B)** Photomicrograph of granular quartz with interstitial K-feldspar (crossed polars). Shawnee Peak. **C)** Photomicrograph of granular quartz without feldspar matrix (plane light). 4021 prospect. **D)** Massive, gold-bearing quartz vein with anhedral, interlocking quartz crystals (crossed polars). Note the even extinction in the quartz crystals. 4021 prospect.

ORE MINERALOGY

Gold-bearing quartz veins and sheeted veinlets contain a simple sulphide assemblage. Sulphides and other ore minerals constitute approximately 3-5 vol. % of the quartz veins, but can range from trace to 20 vol. %. The most common ore minerals are arsenopyrite, pyrite, pyrrhotite and chalcopyrite with lesser löllingite, native bismuth, undifferentiated Bi-Te and Bi-Te \pm S minerals, native gold, maldonite and rare amounts of galena and scheelite. Bismuth-Te-S-Au minerals were identified semi-quantitatively by scanning electron microscope (SEM) analysis.

Gold occurs as isolated grains $<100\text{ }\mu\text{m}$ and commonly as complex intergrowths with native bismuth, bismuth-telluride minerals, and rarely Bi-Te \pm S minerals. Native gold (\pm Bi-Te-S intergrowths) occurs in a variety of textures: as isolated 2-20 μm inclusions within quartz, arsenopyrite and pyrite, along quartz and sulphide grain boundaries, within fractures in arsenopyrite and pyrite (Figure 3-10 a,b,c,d) and rarely in the feldspar matrix surrounding granular quartz in granular quartz veins. Although Bi-Te \pm S minerals most commonly occur as complex intergrowths with gold, they also occur as isolated inclusions within quartz, arsenopyrite, and pyrite (Figure 3-10 e).

Quartz-rich pegmatite contains 0.5 to 1 vol. % interstitial pyrite and pyrrhotite, and lesser arsenopyrite, chalcopyrite, galena and molybdenite. Gold was not identified or detected from any pegmatite at the 4021 prospect. Granular quartz veins contain minor disseminated gold, arsenopyrite, pyrite, pyrrhotite, native bismuth, and bismuth telluride minerals along the grain boundaries and as coarse-grained masses interstitial to the quartz grains. Rarely, gold occurs as inclusions within the granular quartz crystals and even more rarely within the enclosing feldspar.

Arsenopyrite is the most abundant sulphide in the gold-bearing quartz veins, followed by pyrite, pyrrhotite, löllingite and lesser chalcopyrite. These minerals form webby aggregates

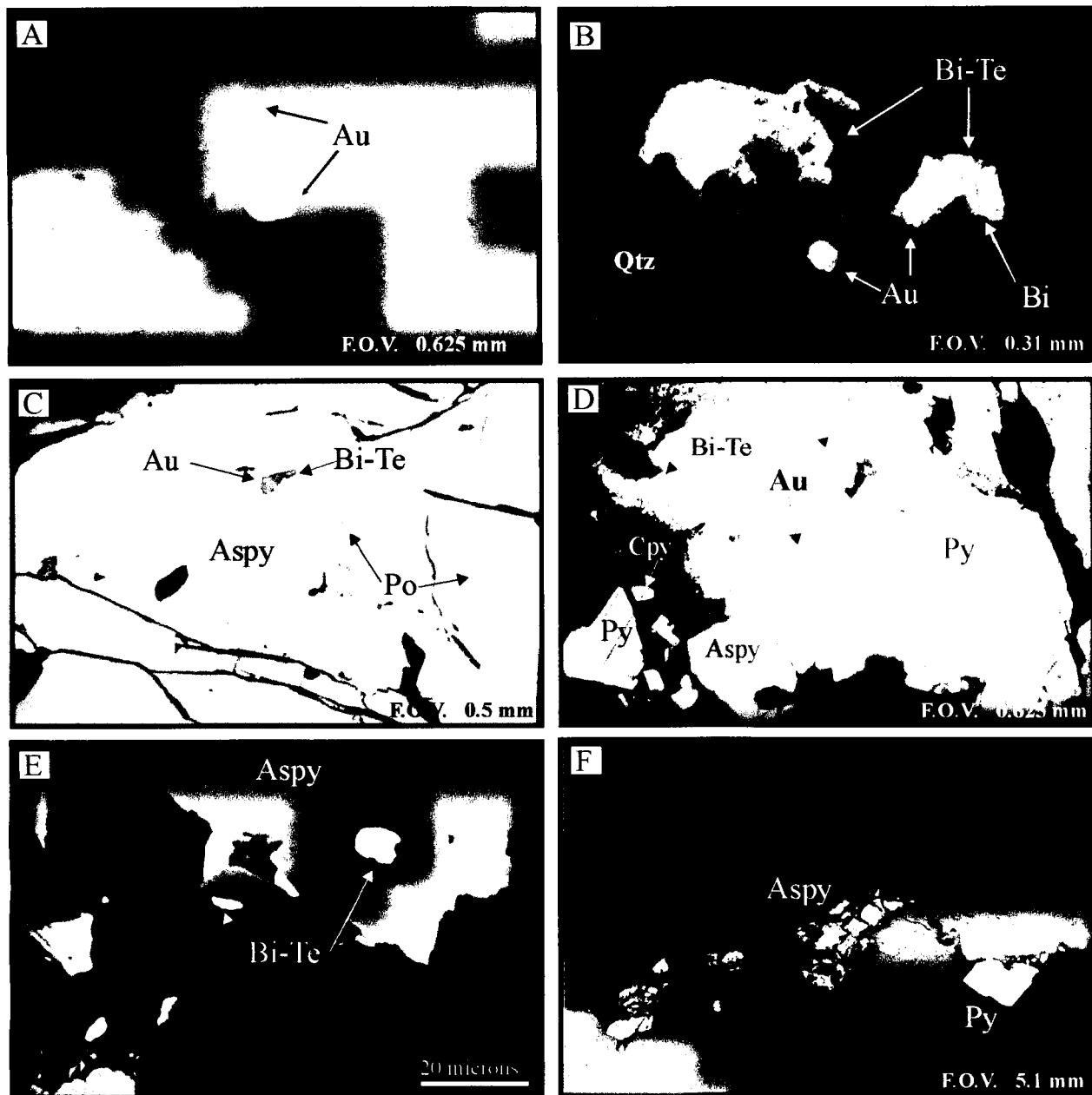


Figure 3-10. Photomicrographs of the nature and occurrence of gold and sulphide minerals in quartz veins and sheeted veinlets. Asp = arsenopyrite, Au = native gold, Bi = native bismuth, Bi-Te = bismuth telluride mineral, cpy = chalcopyrite, py = pyrite, and po = pyrrhotite. **A)** Isolated gold grains within quartz and along quartz grain boundary. **B)** Isolated gold grain within quartz and arsenopyrite. Gold is also intergrown with bismuth telluride. Reflected light **C)** Inclusions of gold, pyrrhotite and bismuth-telluride minerals in arsenopyrite. Reflected light **D)** Gold ± bismuth-telluride inclusions isolated within, and along fractures in, arsenopyrite and pyrite. Pyrrhotite is also enclosed within the arsenopyrite. Pyrite contains abundant fine-grained inclusions of bismuth and bismuth telluride minerals. Reflected light. **E)** Inclusions of bismuth tellurides within, and along fractures, in arsenopyrite. Backscattered image. **F)** Brecciated arsenopyrite and pyrite along a fracture in quartz, and infilled with Mg-rich ankerite. Reflected light.

lying in subparallel bands, as disseminations or coarse-grained blebs within and interstitial to quartz, and along fractures in numerous orientations. Fine-grained native gold, native bismuth, Bi-Te \pm S minerals, pyrrhotite and chalcopyrite commonly occur as inclusions within arsenopyrite, pyrite and quartz, or along fracture planes within pyrite and arsenopyrite. Calcite is commonly interstitial to the webby sulphides and quartz grains. However, calcite deposition is possibly related to a younger alteration event unrelated to the gold mineralization event. Arsenopyrite and pyrite also accumulate along anastomosing stylolites and fractures in the massive quartz veins (Figure 3-8b) and are exploited by later ankerite alteration. Thin, 1-2 mm veinlets containing euhedral pyrite are common in late fractures. A generalized paragenetic sequence for ore mineralization and alteration of the 4021 prospect is shown in Figure 3-11.

METAL ASSOCIATION AND DISTRIBUTION

Correlations between gold and various elements were determined from fire assay and inductively coupled plasma mass spectrometry (ICP-MS) data compiled from the 4021 prospect ore intercepts (Table 3-3). All analyses were prepared at Chemex Laboratories, Fairbanks and completed at ALS-Chemex Laboratories in Vancouver, Canada. Assay results from 151 gold-bearing quartz vein samples with greater than 1 g/t Au indicate veins contain an average of 9 g/t Au, 1.3 ppm Ag, 3764 ppm As, 23 ppm Bi, 42 ppm Cu, 3.6 ppm Mo, 16 ppm Pb, 3 ppm Te, 47 ppm W, and 22 ppm Zn.

Gold correlates strongly with Bi ($r^2=0.93$) and moderately with Te ($r^2=0.49$). This is consistent with the common spatial association of gold with native bismuth and Bi-Te minerals. This relationship is found in many intrusion-related gold deposits. Silver has a low correlation with gold ($r^2= 0.38$). Semi-quantitative SEM analysis of gold grains confirms the

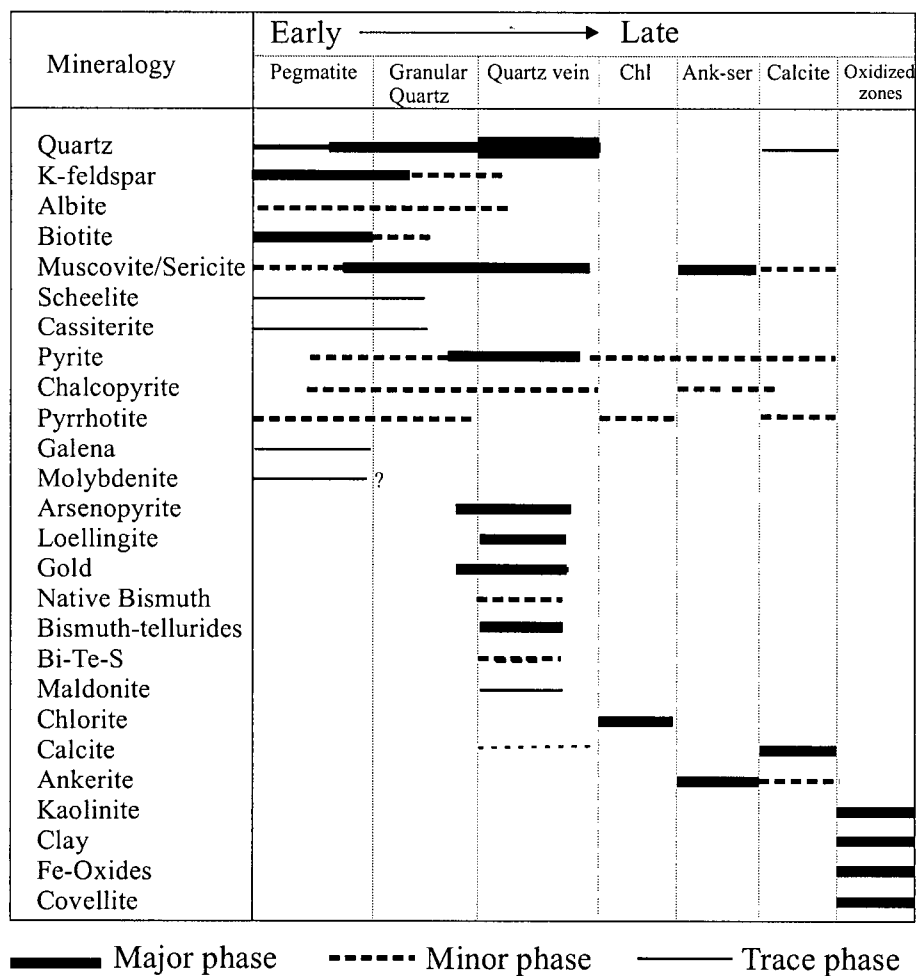


Figure 3-12. Interpreted mineral paragenesis for mineralization and alteration at the 4021 prospect.

presence of trace silver. The presence of trace silver suggests that the gold is actually electrum. However, in view of the lack of quantitative concentration analyses, the electrum is referred to as native gold. Despite arsenopyrite being the most abundant sulphide within gold-bearing quartz veins, arsenic correlates poorly with gold ($r^2 = 0.09$). This poor correlation is probably because arsenopyrite is erratically distributed with gold and gold intermittently occurs as isolated grains in quartz veins lacking sulphides.

An interesting aspect of the metal association is the low to moderate inter-element correlations between copper, lead, zinc, silver and arsenic ($r^2 = > 0.19$ to < 0.54). With the exception of silver, these elements all correlate poorly with gold and bismuth. Their lack of correlation with gold suggests they are likely associated with a different paragenetic stage and/or different hydrothermal fluid event. The mineral hosting silver is not known. However, the low correlation between Au and Ag, and the presence of electrum, suggests that there is another Ag-bearing mineral, such as a base-metal rich sulphide mineral. This could be chalcopyrite, galena or stibnite.

Molybdenum and tungsten correlate with no elements. Although quartz veins locally contain scheelite, elevated tungsten values are generally associated with lower gold values. Many pegmatite and granite rocks from the 4021 prospect, Liese zone and Shawnee Peak also contain elevated W (>200 ppm) values and rare scheelite. Scheelite was also observed in planar, sheeted quartz-feldspar veins suggesting perhaps the elevated W values are associated with early pegmatite and early quartz veins. A further explanation could be attributed to contamination of the samples during tungsten-carbide crushing because W contamination can range up to 300 ppm (ALS-Chemex procedures. www.chemex.ca). Molybdenite was not observed within any gold-bearing quartz veins in this study, and was only observed as isolated grains within wall rock fractures.

Table 3-3: Correlation coefficients (r^2) for 151 quartz vein samples from the 4021 prospect containing greater than 1g/ton gold. Only 66 samples had data for Sb.

	Au	Ag	As	Bi	Cu	Mo	Pb	Sb	Te	W	Zn
Au	1.00										
Ag	0.36	1.00									
As	0.06	0.00	1.00								
Bi	0.93	0.46	0.05	1.00							
Cu	0.02	0.00	0.02	0.05	1.00						
Mo	0.00	0.01	0.05	0.00	0.00	1.00					
Pb	0.00	0.19	0.34	0.00	0.04	0.00	1.00				
Sb	0.07	0.32	0.00	0.07	0.02	0.05	0.54	1.00			
Te	0.49	0.15	0.00	0.95	0.01	0.00	0.00	0.09	1.00		
W	0.00	0.07	0.00	0.00	0.00	0.00	0.00	0.00	0.00	1.00	
Zn	0.00	0.03	0.02	0.00	0.00	0.00	0.29	0.00	0.00	0.00	1.00

FLUID INCLUSIONS

Fluid inclusion microthermometry was undertaken to help characterize the chemical composition of the ore-forming fluids in the gold-bearing quartz veins, and the pressures and temperatures of their formation. Fluid inclusion analysis also included pegmatite because of the textural evidence linking the gold-bearing quartz veins with spatially related pegmatite. The reconnaissance fluid inclusion study was performed on a FLIUD INC[®] adapted USGS gas-flow heating/freezing stage at the University of British Columbia. The stage was routinely calibrated for a range of temperatures using SYN FLYNC standards (Werre et al. 1979). Accuracy of measurements is $\pm 0.1^\circ\text{C}$ for freezing measurements near 0°C and $\pm 2.0^\circ\text{C}$ for heating runs between 30°C and 350°C . Temperature measurements were restricted to an upper limit of 500°C . Where possible, measurements were routinely re-run to check reproducibility of measurements.

The presence of gold as isolated inclusions within quartz requires coeval deposition and it is assumed that primary fluid inclusions in quartz are representative of fluid conditions during gold deposition. Nine samples from the 4021 prospect were used for fluid inclusion petrography. From these, four representative samples were selected for microthermometry: a shallowly dipping main-stage gold-bearing quartz vein, a steeply dipping gold-bearing sheeted quartz veinlet, an unmineralized pegmatite dyke, and a late bladed calcite vein that clearly post-dates the gold mineralizing event. In these samples, quartz had uniform to weak undulatory extinction, suggesting minimal strain. Samples with evidence of high degrees of strain (stylolites, subgrain development, and strong undulose extinction) were avoided to reduce the amount of post entrapment modifications of the inclusions (Shepard et al., 1985)

Several fluid inclusion types were identified based on observations of phases at room temperature and microthermometry results. These are CO₂-H₂O bearing inclusions (type 1), H₂O-rich inclusions (type 2), halite ± sylvite-bearing H₂O-rich inclusions (type 3) and late aqueous inclusions (type 4). Fluid inclusion characteristics are summarized in Table 4.

Type 1 fluid inclusions are further subdivided based on volumetric proportion estimates of CO₂ at room temperature. Type 1A inclusions are aqueous-rich with less than 50% CO₂, whereas type 1B inclusions are CO₂-rich with greater than 50% CO₂.

H₂O-rich type 2 fluid inclusions are subdivided into types 2A and 2B based solely on microthermometric data. Both types contain 10-15% vapour and are indistinguishable at room temperature. Type 2A inclusions are aqueous-low salinity and homogenize over low to moderate temperatures. Type 2B inclusions are aqueous with moderate salinity and homogenize over moderate temperatures.

Type 3 inclusions are polyphase, H₂O-rich aqueous inclusions that contain 5-15% vapour and one to three daughter minerals. Halite is the most common daughter minerals, with rare

sylvite. Halite was identified based on its cubic form and isotropism. Sylvite was identified by its cubic habit with rounded corners (Shepard et al., 1985). Type 3A inclusions are distinguished from type 3B based solely on microthermometric data, with type 3A homogenizing at moderate temperatures and 3B at significantly higher temperatures.

Type 4 inclusions are aqueous inclusions with negligible salinity. They have consistent phase ratios of 5-10% vapour and homogenize at low temperatures.

Table 3-4: Fluid inclusion types and their general characteristics

Type	Description	CO ₂	Salinity	Temperature
1A	Carbonic-aqueous	<50%	low	moderate
1B	Aqueous-carbonic	>50%	low	moderate
2A	Aqueous 2-phase	low	low	low
2B	Aqueous 2-phase	low	moderate	moderate
3A	Hypersaline, aqueous	low	high	moderate
3B	Hypersaline, aqueous	low	high	high
4	Late aqueous 2 phase	low	low	low

Quartz grains contain fluid inclusions that range from 2 to 12 μm . Inclusions smaller than 2-3 μm are abundant but are unsuitable for study because of their small size. Inclusions occur in complex orientations along pseudosecondary and secondary trails, and rarely as inferred primary inclusions. Definitive evidence for primary fluid inclusions, such as growth zones in quartz (Roedder, 1984), are absent in the samples. Nonetheless, inclusions that have consistent phase ratios, are round to oval with regular boundaries, and occur in isolated clusters away from grain boundaries and secondary inclusions trails, are interpreted to be primary (Figure 3-12a). Inclusions that occur along planes or trails that do not cross cut grain boundaries are

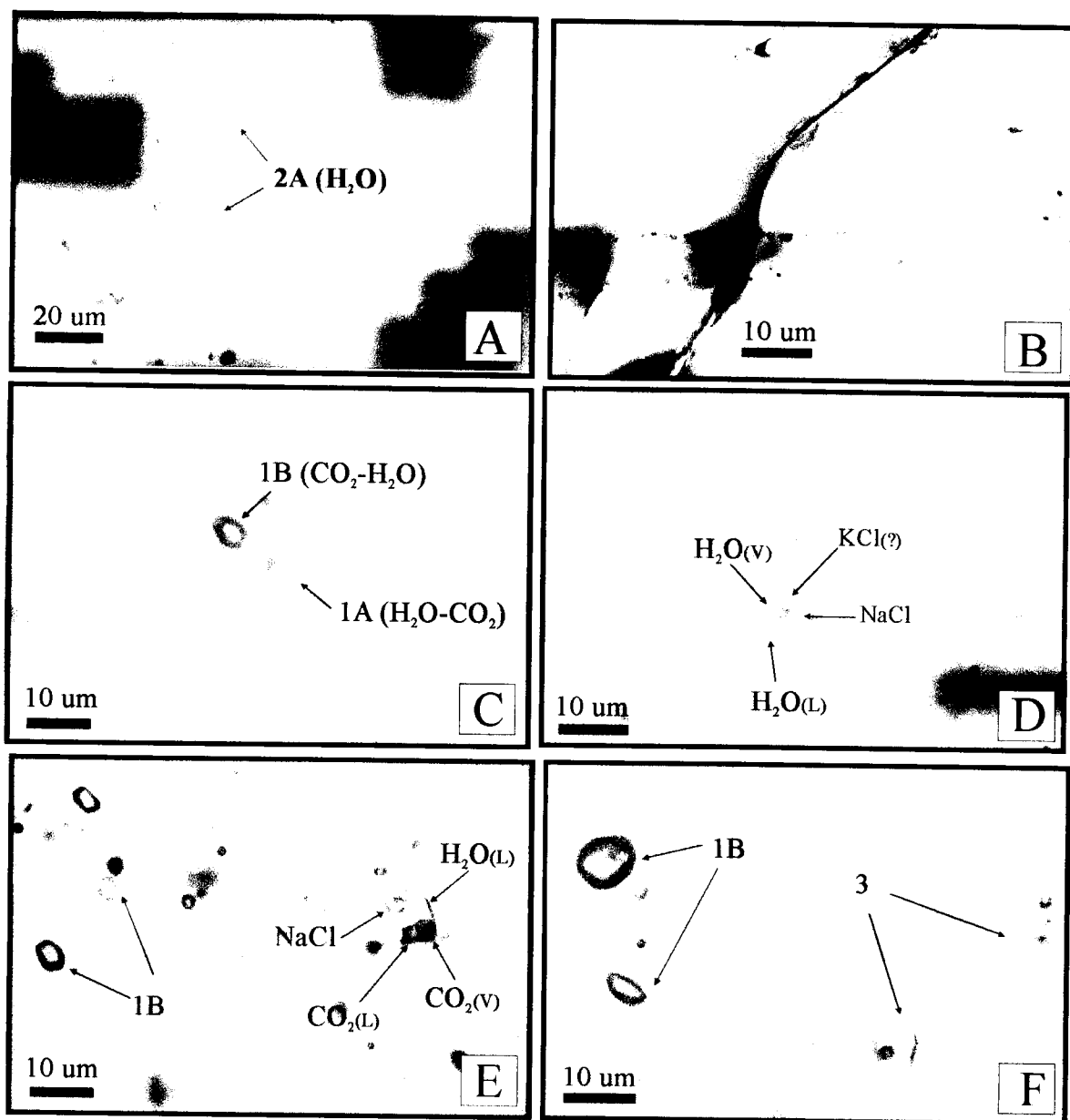


Figure 3-12: Photomicrographs of fluid inclusions in quartz. **A.** A cluster of inferred primary type 2A fluid inclusions with consistent phase ratios (5-10 vol. % vapour). **B.** Secondary type 4 fluid inclusions which occur in trails and cross cut grain boundaries **C.** Primary aqueous-carbonic (type 1A and type 1B) fluid inclusions. **D.** A primary, polyphase, hypersaline inclusion (type 3) with vapour, a halite daughter plus one other daughter mineral, likely sylvite **E.** Primary aqueous-carbonic fluid inclusion with a daughter mineral (inferred halite) in the aqueous portion of the inclusion. Type 1B aqueous-carbonic fluid inclusions are present on the left side of the photomicrograph. **F.** Primary saline fluid inclusions spatially coexisting with primary carbonic fluid (type 1B) inclusions.

pseudosecondary (PS). Inclusions occurring in trails that cut grain-boundaries are classified as secondary (S) and are typically less than 5 μm in size (Figure 3-12b). Most of the inferred primary fluid inclusions occur in groups of type 1 inclusions and less commonly type 2 and rarely type 3 inclusions. All inclusion types are also locally present along pseudosecondary trails. These planes occur in numerous orientations within the quartz and lack any clear cross cutting relationships, thus precluding an interpretation for a paragenetic sequence. Type 4 inclusions are always secondary and occur along trails that cut grain boundaries and trails of all other inclusion types.

MICROTHERMOMETRY

The results of microthermometric analysis are summarized in Tables 5 and 6 and high temperature homogenization results are represented graphically in Figure 3-13. Salinity estimates for type 1 aqueous-carbonic inclusions were determined using the method of Collins (1979) based on clathrate melting temperatures ($T_{m_{\text{clathrate}}}$) and have large uncertainties due to the presence of methane (Shepard et al., 1985). Methane contents were calculated from depressed CO_2 melting temperatures ($T_{m_{\text{CO}_2}}$) (Heyden et al., 1982). Salinity estimates for type 2 and type 4 inclusions were determined from the depression of ice melting temperatures ($T_{m_{\text{ice}}}$) using the method of Bodnar and Vityk (1994). All salinity estimates for type 3 inclusions were estimated using the temperature of halite homogenization (Shepard et al., 1985).

Microthermometric analysis were conducted on inclusions $> 6 \mu\text{m}$. Unfortunately, the small size of some of the inclusions prevented low temperature measurements. Only end member populations for type 1 inclusions were selected for microthermometry (type 1A: 15-20% CO_2 and type 1B: 90-95% CO_2), as heterogeneously trapped phases will have higher homogenization temperatures (T_h) and thus overestimate the actual trapping temperatures and

Table 3-5: Summary of fluid inclusion microthermometric data. T_{mCO_2} =CO₂ melting temperature; T_{hCO_2} = CO₂ homogenization temperature to CO₂ liquid; T_e =eutectic ice melting temperature (first sign of ice melt); T_{mice} = final ice melting temperature; T_{mclath} = clathrate-melting temperature; T_{hfinal} = final homogenization temperature to liquid; T_{hdec} = decrepitation before homogenization; n = total number of inclusions from which measurements were taken. Note that not all inclusions had a complete set of measurements due to their small size, decrepitation and various other inherent difficulties.

	TYPE	<i>n</i>	T_{mCO_2} (°C)	T_{hCO_2} (°C)	T_e (°C)	T_{mice} (°C)	T_{mclath} (°C)	T_h (final) (°C)
247-332 Pegmatite	1A	19	-56.7 to -58.3	6.9 to 25.6	-	-26.0 to -3.0	4.4 to 10.8	265 to 310
	1B	29	-56.6 to -59.2	6.9 to 20.2	-	-	-	263 to 347
	2A	9	-	-	-	-4.4 to -1.5	-	206 to 289
	2B	11	-	-	-40.1 to -34.1	-25.6 to -22.8	-	221 to 335
	3A	5	-	-	-33 to -30.2	-26.2 to -22.1	-	270 to 346
	4	11	-	-	-	-4.4 to -0.5	-	163 to 220
276-192 Sheeted quartz vein	1A	9	-62.1 to -62.2	-9.7 to 4.2	-26.8	-15.1 to -4.1	-	225 to 365
	1B	43	-60.2 to -64.4	-22.8 to 7.4	-	-	-	207 to 370
	2A	5	-	-	-3.2	-3.9 to -0.4	-	211 to 247
	2B	16	-	-	-30.2 to -40.9	-10.1 to -25.6	-	227 to 347
	3A	4	-	-	-36.6 to -40.9	-23.9 to -26.2	-9.0 ?	190 to 319
	3B	21	-	-	-29.2 to -38.0	-26.3 to -22.5	-	452-480 (T_{hdec})
99-2076 Quartz Vein	1A	28	-56.6 to -57.3	21.9 to 28.8	-	-11 to -0.3	5.2 to 10.1	233-302
	1B	24	-56.7 to -59.4	-5.3 to 22.3	-	-	-	225 to 390
	2A	27	-	-	-6.0 to -5.2	-3.0 to -0.6	-	171 to 248
	4	21	-	-	-6.6 to -4	-2.3 to -0.1	-	125 to 219
Bladed Calcite	4	12	-	-	-	0	-	118 to 152

Table 3-6: Summary of fluid inclusion composition data. Fluid composition data calculated from simplified microthermometry and using MacFlincon (Brown and Hagemann, 1995). Where a complete set of measurements was not obtained, estimates from inclusions within the same cluster or trail were used. XH_2O = water proportion ; XCO_2 = carbon dioxide proportion; $XNaCl$ = salt equivalent proportion; $XC H_4$ = methane proportion; Wt. % NaCl= salinity based on weight percent salt equivalent; carb XCH_4 =methane proportion within the carbonic phase.

	TYPE	XH_2O	XCO_2	$XNaCl$	$XC H_4$	Wt. % NaCl	CO ₂ Density (g/cm ³)	carb XCH_4
247-332 Pegmatite	1A	0.85 to 0.92	0.04 to 0.11	0.00 to 0.04	0.00 to 0.00	4.8 to 13.1	0.65 to 0.96	0.00 to 0.07
	1B	0.00 to 0.27	0.83 to 1.00	0.00 to 0.01	0.00 to 0.05	5.7 to 6.3	0.64 to 0.84	0.00 to 0.10
	2A	-	-	-	-	1.8 to 7.0	-	-
	2B	-	-	-	-	21.0 to 25.0	-	-
	3A	-	-	-	-	34.0 to 44.0	-	-
	4	-	-	-	-	0.8 to 7.0	-	-
276-192 Sheeted quartz vein	1A	0.91 to 0.94	0.03 to 0.60	0.02 to 0.03	0.00 to 0.02	6.6 to 8.2	0.66 to 0.71	0.22 to 0.23
	1B	0.00 to 0.26	0.60 to 0.88	0.00 to 0.01	0.12 to 0.35	6.6 to 9.0	0.55 to 0.78	0.14 to 0.37
	2A	-	-	-	-	0.7 to 6.2	-	-
	2B	-	-	-	-	17.4 to 25.0	-	-
	3A	-	-	-	-	32.0 to 40.0	-	-
	3B	-	-	-	-	-	-	-
99-2076 Quartz Vein	1A	0.84 to 0.97	0.30 to 0.16	0.00 to 0.03	0.00 to 0.00	0.02 to 8.7	0.63 to 0.78	0.00 to 0.04
	1B	0.00 to 0.26	0.69 to 0.97	0.00 to 0.01	0.00 to 0.10	5.0 to 7.6	0.71 to 0.83	0.00 to 0.12
	2A	-	-	-	-	1.0 to 4.9	-	-
	4	-	-	-	-	0.0 to 3.8	-	-
Bladed Calcite	4	-	-	-	-	<0.1	-	-

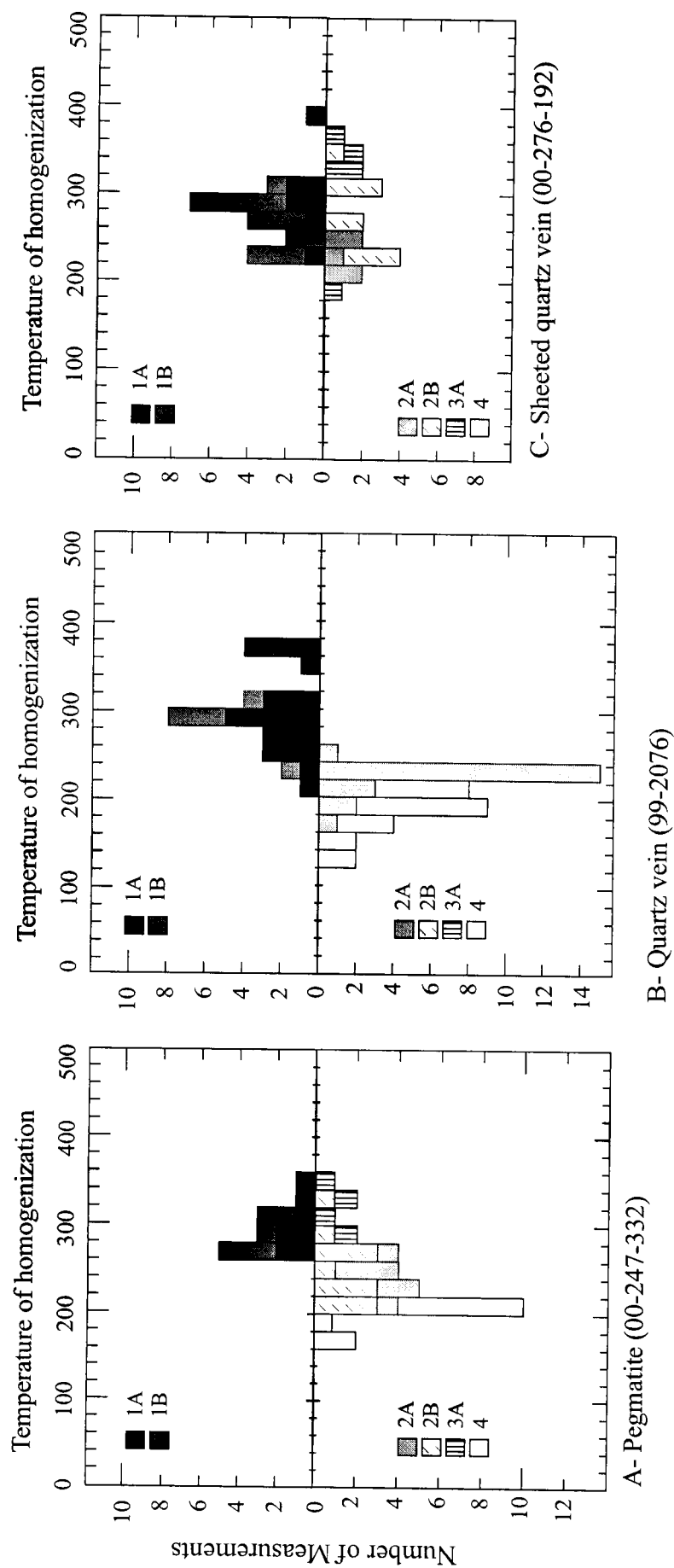


Figure 3-13. Histograms of the final homogenization temperatures (Th) for (A) pegmatite (sample 332-447) (B) a steeply dipping quartz vein (sample 276-192) and (C) a flat lying quartz vein (sample 99-2076). Aqueous-carbonic fluid inclusion (type 1) histograms are shown in the upper portion of the figures to demonstrate overlapping homogenization temperatures for type 1A and Type 1B inclusions. The bottom portion of the figures shows histograms for the low to moderate salinity aqueous fluids (type 2), saline brines (type 3) and secondary aqueous fluids (type 4). Characteristics for each fluid inclusion type are summarized in Table 3-4. Measurements from the calcite sample are not included but range from 118 to 152°C.

pressures (Diamond, 1994). Homogenization temperatures for type 1 inclusions show a considerable range, and some of this range may reflect the difficulty in identifying true end-member inclusions. Leaking of inclusions (sometimes visible during heating) also contributes to the range of temperatures. Observations of homogenization temperatures in CO₂-rich type 1B inclusions were difficult and as such, the values may be overestimated. In addition, many inclusions decrepitated prior to homogenization, and complete measurements on individual inclusions were not always obtained.

Pegmatite

Pegmatite sample 00-247-332 is from a 15 cm-wide vein of pegmatite that contains abundant quartz, graphic potassium feldspar, and muscovite with trace amounts of euhedral pyrite, chalcopyrite, galena, ilmenite, and apatite. Pegmatite is spatially associated with quartz veins and based on field relationships, is earlier than the quartz veins. No assay results are available for this sample but no gold values are documented from any pegmatite samples at the 4021 prospect or in the district.

Type 1A and 1B inclusions are the most common, followed by type 3 and type 2. Type 1A and 1B inclusions occur in primary clusters and along pseudosecondary trails. Homogenization temperatures (Th) range from 265 to 310°C for type 1A inclusions and 263 to 347°C for type 1B inclusions. The coexistence of type 1A and 1B inclusions and similar Th ranges are indicative of immiscible entrapment (Shepard et al., 1985). The temperature of CO₂ melting (T_{mCO₂}) was depressed as low as -58.2°C for type 1A and -59.2°C for type 1B inclusions indicating up to 10 mole % CH₄ (Heyden et al., 1982) in the CO₂ phase. The temperature of CO₂ homogenization (Th_{CO₂}) ranged from -10.6 to 25.6°C for type 1A inclusions and from 6.9 to 20.2°C for type 1B inclusions. In both types, CO₂ homogenized to liquid, indicating a high density for the CO₂ phase. Clathrate melting temperatures between 4.4 and 10.8 °C in type 1A

inclusions indicate salinities < 13 wt. % NaCl equivalent, however the presence of abundant CH₄ in these inclusions affect the estimate. Type 2A inclusions occur along pseudosecondary planes and have Th between 206 and 289°C and salinities between 2 and 7 wt. % NaCl equivalent. Type 2B inclusions have Th of 221 to 335°C. Salinity is estimated between 21-25 wt. % NaCl equivalent and eutectic melting temperatures between -40.1 to -34.6°C suggest a variety of salts, including Na₂CO₃, K₂CO₃, NaCl, KCl, FeCl₂ and MgCl₂ (Borisenko, 1977; Shepard, 1985). Type 3A inclusions locally occur along secondary trails associated with type 2B inclusions, as well as in primary clusters associated with type 1B inclusions. In the analysed sample, type 3A inclusions are generally small (<6 µm) and few measurements were possible. Homogenization temperatures range between 270 and 346°C and halite dissolution temperatures indicate salinities between 35 and 42 wt. % NaCl equivalent. Eutectic melting temperatures of -30.2 to -33.9°C suggest NaCl, MgCl₂ and KCl salts are present (Borisenko, 1977; Shepard, 1985). A few inclusions were found that contain CO₂-H₂O with a halite daughter in the aqueous portion (Figure 3-12b). These inclusions demonstrate that CO₂-rich and hypersaline fluids locally coexisted. Type 4 inclusions always occur along late secondary planes and have Th between 163 to 220°C and salinities of 1 to 7 wt. % NaCl equivalent.

Quartz Veins

Microthermometric analyses were conducted on two auriferous quartz veins. Sample 99-2076 is a quartz vein collected from the surface of the 4021 prospect from a boulder train and is inferred to be from the upper flat lying quartz vein. It contains 291g/t Au, and is gradational from a granular quartz vein. Sample 276-192 is a 1.5 cm thick, sheeted quartz veinlet containing 9 g/t Au and was collected from drill core. This sample is likely a steeply dipping extension veinlet because of the high angle the veinlet makes to the vertical drill hole core which implies a steeply dipping geometry. Both samples have visible gold, are elevated in Bi-Te-W, and contain

<5% arsenopyrite, pyrite, native bismuth and Bi-Te \pm S minerals. Native gold occurs as isolated grains within quartz, arsenopyrite and pyrite, and locally along quartz and sulphide grain boundaries.

99-2076 (*Flat quartz vein*)

Type 1A and 1B inclusions are the most abundant type in sample 99-2076, followed by less abundant type 2A, and very rare type 2B and 3A inclusions. This fluid inclusion assemblage is typical for the gold-bearing quartz veins that were observed petrographically. Type 1 inclusions occur as isolated primary inclusions and along pseudosecondary trails. Homogenization temperatures range from 233 to 302°C for type 1A and from 225 to 390°C for type 1B. T_{mCO_2} values as low as -57.3°C for type 1A and -59.4°C for type 1B indicate up to 12 mol. % CH_4 in the CO_2 phase. Homogenization temperatures for CO_2 range from 21.9 to 28.8°C for type 1A and -5.2 to 22.3°C for type 1B. All inclusions homogenized to CO_2 liquid. Salinity estimates based on $T_{m_{clath}}$ between -5.2 and 10.1°C for type 1A inclusions indicate salinities < 9 wt. % NaCl equivalent. Type 2A inclusions are common and occur along pseudosecondary planes. Homogenization temperatures range from 171°C to 248°C and salinity estimates based on final ice melting are 1 to 5 wt. % NaCl equivalent. Type 3 inclusions are very rare, and no inclusions suitable for microthermometric measurements were found. Type 4 inclusions occur in secondary trails that cross cut grain boundaries and have T_h between 125 and 219°C, and salinities of 0 to 4 wt. % NaCl equivalent. Eutectic temperatures less than -4°C indicate a simple salt system for type 4 inclusions.

Type 1A and 1B inclusions occur in clusters and in pseudosecondary trails with type 1B > 1A. Homogenization temperatures range from 225 to 365°C for type 1A inclusions and from 207 to 370°C for type 1B inclusions. T_{mCO_2} values as low as -62.2°C for type 1A and -64.41°C for type 1B inclusions indicate up to 37 mole % CH_4 in the CO_2 phase. Temperatures of CO_2 homogenization range from -9.7 to 4.2°C for type 1A and -22.8 to 7.4°C for type 1B inclusions. CO_2 homogenizes to liquid in both types, indicating the CO_2 phase has a high density. Ice melting temperatures indicate salinities between 6 and 9 wt. % NaCl, however, these are probably overestimates due to the inferred presence of clathrate (Shepard et al., 1985). Rare low salinity type 2A inclusions occur along pseudosecondary planes or as isolated, inferred primary inclusions. Homogenization temperatures range from 211 to 247°C and inclusions have salinities of 0.7 to 6.2 wt.% NaCl.

Type 2B and type 3 inclusions are abundant and occur together along pseudosecondary and secondary planes, and only rarely as inferred primary inclusions. Type 2B inclusions have T_h of 227 to 347°C and salinities of 17.4 to 25.0 wt. % NaCl equivalent. Type 2B inclusions have eutectic temperatures ranging from -40.9°C to -30.2, suggesting a complex salt system with Na_2CO_3 , K_2CO_3 , NaCl, $FeCl_2$ and $MgCl_2$ (Borisenko, 1977; Shepard, 1985). Many of these inclusions decrepitate before final homogenization.

Measurements for primary type 3A inclusions are scarce because most inclusions decrepitate before final homogenization or are too small for the low temperature measurements. Final homogenization temperatures ranged from 190 to 319°C. Halite and vapour typically homogenize within 20°C of each other, with vapour generally homogenizing first. Salinity estimates range from 32-40 wt. % NaCl equivalent based on halite dissolution. Type 3B

inclusions are abundant and typically occur along secondary planes. Vapour homogenization temperatures range from 312 to 376°C but the inclusions decrepitate between 452 and >480°C, prior to halite dissolution. Eutectic temperatures for type 3A inclusions range from -36.6 to -40.9°C, and between -29.2 to -38°C for type 3B inclusions, indicating a complex salt system.

Bladed calcite vein

Veins containing bladed calcite (sample 00-247-318) are a late alteration event and unrelated to gold mineralization. Bladed calcite veins were examined to constrain the latest fluid known to cross cut quartz veins. The calcite contains 2-phase, aqueous inclusions that are < 2 -10 µm. The inclusions have a rectangular to negative crystal form with consistent phase ratios of 90-95% liquid. One-phase aqueous inclusions are present locally along cleavage planes and are attributed to necking or leakage. Measurements on these inclusions were difficult to obtain due to the double refraction in calcite. Temperatures of homogenization range from 118 to 152°C. Salinity is negligible (<0.01 wt. % NaCl equivalent) and they contain no detectable gases other than H₂O.

INTERPRETATION OF FLUID INCLUSION MICROTHERMOMETRY

Pegmatite and gold-bearing quartz veins contain similar fluid inclusion types and compositions. Both contain rare primary saline and hypersaline fluid inclusions (type 3) in addition to abundant low salinity aqueous-carbonic inclusions (type 1) and low to moderate salinity type 2 inclusions. All samples also contain evidence for a secondary, low temperature and low salinity aqueous fluid (type 4). Type 2B inclusions in pegmatite and quartz veins have a similar range of eutectic temperatures (-41 to -30 °C) that suggests the same complex salt system in the aqueous fluids.

The aqueous-carbonic fluid inclusions in the pegmatite and main-stage quartz veins contain between 1 and 15 mol % CH_4 in the carbonic phase based on depressed final CO_2 melting temperatures (Figure 3-14) and CO_2 homogenization temperatures. Sheeted veinlets have the highest methane content with up to 37 mol % CH_4 in the carbonic phase. The elevated methane content is probably attributed to low initial oxidation states of associated magmas (Lowenstern, 2001) (Chapter 2), or the interaction of the hydrothermal fluids with reduced host rocks (McCuaig and Kerrich, 1994).

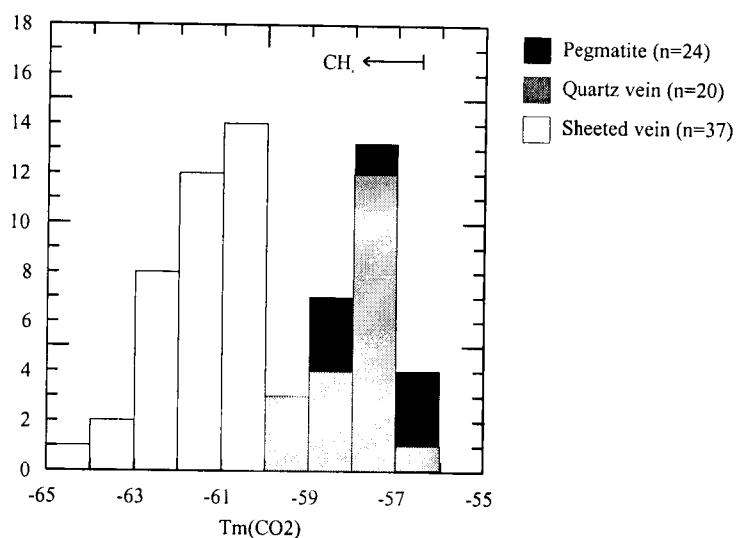


Figure 3-14. Depressed CO_2 melting temperatures for the pegmatite, sheeted quartz vein and main-stage quartz vein samples. n = number of measurements.

Pegmatite and quartz vein samples both contain ubiquitous, coexisting type 1A and type 1B inclusions that show evidence for H_2O - CO_2 phase separation. The inclusions occur in groups with variable ratios or locally as planes of all end member type 1A inclusions and all type 1B inclusions that homogenize to H_2O -liquid and CO_2 -liquid respectively over the same range of temperatures (Figure 3-13). This is strong evidence for H_2O - CO_2 immiscibility (Roedder and Bodnar, 1980; Shepard et al., 1985).

Rare, aqueous-carbonic inclusions containing a halite daughter in the aqueous phase provides evidence that the carbonic and aqueous-saline fluids were contemporaneous in the pegmatite. Similar homogenization temperatures for groups of inferred primary type 1 and type 3A inclusions are also consistent with their coexistence. Temperature of homogenization by daughter dissolution approximately equals temperature of homogenization by vapour ($T_{hd}=T_{hv}$) in type 3A inclusions further supporting an origin by fluid unmixing for some of these inclusions (Shepard et al., 1985). Unfortunately, homogenization data for type 3 inclusions is sparse, making data incomplete and interpretations problematic. Type 2B and 3 inclusions locally occur together along pseudosecondary trails suggesting they are related and reflect an aqueous fluid with a large range of fluid salinities (17 to 42 wt.% NaCl equivalent). Type 3 inclusions that decrepitated before final homogenization at high temperatures may represent a separate fluid event.

The fluid inclusion data suggests a genetic link between pegmatite and gold-bearing quartz veins and infers a complex fluid evolution from late magmatic to hydrothermal processes. A simplified model is proposed where an originally homogenous, moderate salinity, magmatic CO₂-bearing aqueous fluid undergoes phase separation into a hypersaline brine (type 3A) and low salinity, aqueous-carbonic fluid (type 1) (Figure 3-15). We speculate that gold, along with reduced sulphur species, likely portioned into the low salinity aqueous-carbonic fluid and on further cooling, or perhaps changing pressure conditions, was deposited during CO₂-H₂O fluid immiscibility (i.e. Scheelite Dome, Baker and Lang, 2001; Sigma mine, Robert and Kelly, 1987; Hollingetr-MacIntyre mine, Wood et al., 1986a, 1986b, Channer and Spooner, 1991; Roedder, 1984).

The simplified model presented herein explains the distribution of the fluid inclusion types and the inferred hydrothermal fluid chemistry documented at the 4021 prospect. The

model however, is based on a limited data set using complex fluid inclusions. The role of fluid mixing to account for the presence of brine and carbonic fluids cannot be unequivocally excluded. Moreover, metamorphic fluids are characterized by carbonic fluids and their presence can also not be excluded. Despite the limitations, the model does account for the presence of the co-existing brines and carbonic fluids. Other textural, temporal and isotopic evidence also indicates a magmatic linkage to the hydrothermal fluid.

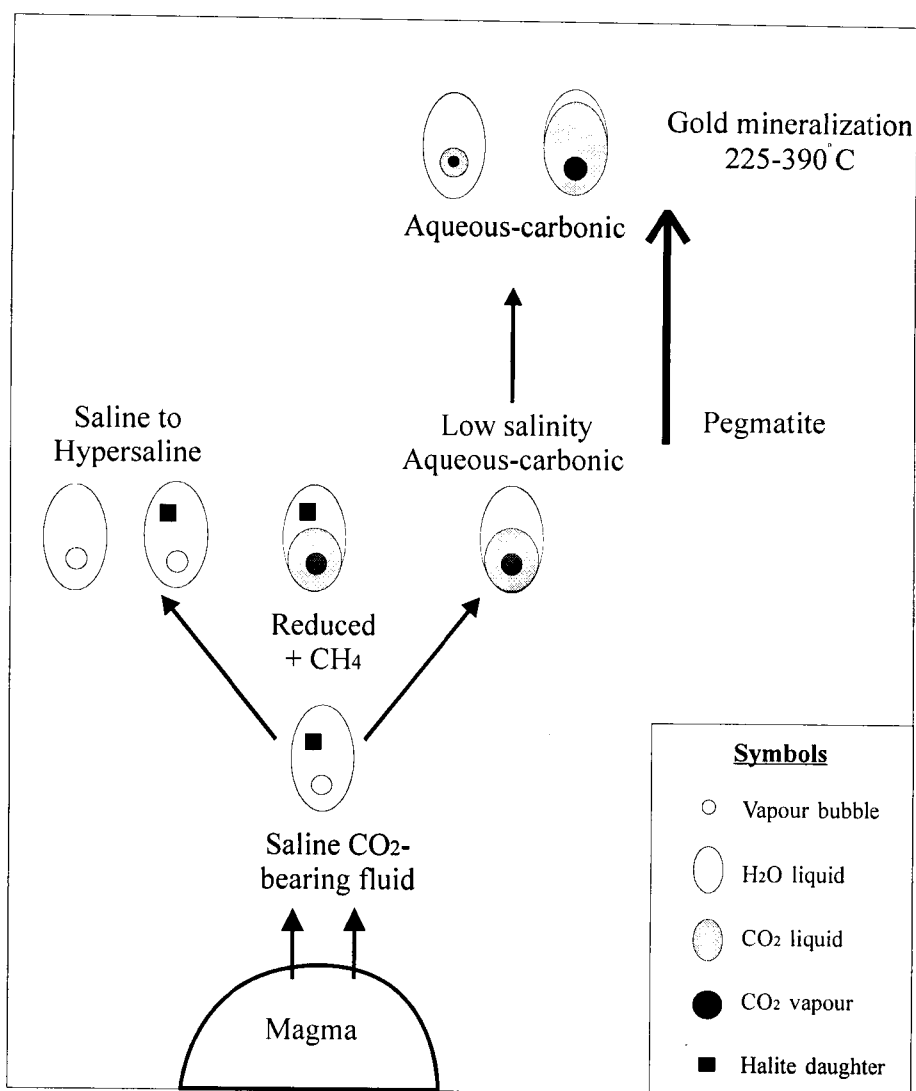


Figure 3-15. Hypothetical fluid evolution model of the 4021 prospect showing possible changes in fluids and fluid inclusion properties with distance from an inferred magmatic source. Modified after Ebert (2001).

PRESSURE ESTIMATES

Minimum trapping pressure estimates from fluid inclusions were obtained by constructing isochors from microthermometric data. Isochores were calculated using MacFlincor (Brown and Hagemann, 1994) and simplified fluid compositions using the equations of Kerrick & Jacobs (1981) for the $\text{CO}_2\text{-H}_2\text{O-CH}_4\text{-NaCl}$ system for Type 1 inclusions, and Bodnar & Vityk (1994) for the $\text{H}_2\text{O-NaCl}$ system for Type 2 inclusions. Where complete data was not available from an inclusion, values were estimated from inclusions within the same group or trail. Problems and uncertainties that arise are due to errors in phase estimation, simplification of the complex chemical system of the fluids, the uncertain paragenetic relationship between the different inclusions, and post-entrapment modification (Roedder and Bodnar, 1980).

Type 1A and type 1B inclusions are assumed to represent $\text{H}_2\text{O-CO}_2$ unmixing. These fluids therefore do not require a pressure correction as temperature of homogenization equals temperature of trapping (Roedder and Bodnar, 1980; Romboz et al., 1982; Shepard et al., 1985). Data for type 1B inclusions are plotted in Figure 3-16 as they provided the most complete microthermometric information. Salinities for type 1B inclusions were assumed to be the same as for immiscible type 1A inclusions. In all samples, trapping pressures estimated from type 1B inclusions ranged between 1300-2350 bar at trapping temperatures between 225 to 390°C.

Type 1B and type 2 inclusions have isochores with significantly different slopes and the intersection of these isochores are also used to estimate pressure (Roedder and Bodnar, 1980). It must be noted, however, that these two fluids at the 4021 prospect have not been proven to be unequivocally contemporaneous. Despite the uncertainty, the intersection of the isochores suggest trapping pressure estimates between 1250 and 2375 kbar. The relationship between fluid inclusion decrepitation before homogenization and inclusion size is a function of pressure

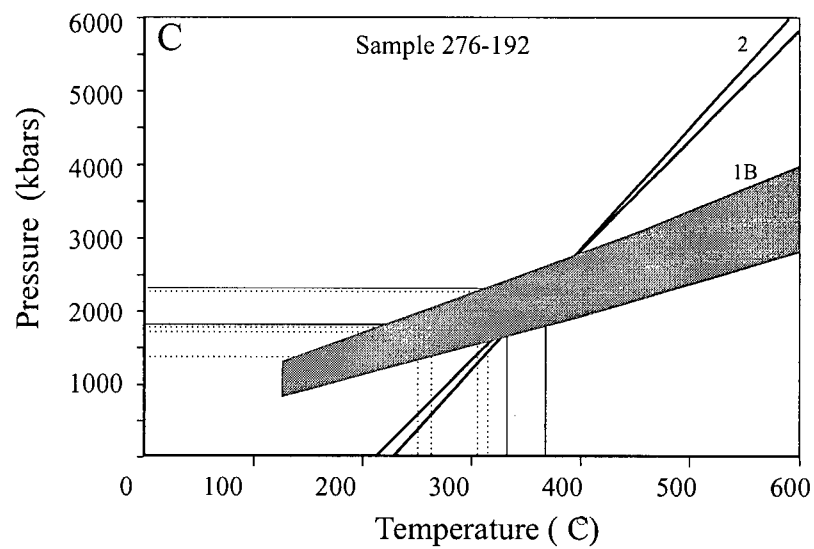
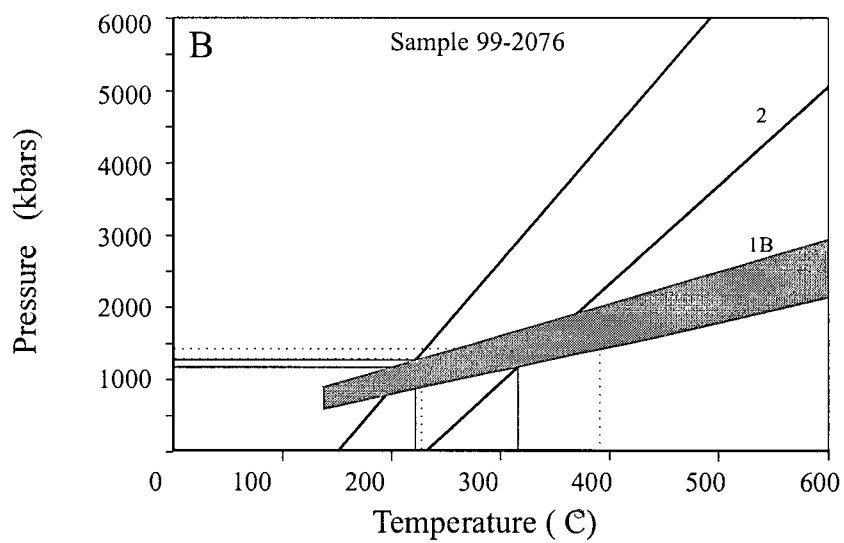
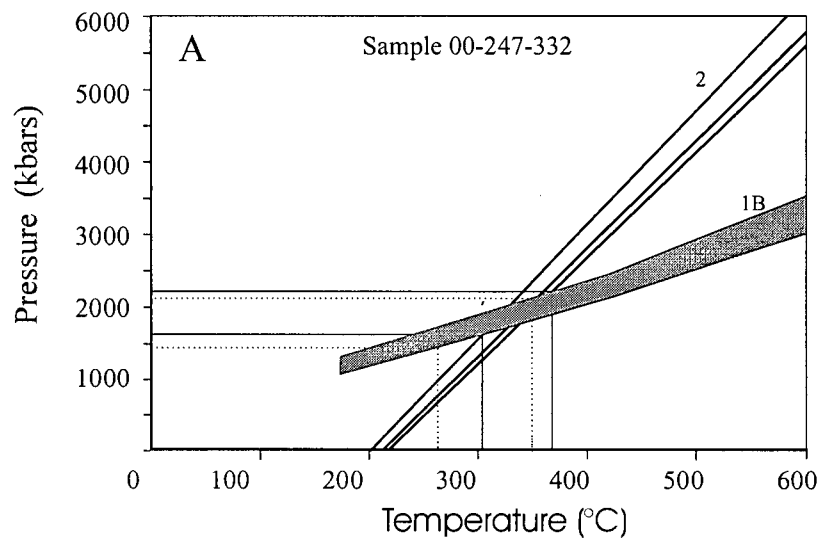


Figure 3-16. Isochore plots and pressure estimates for fluid inclusions for pegmatite (sample 247-332), quartz vein (sample 99-2076) and sheeted vein samples (sample 276-192). Isochores are calculated for type 1B and 2 inclusions that occurred within the same cluster of fluid inclusions. The intersection of type 1B and 2 isochores was used to estimate pressure and is shown as black, full lines. Note that it has not been proven that these fluid types were contemporaneous. Isochores calculated from end-member populations of immiscible type 1 fluid inclusions are shown as grey, dashed lines. Type 1B inclusions are presented, as they have the most complete microthermometric data set. Salinities are estimated based on available data for coexisting type 1A inclusions.

A) Isochore plot for pegmatite sample 247-332. Assuming immiscible entrapment and using the range of homogenization temperatures obtained for type 1B, isochors for type 1B inclusions yield a range of trapping pressure from 1500 to 2200 bars. The intersection of isochors for type 1B and type 2 inclusions gives a pressure estimate between 1650 and 2250 bars.

B) Isochore plot for sheeted quartz vein (sample 276-192). Assuming immiscible entrapment and using the range of homogenization temperatures obtained for type 1B, isochors for type 1B inclusions yield a range of trapping pressure from 1300 to 1500 bars. The intersection of isochors for type 1B and type 2 inclusions gives a pressure estimate between 1250 and 1300 bars.

C) Isochore plot for quartz vein (sample 99-2076). Assuming immiscible entrapment and using the range of homogenization temperatures obtained for type 1B, isochors for type 1B inclusions yield a range of trapping pressure from 1400 to 2350 bars. The intersection of isochores for type 1B and type 2 inclusions gives a pressure estimate between 1800 and 2375 bars.

(Leroy, 1979; Lacazette, 1990). Pressure estimates based on decrepitation of 8-12 μm type 1B fluid inclusions roughly range from 1400-2100 kbar (Leroy 1979; Lacazette, 1990). The largest non-decrepitating inclusion was 15 μm in size, corresponding to a minimum pressure estimate of 1200 kbar (Leroy, 1979).

Although precise estimates of trapping pressures are not possible from the fluid inclusion data, trapping pressures are estimated to be between 1.4 and 2.4 kbars (Figure 3-17). Assuming lithostatic conditions, these pressures correspond to a depth range of approximately 5 to 9 km (or 7 ± 2 km) for both the pegmatite and gold-bearing quartz veins.

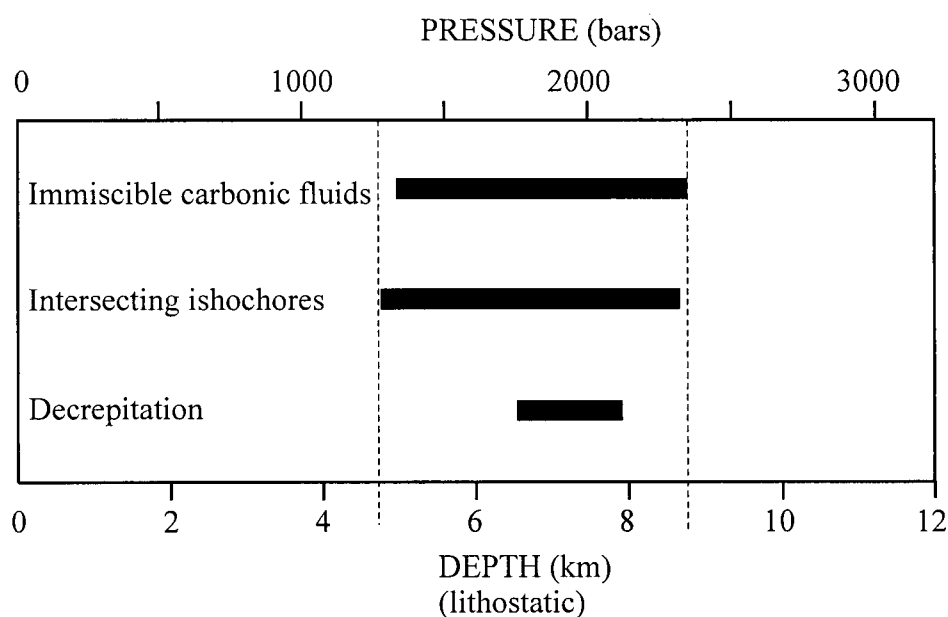


Figure 3-17. Estimated pressure and depth estimates based on intersecting isochores, immiscible type 1 inclusions, and decrepitation temperatures for type 1B inclusions.

LEAD ISOTOPIC COMPOSITIONS AS A SOURCE INDICATOR FOR GOLD VEINS

To further constrain the genetic model for the quartz veins in the Goodpaster district, twenty-six mineral separates were analysed for their lead isotopic compositions at the Pacific

Centre for Isotope and Geochemical Research (PCIGR) at the University of British Columbia, Vancouver. Sulphide samples analysed were from the main gold-bearing quartz veins of the Liese zone, 4021 prospect, and North zone, from the distal Shawnee Peak and Anglo trench prospects, and from a base metal vein from Shawnee Peak. Native gold is commonly included in arsenopyrite and pyrite grains, implying gold precipitated contemporaneously with the sulphides. The Pb isotopic composition of the sulphides are presumably representative of the ore-forming fluid and therefore can be used to identify metal sources of the quartz veins as well as assess the degree of fluid-wall rock interaction (Tosdal et al., 1999). The data is presented in $^{208}\text{Pb}/^{204}\text{Pb}$ vs. $^{206}\text{Pb}/^{204}\text{Pb}$ and $^{207}\text{Pb}/^{204}\text{Pb}$ vs. $^{206}\text{Pb}/^{204}\text{Pb}$ covariation diagrams shown in Figure 3-18. Sulphide Pb isotopic data for the various quartz veins and base metal vein in the district is presented in Table 3-7. Feldspar from the three Cretaceous intrusive suites and an Eocene rhyolite dyke are also presented in Figure 3-18. A detailed discussion of the Pb isotopic compositions of the intrusive rocks, and feldspar analytical data, is presented in Chapter 2.

The shale curve of Godwin and Sinclair (1982) provides a Pb isotopic reference for which to compare the data. The curve is used over the model evolution curve because it best explains the time-integrated Pb isotopic history of sedimentary rock sequences in the northern Cordillera of western Canada. Lead isotopic compositions from Devonian-Mississippian gneiss of the Yukon Tanana Terrane collected from east-central Alaska (Aleinikoff et al., 2000) and sulphides from gold-bearing quartz veins related to reduced intrusions of the younger Tombstone Plutonic Suite near Fairbanks (Aleinikoff et al., 1997) are also plotted for reference.

The granite and diorite suites, the oldest and youngest suites in the Goodpaster district respectively, have distinct Pb isotopic compositions. The granite suite contains a fairly

Table 3-7 : Lead isotopic analyses from sulphide mineral separates from gold-bearing quartz veins and a base metal vein in the Goodpastor district.

Sample ²	Location	Rock type	Mineral ³	²⁰⁶ Pb/ ²⁰⁴ Pb	Error %	²⁰⁷ Pb/ ²⁰⁴ Pb	Error %	²⁰⁸ Pb/ ²⁰⁴ Pb	Error %	²⁰⁷ Pb/ ²⁰⁶ Pb	Error %	²⁰⁸ Pb/ ²⁰⁶ Pb	Error %
Quartz Veins													
97-32	Liese Zone	Quartz-white	as	19.454	0.190	15.684	0.180	39.370	0.190	0.806	0.016	2.024	0.026
97-45	Liese Zone	Quartz-white	as	19.550	0.010	15.739	0.010	39.580	0.010	0.805	0.002	2.025	0.002
97-51	Liese Zone	Quartz- grey	as	19.518	0.020	15.788	0.020	39.753	0.020	0.809	0.009	2.037	0.015
97-49	Liese Zone	Quartz- white	cp	19.505	0.010	15.751	0.010	39.652	0.010	0.808	0.007	2.033	0.005
97-71	Liese Zone	Quartz- grey	as	19.573	0.060	15.763	0.060	39.618	0.060	0.805	0.007	2.024	0.007
97-55	Liese Zone	Quartz- grey	as	19.417	0.010	15.736	0.010	39.491	0.020	0.810	0.006	2.034	0.013
96-19	Liese Zone	Quartz- white	cp	19.499	0.030	15.737	0.020	39.465	0.030	0.807	0.012	2.024	0.009
97-58	Liese Zone	Quartz- white	py	19.427	0.020	15.728	0.010	39.438	0.020	0.810	0.003	2.030	0.008
97-41	Liese Zone	Quartz- grey	py	19.438	0.180	15.808	0.160	39.741	0.190	0.813	0.090	2.045	0.058
00-245-470.5	4021	Quartz Vein	as	19.502	0.011	15.735	0.011	39.553	0.039	0.807	0.000	2.028	0.001
97-54	North Zone	Quartz- white	as	19.545	0.020	15.720	0.020	39.572	0.030	0.804	0.006	2.025	0.012
97-48 b	North Zone	Quartz- grey	as	19.473	0.020	15.780	0.020	39.698	0.030	0.810	0.013	2.039	0.019
15303	Anglo Trench	Quartz Vein	as	19.242	0.009	15.686	0.010	39.043	0.034	0.815	0.000	2.029	0.001
SP-00-11	Shawnee Peak	Quartz Vein	as	19.258	0.009	15.700	0.010	39.220	0.034	0.815	0.000	2.037	0.001
Base metal vein													
44045	Shawnee Peak	Base metal vein	sl	19.202	0.008	15.725	0.010	39.143	0.034	0.819	0.000	2.038	0.001

1. All analysis analyzed by Janet Gabites at the PCIGR Laboratory at the University of British Columbia, Vancouver
All ratios corrected for isotopic fractionation (0.15% per atomic mass unit) based on repeated analyses of NBS SMP981 lead standard.
3. as = arsenopyrite, sl = sphalerite, cp = chalcopyrite, py = pyrite
Uncertainties are obtained by numerically propagating all mass fractionation and analytical uncertainties through the calculations and are presented at the 2σ level.

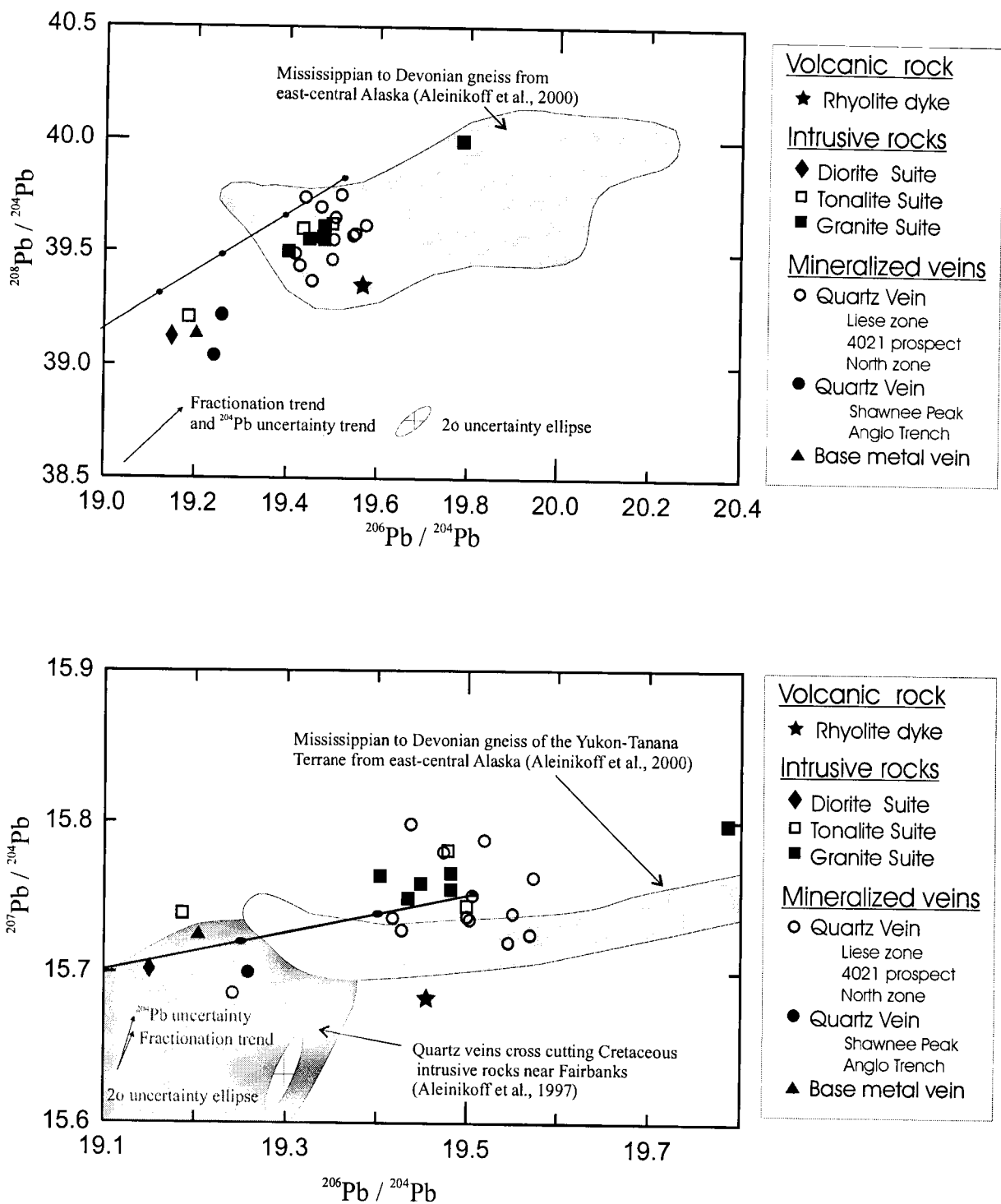


Figure 3-18 A) $^{208}\text{Pb}/^{204}\text{Pb}$ vs. $^{206}\text{Pb}/^{204}\text{Pb}$ diagram and B) $^{207}\text{Pb}/^{204}\text{Pb}$ vs. $^{206}\text{Pb}/^{204}\text{Pb}$ diagram. The growth curve of Godwin and Sinclair (1982) is shown in both diagrams for reference. Tick marks represent growth in 70 Ma increments. Note the change of scale between Figure A and B, due to the higher Pb isotopic values of Mississippian to Devonian gneiss of Yukon-Tanana Terrane (shown in grey) of east-central Alaska (Aleinikoff et al., 2000). The field for Pb values of the quartz veins cross cutting the intrusive rocks in Fairbanks (Aleinikoff et al., 1997) are presented only in the $^{207}\text{Pb}/^{206}\text{Pb}$ vs. $^{208}\text{Pb}/^{206}\text{Pb}$ diagram as only this data was provided.

homogeneous Pb isotopic population and has higher $^{206}\text{Pb}/^{204}\text{Pb}$ values (19.4 to 19.5) than the younger diorite suite ($^{206}\text{Pb}/^{204}\text{Pb}=19.2$). The tonalite suite has isotopic values that lie in the fields for both the granite and tonalite suites and an explanation for this is not obvious but could represent the more mafic nature of the tonalite.

Sulfide minerals from gold-bearing quartz veins of the Liese zone, 4021 prospect, and North zone form a relatively tight isotopic population with $^{206}\text{Pb}/^{204}\text{Pb}$ values of about 19.4 to 19.6. These veins are part of the main gold-mineralization event and have Pb isotopic values that overlap with those of the granite suite, and parts of the tonalite suite, which suggest they shared a similar source. The sulphide samples extend to slightly higher $^{206}\text{Pb}/^{204}\text{Pb}$ values than associated intrusive rocks possibly indicating fluid-rock interaction with the more radiogenic host gneiss of the Yukon Tanana Terrane. Lead exchanged or scavenged from the feldspathic gneisses in the Yukon Tanana Terrane could enhance initially moderately low Pb concentrations in the hydrothermal fluid derived from the granite, or possibly tonalite, suite. If the bulk of the Pb was leached from the Yukon Tanana Terrane, the Pb isotope values should be more radiogenic. Thus, the Yukon Tanana Terrane is not the likely source for the Pb isotopic values for the sulphide minerals. The diorite suite has lower $^{206}\text{Pb}/^{204}\text{Pb}$ values than the granite suite and is thus precluded from contributing Pb to the bulk of the sulfides in the main gold-bearing quartz veins. Lead isotope values of the felsic intrusions and associated main gold-bearing veins have higher $^{206}\text{Pb}/^{204}\text{Pb}$ values than sulphide minerals associated with the Tombstone Plutonic Suite ($^{206}\text{Pb}/^{204}\text{Pb} = 19.4$ to 19.6 versus $^{206}\text{Pb}/^{204}\text{Pb} = 19.0$ to 19.35 respectively).

Sulphides from a base-metal vein hosted in orthogneiss and gold-bearing quartz veins from Shawnee Peak and Anglo Trench have Pb isotopic values that are distinctly lower ($^{206}\text{Pb}/^{204}\text{Pb}=19.1$ to 19.3) and plot outside the main gold mineralization event cluster. Their lead isotopic composition is more similar to the diorite suite and a phase of the tonalite suite. These

gold-bearing quartz veins and base-metal vein may not be related to the main gold-mineralization event. The younger diorite suite, parts of the tonalite suite, the base metal vein and distal auriferous quartz veins have similar lead isotopic values to the Tombstone Plutonic Suite ($^{206}\text{Pb}/^{204}\text{Pb} = 19.1$ to 19.3 versus 19 to 19.35 respectively). The diorite suite is age equivalent to the Tombstone Plutonic Suite (~ 94 Ma).

DISCUSSION

Field relationships, geochronology, fluid-inclusion studies, and lead isotopes, all suggest the ore fluid at the 4021 prospect is magmatically derived. The gold-bearing quartz veins and granite and pegmatite sills and dykes are intimately associated, have similar flat-lying geometries, and have a sericite (-pyrite \pm carbonate) alteration assemblage. The lead isotopic compositional data presented above shows the granite suite is the possible source for the main gold-bearing quartz veins in the Goodpaster district. Granular quartz veins have a similar mineralogy and textures transitional between pegmatite and quartz veins. Granular quartz veins locally contain gold within the quartz grains, and rarely within the interstitial feldspar. The transitional nature of gold-bearing sheeted quartz veinlets with pegmatite and aplite is also reported at Fort Knox deposit (Bakke, 1995; McCoy et al., 1997, Thompson and Newberry, 2000).

Moore (2000) reports a limited number of stable isotope values from gold-bearing quartz vein samples from the Liese zone that provide further evidence for a magmatic origin. Reported $\delta^{34}\text{S}$ values of -0.7 to $+2.8$ per mil from sulphides in the Liese zone (Bressler and Corbett, 1996; Moore, 2000) fall within the range that is common for magmatic sulphur (Ohmoto and Rye, 1979; Rollinson, 1993). Calculated $\delta^{18}\text{O}$ values of ore fluids (assuming an average $\delta^{18}\text{O}$ value of $+15$ per mil for vein quartz and assuming temperature of formation between 300 and 600°C)

range from +7.5 to 13.2 per mil (Moore, 2000), which are permissible for a magmatic or metamorphic source. Nonetheless, the sulphur and oxygen isotope values from the Liese zone are similar to deposits near Fairbanks, Alaska ($\delta^{18}\text{O}_{\text{fluid}} = +5$ to $+10.1$ ‰; $\delta^{34}\text{S} = -3.5$ to $+3.2$ ‰; Fort Knox and Ryan Lode deposits)(McCoy et al., 1997), which are inferred to have a magmatic origin.

Comparison of the 4021 prospect to Liese zone

The 4021 prospect shares many characteristics with the Liese zone and likely formed by similar processes. Similarities include: (1) the flat-lying morphology of shear hosted quartz veins, (2) the arsenopyrite-löllingite-pyrite-pyrrhotite-gold mineral assemblage in addition to bismuth-telluride minerals, (3) the restricted sericite-carbonate alteration assemblages, and (4) similar lead isotopic composition of the sulphides. Early laminated biotite shear zones and alteration found in the Liese zone, however, are notably absent at the 4021 prospect. In contrast, the 4021 ductile shear zones are chlorite-rich and may represent a cooler hydrothermal system. Sheeted veinlets are also more abundant and widespread at the 4021 prospect than in the Liese zone.

Timing of mineralization in relation to metamorphism and Cretaceous magmatism

The timing of hydrothermal activity relative to magmatism is critical in proving a link between ore fluids and the causative intrusive phases. The timing of the gold mineralization event relative to the Cretaceous granitoids in the Goodpaster district is constrained from field relationships at the 4021 prospect and the Liese zone. Gold deposition is constrained between the ~107 Ma host rocks and the 94.5 Ma cross cutting dioritic intrusion (Smith et al., 2000; Chapter 2). Selby et al (2002) report a ^{187}Re - ^{187}Os isochron age of 104.2 ± 1.1 Ma from

molybdenite hosted in thin fracture planes within the L1 quartz vein of the Liese zone. This age places a minimum age on gold deposition, and may date formation if the molybdenum was contemporaneous with gold mineralization. Molybdenite, however, is interpreted to be late in the paragenetic sequence (Moir Smith, personal communication 2003) and the direct genetic link to gold deposition is unequivocal. Nonetheless, gold deposition in the Liese zone, and presumably the genetically related North zone and 4021 prospect, is bracketed between 107 and 104 Ma.

The $^{187}\text{Re}/^{187}\text{Os}$ age temporally overlaps with the tonalite suite and Goodpaster Batholith (106.9 to 103.2 Ma) but is ~ 2 Ma younger than the unfoliated phases of the granite suite (~ 107 Ma) with which gold-bearing quartz veins are spatially associated. The uncertainties associated with the crystallization ages of the intrusions are greater than the lifespan of a typical hydrothermal system (<100 ka; Coulsen et al., 2002) and therefore the duration of hydrothermal activity is not constrained. The 107 Ma, unfoliated phases of the granite suite, and most of the tonalite suite, is within the $^{187}\text{Re}/^{187}\text{Os}$ age uncertainties.

Molybdenite from quartz veins collected from the 4021 and Shawnee Peak prospects returned $^{187}\text{Re}/^{187}\text{Os}$ ages of 95.4 and 93.6 Ma respectively (Selby, personnel communication, 2002). These ages are similar to diorite suite intrusions (94.5 Ma) and $^{40}\text{Ar}/^{39}\text{Ar}$ ages of 96.1 to 91.2 Ma from alteration assemblages in the Liese zone (Smith et al., 2000; Rhys et al., 2003). The molybdenite sample used for Re-Os dating at the 4021 and Shawnee Peak prospects, however, did not contain detectable gold and may represent a different mineralizing event. Furthermore, the molybdenite sample from the 4021 prospect was collected from a talus boulder on surface and therefore its relationship to gold-bearing quartz veins is unknown.

Lead isotopic data supports the presence of two mineralizing fluids with distinct fluid sources, consistent with geochronologic data. The older event (107-104 Ma) is associated with

the main stage gold-bearing quartz veins and is apparently related to the granite suite, and potentially parts of the tonalite suite. The field relationships, supported by the lead isotope evidence, suggests the 4021 prospect is the same age as the Liese zone (~107-104 Ma), and therefore is 13-15 Ma older than typical intrusion-related gold deposits associated with the reduced intrusions of the Tombstone Plutonic Suite.

The younger event, possibly associated with base metal veins and minor quartz veins, occurred at ~94.5 Ma. A younger age for some of the basemetal veins is consistent with rare ankerite-sphalerite-galena veins which cross cut the Liese quartz veins, and the strong Pb-Zn-Sb-As interelement correlation that suggests a different paragenetic event from gold. The younger mineralizing event is presumably somehow related to the diorite suite, or possibly the tonalite suite. It furthermore is similar in age to other IRGD's in the Fairbanks region (~92 Ma) (McCoy et al., 1997; Thompson and Newberry, 2000; Lang et al., 2001).

Additional evidence from the Goodpaster region support the conclusion that the main stage of gold deposition occurred at about 105 Ma. The Blue Lead prospect, located 40 kilometers southeast of the Liese zone, has shear hosted gold-bearing quartz veins that average one meter in width and reach up to 2.5 meters wide (Freegold International Inc. website). Quartz veins and associated quartz stockwork contain gold and a variable assemblage of sulphides including arsenopyrite, covellite, digenite, stibnite, jamesonite, molybdenite and pyrite (Hart et al., 2002). Hydrothermal alteration minerals associated with gold-bearing quartz veins is dated at 105.5 ± 0.5 Ma (Ar-Ar; white mica) and the adjacent intrusive has an age of 105.8 ± 0.4 Ma (Ar-Ar; biotite)(McCoy et al., 1997). This suggests the quartz veins and intrusions were coeval. McCoy et al. (1997) also infer the intrusions were emplaced during the latest stages of regional metamorphism. Despite the Sb-Au geochemical signature, the relationships are like those defined from the Liese zone and 4021 prospect. Evidently, the age of the Liese zone and the

4021 prospect gold-bearing quartz veins are not unique and it is likely that additional examples will be discovered in the future.

Magmatic Linkages and Depths of Formation

Pegmatites and gold-bearing quartz veins share similar fluid compositions, with ubiquitous low salinity aqueous-carbonic fluids and rare saline fluids. Fluid inclusion data is also consistent with pegmatite and quartz veins forming under similar physiochemical conditions.

Granitic pegmatite records the history of late magmatic fluids (Smerekanicz and Dudas, 1999) to hydrothermal fluids (London, 1986). Few fluids are trapped at the magmatic stage (Roedder, 1984; London, 1986; Williams and Taylor 1996). Low salinity, CO₂-rich and mixed H₂O-CO₂ fluids (with or without NaCl) like those interpreted from the 4021 prospect have been found in several pegmatites worldwide (Cook, 1979; London, 1986; Sirbescu, 2001), demonstrating that aqueous-carbonic fluids and locally high salinity fluids are common in the pegmatite environment. The presence of high salinity fluids in some pegmatite likely reflects preservation of the magmatic fluid (Foord et al. 1991). High salinity fluids furthermore are cited as direct evidence for an exsolved magmatic fluid in many shallowly emplaced intrusion-related ore systems in the epithermal and porphyry copper deposit models (Bodnar 1995; Meinert et al. 1997; Hedenquist et al. 1998). Because no evaporitic sequences are known in the Yukon-Tanana terrane to account for the high saline brines, some of the high salinity fluids in the pegmatite and quartz veins are interpreted to be magmatic in origin.

Fluid-inclusion trapping pressures of 1.4 to 2.3 kbar imply depths of 5-9 km for hydrothermal activity at the 4021 prospect. Similar depths of formation (1.7 to 2 kbar) were estimated for parts of the L1 vein in the Liese zone using equilibrium pairs of arsenopyrite and

löllingite with pyrite and pyrrhotite (McCoy and Olsen, 1997). Furthermore, these depths are consistent with emplacement depths of 5-9 km ($\sim 2 \pm 1$ kbar) for the Goodpaster Batholith, based on the Al-in-hornblende geothermobarometer (see Chapter 2).

Orogenic versus reduced intrusion-related gold deposits

The shallowly dipping shear hosted quartz veins at the 4021 prospect, and the Liese zone, have been classified as reduced intrusion-related gold deposits (McCoy et al., 1997; Thompson et al., 1999; Lang and Baker, 2000), and as orogenic gold deposits related to metamorphic fluids or regional processes (Goldfarb et al. 2000; Hart et al., 2002). Hart et al. (2002) suggests that the quartz veins in the Goodpaster district lie in a continuum between the two deposit type styles.

Shear hosted quartz veins, sericite-carbonate alteration, elevated pressure of formation (~ 2 kbar), and abundant carbonic-rich fluid inclusions characterize Archean and Phanerozoic orogenic lode gold systems (Goldfarb et al. 2000; McCuaig and Kerrich, 1994; Roberts, 1988). Orogenic quartz veins form soon after post-peak regional deformation and metamorphism in high angle reverse faults or strike slip structures undergoing compression (Kerrich and Cassidy, 1994; Groves et al., 1998; Cox, 1999; Bierlien and Crowe, 2000). Links to associated granitic rocks are tenuous although there is usually a spatial relationship.

The shallowly dipping veins share some characteristic with orogenic gold deposits but also differ in slight but significant ways. The quartz veins at the 4021 prospect and the Liese zone are immediately post-metamorphic and are spatially and temporally related to reduced late Early Cretaceous felsic intrusions. They furthermore appear to have formed in a normal shear zone (down current dip) or in a localized extensional environment assuming the present orientation of the tectonite fabrics approximates the orientation at the time of formation (Rhys et al., 2003). The veins share many characteristics to intrusion-related gold deposits in Yukon and

Alaska that have an unambiguous magmatic origin (McCoy et al., 1997; Lang et al., 2000; Thompson and Newberry, 2000; Hart et al., 2002). These include a strong correlation of Au with Bi and Te, a reduced ore assemblage (löllingite + pyrrhotite), and primary potassium feldspar in the veins. Geochronology, Pb isotope data, and fluid inclusion evidence discussed above, favours a magmatic over a metamorphic source for metals and ore-forming fluids.

CONCLUSIONS

The data presented here provides compelling evidence for a magmatic origin for the 4021 prospect and are best interpreted within the context of a structurally focused but magmatically-derived hydrothermal system. The gold mineralization event occurred soon after the intrusion of granite to granodiorite between 109 and 107 Ma. The flat lying quartz veins and steeply dipping quartz veinlets at the 4021 prospect are temporally and spatially associated with the late Early Cretaceous granite and tonalite suites. The quartz veins have a reduced ore assemblage including arsenopyrite, löllingite, pyrite and pyrrhotite. Gold occurs as free grains less than 100 μm in diameter or as complex intergrowths with Bi-Te-S minerals. Gold has a strong Bi-Te interelement correlation. The geochemical correlation highlights the Bi-Te-Au association at the 4021 prospect, a relationship common in other intrusion related gold deposits (McCoy et al., 1997; Thompson and Newberry, 2000). Pegmatite and quartz veins have a spatial and temporal association, and contain similar flat lying geometries, mineralogy and textures. The transition from pegmatite to quartz veins through the granular quartz veins provides good evidence for a direct linkage between the felsic intrusions and gold-bearing quartz veins.

Lead isotopes provide the most compelling linkage of the auriferous quartz veins to the felsic intrusions, as feldspar from the granite suite and sulphides from the Liese, North and 4021 zones have similar lead isotopic compositions. Saline fluid inclusions coexisting with carbonic

fluids in both the quartz veins and pegmatite offer an additional connection to intrusions. Limited fluid inclusion data suggest an H₂O-CO₂-salt bearing magmatic-derived fluid undergoes phase separation into saline brine and an aqueous-carbonic fluid. The suspected method of gold deposition occurred during fluid immiscibility of the aqueous-carbonic fluids, where gold was deposited at temperatures between 225 and 390°C. Pressure estimates from fluid inclusions infer the gold-bearing quartz veins were emplaced at ~2 kbar, corresponding to a depth of 7 ± 2 km.

Several lines of evidence require the presence of two mineralizing events in the Goodpaster district. Re-Os ages suggest deposition of molybdenite at 104 Ma and at about 95 Ma. These ages are broadly consistent with the distribution of the two major intrusive events: the granite-tonalite suite at ~104-107 Ma and the diorite suite at 94 Ma. The gold-bearing quartz veins of the 4021 prospect are associated with the older event, at around 107 Ma.

REFERENCES:

- Aleinikoff, J.N., Farmer, G.L. Rye, R.O., and Nokleberg, W.J. 2000. Isotopic evidence for the sources of Cretaceous and Tertiary granitic rocks, east-central Alaska; implications for the tectonic evolution of the Yukon-Tanana terrane. *Canadian Journal of Earth Sciences*, **37**: 945-956.
- Aleinikoff, J.N., and Nokleberg, W.J., 1985a, Age of intrusions and metamorphism of a granodiorite in the Lake George subterranean, northeastern Mount Hayes Quadrangle, *in* Bartsch-Winkler, S., and Reed, K.M., eds., *The United States Geological Survey in Alaska; Accomplishments during 1983: U.S. Geological Survey Circular 945*, p. 62-65.
- Aleinikoff, J.N., Dusel-Bacon, C., Foster, H.L., and Nokleberg, W.J., 1997. Lead isotopic fingerprinting of tectonostratigraphic terranes, east-central Alaska. *Canadian Journal of Earth Sciences*, **24**: 2089-2098
- Bakke, A.A., 1995, The Fort Knox 'porphyry' gold deposit-Structurally controlled stockwork and shear quartz vein, sulfide-poor mineralization hosted by a Late Cretaceous pluton, east-central Alaska, *in* Schroeter, T.G., ed., *Porphyry deposits of the North-western Cordillera of North America: Canadian Institute of Mining, Metallurgy and Petroleum Special*, v. 46, p. 795-802.
- Bressler, J.R. and Corbett, T.J., 1996, 1995 Stone Boy Project Annual Report: WGM, Inc., Unpublished company report, 111 p. (and appendices).
- Baker, T. and Lang, J.R. 2001. Fluid inclusion characteristics of intrusion-related gold mineralization, Tombstone-Tungsten magmatic belt, Yukon Territory, Canada. *In* *Intrusion-Related Gold Systems special Mineralium Deposita Edited by J.R. Lang and T. Baker*. v. 36, pp. 563-582.
- Bierline, F.P., and Crowe, D.E., 2000. Phanerozoic Orogenic Lode Gold deposits. *In* *Gold in 2000*, eds. Hagemann, S.G., and Brown, P.E., *Review in Economic Geology*, v. 13, p. 103-139.
- Brown, P.E. and Hagemann, S.G. (1994) MacFlinCor: A computer program for fluid inclusion data reduction and manipulation. *In* De Vivo and Frezzotti (eds) *Fluid Inclusions in Minerals: Methods and Applications*, VPI Press, 231-250.
- Bodnar, R. J., 1995 Fluid inclusion evidence for a magmatic source for metals in porphyry copper deposits. *In*: Thompson, J.F.H (ed), *Magmas, fluids and ore deposits*. Mineralogical Association of Canada Short Course series, no. 23, pp 139-152.
- Bodnar, R. J., and Vityk, M.O., 1994, Interpretation of microthermometric data for H₂O-NaCl fluid inclusions. *In*: DeVivo, B., Frezzotti, M.L., (eds), *Fluid inclusions in minerals: methods and applications*. IMA shortcourse volume, pp. 117-130.
- Borisenko, A.S., 1977. Study of the salt composition of solutions in gas-liquid inclusions in minerals by the cryometric method. *Soviet Geol. & Geophys.* **18**, 11-19.

- Channner, D.M. DeR., and Spooner, E.T.C., 1991, Grant 364. Multiple fluid-inclusion generations in variably deformed quartz: Hollinger-McIntyre and Kerr Addison-Chesterville Archean gold-bearing quart vein systems, Northern Ontario: Ontario Geologic Survey, Miscellaneous Paper 156, p. 47-64.
- Collins, P.L.F. (1979), Gas Hydrates in CO₂-bearing fluid inclusions and the use of freezing data for estimation of salinity, *Economic Geology*. Volume 74, pages 1435-1444.
- Cook, C.W., 1979, Fluid inclusions and etrogenesis of the Harding pegmatite, Taos County, New Mexico: unpublished MS thesis, University of New Mexico, Albuquerque, 143 p.
- Cox, S.F., 1999, Deformational controls on the dynamics of fluid flow in mesothermal gold systems, in McCaffrey, K.J.W., Lonergan, L., and Wilkinson, J.J. (eds). *Fractures, fluid flow and mineralization: Geological Society, London, Special Publication 155*, p. 123-140.
- Coulson, I.M., Villeneuve, M.E., Dipple, G.M., Duncan, R.A., Russell, J.K. and Mortensen, J.K., 2002. Time-scales of assembly and thermal history of a composite felsic pluton: constraints from the Emerald Lake area, northern Canadian Cordillera, Yukon. *Journal of Volcanology and Geothermal Research*, 114: 331-356.
- Day, W.D., Aleinikoff, J.N., Dusel-Bacon, C., Goldfarb, R., Gough, L.P. and O'Neill, J.M., 2002, Complex Mesozoic deformation in the central part of the Yukon Tanana Uplands, Alaska -Implications for gold deposition in the Tintina Gold Province, *Geological Society of America Programs with Abstracts*.
- Diamond, L.W., 1994, Introduction to phase relations of CO₂-H₂O fluid inclusions. In: De Vivo B, Frezzotti M.L (eds), *Fluid inclusions in minerals: methods and applications*. IMA short course volume, pp 131-158.
- Dusel-Bacon, C., and Aleinikoff, J.N., 1985. Petrology and tectonic significance of augen gneiss from a belt of Mississippian granitoids in the Yukon-Tanana terrane, east-central Alaska. *Geological Society of American Bulletin*, 96: 411-425.
- Dusel-Bacon, C., and Aleinikoff, J.N., 1996, U-Pb zircon and titanite ages for augen gneiss from the divide mountain area, eastern Yukon-Tanana Upland, Alaska, and Evidence for the composite nature of the Fiftymile Batholith, in Moore, T.E and Dumoulin, J.A., eds, *Geologic Studies in Alaska by the U.S. Geological Survey Bulletin 2552*, p. 131-141.
- Dusel-Bacon, C., Lanphere, M., Sharp, W., Layer, P. and Hansen, V., 2002. Mesozoic thermal history and timing of structural events for the Yukon-Tanana Upland, east-central Alaska: ⁴⁰Ar/³⁹Ar data from metamorphic and plutonic rocks. *Canadian Journal of Earth Sciences*, 39: 1013-1051
- Ebert, S., Miller, L., Petsel, S., Dodd, S., and Kowalczyk, P., 2000, Geology, Mineralization, and Exploration at the Donlin Creek Project, Southwest Alaska: in *The Tintina Gold Belt: Concepts, Exploration, and Discoveries*, Special Volume 2, British Columbia and Yukon Chamber of Mines, pp. 99-114.

- Ebert, S., Roberts, P., and Smith, M., 2001. Igneous rocks and gold Prospects in the Pogo District. *In* Regional geologic Framework and Deposit-Specific Exploration Models for Intrusion-related gold Mineralization, Yukon and Alaska. Mineral Deposit Research Unit, Notes from the Second Annual Technical Meeting, p. 33-55.
- Foord, E.E., London, D., Kampf, A.R., Shigley, J.E., and Snee, L.W. (1991) Gem-bearing pegmatites of San Diego County, California. In M.J. Walawender and B.B. Hanan, Eds., Geological Excursions in Southern California and Mexico, p. 128-146. Geological Society of America Guidebook, Boulder, Colorado
- Foster, H.L., Keith, T.E., and Menzie, W.D. 1994. Geology of the Yukon-Tanana Terrane of east-central Alaska. In the geology of Alaska: Boulder, Colorado, Geological Society of America, The geology of North America, v. G-1. Edited by G. Plafker and H.C. Berg, pp. 205-240.
- Godwin, C.I. and Sinclair, A.J. 1982. Average lead isotope growth curves for shale-hosted zinc-lead deposits, Canadian Cordillera. *Economic Geology*, 77: 208-211.
- Goldfarb, R.J., Miller, L.D., Leach, D.L., and Snee, L.W., 1997. Gold deposits in metamorphic rocks of Alaska: *Economic Geology Monograph* 9, p. 151-190.
- Goldfarb, R., Hart, C., Miller, M., Miller, L., Farmer, G.L., Groves, D., 2000. The Tintina gold belt – a global perspective. In: Tucker, T.L., Smith, M.T. (eds). The Tintina Gold Belt: concepts, exploration and discoveries. British Columbia and Yukon Chamber of Mines Special Volume 2. pp 5-34.
- Groves, D.I., Goldfarb, R.J., Gebre-Mariam, M., Hagemann, S.G., and Robert, F., 1998. Orogenic gold deposits: A proposed classification in the context of their crustal distribution and relationship to other gold deposits types: *Ore Geology Reviews*, v. 13, p. 7-27.
- Hansen, V.L., and Dusel-Bacon, C. , 1998, Structural and kinematic evolution of the Yukon Tanana upland tectonites, east-central AK, *GSA Bulletin*, v. 110, no. 2, p. 211-230.
- Hart, C. J.R., Baker, T., and Burke, M. 2000. New exploration concepts for country-rock-hosted, intrusion-related gold systems: In: Tucker, T.L., Smith, M.T. (eds). The Tintina Gold Belt: concepts, exploration and discoveries. British Columbia and Yukon Chamber of Mines Special Volume 2. pp 145-172.
- Hart, C.J.R., McCoy, D.T., Goldfarb, R.J., Smith, M., Roberts, P., Hulstein, R., Bakke, A.A., and Bundtzen, R.K., 2002, Geology, Exploration, and Discovery in the Tintina Gold Province, Alaska and Yukon, *in* Society of Economic Geologists Special Publication 9, p. 241-274.
- Hart, C.J.R. and Goldfarb, R.J., 2003. Targeting Intrusion-related Gold Systems in the Tintina Gold Province, Alaska and Yukon, Abstract *in* Canadian Cordilleran Roundup, p. 3-4.

- Hedenquist, J.W., Arribas, A., and Reynolds, T.J., 1998, Evolution of an intrusion centered hydrothermal system: far Southeast-Lepanto porphyry and epithermal Cu-Au deposits, Philippines, *Economic Geologist*, v. 93: 373-404.
- Heyden, G., Ramboz, C., Dubessy, A., 1982, Simulation des équilibres de phases dans le système $\text{CO}_2\text{-CH}_4$ en dessous de 50°C et de 100 bar. Application aux inclusions fluids. *C R Acad Sci Paris* 294: 204-305.
- Kerrick, R., and Cassidy, K. F., 1994. Temporal relationships of lode gold mineralization to accretion, magmatism, metamorphism and deformation-Archean to present: A review: *Ore Geology Reviews*, v. 9., p. 163-310.
- Kerrick, D.M., and Jacobs, G.K., 1981, A modified Redlich-Kwong equation for H_2O , CO_2 and $\text{H}_2\text{O-CO}_2$ mixtures at elevates pressures and temperatures. *American Journal of Science*, v. 281, p. 735-767.
- Lacazette, Alfred. (1990). Application of linear elastic fracture mechanisms to the quantitative evaluation of fluid-inclusion decrepitation. *Geology*, v. 18, p 782-785
- Lang, J.R., T. Baker, C.J.R. Hart, and J.K. Mortensen. 2000, An exploration model for intrusion-related gold systems: *Society of Economic Geologists Newsletter*. 40,1, 6-15.
- Lang, J.R. and Baker, T. 2001. Intrusion-related gold systems: the present level of understanding. *In* *Intrusion-Related Gold Systems special volume, Mineralium Deposita, Edited by J.R. Lang and T. Baker*. v. 36, pp. 477-490.
- Leroy, J., 1979, Contribution a l'étalonnage de la pression interne des inclusions fluids lors de leur decrepitation: *Societe Francaise, Mineralogie et Cristallographie, bulletin*, v. 102, p. 584-593.
- London, D., 1986, Magmatic-hydrothermal transition in the Tanco rare-earth element pegmatite: Evidence from fluids inclusions and phase-equilibrium experiments. *American Mineralogist*, v. 71, p. 376-395.
- Lowernstern, J.B., 2001. Carbon dioxide in magmas and implications for hydrothermal systems. *Mineralium Deposita*, v. 36, p. 490-502.
- Meinert, L.D., Jefton, K.K., Mayes, D., and Tasiran, I., 1997. Geology, zonation and fluid evolution of the Big Gossan Cu-Au skarn deposit, Ertsber district, Irian Jaya. *Economic Geologists*, 92: 509-535.
- McCoy, D., R.J. Newberry, P. Layer, J.J. DiMarchi, A. Bakke, J.S. Masterman, and D.L. Minehane. 1997, Plutonic-related gold deposits of interior Alaska, *in* Goldfarb, R.J., and Miller, L.D., eds., *Mineral deposits of Alaska: Economic Geology Monograph* 9, p. 191-241.

- McCoy, D., and Olsen, I., 1997, Thermochronology, mineralogy, elemental and microprobe analysis of the Fort Knox, Dolphin and selected Golden Summit deposits, *in* Newberry, R. and McCoy, D., eds., *Geology of bulk-minable, plutonic-hosted and plutonic-related gold deposits of the north Pacific: Short Course Notes*, Alaska Miner's Association Annual Convention and Trade Fair, Anchorage, Alaska.
- McCuaig, T.C. and Kerrich, R., 1994, P-T-t-deformation-fluid characteristics of lod gold deposits: evidence from alteration systematics, *in* Lentz, D.R., ed., *Alteration and Alteration Processes Associated with Ore-forming Systems: Geological Association of Canada, Short Course Notes*, v. 11, p. 339-379.
- Moore, K., 2000. Geology of the gold-bearing L1 and L2 Liese quartz zones, Pogo Deposit, east-central Alaska: Masters Thesis, Colorado School of Mines, June 2000.
- Mortensen, J.K. 1992. Pre-Mesozoic tectonic evolution of the Yukon-Tanana terrane, Yukon and Alaska. *Tectonics*, **11**: 836-853.
- Mortensen, J.K., Hart, C.J.R., Murphy, D.C., and Heffernan, S., 2000. Temporal evolution of Early and Mid-Cretaceous magmatism in the Tintina Gold Belt. *In* *The Tintina Gold Belt: Concepts, exploration, and discoveries*, British Columbia and Yukon Chamber of Mines Cordilleran Roundup Special Volume 2, Vancouver, British Columbia, pp. 49-57.
- Mustard, R., 2001. Granite-hosted gold mineralization at Timbarra, northern New South Wales, Australia. *In* *Intrusion-Related Gold Systems special volume, Mineralium Deposita*, Edited by J.R. Lang and T. Baker. v. 36, pp. 542-562.
- Nokleburg, W.J., Aleinikoff, J.N, and Lange, I.M., 1993, Origin and accretion of Andean-type and island arc terranes of Paleozoic age juxtaposed along the Hines Creek fault, Mount Hayes Quadrangle, eastern Alaska Range, Alaska: *Geological Society of America Abstracts with Programs*, v. 15, p. 427.
- Newberry, R.J. 2000. Mineral deposits and associated Mesozoic and Tertiary igneous rocks within the interior Alaska and adjacent Yukon portions of the "Tintina Gold Belt": A progress report. *In* *The Tintina Gold Belt: Concepts, exploration, and discoveries*, British Columbia and Yukon Chamber of Mines Cordilleran Roundup Special Volume 2, Vancouver, British Columbia, pp. 59-88.
- Ohmoto, H., and Rye, R.O., 1979, Isotopes of sulfur and carbon, in Barnes, H.L., (eds), *Geochemistry of hydrothermal ore deposits*, New York, John Wiley & Sons, p. 509-567.
- Park, V., 1999, Brewery Creek project 1998 exploration progress report, January 20, 1999. Viceroy Exploration (Canada) Inc. company report.
- Rhys, D., DiMarchi, J., Rombach, C., Smith, M., Friesen, R. (in press). Structural setting, style and timing of vein-hosted gold mineralization at the Pogo deposit, east-central Alaska: 38 p. *Mineralium Deposita*.

- Roberts, R.G., 1998, Archean lode gold deposits, in Roberts, R.G., and Sheahan, P.A., eds., Ore deposit models: Geoscience Canada, Reprint Series 3, p. 1-19.
- Roedder, E., 1984. Fluid inclusions: Mineralogical Society of America Review in Mineralogy, v. 12, 644.
- Roedder, E., and Bodnar, R.J., 1980. Geologic pressure determinations from fluid inclusions studies, *Ann. Rev. Earth Planet. Sci.* **8**, 263-301.
- Rollinson, H.R. 1993. Using geochemical data: evaluation, presentation, and interpretation. Longman Group Limited, Essex, England, 352 p.
- Rombach, C., Newberry, R.J., Gordfarb, R.J., Smith, M., 2002. Geochronology and Mineralization of the Liese zones, Pogo Deposit, Alaska. Geological Society of America Program with Abstracts.
- Robert, R., and Kelly, W.C., 1987, Ore-forming fluids in Archean gold-bearing quartz veins at the Sigma Mine, Abitibi greenstone belt, Quebec, Canada: *Economic Geology*, v. 82, p. 56-74.
- Selby D, Creaser RA, Hart C.J., Rombach C.S., Thompson J.F.H., Smith M. T., Bakke A, Goldfarb R., 2002. Timing of sulphide and gold mineralization at the Fort Knox and Pogo gold deposits, Tintina Gold Belt, Alaska: Evidence from Re-Os molybdenite dates for distinct gold mineralization episodes. *Geology*: v. 30, No. 9, pp. 791-794.
- Smerekanicz, J.R., and Dudas, F.O., 1999, Reconnaissance fluid inclusion study of the Morefield pegmatite, Amelia County, Virginia, *American Mineralogist*, v. 84, p. 746-753.
- Smith M, Thompson J, Bressler J, Layer P, Mortensen J, Abe I, Takaoka H, (1999), Geology of the Liese zone, Pogo property, East-central Alaska. SEG Newsletter 38: 1, 12-21.
- Smith, M.T., J.F.H. Thompson, K.H. Moore, J.R. Bressler, P. Layer, J.K. Mortensen, I. Abe, and H. Takaoka. 2000, The Liese zone, Pogo Property: A new high-grade gold deposit in Alaska, in Tucker, T.L., and Smith, M.T., eds., *The Tintina Gold Belt: Concepts, exploration and discoveries*: British Columbia- Yukon Chamber of Mines, Cordilleran Round-Up Special Volume 2, p. 131-144.
- Shepherd, T. J., Rankin, A.H., and Alderton, D.H.M., 1985. A practical guide to fluid inclusion studies: Blackie, Chapman and Hall, New York, 240 p.
- Thompson J.F.H., Sillitoe RH, Baker T, Lang J.R., Mortensen J.K. (1999). Intrusion-related gold deposits associated with tungsten-tin provinces. *Mineral Deposita* 34: 323-334.
- Thompson, J.F.H., and R.J. Newberry. 2000, Gold deposits related to reduced granitic intrusions, in Hagemann, S.G., and Brown, P.E., eds., *Gold in 2000: Reviews in Economic Geology*. v.13 ,377-400.

- Tosdal, R.M., Wooden, J.L., and Bouse, R.M. 1999. Pb isotopes, ore deposits and metallogenic terranes: *Economic Geology Reviews*, **12**: 1-28.
- Weber, F., R., Foster, H.L., Keith, T.E.C., and Dusel-Bacon, C., 1978, Preliminary geological map of the Big Delta Quadrangle: U.S. Geological Survey Open-File Report 78-529-A, scale 1:150,000.
- Werre, R.W. Jr., Bodnar, R.J., Bethke, P.M., and Barton, P.B. Jr. (1979), A novel gas-flow fluid inclusion heating/freezing stage (abstract). *Geological Society of America Abstract with Programs*, **11**, p. 539.
- Williams, A.E. and Taylor, M.C. (1996) Mass spectrometric identification of boric acid in fluid inclusions in pegmatite minerals. *Geochimica et Cosmochimica Acta*, **60**, p. 3435-3443.
- Wilson F.H., Smith, J.G., and Shew, Nora, 1985, Review of radiometric data from the Yukon crystalline terrane, Alaska and Yukon Territory: *Canadian Journal of Earth Sciences*, v. **22**, p. 525-537.
- Wood, P.C., Burrows, D.R., Thomas, A.V., and Spooner, E.T.C., 1986a, The Hollinger-McIntyre Au-quartz vein system: Geologic characteristics, gold occurrence, fluid properties and light stable isotope geochemistry, in Macdonald A.J., ed., *Gold '86, an International Symposium on the Geology of Gold Deposits*, Toronto, p. 56-80.

CHAPTER FOUR

GENERAL CONCLUSIONS AND EXPLORATION CONSIDERATIONS

The second and third chapters in this thesis represent contributions to the Mineral Deposit Research Unit's intrusion-related gold project. Geochronology, field relationships, petrography, granular quartz textures, fluid inclusion studies, and lead isotopic data all suggest the gold-bearing quartz veins of the 4021 prospect formed from exsolved hydrothermal fluids probably from the late Early Cretaceous granite suite, and possibly the tonalite suite. The discovery of the high-grade Liese zone and nearby prospects has resulted in increased exploration activity for high-grade gold mineralization related to reduced intrusions. The empirical observations and theoretical models presented for the 4021 prospect may help aid exploration for similar deposits in the Goodpaster district. Outlined below are the key findings of this study.

Cretaceous Intrusive Rocks

The late Early Cretaceous granite suite intruded late- to post-metamorphism and deformation at 109 to 107 Ma. The suite forms small dykes, sills and tabular sheets of biotite \pm garnet bearing granite and granodiorite intrusions with less abundant leucogranite, aplite and pegmatite. Older phases of the suite are deformed by two main deformation events (D1 and D2). Strongly foliated granitic orthogneiss (~ 109 -107 Ma) constrains the S1 foliation to be as young as ~107 Ma. A folded pegmatite in the Liese zone demonstrates D2 occurred at least locally at ~107-108 Ma. This suggests that D1 and D2 temporally overlap and occurred 107 to 108 Ma. The youngest phases of this suite are unfoliated and form small bodies that locally intrude as flat lying bodies along S2, S3, or other flat lying structures.

The intermediate tonalite suite was emplaced during a slightly younger Cretaceous event between 107 and 103 Ma and forms large plutonic bodies including the Goodpaster Batholith and Shawnee Peak stock. The tonalite suite is characterized by hornblende-biotite bearing tonalite with lesser granite, granodiorite and minor quartz diorite.

Previously, it was interpreted that the Goodpaster Batholith was emplaced during the early Late Cretaceous around 93 Ma (Smith et al., 1999, 2000). New ages presented in this study show the Batholith is a composite intrusion and some phases are much older than previously interpreted (105.7 Ma). Emplacement depths from Al-in-hornblende geobarometry indicate the Goodpaster Batholith was emplaced at depths of 7 ± 2 km.

The youngest, early Late Cretaceous intrusive event formed post-kinematic biotite-hornblende \pm pyroxene bearing diorite, quartz diorite and lesser monzonite and tonalite around 94.5 to 93.7 Ma. This suite forms small, steeply dipping bodies and contains < 1 % primary magnetite. Diorite post-dates gold-bearing quartz veins of the 4021 prospect and the Liese zone.

All the Cretaceous intrusive rocks in the Goodpaster district are reduced. $\text{Fe}_2\text{O}_3/\text{FeO} + \text{Fe}_2\text{O}_3$ ratios less than 0.45, the abundance of ilmenite, scarcity of magnetite and low magnetic susceptibilities all support the reduced origin of the intrusions. The intrusive rocks are subduction related. They are either crustally derived and inherited the arc signature or are mantle derived and are highly contaminated by the continental crust. The intrusive rocks may be reduced due to interaction with the underlying sedimentary rocks of the Yukon-Tanana terrane or North American crust. The diorite suite has less crustal influence than the older granite and tonalite suites. Additional information about the source of the magmas and the degree of crustal contamination may be better understood by Sr, Nd and Hf studies on the intrusive rocks in the Goodpaster district.

4021 Prospect Gold-bearing quartz veins

The 4021 prospect consists of at least two shallowly dipping, low angle quartz veins hosted within shear structures that are surrounded by abundant steeply dipping quartz veins. The quartz veins consist of ~3 vol. % ore minerals which include arsenopyrite, pyrite, löllingite, pyrrhotite, chalcopyrite, native gold, bismuth telluride minerals, Bi-Te \pm S minerals, maldonite and rare galena. Microthermometric analysis of fluid inclusions in pegmatite and gold-bearing quartz veins are similar and are dominated by low salinity H₂O-CO₂-CH₄-NaCl \pm KCl fluids. Gold and sulphide deposition likely occurred during aqueous-carbonic fluid immiscibility at about 225° to 390°C. The presence of rare primary saline and hypersaline fluids further suggests a magmatic origin for the ore-forming fluid. Pressure estimates of 1.4 to 2.4 kbar imply depths of formation at 5-9 km assuming near-lithostatic fluid pressures. At the 4021 prospect, the shallowly dipping quartz veins are thinner and the sheeted veinlets are more widespread and abundant than in the Liese zone. Host rock rheology may play an important role in the size of the quartz veins, due to differences in the formation of faults and propagation of hydrothermal fluid. The presence of sheeted veinlets and ductile shear zones may indicate proximity to thicker, shallowly dipping gold-bearing quartz veins.

The lead isotopic signature for the main gold-bearing quartz veins is consistent with derivation of their lead from the granite suite, or possibly tonalite suite. Distinct differences between the Pb isotopic compositions of main quartz vein and the diorite suite indicate that the mineralizing fluids were neither derived from the diorite suite, nor did they obtain much Pb (or presumably other metals) from them. This lead isotope signature of the granite suite may be effective in distinguishing intrusive rocks with gold potential.

Re-Os ages suggest deposition of molybdenite at 104 Ma and at about 95 Ma. These ages are broadly consistent with the emplacement of the major intrusive events: the granite-

tonalite suite at ~103-109 Ma and the diorite suite at ~94 Ma. The younger Re-Os ages are from non-auriferous quartz-molybdenite vein samples. In addition, lead isotope data suggest two different lead isotopic sources for the granite and the diorite suite. Basemetal veins and minor quartz veins may be associated with phases of the tonalite suite or perhaps the younger diorite suite. Additional lead isotopic data for the tonalite suite and diorite suite are needed in order to assess whether the tonalite suite has two distinct populations, or with more data becomes a continuum between the diorite and granite suite. The recognition of the possibility of two mineralizing events could have important implications for further exploration in the Goodpaster district.

The 4021 prospect and other areas of known mineralization in the Goodpaster district are spatially and temporally related to the granite to tonalite suite intrusions. The veins are most closely spatially related to the youngest unfoliated phases of the granite suite, notably pegmatite and aplite (~107 Ma). The quartz veins postdate metamorphic fabrics and post-metamorphic intrusions, including sulphide-bearing pegmatite. The emplacement of the quartz veins and some pegmatite exploit flat lying structures. The recognition of flat-lying structures is important for determining the location of gold-bearing quartz veins in the Goodpaster district, including the 4021 prospect and the Liese zone.

The Goodpaster Batholith is unmineralized. Intrusive bodies with greater than 4 km² surface exposure typically have no gold-bearing quartz veins, as the apexes have been eroded away and gold veins form in the apexes of the intrusions (McCoy et al., 1997; Thompson and Newberry, 2000). This suggests the Goodpaster Batholith and other large stocks in the Goodpaster district are not likely hosts for gold occurrences. Smaller intrusions, such as the granite suite that forms small, tabular bodies may have better exploration potential. The main gold-bearing veins are 12-15 m.y. older than the intrusion-related gold deposits associated with

the Tombstone Plutonic Suite and deposits associated with the Dawson Range Plutonic suite in Yukon. This broadens the potential age range, and geographic location, for intrusion-related gold deposits in eastern Alaska and Yukon.

Classification

There may still be some debate as to the classification of the gold-bearing quartz veins in the Goodpaster district due to the overlapping characteristics between orogenic gold deposits and intrusion-related gold deposits. Classifying the 4021 prospect and nearby auriferous quartz veins is not merely a semantic problem, as exploration criteria for the regional and camp scale are significantly different between the two mineral deposit classes. The evidence provided in Chapter 2 and Chapter 3 favours an intrusion-related gold deposit classification (McCoy et al., 1997; Thompson et al., 1999; Lang et al., 2000; Thompson and Newberry, 2000). Diagnostic characteristics include: (1) the spatial and temporal association of gold-bearing quartz veins with reduced, I-type intrusions, (2) the associated intrusions are felsic, typically granite to granodiorite in composition, calc-alkaline and weakly metaluminous to peraluminous, (3) the gold veins are post-metamorphism and deformation, (4) gold correlates strongly with bismuth and to a lesser degree tellurium, (5) the metal assemblage includes arsenopyrite, löllingite, pyrrhotite, pyrite, bismuth and variable bismuth-tellurides \pm sulphide minerals, (6) the quartz veins contain ubiquitous, low salinity aqueous-carbonic fluids with local high salinity fluids and (7) quartz veins have a restricted zone of hydrothermal alteration. The shallowly dipping shear hosted nature of the gold veins, the large thickness of the quartz veins, and the high-grade nature of the Liese zone differ from typical auriferous quartz veins within the intrusion-related gold deposit class. The gold-bearing quartz veins of the Goodpaster district are deep-seated manifestations of the intrusion-related gold deposit class.

REFERENCES:

- Lang, J.R., Baker, C.J.R. Hart, and J.K. Mortensen. 2000, An exploration model for intrusion-related gold systems: Society of Economic Geologists Newsletter. v 40,1, 6–15.
- McCoy, D., Newberry, R.J., Layer, P., Dimarchi, J.J., Bakke, A., Masterman, J.S. & Minehane, D.L. 1997. Plutonic-related gold deposits of interior Alaska. *In* Mineral deposits Alaska, Economic Geology Monograph 9, *Edited by* R.J. Goldfarb and L.D. Miller, pp. 191-241.
- Thompson J.F.H., Sillitoe RH, Baker T, Lang J.R., Mortensen J.K. (1999). Intrusion-related gold deposits associated with tungsten-tin provinces. *Mineralium Deposita*, v. 34: 323-334.
- Thompson, J.F.H., and R.J. Newberry. 2000, Gold deposits related to reduced granitic intrusions, *in* Hagemann, S.G., and Brown, P.E., eds., *Gold in 2000: Reviews in Economic Geology*, v.13 ,377–400.

Appendix A

U-Pb Geochronology of intrusive rocks in the Goodpaster Mining District, east-central Alaska

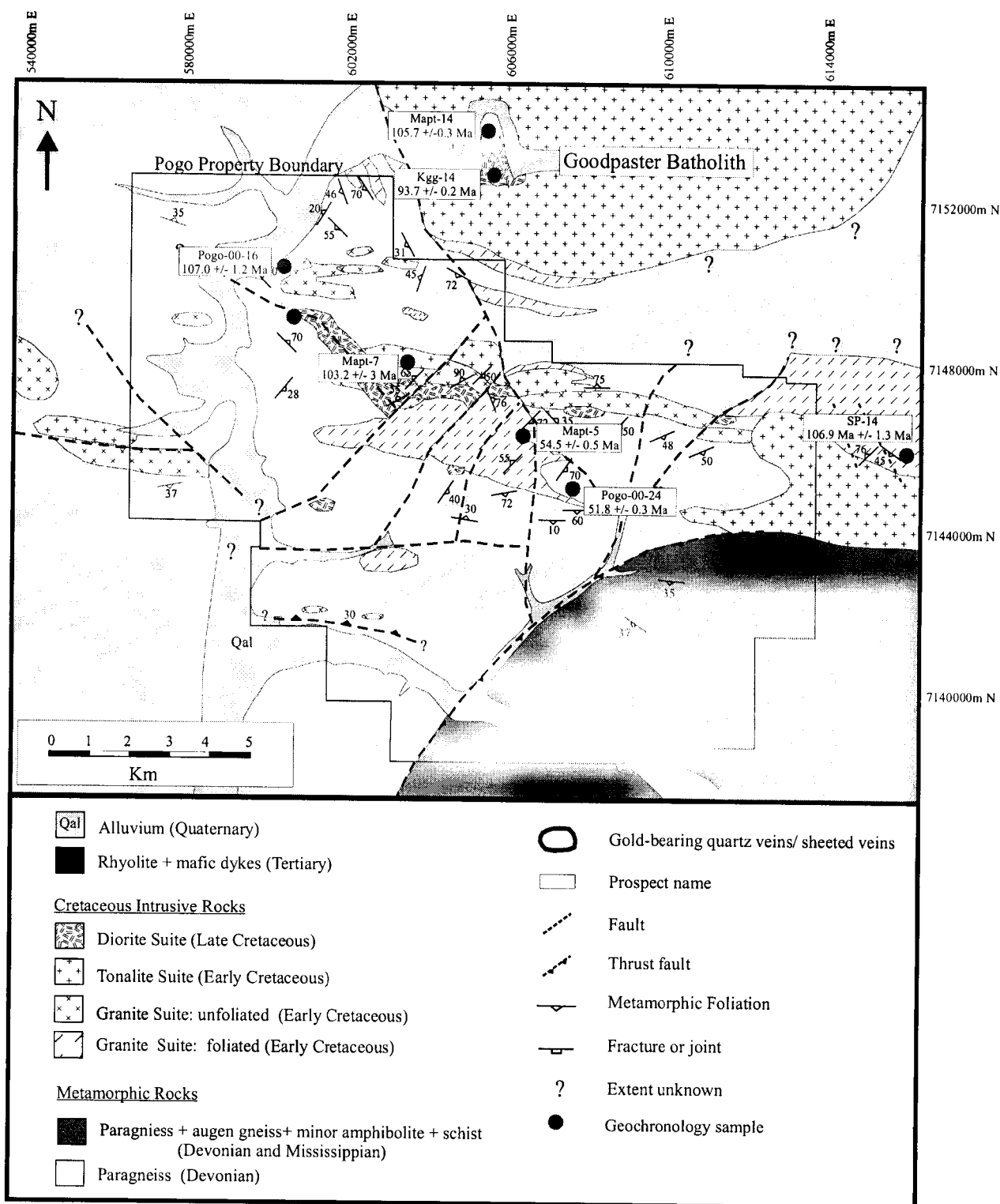


Figure A-1. Geological map of the Goodpaster district and the locations of intrusive rock samples used for U-Pb dating.

Table A-1: Locations and descriptions for samples used for geochronology

Sample	Rock Unit	Age (Ma)	Zone	Location	Description*
U/Pb SHRIMP-RG					
MAPT-7	granodiorite	103.4 ± 2.2 (zircon)	Football Field	603314 N / 7147600 E	equigranular, medium-grained, biotite-granodiorite
U-Pb Conventional					
KG-14	tonalite	93.7 ± 0.2 (zircon)	Goodpaster Batholith	605308 N / 7152204 E	equigranular, coarse-grained, hornblende-biotite tonalite
MAPT-14	tonalite	105.7 ± 0.3 (monazite)	Goodpaster Batholith	604981 N / 7147822 E	equigranular, coarse-grained, biotite-hornblende tonalite
SP-00-14	granite	106.9 ± 1.3 (monazite)	Shawnee Peak	615622 N / 7146190 E	seriate, fine- to medium-grained hornblende-biotite granite
Pogo-00-16	two mica granite	107.9 ± 1.2 (monazite)	North Zone	600320 N / 7149928 E	medium grained, muscovite-biotite granite with rare Fe-Mg garnets
OGNU-98-93	orthogneiss	109.2 ± 0.4 (monazite) 107.0 ± 0.6 (zircon)	Liese Zone	DDH 98-93 852-853.5 ft	medium-grained, strongly folded, hornblende-biotite-rich orthogneiss
PEGM-98-93	Altered Pegmatite	107.5 ± 2.0 (monazite)	Liese zone	DDH 98-93 882-885 ft	coarse-grained pegmatite, sericite altered
GDIB: 97-71	granodiorite	107.3 ± 0.8 (monazite)	Liese zone	DDH 97-71 265.5-266.7ft	coarse-grained pegmatite; graphic K-spar with interstitial quartz and biotite; sericite altered
98-176	granitic orthogneiss	107.3 ± 0.8 (monazite)	Liese zone	DDH 98-176 585.6'-587.8'	weakly foliated, K-spar megacrystic medium- to coarse-grained granitic gneiss
97-75	granodiorite	107.1 ± 0.6 (monazite)	Liese zone	DDH 97-75 1257-1259 ft	biotite-poor granodiorite, sericite altered
MAPT-21	Syn-F2 pegmatite	108.0 ± 1.0 (monazite)	Liese zone	L1 1/2 vein, underground	coarse-grained pegmatite with patches of aplite, folded and deformed by D2 event
105-745	diorite	94.5 ± 0.2 (zircon)	Liese zone	DDH 105-745 745-750 ft	medium-grained, equigranular to seriate, hornblende-biotite +/- pyroxene diorite
MAPT-5	rhyolite	54.5 ± 0.5 (zircon)	East of 4021	605003 N / 7146700 E	Quartz-feldspar phryic rhyolite dyke
POGO-00-24	rhyolite	51.8 ± 0.3 (zircon)	Cholla Ridge	Cholla Ridge	rounded, 3-5mm quartz and feldspar phenocrysts in a fine-grained rhyolite groundmass.

*Grain size is relative to the Pogo region: less than 0.5 mm are aplitic, 0.5 - 1 mm are fine-grained, 1 - 2mm are medium-grained, 2 - 5mm are coarse-grained and greater than 5 mm are pegmatitic.

Conventional U-Pb Geochronology

J.K. Mortensen

INTRODUCTION

Uranium-lead zircon dating of fifteen samples of Cretaceous and Tertiary intrusive rock units from the Goodpaster District in east-central Alaska was undertaken using conventional ID-TIMS methods in order to establish precise crystallization ages for the main intrusive events in the region.

METHODOLOGY

Zircon and monazite were separated from 0.1 - 10 kg samples using conventional crushing, grinding, Wilfley table, heavy liquids and Frantz magnetic separator techniques. U-Pb analyses were done at the Pacific Centre for Isotopic and Geochemical Research at the University of British Columbia. The methodology for zircon and monazite grain selection, abrasion, dissolution, geochemical preparation and mass spectrometry are described by Mortensen et al. (1995). Most zircon fractions were air abraded (Krogh, 1982) prior to dissolution to minimize the effects of post-crystallization Pb-loss. Monazite samples were not abraded prior to analysis. Procedural blanks for Pb and U were 2 and 1 pg, respectively. U-Pb data are plotted on a conventional U-Pb concordia plot in Figures 1 - 3. Errors attached to individual analyses were calculated using the numerical error propagation method of Roddick (1987). Decay constants used are those recommended by Steiger and Jäger (1975). Compositions for initial common Pb were taken from the model of Stacey and Kramer (1975). All errors are given at the 2 sigma level. U-Pb analytical data is provided in Table A1.

Monazite analyses generally plot slightly above concordia due to the presence of a minor component of excess ^{206}Pb related to disequilibrium ^{230}Th effects. For such analyses the $^{207}\text{Pb}/^{235}\text{U}$ age is taken as the most reliable estimate of the age of the fraction. Monazite ages are interpreted to represent the time at which the igneous rock unit cooled through $\sim 725^\circ\text{C}$ following igneous crystallization (Parrish, 1990).

RESULTS

Sample OGNU-98-93: A total of nine zircon and two monazite fractions were analyzed (Table A-1). Zircon grains in this sample were clear and colorless and ranged from multifaceted equant grains to stubby or elongate prisms. Cloudy inherited cores were visible in a small proportion of the zircon grains. Individual zircon fractions were separated on the basis of morphology. One fraction (E) consisted of tips broken off prismatic grains with visible inherited cores. Attempts to obtain a zircon fraction that was completely free of inheritance were for the most part unsuccessful, and eight of the nine zircon analyses plot in a broad array indicative of the presence of older inherited zircon components of more than one age (Fig. A-2a). Fraction O consisted of a single, strongly abraded, elongate prismatic grain. It yields a concordant analysis with a $^{206}\text{Pb}/^{238}\text{U}$ age of 109.2 ± 0.4 Ma. This fraction appears to have been free of inheritance and thus this age is interpreted to give the crystallization age of the sample. Two unabraded fractions of monazite were also analysed

(Fig. A-2b). Both analyses plot slightly above concordia but give identical $^{207}\text{Pb}/^{235}\text{U}$ ages of 107.0 ± 0.6 Ma, which is interpreted as the time at which the protolith of the gneiss unit last cooled through 725°C .

Sample GDIB-97-71: Two fractions of zircon and two fractions of monazite were analyzed. Zircons were similar in appearance to those in the previous sample and both analyzed fractions yield strongly discordant analyses (Fig. A-2c), indicating the presence of a large component of inherited zircon. Two fractions of unabraded monazite from the sample plot slightly above concordia with $^{207}\text{Pb}/^{235}\text{U}$ ages of 107.3 ± 0.8 Ma, which is interpreted as the crystallization age of the sample.

Sample PEGM-98-93: Three fractions of unabraded monazite were analyzed (Table A-1). All plot slightly above concordia (Fig. 2d) with a the total range of $^{207}\text{Pb}/^{235}\text{U}$ ages of 107.5 ± 2.0 Ma, which is interpreted as the crystallization age of the sample.

Sample 98-176: Eight fractions of zircon from this sample were analyzed (Fig. A-1e). All contain a substantial amount of inherited zircon and an age cannot be determined from the zircon data. Three fractions of unabraded monazite from the sample plot on or slightly above concordia (Fig. A-2f) with $^{207}\text{Pb}/^{235}\text{U}$ ages of 107.3 ± 0.8 Ma, which is interpreted as the crystallization age of the sample.

Sample SP00-14: Three fractions of zircon were analyzed (Fig. A-2g) and each contains older inherited zircon. Two fractions of unabraded monazite from the sample plot on or slightly above concordia (Fig. A-2g) with $^{207}\text{Pb}/^{235}\text{U}$ ages of 106.9 ± 1.3 Ma, which is interpreted as the crystallization age of the sample.

Sample 97-75: Four zircon fractions contain moderate to strong inheritance (Fig. A-1h). Two fractions of unabraded monazite from the sample plot on or slightly above concordia (Fig. A-2h) with $^{207}\text{Pb}/^{235}\text{U}$ ages of 107.1 ± 0.6 Ma, which is interpreted as the crystallization age of the sample.

Sample MAPT-14: Three fractions of strongly abraded, elongate, prismatic zircon were analyzed (Table A-1; Fig. A-2i). Two fractions contain a minor older inherited zircon component; however one fraction (C) is concordant with a $^{206}\text{Pb}/^{238}\text{U}$ age of 105.7 ± 0.3 Ma, which is interpreted as the crystallization age of the sample. This sample did not contain monazite.

Sample MAPT-21: Two zircon fractions contain moderate to strong inheritance (Fig. A-2j). Two fractions of unabraded monazite from the sample plot on or slightly above concordia (Fig. A-2j) with $^{207}\text{Pb}/^{235}\text{U}$ ages of 108.0 ± 1.0 Ma, which is interpreted as the crystallization age of the sample.

Sample POGO-00-16: Three fractions of unabraded monazite from the sample plot on or slightly above concordia (Fig. A-2k) with $^{207}\text{Pb}/^{235}\text{U}$ ages of 107.9 ± 1.2 Ma, which is interpreted as the crystallization age of the sample.

Sample 107-745: This sample of the Liese diorite yielded abundant coarse, high quality zircon, in the form of stubby to elongate simple prisms. Four strongly abraded fractions were analyzed (Table A-1). Two fractions are concordant with a total range of $^{206}\text{Pb}/^{238}\text{U}$ age of 94.5 ± 0.2 Ma (Fig. A-2l), which gives the crystallization age of the sample. Fractions B and D contain an older inherited component. A regression line through the four fractions yields an upper intercept age of 1.13 Ga, which gives the average age of the inherited component.

Sample KGG-#14: This sample was very small (<100 g) but yielded sufficient zircon for several analyses. Five strongly abraded fractions were analyzed (Table A-1). One fraction is concordant with a $^{206}\text{Pb}/^{238}\text{U}$ age of 93.7 ± 0.2 Ma, which is interpreted to give the crystallization age of the sample. All of the remaining fractions contain a moderate to strong inherited zircon component. Two-point regressions through Fraction C and each of the discordant fractions yield calculated upper intercept ages of 650 Ma to 2.15 Ga (Fig. A-2m), which gives a minimum age range for the inherited zircon component.

Sample 00-247: Only a small amount of relatively poor quality zircon was recovered. Three fractions all contain moderate to abundant amounts of inherited zircon (Fig. A-2n). No estimate of the crystallization age of the rock can be made from the zircon data. The sample did not yield any monazite or other datable minerals.

Sample CAM-01: The sample yielded abundant zircon, mainly comprising clear, colorless, stubby prismatic grains. A small proportion of the grains contained cloudy inherited cores. Four fractions were analyzed (Table A-1, Fig. A-2o) and all yielded a moderate to strong inherited zircon component. An age cannot be assigned on the basis of the data.

Sample MAPT-5: This sample contained a moderate amount of zircon, most of which comprised stubby to elongate simple prisms with abundant fine clear inclusions. Three fractions were analyzed and all yielded concordant analyses (Table A-1, Fig. A-2p). Fractions B and C give somewhat older, but non-overlapping, Pb/U ages. The best estimate for the crystallization age of the sample is given by the total range of $^{206}\text{Pb}/^{238}\text{U}$ ages for these two fractions of 54.5 ± 0.5 Ma. Fraction A gives a slightly younger age is interpreted to have experienced post-crystallization Pb-loss that was not completely eliminated by abrasion.

Sample POGO-00-24: Zircons in this sample are similar in appearance to those in the previous sample. Four fractions all yield concordant analyses (Table 1, Fig. A-2q). The best estimate for crystallization age of the sample is given by the total range of $^{206}\text{Pb}/^{238}\text{U}$ ages for three overlapping fractions (A, C and D) at 5118 ± 0.3 Ma. Fraction B has experienced post-crystallization Pb-loss.

References

- Krogh, T.E., 1982, Improved accuracy of U-Pb zircon ages by the creation of more concordant systems using an air abrasion technique: *Geochimica et Cosmochimica Acta*, v. 46, p. 637-649.
- Ludwig, K.R., 1980, Calculation of uncertainties of U-Pb isotopic data: *Earth and Planetary Science Letters*, v. 46, p. 212-220.
- Mortensen, J.K., Ghosh, D., and Ferri, F., 1995, U-Pb age constraints of intrusive rocks associated with Copper-Gold porphyry deposits in the Canadian Cordillera, *in* Schroeter, T.G., ed., *Porphyry deposits of the northwestern Cordillera of North America: Canadian Institute of Mining and Metallurgy, Special Volume 46*, pp. 142-158.
- Parrish, R., 1990, U-Pb dating of monazite and its application to geological problems; *Canadian Journal of Earth Sciences*, v. 27, pp. 1431-1450.
- Parrish, R., Roddick, J.C., Loveridge, W.D. and Sullivan, R.W., 1987. Uranium-lead analytical techniques at the geochronology laboratory, Geological Survey of Canada, *in* *Radiogenic age and isotopic studies, Report 1: Geological Survey of Canada Paper 87-2*, p. 3-7.
- Roddick, J.C., 1987, Generalized numerical error analysis with application to geochronology and thermodynamics: *Geochimica et Cosmochimica Acta*, v. 51, p. 2129-2135.
- Stacey, J.S. and Kramer, J.D., 1975, Approximation of terrestrial lead isotope evolution by a two-stage model: *Earth and Planetary Science Letters*, v. 26, p. 207-221.
- Steiger, R.H. and Jäger, E., 1977, Subcommittee on geochronology: convention on the use of decay constants in geo- and cosmochemistry: *Earth and Planetary Science Letters*, v. 36, p. 359-362.

Table A-2. U-Pb analytical data for intrusive rocks in the Goodpaster District, Alaska.

Sample Description ¹	Wt (mg)	U (ppm)	Pb ² (ppm)	206Pb/204Pb (meas.) ³	total Pb (pg)	% 208Pb ²	206Pb/238U ¹⁴ ($\pm 1\sigma$)	207Pb/235U ¹⁴ ($\pm 1\sigma$)	207Pb/206Pb ¹⁴ ($\pm 1\sigma$)	206Pb/238U age	207Pb/206Pb age (Ma, $\pm 2\sigma$)
Sample OGNU-98-93											
A: N2,+105,e	0.04	627	18.9	10650	4	9.2	0.02999(0.10)	0.2488(0.16)	0.06017(0.08)	190.5(0.4)	609.8(3.8)
B: N2,+105,e	0.052	694	26.3	6549	13	11.9	0.03616(0.20)	0.3528(0.17)	0.07077(0.08)	229.0(0.5)	950.7(3.4)
C: N2,+105,i	0.016	883	17.5	3396	5	7.5	0.02031(0.09)	0.1389(0.18)	0.04961(0.11)	129.6(0.2)	176.6(5.2)
D: N2,+105,i	0.014	356	11.6	182	59	10.8	0.03153(0.28)	0.2972(0.99)	0.06837(0.81)	200.1(1.1)	879.7(33.6)
E: N2,+105, tips	0.02	881	20.3	4092	7	5.1	0.02416(0.09)	0.1796(0.17)	0.05392(0.10)	153.9(0.3)	367.9(4.5)
L: N5,44-74,e,u	0.042	801	16.6	5654	8	5.4	0.02162(0.11)	0.1627(0.19)	0.05457(0.10)	137.9(0.3)	394.7(4.4)
M: N5,44-74,e,u	0.037	1004	21	10400	5	6.4	0.02172(0.10)	0.1507(0.19)	0.05034(0.13)	138.5(0.3)	210.8(6.1)
N: N5,44-74,e,u	0.019	237	6.8	1180	7	10.6	0.02848(0.15)	0.2044(0.35)	0.05206(0.29)	181.0(0.5)	288.1(13.2)
O: N2,105-134,e,1	0.015	544	8.8	1502	6	5.4	0.01708(0.19)	0.1133(0.71)	0.04812(0.65)	109.2(0.4)	105.2(30.8)
M1: monazite,2,u	0.027	1602	279	4695	10	91.3	0.01674(0.14)	0.1111(0.21)	0.04815(0.14)	107.0(0.3)	106.7(6.5)
M2: monazite,3,u	0.021	1580	230	4022	9	89.4	0.01682(0.15)	0.1112(0.23)	0.04796(0.17)	107.5(0.3)	97.3(7.8)
Sample GDIB-97-71											
A: N5,+74,e	0.01	280	11.8	1805	4	16.8	0.03866(0.12)	0.2821(0.24)	0.05291(0.17)	244.5(0.6)	325.1(7.8)
C: N5,+74,s	0.011	310	13.9	1604	6	12.9	0.04302(0.12)	0.3415(0.23)	0.05758(0.16)	271.5(0.7)	513.8(7.1)
M1: monazite,2,u	0.018	1246	141	3925	6	86.7	0.01649(0.12)	0.1095(0.31)	0.04816(0.26)	105.4(0.2)	107.3(12.2)
M2: monazite,3,u	0.014	426	69.1	2697	2	90.6	0.01681(0.14)	0.1114(0.40)	0.04809(0.36)	107.4(0.3)	103.9(17.3)
Sample PEGM-98-93											
M1: monazite,1,u	0.05	5852	376	2927	105	76.4	0.01670(0.18)	0.1101(0.24)	0.04782(0.13)	106.8(0.4)	91.5(6.2)
M2: monazite,1,u	0.018	5060	349	7578	13	77.8	0.01690(0.17)	0.1113(0.22)	0.04776(0.11)	108.0(0.4)	87.5(5.4)
M3: monazite,1,u	0.032	5472	369	330	597	77.1	0.01703(0.18)	0.1124(0.66)	0.04785(0.56)	108.9(0.4)	91.8(26.4)
Sample 98-176											
A: N1,+149,s	0.055	697	33.1	6668	16	12.7	0.04563(0.10)	0.3358(0.17)	0.05336(0.09)	287.7(0.6)	344.3(3.8)
B: N1,+149,s	0.046	652	30.6	8043	11	10.8	0.04615(0.12)	0.3464(0.17)	0.05444(0.09)	290.8(0.7)	389.3(4.0)
C: N1,+149,s	0.034	950	42.6	3215	28	9.5	0.04482(0.10)	0.3291(0.18)	0.05326(0.11)	282.6(0.6)	339.7(4.8)
D: N1,+149,s	0.055	505	23.2	2388	33	11.5	0.04465(0.11)	0.3520(0.20)	0.05719(0.14)	281.6(0.6)	498.8(6.1)
E: N1,+149,s	0.072	708	33.7	211	766	11.2	0.04648(0.28)	0.3662(0.93)	0.05714(0.75)	292.8(1.6)	496.9(33.1)
H: N1,+149,s	0.062	880	36.1	6992	20	8	0.04157(0.13)	0.3051(0.18)	0.05322(0.09)	262.6(0.6)	338.4(3.9)
I: N1,+149,s	0.063	744	32.7	4003	32	9	0.04413(0.10)	0.3249(0.18)	0.05339(0.09)	278.4(0.5)	345.5(4.2)
J: N1,+149,s	0.07	647	29	9490	13	9.7	0.04456(0.11)	0.3404(0.17)	0.05539(0.08)	281.1(0.6)	428.1(3.6)
M1: monazite,3,u	0.018	3914	359	10890	7	83.4	0.01673(0.16)	0.1110(0.19)	0.04813(0.14)	106.9(0.3)	105.8(6.4)
M2: monazite,2,u	0.023	3665	291	4591	19	80.8	0.01683(0.16)	0.1118(0.22)	0.04820(0.13)	107.6(0.3)	109.1(6.0)
M3: monazite,3,u	0.023	4602	391	4394	25	82.1	0.01680(0.16)	0.1114(0.22)	0.04809(0.12)	107.4(0.3)	103.2(5.5)
Sample SP-00-14											
A: N2,134-149,s	0.018	296	5.8	1969	3	9.6	0.01963(0.13)	0.1365(0.37)	0.05043(0.33)	125.3(0.3)	215.9(15.1)
B: N2,134-149,s	0.02	288	11.9	2339	6	15.6	0.03946(0.16)	0.3009(0.26)	0.05530(0.19)	249.5(0.8)	424.5(8.6)
C: N2,134-149,s	0.013	392	19.7	3714	4	14.1	0.04660(0.16)	0.4910(0.23)	0.07642(0.15)	293.6(0.9)	1106.0(6.0)
M1: monazite,4,u	0.028	1946	234	1899	30	878.3	0.01678(0.17)	0.1111(0.57)	0.04805(0.52)	107.0(0.4)	101.8(24.7)
M3: monazite,3,u	0.019	1921	224	1224	31	87	0.01670(0.11)	0.1107(0.52)	0.04806(0.48)	106.8(0.2)	102.4(22.7)

Sample Description ¹	Wt (mg)	U (ppm)	Pb ² (ppm)	²⁰⁶ Pb/ ²⁰⁴ Pb (meas.) ³	total Pb (pg)	% ²⁰⁸ Pb ²	²⁰⁶ Pb/ ²³⁸ U ⁴ (± % 1σ)	²⁰⁷ Pb/ ²³⁵ U ⁴ (± % 1σ)	²⁰⁷ Pb/ ²⁰⁶ Pb ⁴ (± % 1σ)	²⁰⁶ Pb/ ²³⁸ U age (Ma. ± % 2σ)	²⁰⁷ Pb/ ²⁰⁶ Pb age (Ma. ± % 2σ)
Sample 97-75											
A: N10,+134,s	0.041	418	19.3	15840	3	8.7	0.04557(0.10)	0.4767(0.16)	0.07586(0.09)	287.3(0.6)	109.1(3.4)
B: N10,+134,s	0.025	667	15.2	9314	3	6.1	0.02364(0.14)	0.1748(0.19)	0.05363(0.13)	150.6(0.4)	355.5(5.7)
C: N10,+134,s	0.03	710	16.1	8400	4	5.7	0.02333(0.09)	0.2218(0.16)	0.06896(0.08)	148.7(0.3)	897.4(3.5)
D: N10,+134,s	0.025	422	13.7	75452	3	7	0.03243(0.14)	0.3613(0.18)	0.08105(0.100)	205.7(0.6)	1222.5(4.1)
M1: monazite,1,u	0.016	4374	248	4681	16	73.1	0.01687(0.13)	0.1115(0.20)	0.04793(0.11)	107.8(0.3)	96.0(5.1)
M2: monazite,3,u	0.011	5033	282	9625	6	72.9	0.01675(0.10)	0.1110(0.16)	0.04809(0.09)	107.1(0.2)	103.7(4.4)
Sample MAPT-14											
A: N2,134-149,c	0.02	609	11.4	3112	4	14.1	0.01774(0.12)	0.1199(0.21)	0.04900(0.14)	113.4(0.3)	147.8(6.7)
B: N2,134-149,c	0.025	578	11.4	2570	7	9.9	0.01962(0.16)	0.1330(0.23)	0.04916(0.14)	125.3(0.4)	155.6(6.5)
C: N2,134-149,c	0.018	561	9.4	1761	6	11.3	0.01653(0.14)	0.1095(0.24)	0.04807(0.16)	105.7(0.3)	102.7(7.5)
Sample MAPT-21											
A: N2,105,e	0.018	421	21.8	3598	7	8.2	0.05232(0.10)	0.4047(0.18)	0.05609(0.11)	328.8(0.7)	456.1(4.8)
C: N2,105,e	0.005	435	11.4	696	5	7.3	0.02681(0.17)	0.1886(0.47)	0.05102(0.40)	170.6(0.6)	241.7(18.4)
M1: monazite,2,u M2:	0.007	4695	276	4673	7	73.8	0.01698(0.17)	0.1128(0.26)	0.04816(0.16)	108.5(0.4)	107.1(7.6)
	0.005	11714	552	3494	17	67.6	0.01682(0.14)	0.1116(0.22)	0.04814(0.14)	107.5(0.3)	106.0(6.7)
Sample POGO-00-16											
M1: monazite,1,u	0.02	5110	199	2099	52	60.6	0.01696(0.13)	0.1122(0.53)	0.04799(0.49)	108.4(0.3)	98.6(23.3)
M2: monazite,2,u	0.013	7470	320	3256	31	59.1	0.01693(0.11)	0.1121(0.20)	0.04801(0.12)	108.2(0.2)	99.9(5.8)
M3: monazite,1,u	0.019	8160	461	3406	47	59.7	0.01676(0.11)	0.1113(0.20)	0.04814(0.13)	107.2(0.2)	106.0(6.1)
Sample 105-745											
A: M2,+149,s	0.036	638	10.3	2389	9	17.3	0.01476(0.11)	0.09752(0.24)	0.04791(0.18)	94.5(0.2)	94.8(8.7)
B: M2,+149,s	0.03	544	9.2	1292	12	20.5	0.01494(0.15)	0.0954(0.31)	0.04834(0.23)	95.6(0.3)	15.7(11.0)
C: M2,+149,s	0.05	591	9.8	1897	15	19.5	0.01477(0.12)	0.09758(0.27)	0.04891(0.20)	94.6(9.4)	94.6(9.4)
D: M2,+149,s	0.054	571	9.5	1708	17	19	0.01492(0.10)	0.09919(0.22)	0.04821(0.14)	95.5(0.2)	109.8(6.8)
Sample KGG #14											
A: N2,+134,s	0.057	563	9.2	3862	9	8.7	0.01642(0.09)	0.13058(0.17)	0.05769(0.09)	105.0(0.2)	517.9(4.1)
B: N2,+134,s	0.068	659	10	4564	9	8.3	0.01534(0.13)	0.10727(0.18)	0.05071(0.12)	98.2(0.3)	227.7(5.7)
C: N5,+74,e	0.016	830	11.8	1666	7	7.3	0.01464(0.11)	0.09669(0.24)	0.04789(0.17)	93.7(0.2)	93.9(8.2)
D: N5,+74,e	0.027	748	10.9	2588	7	7.8	0.01495(0.11)	0.09939(0.20)	0.04822(0.12)	95.7(0.2)	109.8(5.7)
E: N5,+74,e	0.018	703	10.2	1660	7	8.6	0.01468(0.11)	0.09825(0.27)	0.04853(0.22)	94.0(0.2)	125.2(10.3)
Sample POGO-00-247											
B: N5,74-104,s	0.021	1022	52.9	2507	27	8.9	0.05205(0.17)	0.3858(0.25)	0.05377(0.16)	327.1(1.1)	361.3(7.4)
C: N5,74-104,s	0.03	798	39.9	8861	8	9.9	0.04834(0.12)	0.3728(0.18)	0.05594(0.09)	304.3(0.7)	449.9(4.1)
D: N5,74-104,s	0.042	1259	58.6	6789	22	10.6	0.04588(0.11)	0.3389(0.18)	0.05558(0.09)	289.2(0.6)	353.5(4.2)

Sample Description ¹	Wt (mg)	U (ppm)	Pb ² (ppm)	206Pb/204Pb (meas.) ³	total Pb (pg)	% 208Pb ²	206Pb/238U ⁴ (± % 1σ)	207Pb/235U ⁴ (± % 1σ)	207Pb/206Pb ⁴ (± % 1σ)	206Pb/238U age (Ma; ± % 2σ)	207Pb/206Pb age (Ma; ± % 2σ)
Sample CAM-01											
A: N2,+149,s	0.055	669	18.2	23950	3	12	0.02644(0.09)	0.1872(0.16)	0.05134(0.09)	168.3(0.3)	256.0(3.9)
B: N2,+149,s	0.034	597	18.6	4942	8	8.2	0.09428(0.15)	0.2345(0.21)	0.05387(0.13)	200.4(0.6)	365.7(5.8)
C: N2,+149,s	0.045	523	24.4	10030	6	18.4	0.04176(0.17)	0.3226(0.24)	0.05603(0.16)	263.7(0.9)	453.4(6.9)
D: N2,+149,s	0.034	278	13.8	6892	4	10	0.04681(0.11)	0.6831(0.17)	0.10584(0.10)	294.9(0.6)	1728.9(3.5)
Sample MAPT-5											
A: N2,+134,s	0.067	343	2.7	453	25	13	0.00761(0.35)	0.05024(2.16)	0.04788(2.05)	48.9(0.3)	93.5(97.0)
B: N2,+134,s	0.072	202	1.8	762	10	12.1	0.00853(0.16)	0.05531(1.38)	0.04702(1.31)	54.8(0.2)	50.3(62.3)
C: N2,+134,s	0.051	474	4	570	23	10.8	0.00843(0.14)	0.05483(1.29)	0.04717(1.23)	54.1(0.2)	57.6(58.7)
Sample POGO-00-24											
A: N5,+74,e	0.015	5335	41.9	200	219	7.8	0.00804(0.22)	0.05225(1.95)	0.04715(1.86)	51.6(0.2)	56.9(88.5)
B: N5,+74,e	0.014	6073	46.9	213	214	7.5	0.00793(0.24)	0.05150(1.53)	0.04713(1.43)	50.9(0.2)	55.6(68.2)
C: N5,+74,e	0.016	2063	16.1	746	23	7.2	0.00806(0.14)	0.05233(0.64)	0.04707(0.59)	51.8(0.1)	52.9(28.5)
D: N5,+74,e	0.014	1761	13.8	1057	12	7.2	0.00808(0.16)	0.05250(0.99)	0.04710(0.95)	51.9(0.2)	54.5(45.3)

¹ N1, N2 = non-magnetic at n degrees side slope on Frantz magnetic separator; grain size given in microns; number = number of grains in the analysis; t = tabular grains; s = stubby prisms; e = elongate prisms; u =

² radiogenic Pb; corrected for blank, initial common Pb, and spike

³ corrected for spike and fractionation

⁴ corrected for blank Pb and U, and common Pb

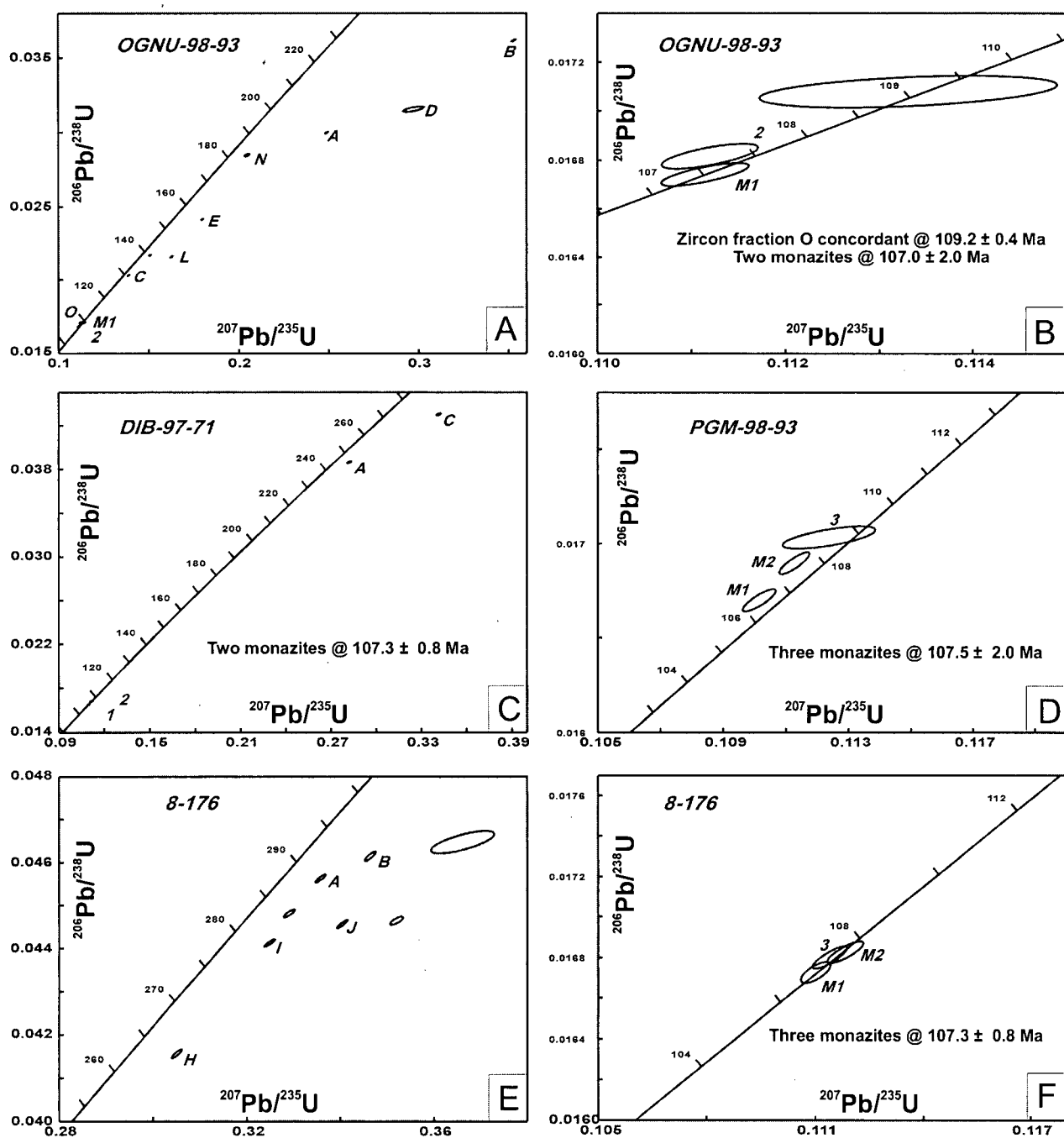


Figure A-2. U-Pb concordia plots for Goodpaster district intrusive rock samples.

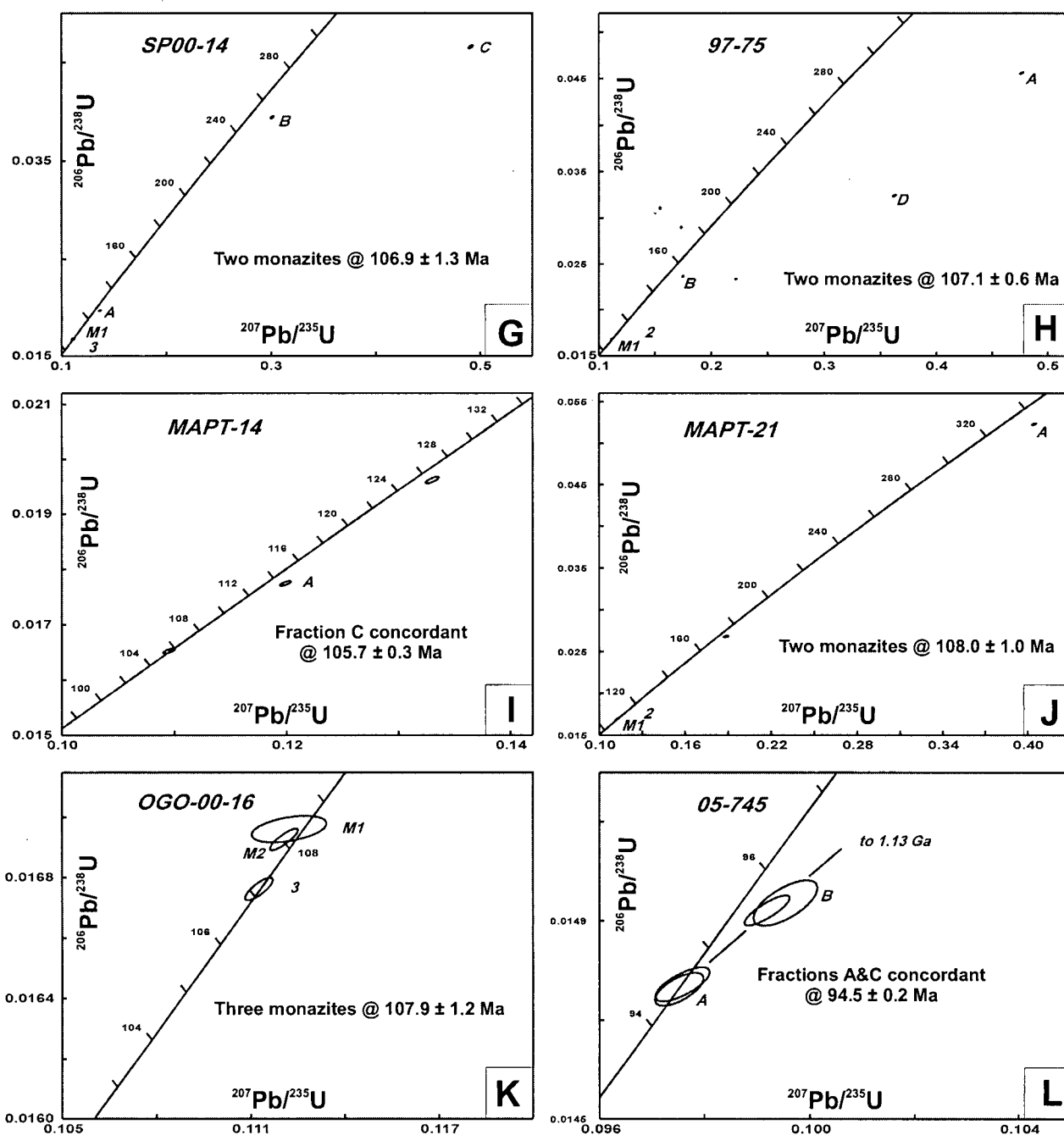


Figure A-2. U-Pb concordia plots for Goodpaster district intrusive rock samples.

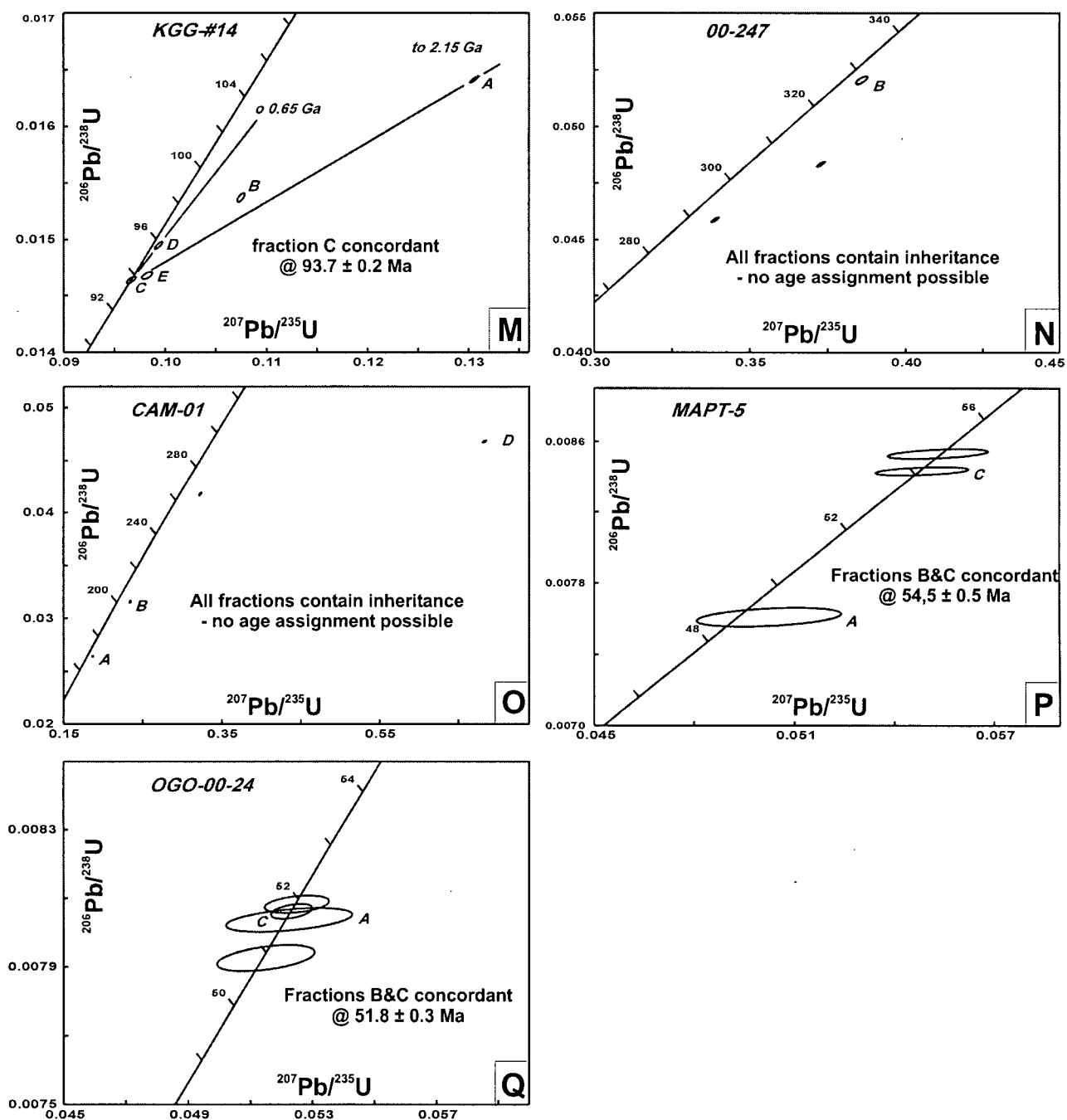


Figure A-2. U-Pb concordia plots for Goodpaster district intrusive rock samples.

SHRIMP-RG U-Pb Geochronology

Introduction

Sample MAPT-7, located approximately 3 km east of the Liese zone in the composite plutonic belt, was analysed using the Stanford-U.S. Geological Survey SHRIMP-RG (Sensitive High-mass Resolution Ion MicroProbe-Reverse Geometry) by Richard Tosdal. Previous attempts to obtain a U-Pb crystallization age by conventional U-Pb methods at the University of British Columbia failed because the zircons were small and had highly inherited cores.

METHODOLOGY

The sample was prepared at the University of British Columbia using the methods outlined for conventional U-Pb analysis. The population of zircon was dated using the SHRIMP-RG at Stanford University, California. This method has an advantage over conventional methods as it allows determination of U-Pb ages from 30-micron spots on individual zircon grains and allows for analysis of growth zones in complicated zircon populations. Small transparent zircons crystals, or zircons with clear rims surrounding a turbid core, were analysed. Extremely turbid grains with inherited crystals were avoided where possible. The SHRIMP-RG has a reverse geometry design and has improved mass resolution compared to conventional SHRIMP designs (Williams, 1998; Bacon et al., 2000). Bacon et al., (2000) summarize the operational conditions for the SHRIMP-RG. Reviews on the ion microprobe technique and data interpretation are provided in Ireland (1994) and Compson (1999). Compositions for initial common Pb compositions were used from the model of Cumming and Richards (1975). Zircon and Pb isotope data were reduced using the PRAWN and LEAD programs (Ireland, 1994) and ISOPLOT (Ludwig, 1999). Spot U-Pb analyses are provided in Table A-3 and are plotted on a concordia diagram in Figure A-3. All errors are given at the 1σ level.

RESULTS

MAPT-7

The zircons in this sample were prismatic to stubby with turbid to opaque cores and showed multiple generations of overgrowth. An episode of Early Cretaceous zircon growth nucleated on older turbid zircons scavenged from older rocks. A total of 12 zircon tips were analysed. Three of the tips (spot 1-2, 1-6, 1-11) yielded Mesozoic ages that may or may not have any age significance and are not considered in statistical analysis. Spots 1'-1, 1-3 and 1-8 give ages of 110-120 Ma. These ages could be a mix of Paleozoic or older inherited zircon and Early Cretaceous zircon. Ignoring points 1, 2, 3, 6, 8 and 11 the weighted mean average is $103.4 \text{ Ma} \pm 2.2 \text{ Ma}$. $\text{MSWD}=0.36$ and Probability = 0.87.

REFERENCES

- Bacon, C.R., Persing, J.M., Wooden, J.L., and Ireland, R.R., 2000, Late Pleistocene granodiorite beneath Crater Lake Caldera, Oregon, dated by ion microprobe: *Geology* (Boulder), v. 28, p. 467-470.
- Cumming, G. L., and Richards, J.R., 1975, Ore lead isotope ratios in a continuously changing Earth: *Earth and Planetary Science Letters*, v. 28, p. 155-171.
- Compson, W., 1999, Geological age by instrumental analysis; the 29th Hallimond Lecture" *Mineralogical Magazine*, v. 63, p. 297-311.
- Ireland T. R., 1994, Ion Microprobe mass spectrometry: Techniques and applications, in Hyman, M. and .R., eds, *Cosmochemistry, geochemistry and geochronology: Advances in analytical Geochemistry*, JAI Press, p. 1-118.
- Ludwig, K. R., 1999, ISOPLOT: A plotting and regression program for radiogenic-isotope data: U.S. Geological Survey Open File, v. 91-445, 41p.
- Williams, I.S., 1998, U-Th-Pb geochronology by ion microprobe, in McKibben, M.A., Shanks, W.C., III, and Ridley, W.I., eds, *Applications of micro analytical techniques to understanding mineralizing processes, Volume 7: Reviews in Economic Geology*: Socorro, NM, United States, Society of Economic Geologists, p. 1-35.

Table A-3. U-Pb analytical data for sample MAPT-7

Spot Name	percent comm 206	ppm U	ppm Th	$^{232}\text{Th}/^{238}\text{U}$	ppm Rad ^{226}Ra	$^{207}\text{Pb}/^{235}\text{U}$ 207corr	1s err (Ma)	$^{206}\text{Pb}/^{238}\text{U}$	Percent error	$^{207}\text{Pb}/^{235}\text{U}$	Percent error	$^{207}\text{Pb}/^{206}\text{Pb}$	Percent error	err corr
MAPT7-1.1	0.60	4272	372	0.09	64.4	111.3	2.9	0.01743	2.6	0.11742	5.8	0.048867	5.2	0.45
MAPT7-2.1	2.82	6594	513	0.08	126.5	140.6	4.1	0.02170	3.1	0.10785	27.5	0.036044	27.3	0.11
MAPT7-3.1	0.00	3708	411	0.11	59.9	119.6	3.3	0.01880	2.8	0.13287	4.7	0.051269	3.7	0.60
MAPT7-4.1	1.19	6621	361	0.06	93.4	104.4	2.8	0.01622	2.7	0.09680	10.1	0.043278	9.7	0.27
MAPT7-5.1	0.55	4142	415	0.10	57.2	102.8	2.7	0.01599	2.6	0.09723	5.8	0.044095	5.2	0.45
MAPT7-6.1	1.61	11509	531	0.05	231.0	148.5	3.9	0.02299	2.7	0.12144	11.2	0.038309	10.9	0.24
MAPT7-7.1	0.71	10397	384	0.04	146.9	104.9	2.7	0.01633	2.6	0.10016	3.8	0.044484	2.7	0.69
MAPT7-8.1	0.91	6628	490	0.08	101.6	113.7	3.0	0.01769	2.6	0.10571	6.2	0.043342	5.6	0.43
MAPT7-9.1	0.80	9665	543	0.06	134.8	103.5	2.7	0.01610	2.6	0.09839	6.1	0.044311	5.6	0.43
MAPT7-10.1	1.14	6037	873	0.15	82.8	100.6	2.7	0.01578	2.6	0.11135	7.7	0.051165	7.2	0.34
MAPT7-11.1	4.95	5326	369	0.07	112.1	155.7	4.4	0.02329	3.4					
MAPT7-12.1	0.95	14404	1194	0.09	204.3	104.6	2.8	0.01635	2.7	0.10707	6.6	0.047490	6.0	0.40

Errors are 1s unless otherwise specified

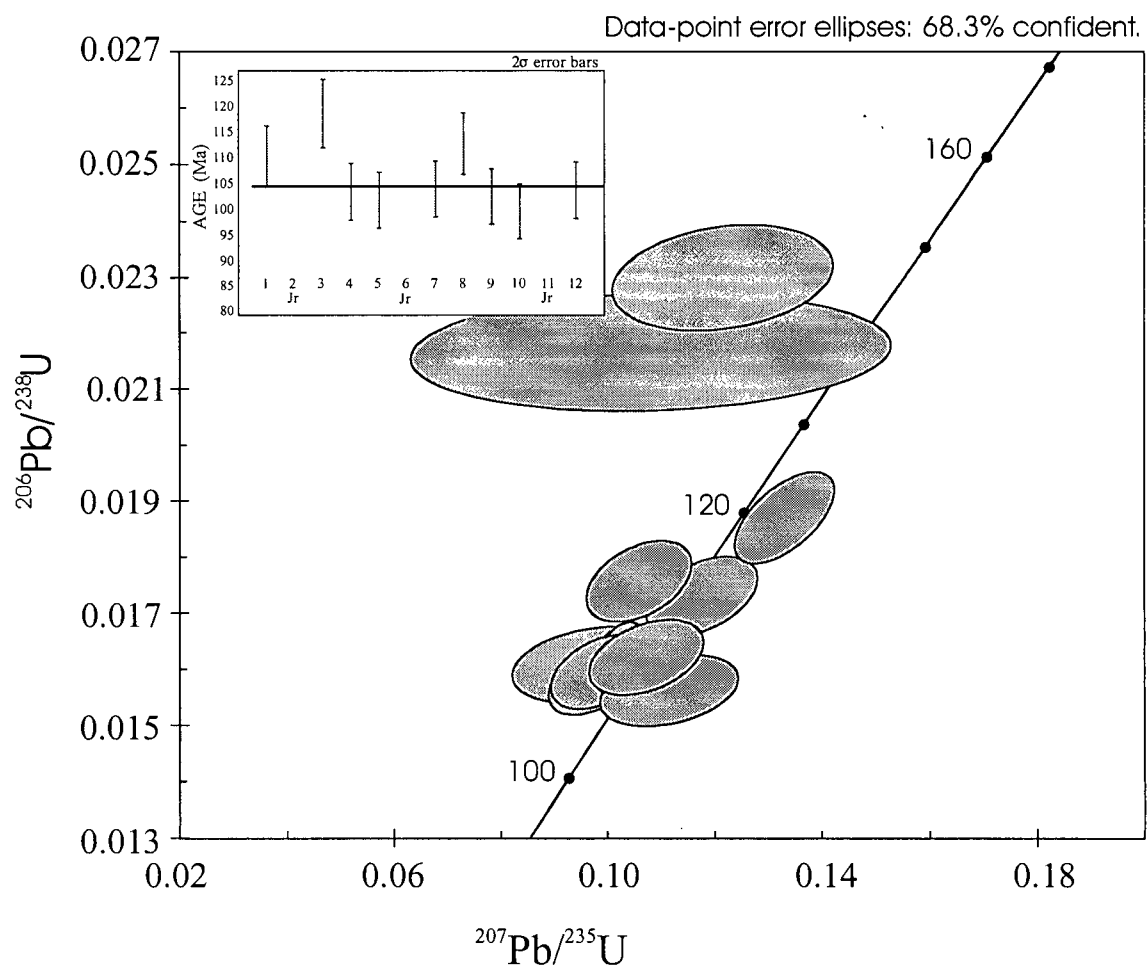


Figure A-3. U-Pb concordia plot for sample MAPT-7. A histogram of $^{206}\text{Pb}/^{238}\text{U}$ ages is shown in inset.

APPENDIX B

Geochemistry analytical methods

Collection, Crushing, and Analytical Methods

Fifty-nine Cretaceous intrusive rocks samples and two volcanic rock samples from the Goodpaster district were collected during regional mapping and from drill core for geochemical analysis. Most samples were collected from rubble crop and least altered samples were attempted to be collected. Geochemical analyses from two volcanic rocks that were not used in this study and are provided in Table B-1.

Samples were prepared for processing by cutting away weathered edges with a diamond saw and were sent to ALS-Chemex Laboratory Services Ltd. in North Vancouver, Canada. Samples were then crushed and pulverized to approximately 150 mesh in tungsten-carbide. Tantalum contamination during tungsten-carbide crushing is problematic and therefore all samples processed by this method likely have excess Ta. All Ta values have therefore been viewed as suspect and were not used in geochemical analysis. In addition, because of the tungsten-carbide grinding media, tungsten and cobalt may have been carried over to the samples. Typical ranges of contamination for granite range between 30 and 300 ppm for tungsten and between 10 and 30 ppm for cobalt (www.alschemex.com).

All samples were analysed for major, trace and rare earth elements abundances. Major element analyses were determined on fused disks by X-ray fluorescence (XRF). Reported Fe_2O_3 (T) is a measure of the total iron in the sample assuming all iron is ferric. Ferrous iron (FeO) was determined by Wilson titration method. Trace and rare earth elements were prepared by dissolving the rock powders in nitric, perchloric and/or hydrofluoric acids, followed by lithium metaborate fusion. The solutions were then analysed by inductively coupled plasma mass-spectrometry (ICP-MS). Detection limits for the major, trace and rare-earth elements are listed in Table B-2.

DUPLICATE AND STANDARDS

Duplicate analysis for MDRU standard samples PA-1 (granodiorite from the Coast Plutonic Complex) and BAS-1 (basalt from near Cheakamus, British Columbia) were submitted as unknowns to test for analytical precision and accuracy. Duplicate analyses of these samples are precise and are within two standard deviations of the standard values (Table B-3).

Table B-1. Geochemical data for an Eocene rhyolite dyke and a mafic dyke in the Goodpaster district not used in this study.

Sample No.:	Pogo-00-R24	Pogo-00-R53
Suite	Rhyolite	Mafic Dyke
Major Elements (%)		
SiO ₂	73.66	50.17
TiO ₂	0.04	1.88
Al ₂ O ₃	13.48	13.88
FeO (T)	1.42	8.84
MnO	0.04	0.23
MgO	0.03	4.28
CaO	0.45	9.05
Na ₂ O	3.03	2.05
K ₂ O	4.43	1.74
P ₂ O ₅	0.03	0.42
LOI	1.99	6.63
TOTAL	98.6	99.17
FeO	0.13	6.67

Sample No.:	Pogo-00-R24	Pogo-00-R53
Suite	Rhyolite	Mafic Dyke
Trace elements (ppm)		
Ba	126.5	500
Ce	13	58.5
Cs	10.2	2.4
Co	11.5	36
Cu	15	40
Dy	9.3	6
Er	7.2	3.5
Eu	0.1	2
Gd	4.4	6
Ga	25	18
Hf	6	6
Ho	2.5	1.3
La	5	27
Pb	40	20
Lu	1.3	0.5
Nd	6.5	32
Ni	5	130
Nb	27	18
Pr	1.7	7.9
Rb	498	48.6
Sm	3.2	6.6
Sr	32.4	386
Ta	9.5	2.5
Tb	1.3	1.2
Tl	2.5	<0.5
Th	37	9
Tm	1.4	0.5
Sn	40	3
W	98	28
U	22	4
V	5	145
Yb	9.1	3
Y	74.5	32
Zn	40	100
Zr	93.5	221

Table B-2. Detection limits for major, trace and rare earth elements at ALS-Chemex Labs.

Element	Method	Lower Limit (ppm)	Upper Limit (ppm)
Ag	ICP-MS	1	1000
Ba	ICP-MS	0.5	10000
Ce	ICP-MS	0.5	10000
Co	ICP-MS	0.5	10000
Cr	ICP-MS	10	10000
Cs	ICP-MS	0.1	10000
Cu	ICP-MS	5	10000
Dy	ICP-MS	0.1	1000
Er	ICP-MS	0.1	1000
Eu	ICP-MS	0.1	1000
Ga	ICP-MS	1	1000
Gd	ICP-MS	0.1	1000
Hf	ICP-MS	1	1000
Ho	ICP-MS	0.1	10000
La	ICP-MS	0.5	1000
Lu	ICP-MS	0.1	10000
Mo	ICP-MS	2	1000
Nb	ICP-MS	1	10000
Nd	ICP-MS	0.5	10000
Ni	ICP-MS	5	10000
Pb	ICP-MS	5	10000
Pr	ICP-MS	0.1	10000
Rb	ICP-MS	0.2	1000
Sm	ICP-MS	0.1	10000
Sn	ICP-MS	1	1000
Sr	ICP-MS	0.1	10000
Ta	ICP-MS	0.5	10000
Tb	ICP-MS	0.1	1000
Th	ICP-MS	1	1000
Tl	ICP-MS	0.5	1000
Tm	ICP-MS	0.1	1000
U	ICP-MS	0.5	1000
V	ICP-MS	5	10000
W	ICP-MS	1	10000
Y	ICP-MS	0.5	1000
Yb	ICP-MS	0.1	1000
Zn	ICP-MS	5	10000
Zr	ICP-MS	0.5	10000

Element	Method	Lower Limit (%)	Upper Limit (%)
Al	XRF	0.01	100
Ba	XRF	0.01	100
Ca	XRF	0.01	100
Cr	XRF	0.01	100
Fe (T)	XRF	0.01	100
K	XRF	0.01	100
Mg	XRF	0.01	100
Mn	XRF	0.01	100
Na	XRF	0.01	100
P	XRF	0.01	100
Si	XRF	0.01	100
Sr	XRF	0.01	100
Ti	XRF	0.01	100
LOI	XRF	0.01	100
FeO	titration	0.01	100

Table B-3. Mean values and duplicate analyses of standards P1 and BAS-1

P-1 (n=5)* std deviation			BAS-1 (n=5)* std deviation					
mean			P-1-A	P-1-B	mean		BAS-1-A	BAS-1-B
Majors (wt. %)								
SiO ₂ (wt%)	70.96	0.17	69.90	69.83	53.56	0.36	52.41	52.45
TiO ₂	0.38	0.00	0.40	0.38	1.31	0.01	1.33	1.31
Al ₂ O ₃	14.10	0.06	14.27	14.24	15.12	0.07	15.06	15.08
Fe ₂ O ₃ T	3.90	0.00	3.89	3.85	11.16	0.05	11.09	11.10
FeO	2.34	0.08	2.25	2.25	8.86	0.12	8.73	8.76
MnO	0.08	0.00	0.08	0.08	0.14	0.00	0.15	0.14
MgO	1.11	0.01	0.91	0.93	7.35	0.05	7.10	7.11
CaO	3.49	0.02	3.35	3.38	8.28	0.05	8.28	8.30
Na ₂ O	3.80	0.00	3.78	3.80	3.28	0.04	3.05	3.06
K ₂ O	2.12	0.01	2.19	2.21	0.56	0.02	0.61	0.60
P ₂ O ₅	0.08	0.04	0.07	0.08	0.22	0.00	0.23	0.23
TOTAL	100.56	0.22	99.28	99.20	100.96		99.15	99.26
Trace and rare earth elements (ppm)								
Ag	0.3		<1	<1	0.28	0.08	<1	<1
Ba	724	8.00	825	932	194	18.55	209	184
Ce	28	1.26	25	29.5	21.8	0.75	20.5	20.5
Co	6.2	0.40	5.5	6.0	42.2	0.40	39.0	41.0
Cs	1.2	0.10	1.1	1.1	0.1	0.01	<0.1	<0.1
Cu	15.5	5.50	5.0	5.0	59.0	0.80	55.0	65.0
Dy	3.3	0.15	2.3	3.1	3.3	0.15	2.6	2.7
Er	2.1	0.09	1.9	2.1	1.5	0.08	1.4	1.4
Eu	0.8	0.03	0.7	0.7	1.3	0.07	1.0	1.0
Ga	15.0	1.10	12.0	13.0	19.6	1.02	16.0	17.0
Gd	3.1	0.10	2.7	2.5	3.8	0.11	3.0	3.3
Hf	3.8	0.14	3.0	4.0	2.4	0.08	2.0	1.0
Ho	0.7	0.04	0.5	0.5	0.6	0.02	0.5	0.5
La (ppm)	13.2	0.40	14.0	16.0	9.3	0.44	10.5	9.5
Lu	0.4	0.01	0.3	0.3	0.2	0.01	0.1	0.1
Nb	3.8	0.17	2.0	3.0	8.2	0.49	6.0	6.0
Nd	13.0	0.63	10.5	12.0	13.6	0.80	11.0	11.5
Ni	-	-	<5	<5	172.0	1.90	160.0	170.0
Pb	10.2	1.47	15.0	5.0	4.4	4.32	40.0	<5
Pr	3.4	0.10	2.6	2.6	3.0	0.13	2.2	2.3
Rb	50.4	3.14	40.4	43.2	7.0	0.14	5.2	5.6
Sm	2.9	0.12	1.9	2.7	3.5	0.48	2.5	2.4
Sn	2.4	0.88	1.0	1.0	1.2	0.21	1.0	1.0
Sr	256.0	4.90	194.5	207.0	502.0	7.48	401.0	426.0
Ta	0.3	0.01	0.4	0.5	0.5	0.02	0.5	0.5
Tb	0.5	0.02	0.4	0.5	0.6	0.03	0.5	0.5
Th	4.4	-	<0.5	<0.5	0.8	0.03	<0.5	<0.5
Tl	0.3	-	<0.5	<0.5	0.1	0.00	<0.5	<0.5
Tm	0.4	0.01	0.3	0.3	0.2	0.01	0.1	0.1
U	1.5	0.07	1.5	1.5	0.3	0.01	<0.5	<0.5
V	58.2	0.40	45.0	45.0	152.0	1.10	125.0	140.0
Y	22.8	0.75	18.0	19.0	18.4	1.02	14.0	14.5
Yb	2.5	0.15	1.9	2.0	1.4	0.06	1.2	1.1
Zn	44.0	0.89	30.0	40.0	91.4	1.02	85.0	90.0
Zr	126.0	10.20	126.0	123.0	94.5	2.18	93.0	90.0

P-1 and BAS-1 are MDRU standards

* Mean values of P-1 and BAS-1 are based on the average of 5 previous repeat analyses

A and B are duplicate analyses of the standards that were analysed to test for precision

APPENDIX C

Fluid Inclusion Microthermometry Data

4021 PROSPECT FLUID INCLUSION DATA

- Notes: 1. Volume degree of fill based on visual estimation at room temperature (20° C)
2. CO₂ homogenized to the liquid state
3. Group refers to chip number, followed by fluid inclusion group letter
4. D= decrepitation temperature before homogenization
5. L= temperature at which the fluid inclusion leaked

Type 1A Aqueous-Carbonic (< 50% CO₂)

Quartz Sample	Size microns	Group	Degree of Fill (CO ₂)	T _{mCO2} (°C)	(% CO2 V)	T _{hCO2} (°C)	T _{fmH2O} (°C)	T _{mH2O} (°C)	T _{hH2O} (°C)	T _{clath} (°C)
332-247 Pegmatite	10	1a	0.2	-	-	25.6	-	-	D 330	-
	12	1a	0.2	-56.7	0.4	23.5	-	-	L 330	-
	8	1a	0.25	-57.2	0.3	-	-	-	D 330	-
	8	1a	0.25	-	-	18.4	-	-	-	-
	10	4a	0.1	-	-	-	-	-	265.1	-
	11	3a	0.1	-57.3	0.4	-10	-	-26	-	-
	7	6a	0.15	-	-	-10.6	-	-	269	-
	9	2a	0.2	-	-	12.5	-	-	302.3	10.8
	10	2a	0.2	-	-	21.8	-	-9.2	D 300.1	-
	8	2a	0.2	-	-	18.6	-	-7.6	D 300.1	-
	10	2a	0.2	-	-	23.4	-	-	L 304	-
	8	2b	0.2	-	-	20.4	-	-3	D 300	-
	10	2b	0.3	-57.7	0.5	12.7	-	-7.3	D 300	-
	8	5	0.15	-57.7	0.4	-	-	-	269	5.6
	10	6a	0.2	-	-	-	-	-8.8	310	4.4
	12	6a	0.2	-	-	-	-	-	290	-
	18	6a	0.2	-	-	-	-	-	300	-
	10	6a	0.2	-	-	9.6	-	-12	-	-
	8	6a	0.2	-	-	25.1	-	-	-	-
276-192 steeply dipping quartz veinlet	8	4a	0.1	-	-	-	-	-	289.6	-
	6	3b	1	-62.1	0.25	-9.7	-	-	-	-
	6	3b	0.1	-	-	-	-	-	294.8	-
	6	4b	0.2	-62.2	0.5	4.2	-	-4.1	D 300	-
	10	4c	0.1	-	-	-	-	-8.1	D 450	-
	6	4c	0.05	-	-	-	-	-	282.1	-
	20	4c	0.2	-	-	-	-26.8	-15.8	225.4	-
	10	5c	0.1	-	-	-	-	-	364.5	-
	10	5c	0.3	-56.7	0.4	-	-	-	-	-
99-3076 Quartz vein	20	2a	0.25	-56.3	-	28.8	-19	-11	233.3	5.2
	11	2a	0.1	-57.3	0.5	22.8	-	-2.8	D	-
	22.5	2b	0.1	-57.3	0.5	21.9	-10	-4.5	D	10.1
	10	2b	0.1	-	-	-	-	-1.8	-	-
	22.5	2c	0.1	-	0.5	21.9	-	-	-	10.1
	15	2c	0.1	-	-	-	-	-0.3	226.8	-
	7	3a	0.2	-	-	-	-	-	270.2	-
	8	3b	0.5	-	-	-	-	-24	265.7	-
	6	3d	0.1	-	-	-	-	-7.2	302.3	-
	10	3c	0.15	-	-	-	-	-1.6	233	-
	15	3c	0.2	-	-	-	-	-1.2	294.7	-
	16	3h	0.2	-	-	-	-	-	251.6	-
	12.5	3h	0.2	-	-	-	-	-2.4	258.4	-
	9	3f	0.15	-	-	-	-	-	276.9	-
	8	3f	0.15	-	-	-	-	-2.5	D 330	-
	8	3j	0.1	-	-	22.8	-	-	-	5.2
	18	6a	0.2	-	-	-	-	-	D 340	-
	10	6a	0.2	-	-	-	-	-	D 341	5.2
	10	6a	1	-57.3	0.4	13.5	-	-	D 342	-
	14	6a	0.2	-56.3	0.4	-	-	-	D 343	-
	14	6a	0.15	-	-	-	-	-	D 340	-
	7	6b	0.25	-56.5	-	24.4	-	-	284.4	9.7
	10	6b	0.2	-	-	28.7	-	-	288.2	-
	8	6b	0.2	-	-	-	-	-	290.1	-
	9	6b	0.4	-	-	27.2	-	-	-	-
	10	6a	0.1	-	-	-	-	-	D 340	5.2
	8	9	0.1	-	-	-	-	-2.1	-	6.9
	9	9	0.1	-	-	-	-	-	289	-

4021 PROSPECT FLUID INCLUSION DATA

- Notes: 1. Volume degree of fill based on visual estimation at room temperature (20° C)
2. CO₂ homogenized to the liquid state
3. Group refers to chip number, followed by fluid inclusion group letter
4. D = decrepitation temperature before homogenization

Type 1B Aqueous-Carbonic (> 50% CO₂)

Quartz Sample	size microns	Group	Degree of Fill (CO ₂)	T _{mCO2} (°C)	% CO ₂ vapour	Th _{CO2} (°C)	Th _{H2O} (°C)
332-247 Pegmatite	10	1a	0.9	-57.6	0.3	20.1	330.8
	9	1a	0.95	-57.8	0.4	14.8	D 330
	8	1a	0.85	-58.2	0.3	12.9	D 330
	8	1a	0.9	-57.3	0.5	17.1	-
	8	1a	0.95	-58.2	0.5	14.5	-
	10	1a	0.95	-57.4	0.3	15.2	-
	9	1a	1	-56.6	0.6	20.1	-
	10	1a	0.8	-56.6	0.4	17.1	-
	12.5	1a	0.95	-57.2	0.3	19.6	-
	15	1a	0.85	-56.8	0.5	12.4	D 330
	10	1a	0.8	-57	0.5	18.7	-
	8	1a	0.9	-57.4	0.4	19.2	-
	8	1a	0.9	-58.2	0.4	16.6	-
	8	1a	0.95	-	-	18.6	-
	10	1a	0.95	-57.3	0.4	16	-
	10	1c	0.85	-57.5	0.3	-	-
	10	1c	0.85	-57.4	0.4	10.3	-
	9	1c	0.95	-57.9	0.2	6.9	-
	7	3a	0.95	-57.7	0.4	12.4	278.6
	8	3a	0.95	-	-	14.2	-
	8	3a	0.9	-57.2	0.3	-	-
	7	3a	0.95	-58.6	0.5	-	-
	8	3a	0.95	-58.5	0.35	14.9	289
	10	3a	1	-57.3	-	-	-
	10	2a	0.9	-57.4	0.4	18.7	262.6
	12	4a	0.85	-58.3	-	12	346.6
	12	6b	0.95	-59.2	0.4	-	D 300
	10	6b	0.95	-58.3	0.4	20.2	D 300
	8	6b	1	-	-	8.8	300
276-192 steeply dipping quartz veinlet	25	1a	1	-61.6	0.33	-10.9	-
	10	1a	1	-62.5	0.33	-15.3	-
	9	1a	1	-64.4	0.25	-22.8	-
	12	1a	1	-62.5	0.8	-	-
	8	1a	1	-62.9	0.5	-6.9	-
	5	1a	1	-62.5	0.5	-7.4	-
	8	1a	1	-63.7	0.5	-10.8	-
	12	1a	1	-62.2	0.3	-9.9	-
	8	1a	1	-61.9	0.5	-5.2	-
	12	1a	1	-61.4	0.5	-14.1	-
	12	1a	1	-61.2	0.5	-13.6	-
	12	1b	0.9	-64	0.3	-15.5	-
	8	1b	0.9	-62.5	0.4	-17.8	306.2
	10	2a	0.9	-60.8	0.5	5.4	250.8
	8	2a	0.9	-62.6	0.6	3.6	287.9
	8	1b	0.95	-61.2	0.4	-9.7	NC at 344

Quartz Sample	size microns	Group	Degree of Fill (CO ₂)	T _{mCO2} (°C)	(% CO ₂ V)	Th _{CO2} (°C)	Th _{H2O} (°C)
276-192 con't	6	2a	0.85	-59.2	0.4	-	
	12	2a	0.9	-61.8	0.5	9	270.9
	15	2a	0.95	-59.9	0.5	-	D 270
	6	2b	0.9	-61.2	0.5	-4.8	290.2
	16	2b	0.9	-62.2	0.25	-4.9	D 270
	8	2b	0.9	-61	0.4	-1.8	291
	12	2b	0.95	-61.1	0.5	3	D 270
	8	2b	0.95	-60.7	0.4	-0.5	D 270
	10	2b	0.95	-60.8	0.4	-	D 270
	11	2c	0.95	-60.3	0.3	-0.4	D 270
	8	2c	0.95	-60.2	0.3	3.5	D 270
	10	2c	0.9	-60.6	0.3	7.4	207
	20	2d	0.95	-61	0.4	4	D 270
	12	2d	0.9	-61	0.4	2.6	D 270
	11	3c	0.9	-61.2	0.55	-21.1	270.1
	8	4a	0.9	-	-	-	288.8
	6	4b	1	-62.1	0.25	-9.2	-
	8	4d	0.9	-61.6	0.6	-23	259
	8	4c	0.95	-60.8	0.6	4.8	270
	10	5a	0.9	-60.3	0.5	2.5	D 470
	-	5a	0.9	-60.8	0.6	4.8	288.6
	8	5c	0.8	-60.9	0.6	-3.5	370.3
	10	5d	0.95	-60.6	0.7	2.7	300
	15	5d	0.9	-60.8	0.5	4.2	313
	7	5e	95	-61.4	0.3	-8.8	350
	12	5e	0.9	-60.8	0.3	-3.2	228.6
	11	5e	0.9	-61.1	0.4	5	240
99-3076 Quartz vein	10	1a	0.9	-56.7	-	22.3	-
	8		1	-57.6	-	-	-
	12	2c	0.95	-	-	18.7	-
	8	2e	1	-57.5	0.4	18.7	D 377
	7	2e	0.95	-57.3	0.25	19	D 377
	8	2e	1	-58	0.4	-	-
	7	3a	0.8	-58.2	0.5	too dark	304.8
	7	3a	0.95	-59.4	0.6	15.4	390
	8	3f	0.95	-	22.1	-	269
	8	3f	0.9	-57.9	0.5	-	-
	8	4c	1	-58.4	0.5	3.6	-
	6	4c	1	-57.5	0.4	12.8	-
	8	4c	0.95	-58.7	0.3	8.2	-
	12	4e	1	-58	0.25	-5.3	-
	11	4g	1	-57.4	0.5	15.9	-
	6	4h	1	-	-	18.4	-
	12	4j	0.9	-58.4	0.4	15	280
	10	4j	0.95	-57.4	0.8	-	-
	11	4j	0.95	-58	0.5	19.3	-
	10	4j	1	-57.3	-	21.2	-
	8	4j	0.95	-57.5	0.3	-	286
	6	4j	0.9	-	-	-	317
	10	5a	0.9	-	-	16	-
	10	5a	0.9	-	-	-	225.2
	10	6a	1	-	13.5	-	D 340

4021 PROSPECT FLUID INCLUSION DATA

- Notes: 1. All volume estimates based on phase proportions at room temperature (20° C)
2. Group refers to chip number followed by fluid inclusion group number
3. Type 2: P = primary, PS = pseudosecondary
4. Type 4: S = secondary
5. Type according to classification in text

Type 2 and Type 4 Aqueous

Sample	size	Group	Degree of Fill (vapour)	TfmH2O (°C)	TmH2O (°C)	ThH2O (°C)	Tclath (°C)	Type	P, PS, S
332-247 Pegmatite	7	1a	0.05	-	-	335	-	2B	PS
	5	1b	0.1	-34.1	-22.8	265.4	-8.9	2B	PS
	5	1b	0.05	-40.1	23.8	254.8	-11	2B	PS
	6	1b	0.1	-	-	211.4	-	2B	PS
	7	1b	0.1	-39.8	-25.3	257	-12.8	2B	PS
	7	1b	0.1	-	-23.3	226.3	-8	2B	PS
	8	1b	0.1	-	-23.8	258.6	-13.8	2B	PS
	7	1b	0.1	-34.6	-23.9	-	-11.5	2B	PS
	6	3b	0.05	-	-	269.6	-	2A	PS
	11	3b	0.1	-	-4.4	255.7	-	2A	PS
	8	3b	15%	-	-	289.1	-	2A	PS
	9	3b	0.1	-	-	277.7	-	2A	PS
	22	3b	0.1	-	-2.1	218	-	4	S
	12	3b	0.05	-	-0.5	187.2	-	4	S
	6	3b	0.05	-	-	206.1	-	4	S
	10	2a	0.1	-	-4	202.6	-	4	S
	8	2a	0.1	-	-	162.9	-	4	S
	8	2a	0.1	-	-3.4	215.1	-	4	S
	7	2a	0.1	-	-	170.8	-	4	S
	-	2c	0.1	-	-1.1	229.9	-	2A	PS
	5	2c	0.1	-	-	215.9	-	4	S
	9	2c	0.15	-	-0.5	219.5	-	4	S
	9	4a	0.05	-	-	206.2	-	2A	p
	8	4b	15%	-	-	265	-	2A	PS
	8	5a	0.05	-	-23.8	D 340	-	2B	PS
	10	5a	0.1	-	-1.5	234.2	-	2A	PS
	8	5a	0.1	-	-25.6	220.6	-	2B	P
	9	5a	0.1	-	-	225.8	-	2A	P
	9	5a	0.01	-	-4.4	206	-	4	S
	8	5a	0.01	-	-4	213	-	4	S
	8	4A	0.1	-	-27.2	-	-	2B	PS
276-192 steeply dipping quartz veinlet	6	2b	0.05	-3.2	-0.4	246.8	-	2A	P
	10	2a	0.15	-33	-23.6	L 370	-	2B	
	10	2a	0.1	-	-13.6	227	-	2B	S
	10	5b	0.1	-	-	232.6	-	2B	P
	9	5b	0.1	-	-3.9	210.6	-	2A	P
	8	5b	0.15	-	-2.6	213.2	-	2A	P
	9	3a	0.05	-40.9	-23.9	346.7	-	2B	P
	15	2a	0.1	-43	-24	311.6	-	2B	PS
	12	2b	0.1	-35.6	-25.1	D 270	-	2B	P
	12	2b	0.1	-	-25.8	D 270	-	2B	P
	7	2b	0.01	-35.9	-22.5	D 270	-	2B	P
	10	4b	0.05	-30.2	-24.8	269.7	-	2B	P
	6	4b	0.05	-	-24	265.1	-	2B	PS
	6	4b	0.05	-	-3.2	246.8	-	2A	P
	8	4d	0.1	-	-10.1	302	-	2B	PS
	7	4d	0.1	-	-	305	-	2B	PS
	12	5b	0.15	-40	-23.6	D at 370	-	2B	PS
	10	5b	0.1	-	-13.6	227	-	2B	PS

Sample	size	Group	Degree of Fill (vapour)	TfmH2O (°C)	TmH2O (°C)	ThH2O (°C)	Tclath (°C)	type	P, PS, S
276-192 con't	6	5d	0.1	-26.8	-16.2	D at 300		2B	PS
	7	5d	0.1			225.4		2A	PS
	10	5f	0.1	-29.2	-23.9	D		2B	P
99-3076 Quartz vein	16	2a	0.1	-5.2	-2.2	224.6	-	2A	P
	14	2a	0.1		-2	212.8		4	S
	10	2a	0.1	-6.6	-1.9	209	-	2A	PS
	10	2a	0.1	-	-2	224.9	-	2A	PS
	10	2a	0.1	-6	-1.4	206.8	-	4	S
	9	2a	0.1	-	-2	206	-	4	S
	7	2a	0.1	-	-1	210	-	2A	PS
	16	2b	0.15	-	-2.1	225.1	-	2A	PS
	25	2b	0.15	-	-2.8	225	-	2A	PS
	12	2b	0.1	-	-3	225	-	2A	PS
	20	2c	0.1	-	-2.2	225.4	-	2A	PS
	15	2c	0.1	-	-1.7	225	-	2A	PS
	8	2c	0.1	-	-1.6	-	-	2A	PS
	9	2c	0.1	-	-1.6	-	-	2A	PS
	10	2c	0.1	-	-1.8	-	-	2A	PS
	7	3a	0.1	-6.3	-2.3	154.5	-	4	S
	15	3a	0.1	-6	-1.9	186.1	-	2A	PS
	8	3a	0.05	-	-2.4	226.4	-	2A	PS
	6	3c	0.05	-	-2	213		2A	PS
	7	3c	0.1	-	-2.9	248		2A	P
	15	3e	0.1	-	-1.9	233.1	-	2A	PS
	8	3e	0.1	-	-1.8	190	-	2A	PS
	10	3e	0.15	-	-1.1	189.7	-	4	S
	10	3e	0.15	-	-1.5	-	-	4	S
	20	3h	0.15	-	-0.9	171	-	2A	PS
	12	3h	0.15	-	-1.4	212	-	2A	PS
	10	3h	0.25	-	-0.6	214	-	2A	PS
	8	3h	0.1	-	-1	176.8	-	4	S
	10	3h	0.1	-4	-1.4	-	-	4	S
	10	4a	0.1	-	-1.6	145.1	-	4	S
	12.5	4a	0.1	-	-0.6	124.8	1.1	4	S
	12	4b	0.1	-	-1	188.9	-	4	S
	5	4b	0.1	-		180.5	-	4	S
	9	4d	0.1	-	-1.8	223.7	-	2A	PS
	8	4d	0.1	-	-	221.4	-	2A	PS
	10	4d	0.05	-	-	221.9	-	2A	PS
	6	4d	0.1	-	-	220.4	-	2A	PS
	10	4f	0.1	-5.5	-1.6	184.7	-	4	S
	8	4h	0.1	-	-1.1	184.7	-	4	S
	10	4h	0.1	-	-1.4	202.6	-	4	S
	10	4f	0.1	-	0.7	233.5	-	2A	P
	8	4f	0.1	-	-0.6	221	-	2A	P
	8	5a	0.1	-	-2.1	183	-	4	S
	10	5a	0.1	-	-0.9	133	3.7	4	S
	12	5a	0.1	-	-	218.5	-	4	S
	9	5a	0.5	-	-	166.4	-	4	S
	6	5a	0.5	-	-	194.5	-	4	S
	6	5a	0.5	-	-	164	-	4	S

4021 PROSPECT FLUID INCLUSION DATA

- Notes: 1. All volume estimates based on phase proportions at room temperature
2. Group refers to chip number followed by fluid inclusions group number
3. P = primary, PS = pseudosecondary, S = secondary
4. D = decrepitation temperature,
5. NC = cubic inclusion has not changed at this temperature. The upper temperature limit of the stage was 480°C
6. L = leakage temperature

Type 3 Saline Fluids with Daughter Minerals

Sample	size	Group	Degree of Fill (vapour)	Degree of Fill (daughter)	T _{fmH2O} (°C)	T _{mH2O} (°C)	T _{clath} (°C)	Th _{H2O} (°C)	Th _{daughter} (°C)	P,PS,S
332-248 pegmatite	14	1b	0.1	0.1	-32.2	-24.8	9.7 (?)	L 330	-12.7	PS
	12	1b	0.1	0.05	-33	-25.2	8.8 (?)	L 330	210	PS
	8	4a	0.1	0.02	-30.2	-22.1	-	274.5	D 340	PS
	10	4a	0.1	0.05	-	-24.5	-	282	300	P
	12	4a	0.1	0.05	-	-26.2	-	270	274	PS
	8	5b	0.1	0.05	-	-	-	NC 320	240	P
	8	5b	0.1	0.05	-30.8	-	-	238	246	P
	10	5b	0.1	0.05	-	-	-	338	321	P
	14	3a	0.2	0.05	-	-	-	D 300	-	P
276-192	12.5	1b	0.05	0.05	-28.2	-	-	-	-	P
00-276-192	9	2b	0.05	.1 (2)	-43	-	-	L	-	PS
	8	2b	0.1	0.05	-35.9	-	-	-	-	PS
	10	3a	0.05	0.05	-35.6	-	-	338.1	NC 470	P
	10	3a	0.05	0.05	-40.9	-23.9	-	346.7	352.4	P
	14	3a	0.05	0.05	-39	-23.4	-	312	NC 475	PS
	11	3a	0.05	0.05	-	-23.9	-	376	D 480	PS
	6	3a	0.05	0.015	-	-22.8	-	NC 380	D 480	PS
	7	3a	0.05	0.05	-	-	-	312	D 480	PS
	10	3a	0.05	0.025	-	-	-	292.8	NC 480	PS
	8	3a	0.05	0.025	-	-	-	298.9	NC 480	PS
	8	4d	0.05	0.05	-40.1	-26.3	-	244.9	NC 450	P
	10	4d	0.05	0.05	-	-22.5	-	319	300	P
	12	5a	0.05	0.05	-36.6	-23.7	-9 (?)	169.6	190.2	P
	-	5b	0.1	0.05	-	-24.6	-	D 300	-	P
	10	5b	0.1	0.025	-39.2	-	2.2	362	L 420	P
	12	5b	0.1	0.08	-31.2	-24.5	-	L 370	-	PS
	8	5b	0.5	0.05 (2)	-36	-24.8	2.2	D 370	-	PS
	15	5b	0.05	0.025	-33.7	-24.8	-12.4 (?)	L 300	-	PS
	7	5f	0.05	0.05	-32	-	-	139.5	D 350	PS
	10	5f	0.1	0.05	-29.2	-26.2	-	300.4	L 452	PS
	15	5f	0.1	0.05	-38	-23.7	-	314.4	L 452	PS
	12	5f	0.015	0.05	-	-23.9	-	300.6	320	PS

4021 PROSPECT FLUID INCLUSION DATA

Notes: 1. Volume degree of fill based on visual estimation at room temperature (20° C)
2. All samples homogenized to the liquid state

Bladed Calcite

Inclusion number	size (microns)	Degree of Fill (vapour)	T _{fm} H ₂ O (°C)	T _h H ₂ O (°C)
1	12.5	0.05	-	118
2	12	0.05	-	118.6
3	10	0.05	-	150.2
4	10	0.05	-	124
5	5	0.05	-	124.2
6	5	0.05	-	124.8
7	10	0.05	-	138.4
8	10	0.05	-0.2	-
9	42	0.05	-0.01	-
10	10	0.05	-0.01	-
11	14	0.05	-0.2	-
12	17	0.05	-0.01	127.6
13	7.5	0.05	-	141.6
14	18	0.05	-	124.5
15	6	0.05	-	126.6
16	10	0.05	-	152.2